Discovery and characterization of formate dehydrogenases for enzymatic conversion of CO_2

Nielsen, Christian Førgaard

Publication date:
2020

Document Version
Publisher's PDF, also known as Version of record

PhD thesis

Discovery and characterization of formate dehydrogenases for enzymatic conversion of CO_2

Christian Førgaard Nielsen
November 2020

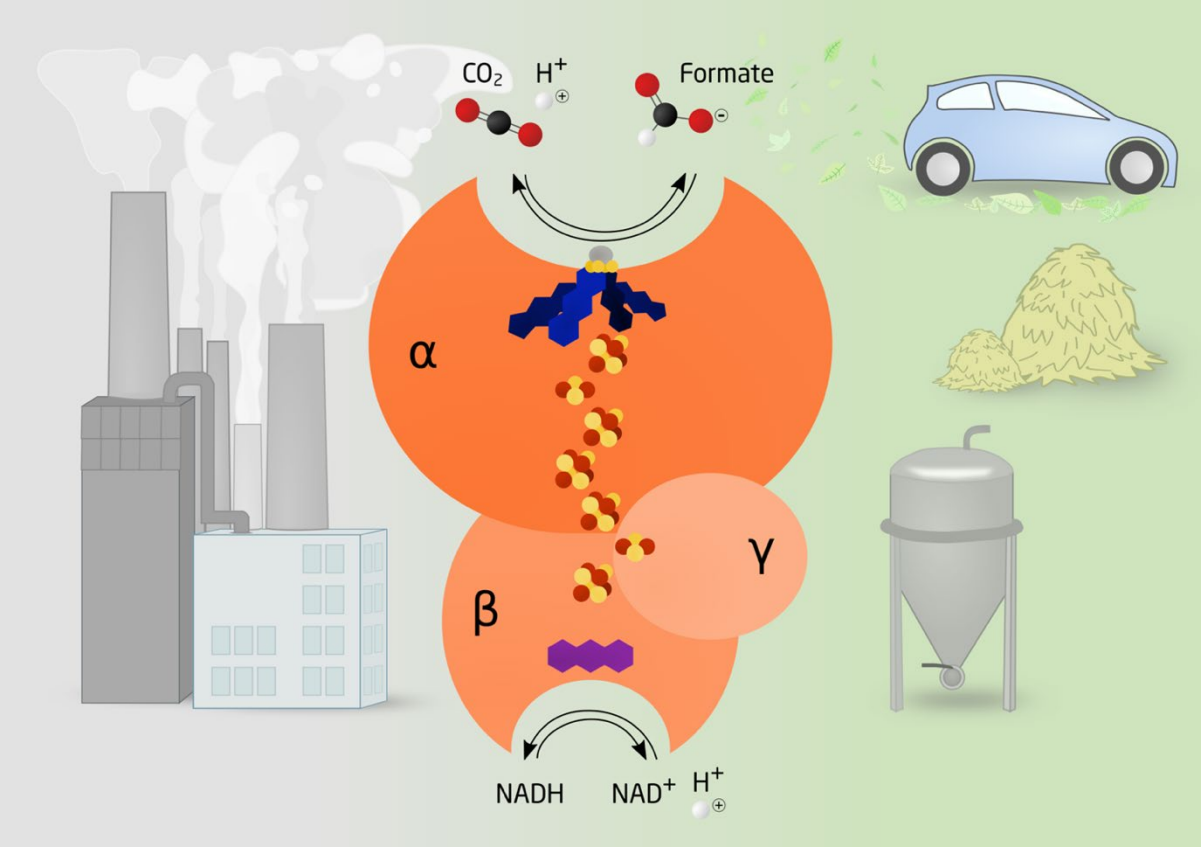

Preface

This PhD thesis was submitted to the Technical University of Denmark, Department of Biotechnology and Biomedicine, to fulfil the requirements to obtain a PhD degree. The work presented in this thesis was conducted first at the Center for Bioprocess Engineering, Department for Chemical and Biochemical engineering, and then continued at the Section for Protein Chemistry and Enzyme Technology, Department of Biotechnology and Biomedicine. The project was initiated in April 2017 and supervised by main supervisor Professor Anne Meyer and co-supervisors Professor Lene Lange and Professor Preben Morth. The work was supported by BioValue SPIR – A Strategic Platform for Innovation and Research on Value Added Products from Biomass, which is co-funded by The Innovation Fund Denmark, case no: 0603 - 00522B, and the Technical University of Denmark.

Christian Førgaard Nielsen
Kgs. Lyngby, November 10, 2020

Abstract

Among the developments aimed at addressing the climate crisis, the field of carbon capture and utilization (CCU) contains promising technologies.

Enzymatic solutions for CO_2 conversion are of interest given their high selectivity and mild reaction conditions. Metal-dependent formate dehydrogenases (FDHs) are particularly interesting since it is the only class of enzymes capable of producing a liquid in-demand product using CO_2 and electricity as the only substrates.

However, due to the incredible FDH diversity, selection of promising candidates for CCU proves non-trivial. Additionally, their inherent complexity and preference for anaerobic conditions have been shown to confer challenges for expression and characterization. This is reflected in literature, where a majority of studies are based on natively expressed FDHs and no study characterizes more than a single metal-dependent FDH variant at a time.

This thesis aims to develop and present a novel classification scheme for metal-dependent FDHs that allows discussion and selection of FDH candidates relevant for CCU. Additionally, through characterization of relevant FDHs, this thesis aims at expanding and consolidating the current understanding of FDHs in a CCU context.

By comparing structural and compositional qualities of all metal-dependent FDHs from the RefSeq sequence database, a classification scheme consisting of six FDH 'types' was developed. Here, the only two previously described oxygen tolerant FDH variants, RcFDH and CnFDH, were both classified as 'type 5 FDHs'. These variants and a third novel type 5 FDH, RsFDH, were subsequently expressed recombinantly, purified, and then characterized in terms of co-factor saturation, pH and temperature optima, catalytic parameters, and oxygen tolerance.

Interestingly, it was observed that hypothesized best practices for expression of metal-dependent FDHs were inferior in terms of yield and specific activity to a previously demonstrated simpler protocol. In terms of catalytic rate, CnFDH clearly outperformed the other type 5 FDHs, although RsFDH showed a higher relative preference for CO_2 reduction. Remarkably, oxygen tolerance turned out to involve complex dynamics between the enzyme, substrates, oxygen, and nitrate ions. Adding to this complexity, all three FDHs displayed previously unreported interaction with phosphate.

In conclusion, this thesis expands the previous knowledge on metal-dependent FDHs by demonstrating that type 5 FDHs represent a distinct sub-group, which is able to convert CO_2 under aerobic conditions with complex catalytic dynamics. Combined with a broad investigation of expression and purification methods, this thesis provides valuable insights for future research on these fascinating enzymes.

Dansk resumé

Blandt teknologier udviklet i kampen mod den verdensomspændende klimakrise er CCU (*carbon capture and utilization*) en af de mest lovende muligheder.

Enzymatisk omdannelse af CO_2 er en lovende teknologi, idet enzymer er meget selektive og fungerer under milde reaktionsbetingelser. Metal-afhængige format dehydrogenaser (FDH'er) er særligt interessante, idet de er den eneste type enzymer, der muliggør produktion af et flydende og efterspurgt produkt udelukkende ved brug af CO_2 og elektricitet som substrater.

På grund af en imponerende grad af diversitet blandt FDH'er er det dog ikke trivielt at udvælge lovende kandidater til CCU. Ydermere har tidligere studiers ekspression og karakterisering af enzymerne været udfordret af FDH'ernes høje kompleksitet samt deres præference for anaerobe forhold. Dette ses også i litteraturen, hvor størstedelen af studierne er baseret på nativt udtrykte FDH'er, og idet ingen studier har karakteriseret mere end en enkelt metal-afhængig FDH ad gangen.

Målet med denne afhandling er at udvikle og præsentere en ny metode til klassifikation af metal-afhængige FDH'er, som muliggør diskussion og udvælgelse af FDH-kandidater til CCU. Ydermere, vil afhandlingen gennem karakterisering af relevante FDH-varianter forsøge at udvide og sammenfatte den nuværende forståelse af FDH'er i CCU-kontekst.

Gennem sammenligning af alle metal-afhængige FDH'er fra RefSeq-sekvensdatabasen, blev der udviklet en klassifikationsmetode med seks 'typer' af FDH'er. De eneste to tidligere beskrevne FDH-varianter med ilt-tolerance, RcFDH og CnFDH, blev begge klassificeret som 'type 5 FDH'er' med denne metode. Disse varianter samt en tredje, hidtil ubeskrevet type 5 FDH, RsFDH, blev rekombinant udtrykt og oprenset, hvorefter de blev karakteriseret i forhold til deres cofaktor-mætning, pH og temperatur optima, katalytiske parametre og ilt-tolerance.

Først blev det observeret at den metode, der var hypotetiseret til at være mest optimal til ekspression af metal-afhængige FDH'er faktisk resulterede i lavere udbytte og specifik aktivitet sammenlignet med en tidligere anvendt, simplere protokol. CnFDH opnåede den klart højeste katalytiske hastighed af de tre FDH'er på trods af, at RsFDH faktisk havde en højere relativ præference for CO_2-reduktion. Derudover viste det sig, at ilt-tolerance var et komplekst spørgsmål, hvori dynamikken mellem enzymet, substraterne, ilt og nitrat-ioner var afgørende. Derudover blev der tilføjet endnu et lag af kompleksitet, idet der blev observeret en interaktion mellem fosfat og samtlige af de tre FDH-varianter, som ikke tidligere er beskrevet.

Overordnet set, udbygger denne afhandling den eksisterende viden om metal-afhængige FDH'er ved at demonstrere, at type 5 FDH'er udgør en distinkt undergruppe, der med kompleks dynamik er i stand til at omdanne CO_2 under aerobe forhold. Når dette sammenholdes med en bredere undersøgelse af metoder til ekspression og oprensning, bidrager denne afhandling med værdifuld viden til fremtidig forskning i disse fascinerende enzymer.

Acknowledgements

Throughout the past three and a half years I have received a great amount of supervision, help, and support, without which I could have not completed this work.

Firstly, I would like to express my gratitude to my main supervisor Anne Meyer, who not only entrusted me with this very exciting project, but also supported me continuously and tirelessly over the whole period. Her unwavering dedication and belief in the project and me as student have been of critical value to me. From Anne, I have learnt a lot about drive, leadership, and most importantly how to be a proper scientist.

Secondly, I want to thank my co-supervisors Preben Morth and Lene Lange. The long intricate talks on both science and scientific context have been a great source of learning, and their creative thinking has opened doors that I did not know existed. Travelling with Lene to Lolland or sitting in Preben's office has been not only inspiring and enlightening but also equipped me with a strong perspective on research as a whole.

I feel fortunate to have worked among some great colleagues during my time as a PhD student. I would particularly like to thank the members of the Enzyme Technology, Structural Enzymology, and Protein Biophysics groups for making the journey both fun and intellectually stimulating. I would like to specially mention Kristian Barrett, who not only helped me conduct a CUPP analysis but was also a great friend and brainstorm partner over the past six years at DTU. Furthermore, I would like to particularly thank Marlene Vuillemin, Lisa Merklinger, Julia Weikum, Emil Stender, Jesper Holck, Mateusz Lezyk, and Casper Wilkens who all have helped me tremendously in the lab.

In addition, the journey would not have been the same without the amazing social network I experienced in building 224, 225 and 227. Thank you for all the good times in the lab and lunchroom with board game nights, bar crawls, raclette eating, breakfast clubs, birthday parties, and hot pot dinners.

I am sincerely grateful to my collaborator at Boston University, Sean Elliott, who provided valuable insights on the electrochemical aspects of this work. I would also like to thank Malgorzata Rizzi at DTU Environment, for helping me quantify co-factor saturation via ICP-MS.

Finally, I am very thankful to my friends and family, who have always supported my scientific path – also by accepting that the lab sometimes comes first. I would like to mention Michael Schantz, who took the time to help me in the final proof-reading phase, and my wife Christina, who is always there for me and who has been my rock, cheerleader, and detail polisher during the thesis writing process.

Contents

List of publications

- **PAPER I**: Nielsen, C. F., Lange, L., & Meyer, A. S. (2019). Classification and enzyme kinetics of formate dehydrogenases for biomanufacturing via CO_2 utilization. *Biotechnology advances*, *37*(7), 107408.

- **PAPER II**: Nielsen, C. F., Morth, J. P., & Meyer, A. S. (*In preparation*). Enzyme reaction kinetics and O_2 tolerance of bacterial formate dehydrogenases for CO_2 utilization. *Journal of CO_2 Utilization.*

List of abbreviations

ADH	Alcohol dehydrogenase
ATP	Adenosine triphosphate
AUC	Area under curve
BmFaldDH	Formaldehyde dehydrogenase of *Burkholderia multivorans*
CA	Carbonic anhydrase
CbFDH	Formate dehydrogenase from *Candida boidinii*
CCU	Carbon capture and utilization
CI	Confidence interval
ClFDH	Formate dehydrogenase from *Clostridium ljungdahlii*
CnFDH	Formate dehydrogenase from *Cupriavidus necator*
$CO_{2(aq)}$	Aqueous CO_2
$CO_{2(g)}$	Gaseous CO_2
CODH	Carbon monoxide dehydrogenase
CV	Column volume
DdFDH	Formate dehydrogenase from *Desulfovibrio desulficans*
DET	Direct electron transfer
DvFDH	Formate dehydrogenase from *Desulfovibrio vulgaris* Hildenborough
EC number	Enzyme Commission number
ED	Electron donor
EDTA	Ethylenediaminetetraacetic acid
EES	Enzymatic electrosynthesis
FAD	Flavin adenine dinucleotide
FaldDH	Formaldehyde dehydrogenase
FDH	Formate dehydrogenase
FHL	Formate hydrogenlyase
FMN	Flavin mononucleotide
HDCR	Hydrogen-dependent carbon dioxide reductase
Hdr-SC	Heterodisulfide supercomplex
ICP	Inductive coupled plasma
ICP-MS	Inductive coupled plasma-mass spectrometer
IMAC	Immobilized metal affinity chromatography
IPTG	Isopropyl β-D-1-thiogalactopyranoside
k_{cat}	Turnover number
K_i	Inhibition constant
K_M	Michaelis constant
k_{obs}	Observed rate constant
LCA	Life cycle analysis
MET	Mediated electron transfer
MGD	Metallopterin guanine dinucleotide
Mo/W-bis-PGD	Mo/W-bis-pyranopterin guanine dinucleotide
MV	Methyl viologen
NAD^+	Nicotinamide adenine dinucleotide (oxidized)

NADH	Nicotinamide adenine dinucleotide (reduced)
$NADP^+$	Nicotinamide adenine dinucleotide phosphate (oxidized)
NADPH	Nicotinamide adenine dinucleotide phosphate (reduced)
NREL	National Renewable Energy Laboratories
ODC	Oxaloacetate decarboxylase
P	Pellet
PEPC	Phosphoenolpyruvate carboxykinase
PpFaldDH	Formaldehyde dehydrogenase from *Pseudomonas putida*
RaFDH	Formate dehydrogenase from *Rhodobacter aestuarii*
RcFDH	Formate dehydrogenase from *Rhodobacter capsulatus*
RsFDH	Formate dehydrogenase from *Rhodobacter sphaeroides*
RSM	Response surface methodology
RT	Room temperature
RuBisCO	Ribulose-1,5-bisphosphate carboxylase/oxygenase
ScADH	Alcohol dehydrogenase from *Saccharomyces cerevisiae*
SDS-PAGE	Sodium dodecyl sulfate-polyacrylamide gel electrophoresis
SEC	Size exclusion chromatography
SfFDH	Formate dehydrogenase from *Syntrophobacter fumaroxidans*
SHE	Standard hydrogen electrode
SN	Supernatant
TCL	Total cell lysate
TkHDCR	Hydrogen-dependent carbon dioxide reductase from *Thermoanaerobacter kuvui*
TRL	Technology readiness level
WLP	Wood-Ljungdahl pathway

Introduction

Anthropologically caused climate change is a reality caused by increased saturation of especially CO_2 in the atmosphere (Masson-Delmotte et al., 2018). While problematic, the atmospheric carbon also represents a potential sustainable resource: If able to efficiently capture and convert carbon, one would not only contribute to mitigating climate change but also to generating a potentially valuable and environmentally sustainable revenue chain (Aresta et al., 2016; Hepburn et al., 2019).

Among the many possible technologies aimed at sustainably converting CO_2 to in-demand chemical products, enzymatic solutions are of particular interest. This is due to the mild reaction conditions and high selectivity of enzymatic solutions. Within the realm of enzymes, the class of formate dehydrogenases (FDHs) contains interesting candidates for CO_2 conversion (Maia et al., 2017). Intriguingly, despite extensive diversity among FDHs, no classification scheme has yet been developed. Additionally, no study has been published where multiple FDH variants relevant for CO_2 conversion have been expressed in parallel and directly compared.

Scope of thesis

The scope of this thesis is to develop and consolidate the understanding of FDHs for conversion of CO_2.

To accomplish the scope, this thesis follows a linear structure, separated into five chapters. Combined, the chapters describe the full exploratory process from understanding the context of enzymatic CO_2 conversion to evaluating the potential of the characterized FDH candidates.

(Chapter 1) 'Context of study': The context of enzymatic CO_2 conversion. This chapter comprises the contextual background of the study. Here, challenges and opportunities with carbon capture and utilization are presented leading to a discussion on the parameters relevant for enzymatic conversion. Based on these parameters, both a general overview of enzymatic reactions involving CO_2 and arguments for the selection of FDH as best suited enzyme class are presented.

(Chapter 2)(PAPER I) 'Formate dehydrogenases': **Description and classification of formate dehydrogenases.** This chapter contains enzyme-specific background knowledge on FDHs to allow for discussion in the following chapters. Importantly, an investigation of the inherent diversity among FDHs is presented, followed by a presentation and discussion on division of FDHs into meaningful classification scheme. Additionally, by comparing kinetic qualities, the influence of electron donors is presented and discussed. Based on the derived classification scheme and subsequent discussion, specific FDH variants are selected for expression and purification.

(Chapter 3)(PAPER II) 'Enzyme production': Production of selected enzyme candidates, while addressing potential optimization options. This chapter tests and evaluates the current best practices for recombinant expression of selected FDH variants.

(Chapter 4)(PAPER II) 'Type 5 formate dehydrogenases as catalysts': Characterization of selected FDH variants. Here, pH and temperature optima, catalytic parameters, and oxygen tolerance are evaluated and compared for selected FDH variants.

(Chapter 5) 'Perspectives on application': Evaluation of potential for application of selected enzymes. Discussion on the perspectives of large-scale implementation of CO_2 reduction to formate.

Through the information presented and discussed in these five chapters, this thesis contributes to the overall understanding of formate dehydrogenases for CO_2 conversion by presenting and discussing a novel classification scheme, and additionally by characterizing and comparing relevant FDHs.

Chapter 1. Context of study

1.1. Carbon capture and utilization

As mentioned in the introduction: Climate change is a reality. It is a full-fledged crisis that we need to act on with a high level of urgency if we wish to avoid the worst of its consequences (Intergovernmental Panel on Clima Change, 2013). Recent estimates set the annual total carbon emission to roughly 11.3 Gt carbon emitted per year. The majority of the carbon is bound in CO_2, meaning a total annual emission of roughly 41 Gt CO_2. Of this, 17 Gt CO_2 is causing an atmospheric CO_2 concentration increase, and the remainder is taken up in ocean and land mass (Hepburn et al., 2019). Currently, the atmosphere contains approximately 3,150 Gt CO_2. This corresponds to approximately 410 ppm CO_2 assuming equal distribution over a year (Quéré et al., 2018). In the preindustrial year of 1750, the CO_2 concentration was 277 ppm (Joos and Spahni, 2008). Returning to this concentration would entail a removal of roughly 995 Gt atmospheric CO_2 on top of the yearly 17 Gt CO_2 emission. Or to put it in sensational terms: We need to remove a full teratonne of CO_2 from the atmosphere just to return to 'normal'.

The only actual long-term solution to achieve this momentous goal would be to become completely independent of any kind of fossil fuel, while simultaneously introducing net negative carbon emission processes at truly massive scales (Chohan, 2018). This is of course is an incredibly daunting and complex task. In fact, it is most likely the biggest global challenge ever.

Among the many possible solutions to achieve significant reduction in CO_2 emissions, carbon capture and utilization (CCU) has gained increasing interest. As the name implies, CCU technologies are technologies allowing capture and conversion of CO_2 into useful products. Essentially, CCU technologies hold the promise of providing existing in-demand chemical commodities, but produced with CO_2 as the carbon source. This effectively allows substitution of fossil fuels with CO_2 and renewable energy. Additionally, CCU is promoted as an option which – unlike other technologies – allows introduction of revenue. In a free market economy, generation of revenue could aid scaling and implementation independently of national politics.

Without delving too deeply into definitions and semantics it should be mentioned that 'carbon capture' and 'CO_2 utilization' are actually often two distinct technologies or methods that can be coupled. 'Carbon capture' is the process of capturing CO_2 to be processed for other uses. 'CO_2 utilization' is loosely defined as the use of CO_2 as a feedstock to produce carbon containing products. It is important to realize that the technologies revolve around *substitution* of CO_2 net positive emission processes with net neutral processes, although some approaches do also allow net negative emission depending on the lifetime of the given product (Aresta et al., 2014; Hepburn et al., 2019). In other words, CCU on its own will mainly contribute to diminishing – and ultimately completely removing – further emission of CO_2. It will *not* significantly contribute to removing the legacy CO_2 that is already in the atmosphere.

To further complicate matters, some definitions only consider something to be 'CO_2 utilization' if the CO_2 substrate is above atmospheric level concentrations. In other words, if the product is made from a plant biomass, it is not CCU but something else. One could argue that wood products and soil carbon sequestration are also CCU and if so, really attractive, already economically feasible CCU approaches do exist. Additionally, many of the plant-based approaches have gigaton potential for reducing CO_2 emissions (Hepburn et al., 2019). Although these are interesting and exciting, for the purpose of this

thesis, CCU will be defined as the process of converting CO_2 from a single point source, with high CO_2 concentration, directly into a single in-demand chemical.

1.1.1. Current developments within CCU

CCU is new territory. Different people, with different viewpoints, agendas, backgrounds, and geography, are all lobbying for their particular solution (Patricio et al., 2017). No consensus regarding the optimal solution has yet been reached. Then again, turning CO_2 emissions into net negative emissions is not a task that can be completed with a single technology.

The promise of CO_2 conversion has led to the technology and dream of CCU to be on the rise and gaining traction. Industrial and academic research efforts are rapidly growing with ever increasing funding opportunities. Global prizes for researchers and companies are awarded. Established chemical producers are building collaborations and adapting existing devices. Startup companies emerge in droves. All to help achieve the common goal of establishing the production processes for the future. However, despite the progress and immense initiative, challenges remain. Ultimately, cost economics, market barriers, and technology-specific limitations will determine if any of these new approaches achieve sufficient implementation (De Luna et al., 2019; Naims, 2016).

To the best of our knowledge, without discussing the political aspects of the chemical industry, chemical companies are waiting for economic incentive to adapt away from petrochemical production. This could be in the form of increased carbon taxation or removal of subsidies for petrochemical production. Without these incentives it is reasonable to state, this time without discussing the techno-economic feasibility of existing technologies, that the industry is *also* waiting for the right technology to make CCU profitable enough. This 'right technology' could potentially be derived with/from enzymes.

This thesis will not provide a techno-economic analysis comparing the current state-of-the-art CCU methods. Additionally, it will not go into detail with the abundant non-enzymatic approaches that have been developed recently. However, briefly put, interesting new chemical advances have been achieved for both heterogenous and homogenous catalysts in both thermochemical and electrochemical contexts (Al-Mamoori et al., 2017; Apaydin et al., 2017; P Chiranjeevi et al., 2019; Goeppert et al., 2014; Song et al., 2017). And, of course, numerous interesting biological technologies have also been developed. Engineered and native strains of bacteria, archaea, algae, and plants have been studied and applied in CCU contexts (Aresta et al., 2014; Bajracharya et al., 2016; Canadell and Schulze, 2014; Claassens et al., 2016; Humphreys and Minton, 2018; Yuan et al., 2016).

Common for any of the above technologies is that they all require a source of energy. For the chemical approaches, many of the most established technologies are based on thermochemically driven approaches (Aresta et al., 2016; Goeppert et al., 2014). The biological approaches are often driven directly or indirectly by solar energy. However, interestingly, for both chemical and biological approaches, electricity is becoming a more and more prevalent energy source. With good reason: Electricity is the cleanest and cheapest energy we have. Implementation of electricity is the key to turning extremely high volume reactions sustainable (Artz et al., 2018).

Point sources of CO_2, including up-concentrated atmospheric CO_2 via direct air capture, combined with the use of renewable energy may form the basis for a new chemical industry. The terminology of so-called 'electron foundries' is being used by National Renewable Energy Laboratories (NREL) in the US, exemplifying the ideology behind the new CO_2-based chemical production driven by sustainable

electricity (NREL, 2020). This talk reflects European work on implementation of Power-to-X production facilities and a general global trend of implementing electricity as *the* foundational energy source.

In a recent review, De Luna et al. explores the question of what it would take for renewable powered electrosynthesis to displace petrochemical processes (De Luna et al., 2019). Unsurprisingly, electricity prices are the main cost driver that limits electrochemical production. If electricity prices fall below 4 cents per kWh and conversion efficiencies reach at least 60%, then electrochemical processes can compete. It is beyond the scope of this thesis to assess the conversion efficiency of a suggested enzymatic approaches, since such a solution would first have to be implemented in a device. However, our best-informed prediction would be that technologies driven by clean electricity will become a cornerstone in future chemical production if we are to have any hope of replacing petrochemical production.

1.1.2. CCU in a Danish context

In a Danish context, CCU makes sense in two ways. First of all, Denmark has strong point sources of CO_2 from a host of differences origins:

- Production of biogas is increasing through heavy subsidies (The Danish Energy Agency, 2017). When producing biogas, only 60% of the emitted gaseous product is methane. Almost the entirety of the remaining gas phase is CO_2 (Aryal et al., 2018). Already, biogas plants need to 'upgrade' the outlet gas by removing CO_2 and other gasses, leaving the CO_2 as a wasted resource (Adnan et al., 2019).

- The Danish bio sector is strong and large. Fermentations in Danish biotech companies and breweries produce outlet gas containing CO_2.

- Combustion-based power plants are likely to remain a reality until efficient energy storage is implemented. In Denmark, there is a strong trend of increasingly using agricultural waste, energy crops, and municipal waste for incineration instead of the traditional use of coal and natural gas. Flue gas from these power plants will however still contain significant levels of CO_2 (Johnke, 1996).

- Steel and cement production are heavy emitters and will likely continue to be so unless heavy carbon taxation is introduced (van Ruijven et al., 2016).

Secondly, a large percentage of Danish electricity production is based on wind energy (Energinet Elsystemansvar, 2020). While relying *only* on surplus electricity is currently considered unfeasible due to the inherent instability of wind power production, wind energy does promise the opportunity of increasingly cheaper electricity on the grid as whole.

1.1.3. Considerations for enzymatic CCU

Based on the discussion presented in the previous two sections, it becomes clear that an ideal enzymatic CCU technology is driven (directly or indirectly) by sustainable electricity. However, a number of other parameters are also important when gauging the relevance and performance of a given enzymatic CCU technology. Of particular relevance is the composition and conditions of the carbon source.

CO_2 can be delivered in large variety of conditions. The key differentiator is the level of purification. At one end of the scale you have 99.99% pure, ambient temperature, pressurized CO_2 derived from

direct air capture with state-of-the-art equipment. A metric ton of CO_2 in this quality from this source would cost between USD 94 and USD 232 per tonne depending on the location of the capture device (Keith et al., 2018). This cost is mainly driven by energy requirements of the capture device.

Then, at the other end of the scale, you have flue gas from an outdated combustion power plant. Here particles and harmful NO_x gasses are often removed, but otherwise the flue gas would be derived straight from the chimney. The CO_2 concentrations here are in the range of 10-14% with temperatures reaching 160-180 °C (Aouini et al., 2014; Arachchige and Melaaen, 2012; Trachtenberg, 2006). The cost of this point source is unknown but would likely be low since it is quite literally considered problematic waste.

Obviously, in between the above two types of CO_2 point sources, different combinations of cost, purity, and conditions exist. The point is: Each point source, via its composition and condition, infers its own unique challenges for an enzymatic solution. Temperature, pH, CO_2 concentration, and presence of inhibitors will vary from point source to point source.

This leads to the final – but equally fundamental – consideration for enzymatic CCU: The output of a given technology. Which product is produced? If aiming to achieve any significant CO_2 climate impact, the product also needs to be in large enough demand to matter in terms of sheer volume.

In relation to this study, these considerations helped formulate the requirements for a potential enzymatic CCU technology. An ideal solution would involve the use of sustainable electricity and produce a relevant product in manner that is able to tolerant the challenges invoked by the CO_2 point sources. The question now becomes, based on these considerations, which enzyme would be an interesting candidate to study?

1.2. Enzymatic reactions with CO_2

CO_2 is known to be involved in quite literally thousands of biological reactions. According to BRENDA, more than 3,400 enzyme-catalyzed reactions exist with CO_2 as either a product, substrate, activating compound, or inhibitor. These have been reported in more than 2,600 literature references (Jeske et al., 2019; Schomburg et al., 2017).

Looking closer, it can be observed that out of the total amount of enzyme-catalyzed reactions, only 191 reactions are known to have CO_2 as a substrate. Upon further examination, the enzymes catalyzing these 191 reactions can be described with 48 distinct EC numbers (Figure 1). For a complete overview of EC numbers for enzymes registered in BRENDA as utilizing CO_2 as substrate, please refer to Appendix B.

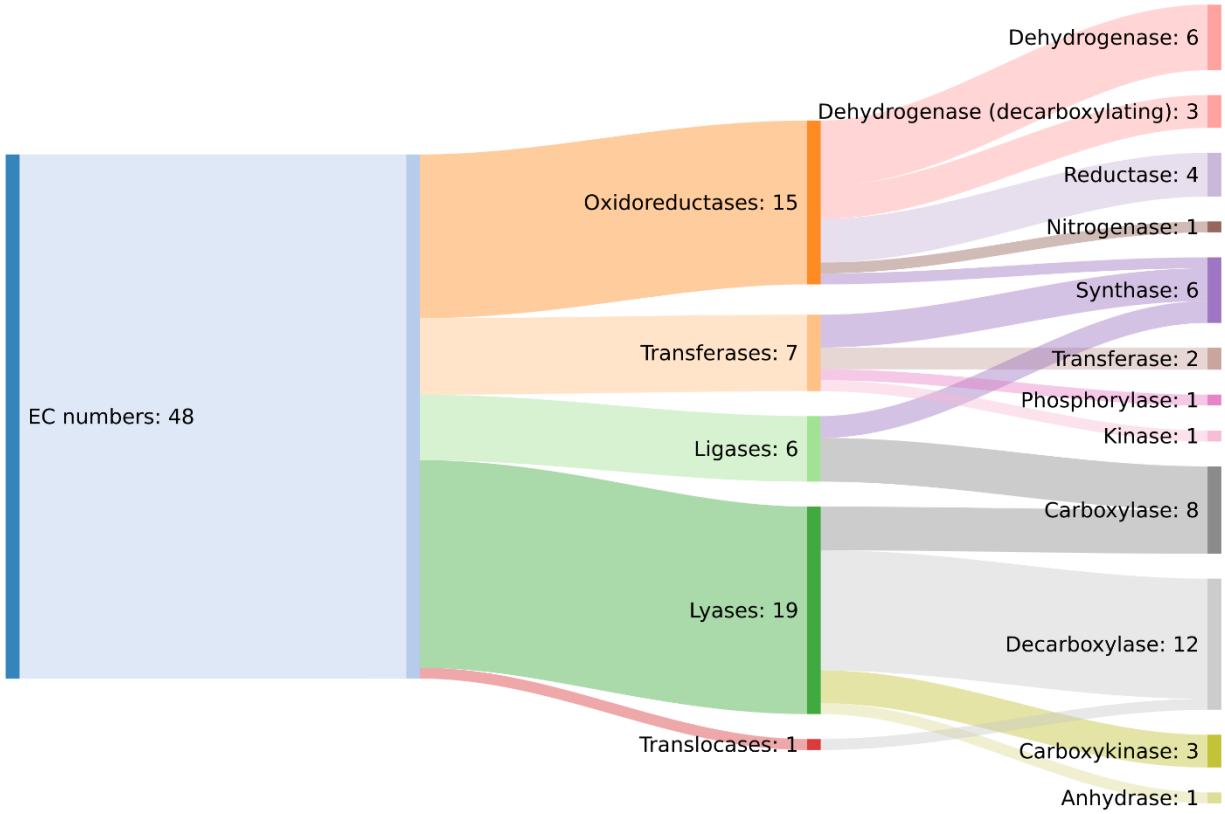

Figure 1: Santay diagram showing the 48 EC numbers found for the 191 reactions in BRENDA, which have CO_2 as a substrate.

From Figure 1, it is seen that five major groups of enzymes are found to interact with CO_2 as substrate, with oxidoreductases and lyases being the most diverse. The diversity does not reflect the natural abundance or prevalence of the enzymes, but it does provide some insight into the general role of CO_2 when acting as a substrate.

Two general notes of caution should be mentioned. To begin with, while the enzymes above are listed in BRENDA as catalyzing reactions with CO_2 as a substrate, it is entirely likely that the reverse reaction with CO_2 as a product is more favorable in most conditions. Then again, some of the reactions *not* listed as using CO_2 as a substrate may in fact be able to do just that. Secondly, although the actual number of remaining undiscovered microbial diversity remains somewhat debated (Lennon and Locey, 2016; Schloss et al., 2016), it is clear that natural diversity still has enormous room for discovery of organisms, and as an extrapolation, enzymes as well. As such, even though the list from BRENDA reasonably represents our current knowledge within CO_2-catalyzing enzymes, it is far from complete.

CO_2 is an incredibly stable compound, which is why enzymes using it as a substrate need another substrate to provide the energy (Wu et al., 2017). These are often in the form of energy-rich co-substrates such as ATP, redox active molecules or proteins, or even ion gradients. For a detailed exemplified presentation of enzymes catalyzing reactions involving CO_2, please refer to Appendix C.

In the context of CCU, a single group of enzymes stands out: the oxidoreductases. Oxidoreductases contain two enzyme classes defined by being able to catalyze reactions without any other co-substrate than an electron donor (ED). Specifically, carbon monoxide dehydrogenases (CODHs) that catalyze the interconversion between CO_2 and CO, and formate dehydrogenases (FDHs) that catalyze interconversion between CO_2 and formate.

Furthermore, the oxidoreductases have been shown to operate with electrodes as electron donors in bioelectrochemical setups (Jenner and Butt, 2018; Yang et al., 2016). With the considerations of the previous section in mind, the emerging platform of enzymatic electrosynthesis is incredibly exciting (Wu et al., 2020). Additionally, when comparing CODHs and FDHs, it can be argued that FDHs is more interesting. Although CO also has its purposes, formate is liquid non-toxic product that is water-miscible and also in demand.

Formic acid, the acid counterpart of formate, is the simplest carboxylic acid. It was first described in ants, given rise to its name ('formica' in latin translates to 'ants') (Wray, 1670). Formic acid and formate salts have very diverse applications across many industries. Formic acid is primarily used in the feed industry where it has nutrient-preserving effects on silage. Additional uses for the acid and salts include leather tanning, anti-icing, textile dyeing, food additives, and drilling fluid (Hietala et al., 2016). In 2012, worldwide production and consumption of formic acid was approximate 0.62 Mt/yr (Pérez-Fortes and Tzimas, 2016). An increase in production, particularly in China has since been observed (IHS, 2016). The best current global production estimates are behind paywall, but a reasonable estimate based on a conservative 4% annual growth rate (IndustryARC, 2019) would be a current global production of approximate 0.85 Mt/yr in 2020. This represents a market value of approximately 430-510 million EUR per year at 2013-prices of 0.51-0.6 EUR/kg (Afshar, 2014).

The potential of formate as a chemical product is foundational for the discussion of application of FDHs. An extended presentation of the interesting opportunities for processing of formate will be discussed in Section 5.2.

With both CO_2 and electricity having potential of being extremely low-cost substrates, the FDH class is an interesting candidate to investigate further for the purpose of enzymatic CCU.

Chapter 2. Formate dehydrogenases

Please note

This chapter is based on work published in Paper I: Classification and enzyme kinetics of formate dehydrogenases for biomanufacturing via CO_2 utilization. See Appendix M for full paper.

2.1. General characteristics

FDHs facilitate the interconversion between formate and CO_2 via a redox reaction (Eq. 1). The specific characteristics of the electron donor/acceptor often define the FDH as a whole.

$$HCOO^- \rightleftharpoons CO_2 + H^+ + 2e^- \quad (Eq. 1)$$

Formic acid, in the form of the anionic 'formate' at physiological pH, is the simplest possible carboxylic acid. It is present in all microbial life and broadly used in various C1 metabolisms (Maia et al., 2015). As a direct consequence, FDHs, facilitating reactions involving formate, are also present in all microbial life. In fact, with just a brief glance at FDHs as a class of enzymes, it becomes clear that a tremendous diversity in structure and function exists. For the purpose of studying FDHs in a CCU context, it can be considered prudent to first obtain an overview of the available variants of FDH. Grouping and classifying the FDHs into sub-groups could reveal information relevant for selection of CCU catalyst candidates.

Currently, FDHs are most commonly divided into two separate groups: The metal-dependent FDHs and the metal-independent FDHs. The two groups are completely unrelated in structure and mechanism with the only common ground being that they catalyze the same chemical reaction (Maia et al., 2017).

Metal-independent FDHs

Metal-independent FDHs are highly conserved globular proteins with a molecular weight in the range of 40-45 kDa per subunit (Choe et al., 2014) (Figure 2A-D). They are most often found as homodimers and do not contain any co-factors (Sultana et al., 2016).

In regards to electron donors/acceptors, the metal-independent enzymes are only able to react with either NAD^+/NADH or $NADP^+$/NADPH (Castillo et al., 2008; Marpani et al., 2017). This is due to the rather straight-forward close-proximity mechanism employed by this enzyme.

Interestingly, the only two commercially available FDHs are two metal-independent variants. This is likely a major contributing factor to studies involving metal-independent FDHs being more prominent in literature than those of metal-dependent FDHs. Particularly the FDH derived from the yeast *Candida boidinii* (CbFDH) is very well studied (Sultana et al., 2016). Another possible rationale for this research interest, is that metal-independent FDHs have been hailed by some as the best possible solution for CO_2 reduction (Takacs et al., 2017). This is, however, a matter for debate (Cotton et al., 2018), as will be discussed further in Section 2.3.

For the purpose of this chapter, metal-independent FDHs are noted as a remarkably uniform and simple protein group: A single type of subunit, soluble, no co-factors, no chaperones, and no known conjunction with other proteins. As a result, no further sub-grouping makes sense for this group of enzymes.

Metal-dependent FDHs

Relative to the metal-independent FDHs, the metal-*dependent* FDHs are entirely different beasts. Molded by the hydrothermal vents of the deepest seas, these enzymes are truly ancient (Berg et al., 2010; Fuchs, 2011; Hügler and Sievert, 2011). Not only do they have an impressive ancestry, but they are incredibly diverse in structure, composition, and function. Either soluble in cytoplasm or periplasm or as part of membrane bound complexes, these enzymes are located throughout the microbial cell (Hille et al., 2014).

First of all, unlike metal-independent FDHs, metal-dependent FDHs interact with a host of different electron donors/acceptors. In fact, it can be argued that most naturally occurring prokaryotic electron donors/acceptors have been shown to interact with an FDH or an FDH-containing protein complex (Maia et al., 2015). This is a major contributing factor as to why such a diversity is observed.

The only common denominator for metal-dependent FDHs is the central alpha subunit. The alpha subunit is commonly found in the range of 80-95 kDa in size. This subunit contains the ubiquitous and essential metallopterin guanine dinucleotide (MGD) co-factor (Hille et al., 2014) (Figure 2E-G). The MGD co-factor is often present as a bis-MGD. Together with a cysteine or selenocysteine residue in the alpha subunit, it coordinates the molybdenum or tungsten heavy metal that is central for activity (Moura et al., 2004). As such, the co-factor is often referred to as Mo-bis-MGD or W-bis-MGD if the metal is known, or Mo/W-bis-MGD if it is not. An alternative name is Mo/W-bis-pyranopterin guanine dinucleotide (Mo/W-bis-PGD), which is also commonly used (Grimaldi et al., 2013).

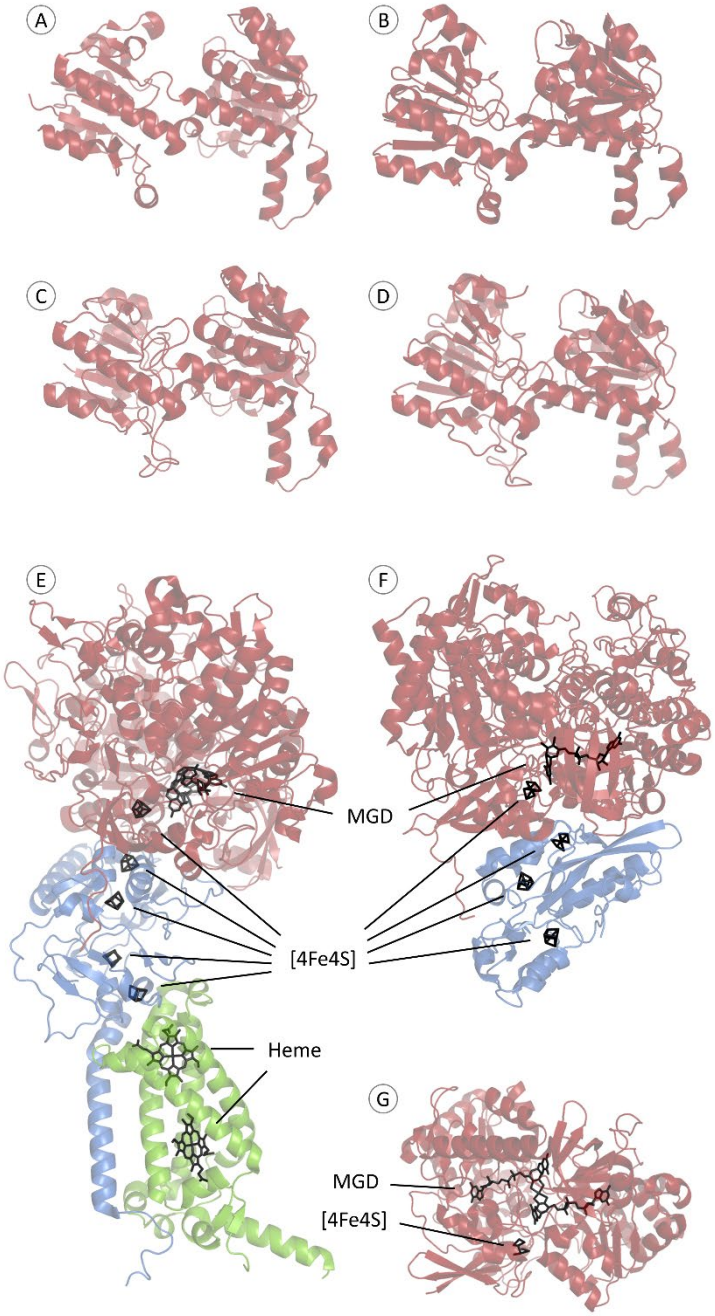

Figure 2: Three-dimensional crystal structures of FDHs. The main subunit, catalyzing formate oxidation/CO_2 reduction, is presented in red. For metal-dependent FDHs, this is the alpha subunit (α). The beta subunit (β) is represented in blue and the gamma subunit (γ) is represented in green. (A) FDH from Arabidopsis thaliana (metal-independent)(3JTM)(Shabalin et al., 2010). *(B) FDH of Candida boidinii (Metal-independent)(5DNA)*(Guo et al., 2016). *(C) FDH of Pseudomonas sp. 101 (Metal-independent)(2GO1)*(Filippova et al., 2005). *(D) FDH of Granucella mallencis MP5ACTX8 (Metal-independent)(4XYG)*(Fogal et al., 2015). *(E) FDH-N of Escherichia coli (Metal-dependent)(1KQG)*(Jormakka et al., 2003). *(F) FDH of Desulfovibrio gigas (Metal-dependent)(1H0H)*(Raaijmakers et al., 2002). *(G) FDH-H of Escherichia coli (Metal-dependent)(2IV2)*(Raaijmakers and Romão, 2006). *(Figure derived from* (Nielsen et al., 2019)*, see Appendix M).*

2.1.2. Subunits and chaperones

Beyond the central alpha subunit, metal-dependent FDHs are often found with a so-called 'beta subunit' and even sometimes a 'gamma subunit' (Figure 2E-F). The beta subunit is commonly seen at around 20-35 kDa in weight with the gamma subunits being smaller at 12-18 kDa in weight (Hartmann et al., 2015).

The role of the beta subunit is most often to transport electrons to and from the main active site. Additionally, an extra active site may be found in the beta subunit that catalyzes a redox reaction with an electron carrier as seen for the FDH from *Rhodobacter capsulatus* (Hartmann and Leimkühler, 2013) or FDH from *Cupriavidus necator* (Yu et al., 2019). In such cases, the electrons are transported from the active site in the beta subunit, through the beta and alpha subunits via FeS groups to the main active site (Jormakka et al., 2003). In this case, the 'main' active site is considered to be the formate oxidizing/CO_2 reducing active site of the alpha subunit.

Likewise, the gamma subunit may contain an active site catalyzing a redox reaction as can be seen for FDH-N from *Escherichia coli* (Jormakka et al., 2003). However, subunits annotated as 'gamma subunit' may also simply be smaller subunits with a single FeS group. The role of those is likely to stabilize and transfer electrons.

The synthesis and assembly of the Mo/W-bis-MGD is a process requiring multiple specialized intracellular proteins and often even FDH specific chaperones. These chaperones are known as FdhD, FdhE, FdsC and FdsD, with FdsC and FdhD being close homologs (Böhmer et al., 2014; Hartmann et al., 2015; Iobbi-Nivol and Leimkühler, 2013; Niks and Hille, 2019).

2.1.3. Co-factors

Beyond the Mo/W-bis-MGD co-factor, FDHs most commonly have other co-factors as well. These have one of two functions: To direct electrons through the enzyme or to interact with electron carriers.

For directing electrons, FDHs utilize FeS groups. Most commonly the cubane [4Fe-4S] groups are found, but also the smaller [2Fe-2S] groups are known to be used.

When a metal-independent FDH is soluble and not part of a multi-functional complex, flavin adenine dinucleotide (FAD), flavin mononucleotide (FMN), and heme groups constitute the most common co-factors that facilitate interaction with electron carriers (Hartmann et al., 2015).

2.1.4. FDHs in combinations with other enzymes

When an FDH does not contain a secondary active site to interact with electron carriers, it instead derives/provides electrons from/to other proteins.

A good example is the soluble protein complex known as 'hydrogen-dependent carbon dioxide reductase' (HDCR). These enzymes are essentially composed of an FDH coupled to a hydrogenase through two FeS-containing subunits (Schuchmann and Muller, 2013; Schwarz et al., 2018).

Other times, an FDH is part of much larger protein complexes. Two good examples are the membrane bound formate hydrogenlyase (FHL) complex of *E. coli* (McDowall et al., 2014) and the heterodisulfide supercomplex (Hdr-SC) of *Methanococcus maripaludis* (Lienemann et al., 2018). Interestingly, in Hdr-SC the FDHs are also coupled to a hydrogenase, although additional functionality beyond what is found in HDCR is included as well.

2.1.5. Potential for meaningful sub-division

Although metal-dependent FDHs have an alpha subunit containing the main active site in common, a lot of variability can be observed beyond the alpha subunit. As presented above, particularly the nature of other proteins and subunits attached to the alpha subunit varies. Additionally, the manner of assembly holds variation. Furthermore, and importantly, the manner with which the enzymes obtain/deliver the electrons used/generated in the main active site holds additional variability. As such, it is possible to further divide the metal-dependent FDHs into subgroups based on their subunit composition and manner of obtaining/delivering electrons.

Now the question becomes: How would a classification scheme for division into subgroups look? And then: Would such a scheme provide meaningful information?

2.2. Classification

2.2.1. Existing classification scheme for FDHs

As described above, FDHs are commonly divided into metal-dependent FDHs and metal-independent FDHs. Due to the limited variability of metal-independent FDHs, no further division of this type of FDHs would be meaningful. Metal-dependent FDHs, however, have potential for further classification.

Currently, metal-dependent FDHs are referred to as a subfamily of the 'DMSO reductase family' (Hille et al., 2014). This family is named after its first characterized member (Schneider et al., 1996). Metal-dependent FDHs are also placed, in a separate less complex categorization scheme, in the categories of 'complex iron-sulfur molybdo-enzymes' (Rothery et al., 2008) and 'Mo/W-bisPGD enzymes' (Grimaldi et al., 2013). These categories were coined later and are based on structure and co-factor content, rather than sequence relatedness. However, although metal-dependent FDHs belong in the above three classifications, no further sub-division exists.

2.2.2. Novel classification scheme for FDHs

As presented in the previous section, metal-dependent FDHs have extensive levels of diversity. When studying this group of enzymes more deeply, it was observed that different gene organizations existed for metal-dependent FDHs. Secondly, it was observed that different unique co-factors were employed by metal-dependent FDHs. Interestingly, the gene organization for known FDHs was associated with employment of certain co-factors. When combining information on these two features, a classification scheme with six 'types' of metal-dependent FDHs may be derived (Table 1).

The six types proposed here could then be annotated solely based on gene organization. It is the assumption that it is possible to extrapolate on the existing information in literature on co-factor content. Or, in other words, it is assumed that: A certain gene organization will always have a certain characterizing co-factor.

*Table 1: Proposed novel classification scheme. Gene organization allow for annotation of type. *: old nomenclature used for* E. coli. **: old n*omenclature used for homologs to CnFDH.*

Type	Gene segment organization	Subunit composition (per monomer)	Characterizing Co-factor
1	fdhA	α	None
2	fdhAB	αβ	None
3	fdhAB	α + FAD F420	FAD
4	fdhABC (fdnGHI*)	αβγ	Heme
5	fdhCBA (fdsGBA**)	αβγ	FMN
6	With NADH oxidoreductase	-	-

To understand if the classification scheme provides meaningful information, sequence relatedness studies were performed. Initially, the amino acid sequence of alpha subunits for the 23 currently known metal-dependent FDHs were compared and grouped according to sequence similarity. A type was then assigned based on gene organization. FDHs of the same type formed clades of enzymes with similar amino acid sequences (Figure 3).

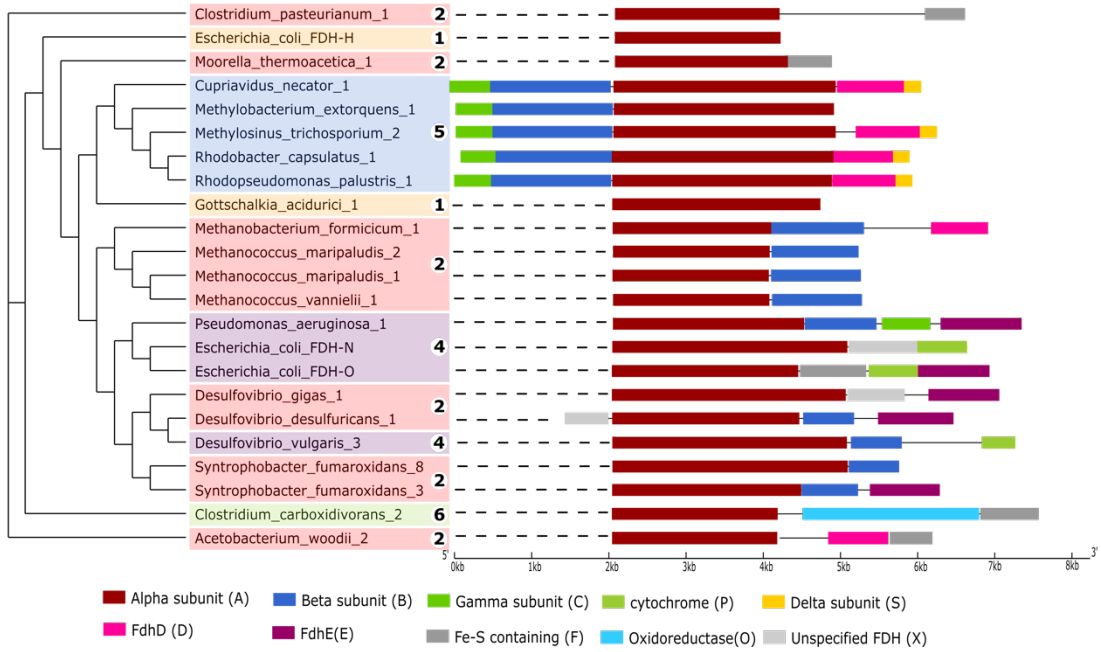

Figure 3: The 23 previously described metal-dependent FDHs annotated according to suggested classification scheme (number between 1-6 in white circle). FDHs are grouped according to alpha subunit amino acid sequence homology. The criterion for inclusion of each of the 23 enzymes was a possibility to correlate the described enzyme to the encoding genes and origin organism. Gene annotations for genes immediately upstream or downstream from the gene encoding the alpha subunit were logged. This includes FDH subunits, sulfurtransferase FdhD, FDH accessory protein FdhE, cytochrome (all types), unspecific FeS-containing proteins, and NAD(P)H related oxidoreductases. Individual enzymes are named according to the microbial origin and operon number encoding FDH found in the given organism. For instance, Syntrophobacter_fumaroxidans_3 and _8 denominate the 3rd and 8th FDH operon in the Syntrophobacter fumaroxidans *genome. (Figure derived from* (Nielsen et al., 2019)*, see Appendix M)*

It was noted that FDHs belonging to type 4 and type 5 grouped particularly strongly. This makes sense due to their more defined gene organization. In contrast, type 1 includes a large variety of proteins defined by containing at least a single FDH subunit. As mentioned previously, the electrons produced or required in the active site need to be transported to or from another redox reaction elsewhere. An alpha subunit on its own is typically not a complete protein. With type 1 and type 2, it is recognized that FDHs exist in a large range of different contexts.

Large scale sequence analysis

To investigate the classification scheme further, a larger scale sequence analysis was performed. The data applied for this study was derived from the RefSeq database, a collection of comprehensive and well-annotated sequences (O'Leary et al., 2016; Tatusova et al., 2016). From this database, 1,597 protein sequences encoding FDH alpha subunits were extracted from full genomes. To avoid selection bias, *all* FDH alpha subunits sequences from full genomes were extracted. No other selection parameters were included.

The predicted gene products for the adjacent genes were logged to gain information on the gene organization context of a given alpha subunit gene. Specifically, the four genes directly upstream and downstream of the alpha subunit gene were logged. Additionally, the directions of the genes were noted to assign the order of the genes. Finally, the organism of origin for the given alpha subunit sequence was logged.

The data was then processed. To reduce similarity bias in the final dendrogram, a 90% sequence identity threshold was enforced using the CD-hit tool (Li and Godzik, 2006). Following this reduction, 965 protein sequences remained. These were aligned using version 7 of the MAFFT multiple sequence aligner (Katoh et al., 2017; Katoh and Standley, 2013). The alignment was then analyzed with RAxML maximum likelihood software to generate a dendrogram (Le and Gascuel, 2008; Miller et al., 2010; Stamatakis, 2014).

Additionally, the 965 FDH alpha subunit sequences were grouped according to predicted function using the CUPP software (Barrett and Lange, 2019). CUPP is a novel clustering approach developed on the basis of conserved peptide patterns in proteins. These patterns can be used to identify similarities between proteins and create clusters of likely functionally similar proteins. In this regard, it adds an additional level of resolution to the analysis of FDH diversity. The FDH sequences in this study were divided into 17 CUPP groups.

Relying the on the annotation provided in the RefSeq database, the logged genes adjacent to the alpha subunit were assigned with a letter depending on the protein. For instance, 'A' for 'alpha subunit' and 'B' for 'beta subunit'. Also, more general annotations were employed. For example, 'X' for 'unspecified formate dehydrogenase subunit' and 'F' for '4Fe-4S containing protein'. These letters were assigned to the genes adjacent to the alpha subunit if possible. In this way, each alpha subunit gene was assigned a gene organization profile to use for annotation. For example enzymes with 'XBA' gene organization were annotated as type 5, and enzymes with 'AFC' were annotated as type 4 (See Table 1). For the complete list of search terms for letter assignment, see Appendix A.

In addition to the FDH type and CUPP group, the sequences were also annotated with species and taxonomy. Taxonomy was annotated at three levels: Superkingdom, phylum, and class. Combined with the dendrogram of sequence relatedness, a broader and more detailed picture of metal-dependent FDH emerges (Figure 4).

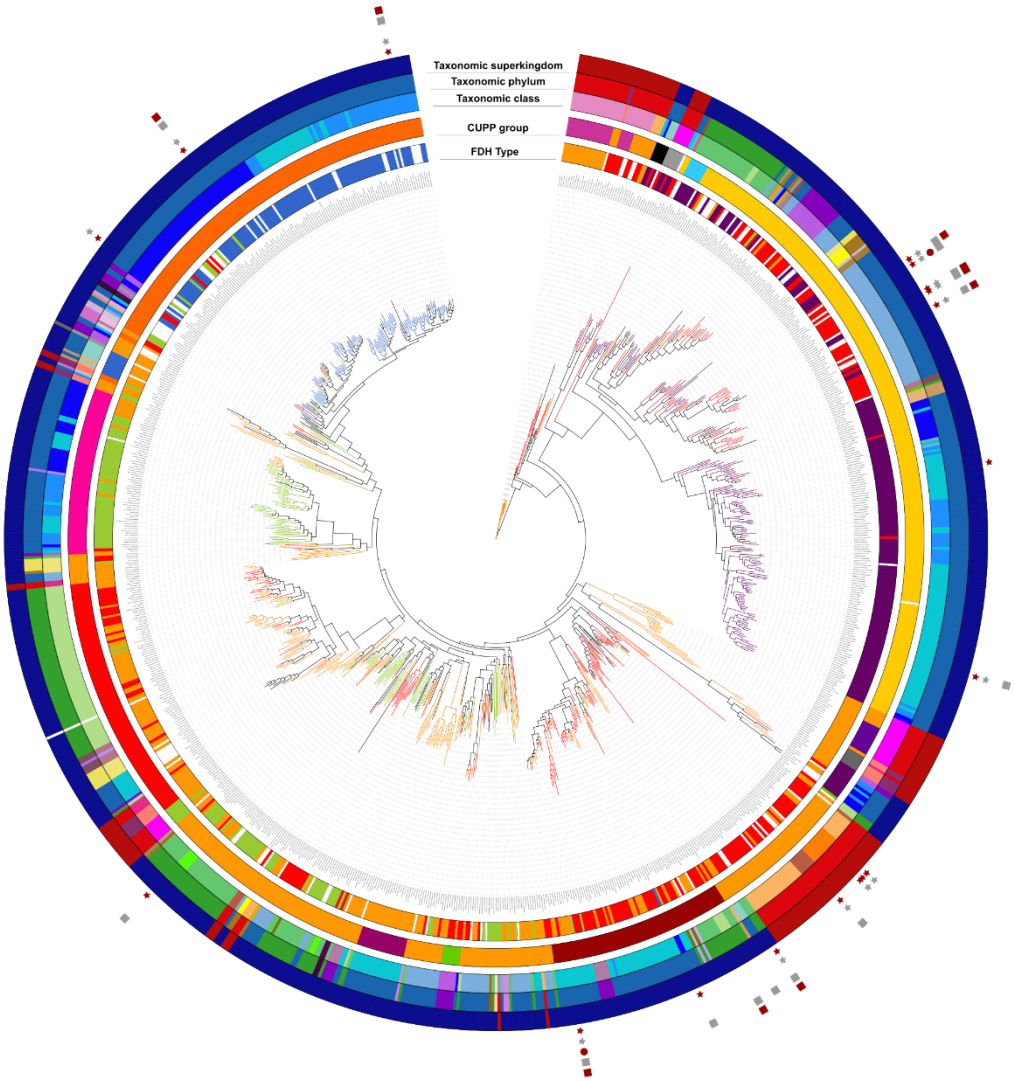

FDH Type

- Type 1: A, DA
- Type 2: (E)AB(E), AX(E), XA, AF, FA, XAD, AFD
- Type 3: Not able to annotate
- Type 4: ABC(E), ABP(E), AFC(E), ABCD, DABC(E), DABP(E), DAFCE
- Type 5: CBADS, CBADX, CXADS, CBAD, CXAD, CBAX, CBAS, CXAS, CXA
- Type 6: OA, OAF, OBAD, OAD, OXA, OXAD, AO, OBA, AOF, COA

Taxonomic superkingdom	Taxonomic phylum	Taxonomic class	Percentage of data (Phylum)
Archaea	Euryarchaeota	Thermococci Methanococci Methanobacteria Thermoplasmata Methanomicrobia Halobacteria	9.5 %
	Crenarchaeota	Thermoprotei	1.1 %
Bacteria	Proteobacteria	Alphaproteobacteria Betaproteobacteria Gammaproteobacteria Deltaproteobacteria Epsilonproteobacteria	64.3 %
	Firmicutes	Bacilli Clostridia Tissierellia Negativicutes Limnochordia	17.5 %
	Actinobacteria	Actinobacteria Acidimicrobiia Coriobacteriia Rubrobacteria	3.0 %
Other bacteria	Other phyla (16)	Other classes (21)	4.5 %

CUPP group

- FDH:1
- FDH:2
- FDH:3
- FDH:4
- FDH:5
- FDH:6
- FDH:7
- FDH:8
- FDH:9
- FDH:10
- FDH:11
- FDH:12
- FDH:13
- FDH:14
- FDH:15
- FDH:16
- FDH:17

Known attributes

- Gene organization
- Subunit composition
- Crystal structure
- Formate oxidation
- CO2 reduction

Figure 4: Phylogenetic tree generated based on alignment of 965 metal-dependent FDH alpha subunit sequences. Inter-sequence identity was reduced to a maximum of 90% between any two sequences. Each branch tip represents a single sequence. Each sequence is annotated with an FDH type based on gene segment organization. Gene segment organization is defined as the genetic makeup of the surrounding genes of a given FDH alpha subunit sequence. Here 'A': alpha (α) subunit, 'B': beta (β) subunit, 'C': gamma (γ) subunit, 'D': accessory sulfurtranferase fdhD, 'E': accessory protein fdhE, 'S': delta subunit, 'X': unspecified formate dehydrogenase subunit, 'O': NADH-quinone oxidoreductase related subunit, 'F': 4Fe-4S containing protein, and 'P': cytochrome formate dehydrogenase subunit ***PLEASE NOTE: An 'easier-to-read' large version of this figure can be found in Appendix D****.*

Discussion on validity of novel classification scheme

When looking more closely at the annotated dendrogram of metal-dependent FDHs (Appendix D), several points of interest emerge.

CUPP group 'FDH:1' is dispersed throughout the entire tree. In other words, the dendrogram built on the MAFFT based alignment does not completely correlate with the clustering method used for CUPP. This is to be expected, as two method will often provide two slightly different results due to differences in clustering algorithms. However, it beckons the question if further improvements could be made to the tree. Nonetheless, since the remaining 16 CUPP groups nicely overlap with distinct clades in the dendrogram, another possibility is that the CUPP group FDH:1 is simply a catch-all group with less defined traits.

FDH type 3 is not annotated for the sequences studied for this thesis at all. Although the type is distinct from the remaining five types through its unique use of FAD as a co-factor, it is not possible to annotate via gene organization alone. As such, enzymes annotated as type 2 are potentially instead a type 3 if containing FAD. Interestingly, when locating the known type 3 FDHs they group strongly with FDHs from other methanogenic archaea (Figure 5). Although, the annotated CUPP group is the promiscuous 'FDH:1', it likely that the FDH annotated here are in fact type 3 and not type 1 or 2 as seen in Figure 5.

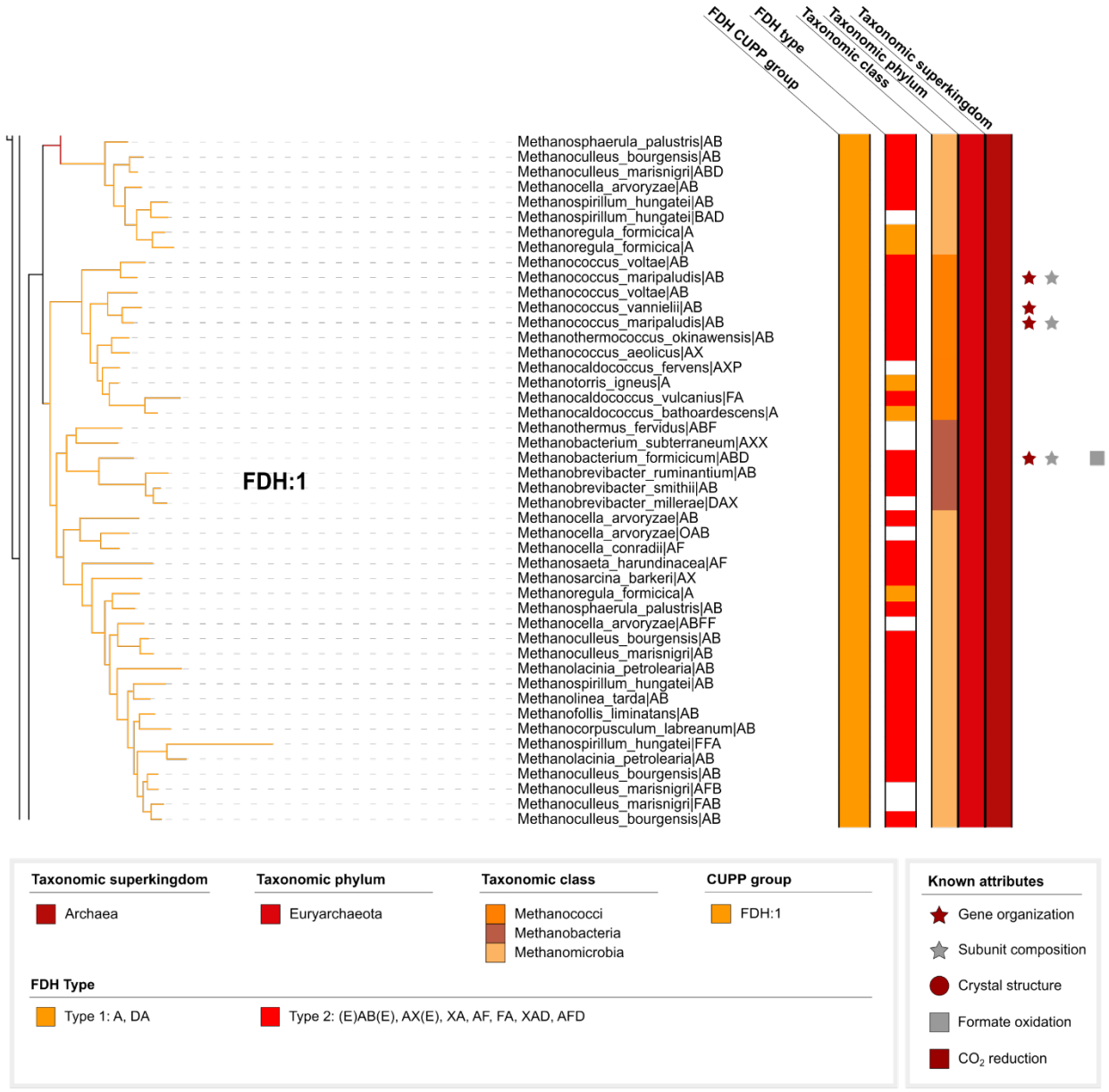

Figure 5: Subsection of Figure 4. Each branch tip represents a single FDH. Each sequence is annotated with origin organism and FDH type based on gene segment organization. Gene segment organization is defined as the genetic makeup of the surrounding genes of a given FDH alpha subunit sequence. Here, 'A': alpha (α) subunit, 'B': beta (β) subunit, 'D': accessory sulfurtranferase fdhD, 'E': accessory protein fdhE, 'X': unspecified formate dehydrogenase subunit, and 'F': 4Fe-4S containing protein.

Through removal of identical sequences, it was attempted to remove as much bias as possible. All data is biased to some extent. In this case, it was chosen to rely on the annotations provided in the RefSeq database. It is likely that some organism groups or FDH variants have received more attention than others. As such, this study makes no claim that the overview presented is representative of the actual natural distribution of FDHs. However, as it is the scope of the RefSeq database to include taxonomically diverse organisms (O'Leary et al., 2016), it is the best approximation known and available at the time of study.

Interestingly, the FDHs for which it was possible to link literature information with sequence (Figure 4) can be described with just four of the 17 CUPP groups. These are CUPP groups FDH:1, FDH:2, FDH:4,

and FDH:6. Admittedly, these four CUPP groups are also by far the largest, but it is interesting that the remaining 13 CUPP groups are unrepresented by any characterized FDH in literature. In other words, likely functionally different variants of FDH are left undescribed in literature. Nonetheless, since CUPP groups FDH:1, FDH:2, FDH:4, and FDH:6 comprise the vast majority of included FDHs here, the bias is somewhat negligible.

Finally, similarly to the results of the previous smaller study on known FDHs, it is observed for this larger study that clades of FDH alpha subunit sequences group according to the types presented in classification scheme proposed for this study. And again, it is especially the more tightly defined type 4 and type 5 that form coherent clades. Interestingly, also type 6 forms a coherent clade. This clade belongs solidly to CUPP group FDH:5 (Figure 6).

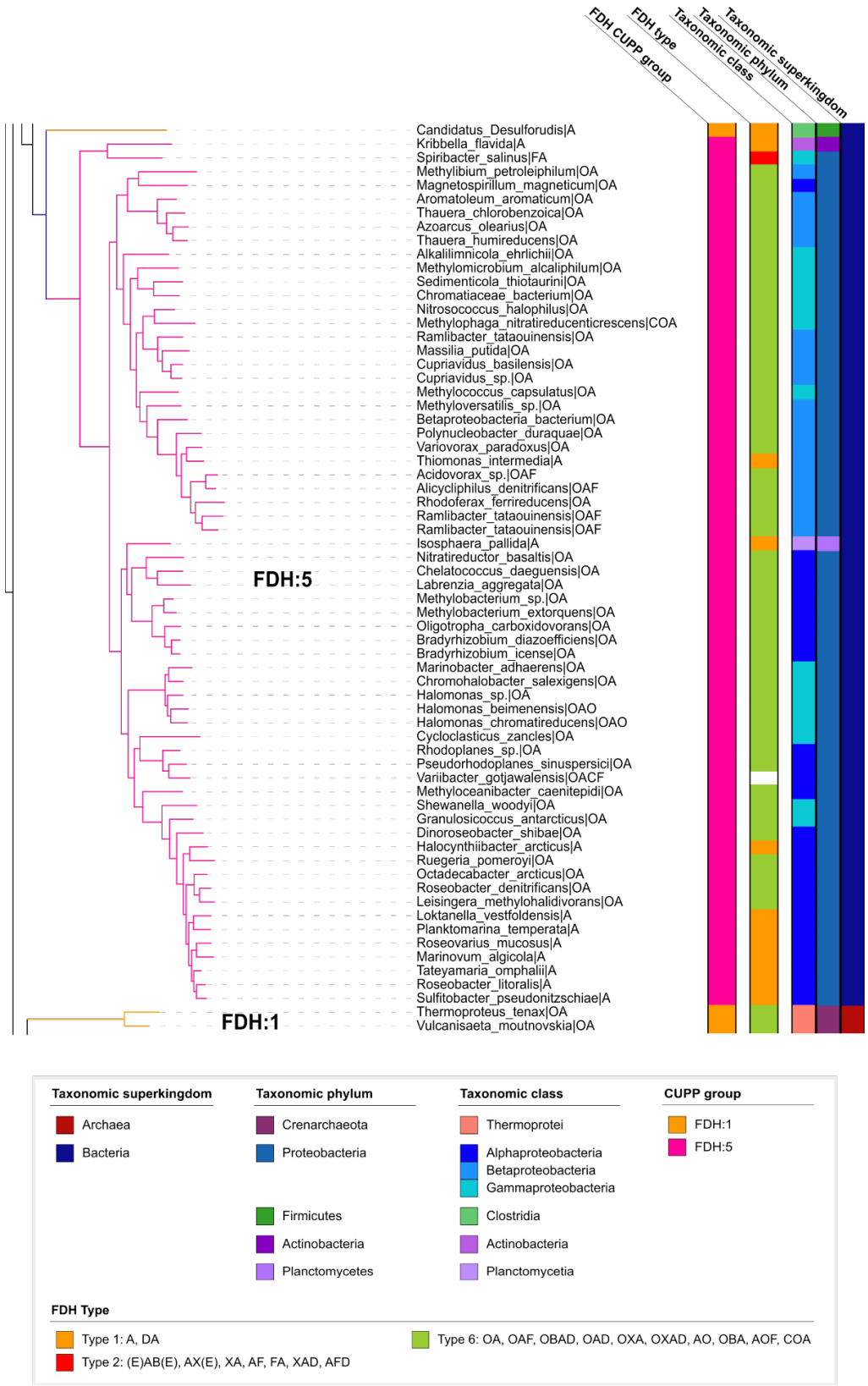

Figure 6: Subsection of Figure 4. Each branch tip represents a single FDH. Each sequence is annotated with origin organism and FDH type based on gene segment organization. Gene segment organization is defined as the genetic makeup of the surrounding genes of a given FDH alpha subunit sequence. Here, 'A': alpha (α) subunit, 'B': beta (β) subunit, 'C': gamma (γ) subunit, 'D': accessory sulfurtranferase fdhD, 'E': accessory protein fdhE, 'S': delta subunit, 'X': unspecified formate dehydrogenase subunit, 'O': NADH-quinone oxidoreductase related subunit, 'F': 4Fe-4S containing protein, and 'P': cytochrome formate dehydrogenase subunit.

In summary, while the starting data set for this classification analysis may be somewhat biased, it also contains data from a reasonable distribution of organisms and known traits. In other words, although it has room for further improvements, the dendrogram is a reasonable representation of the diversity within metal-dependent FDHs. This knowledge combined with the observation that coherent and distinct clades are able to be annotated with single FDH types corroborates the validity of the proposed classification scheme.

Regarding taxonomy, the cataloged FDHs have a prokaryotic background with emphasis on bacteria. This is useful in relation to recombinant production. Although fungal expression systems are able to secrete their protein product, prokaryotic systems have a high turnaround and well-developed synthetic biological toolbox. For a broader discussion on FDH taxonomy please refer to Appendix J.

Metabolically speaking, FDHs of organisms such as acetogens that are known to reduce CO_2 as their main function in the organism, would be interesting for CCU application (Müller, 2019; Schuchmann and Müller, 2014). However, it was not possible to identify an FDH derived from an acetogenic bacteria which had been shown to be oxygen tolerant, or even have a reasonable chance of being oxygen tolerant. For a description on FDH roles in metabolism please refer to Appendix J.

2.3. Kinetics

2.3.1. Generalized reaction mechanism

The reaction mechanism of metal-independent FDHs is fairly simple. Essentially, the active site catalyzes the reaction by forcing the NAD^+ (or $NADP^+$) and formate or NADH (or NADPH) and CO_2 into close proximity. This allows for a hydride transfer (Castillo et al., 2008).

In contrast to reaction mechanism for metal-independent FDHs, the reaction mechanism for a metal-dependent FDH is more complex. Essentially, the metal-dependent FDHs are divided into 3 separate functions.

1. The main active site facilitates reduction of CO_2 or oxidation of formate via a redox active Mo/W-bisPGD co-factor that is coordinated with a Cys or a SeCys (Maia et al., 2015).
2. The electron transport to the active site. A chain of FeS clusters can transport the electron through the enzyme to the heavy metal in the active site (Jormakka et al., 2002).
3. The electrons generated/consumed in the main active site is delivered to/received from a separate source. If not receiving electron from a high reduction potential molecule, then likely from another protein or even directly from an electrode (Figure 7)(Amao, 2018).

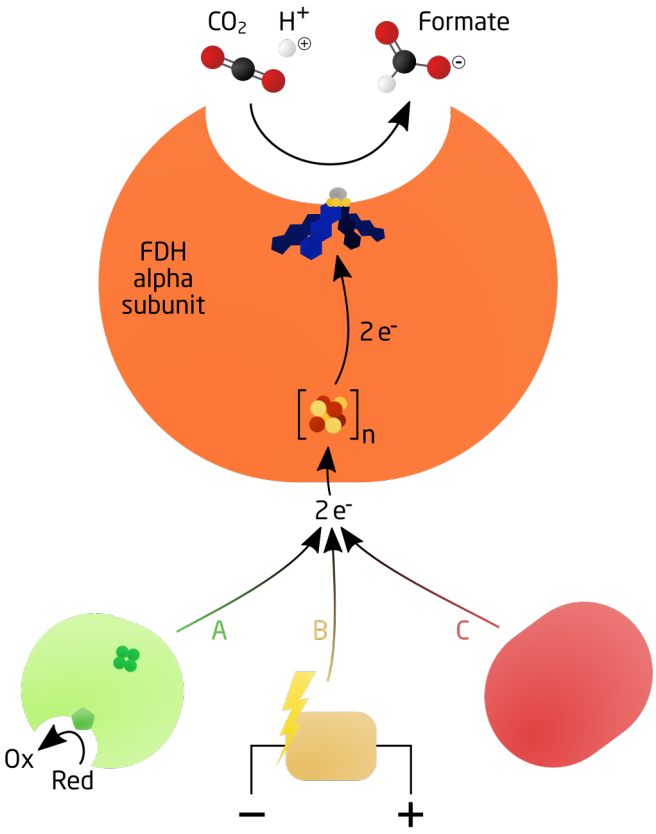

Figure 7: The alpha subunits of the metal-dependent FDH are designed to interact with different electron carriers. (A) A separate protein, often in complex with the alpha subunit, facilitates a redox reaction that provides or absorbs an electron. (B) Electrodes perform as electron carriers. (C) FDH alpha subunits may interact with proteins transporting electrons as part of a larger system (e.g. cytochromes). Independent of the electron carrier, electrons are transported via one or more [Fe-S] clusters to/from the molybdenum containing co-factor of the main active site. Here, CO_2 is reduced or formate is oxidized.

As a note, for some FDH variants, incomplete enzymes without the main active site are able to have diaphorase activity (Hartmann and Leimkühler, 2013).

The ability to deliver/receive electrons from a variety of electron carriers is one of the key premises for the diversity observed for FDHs in general.

2.3.2. Electron donors

Chemical electron donors

Chemical electron donors are soluble redox active molecules with an inherent redox potential as described above. Natural electron donors of interest include NADH, NADPH, and H_2. However, synthetic electron donors are also relevant. Predominantly viologens such as methyl viologen (MV^+).

For the application of chemical electron donors, considerations of concentration are important. In essence, an enzyme-catalyzed reaction is still just a chemical reaction that goes towards equilibrium. As such, a surplus of electron donor is often necessary to force the reaction towards the reduced product.

However, other considerations are also in play for the electron donor selection. For application, the electron donor represents a cost. This is why several studies have employed use of regenerating the electron donor through coupling to another reaction or electrochemically (Marpani et al., 2017; Singh et al., 2018).

Metal-independent FDHs only function with NADH or in rare cases with NADPH as electron donors (Alpdağtaş et al., 2018). This is suspected to be due to the close proximity mechanism (Castillo et al., 2008). NADH and NADPH are differentiated only by an additional phosphate group for NADPH (Figure 8). Due to the close relationship between the two molecules, there are examples of engineered metal-independent FDH that used to accept only NADH but now also work with NADPH (Tishkov and Popov, 2006).

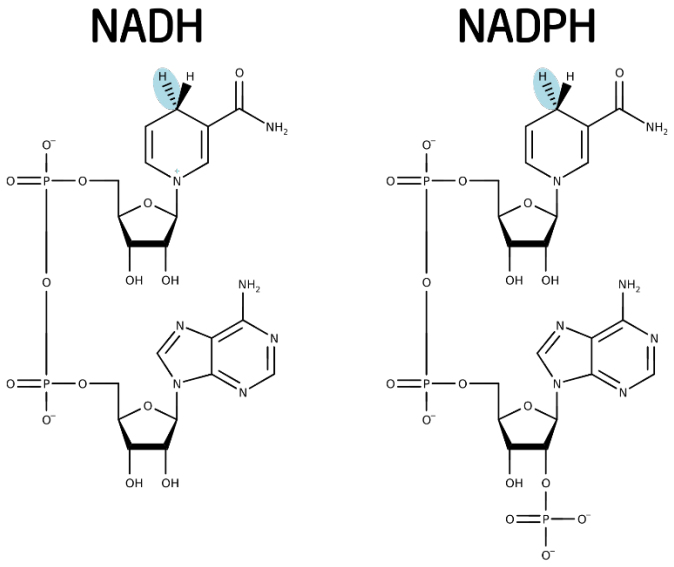

Figure 8: Chemical structures of NADH and NADPH. Hydrogen atoms highlighted in blue represent the proton that either molecule donates when acting as an electron donor.

In contrast to the metal-independent FDHs, metal-dependent FDHs are able to use NADH and NADPH *and* other electron donors as well.

Protein electron donors

Protein electron donors simply entail proteins that are able to provide electrons. This is done in one of two ways: Either, the protein is redox active. Strong examples include cytochromes and ferredoxin (Figure 7C). Or, the protein is able to generate electrons, often via facilitating a redox reaction on its own, and then transport them other proteins (Figure 7A).

For this study, it was observed that FDHs classified as metal-dependent FDH type 4 are seen to interact with cytochromes as their redox partner.

Proteins that are able to generate electrons and transport them to a metal-dependent FDH is a broad topic that extends beyond the scope of this thesis. However, two good examples include the previously mentioned HDCR and the Hdr-SC.

HDCR is essentially an FDH combined with a hydrogenase in one highly efficient complex. Here, a thermostable variant derived from *Thermoanaerobacter kuvui* (TkHDCR) was recently described. TkHDCR has an incredible high turnover frequency of nearly 160,000 min^{-1}. Instead of NADH or an electrode, the electron donor is molecular hydrogen (Schwarz et al., 2018). Applying HDCR for CO_2 reduction would involve electrolysis, a process that it still energetically expensive.

Electrodes as electron donor

Conversely to chemical and protein electron donors, electrodes have the unique advantage of not being limited to a single redox potential. It is possible to, quite literally, set the exact potential desired. One can also accurately monitor and control the reaction by measuring the current, which directly corresponds to the reaction rate. Importantly, electricity directly from an electrode is the cheapest possible electron source available. In other words, electrodes are the ultimate electron donor when it comes to *providing* the electrons.

However, getting the electrons from electrode to active site of the redox protein is not trivial (Sakai et al., 2017). Again, it goes beyond the scope of this thesis to discuss protein-electrode interactions in detail. Briefly, it can be mentioned that electrode shape/texture, electrode material, and method for immobilization influence the reaction rate of the immobilized enzyme drastically (Bernal et al., 2018a; Mateo et al., 2007).

Interestingly, electrochemical characterization of metal-dependent FDHs has recently seen an increased interest. FDH of *Desulfovibrio desulficans* (DdFDH) was recently studied as immobilized on pyrolytic graphite (Cordas et al., 2019), FDH from *Clostridium ljungdahlii* (ClFDH) has been studied on a hydrogel (Kuk et al., 2019), and finally FDH from *Desulfovibrio vulgaris* Hildenborough (DvFDH) on metal-oxides (Miller et al., 2019). In parallel, FDH from *Rhodobacter capsulatus* (RcFDH), CbFDH, along with DvFDH have been studied separately in indirect electrochemical setups (Chen et al., 2019; Choi et al., 2018; Szczesny et al., 2020). All of these sixstudies are from within the last two years, indicating a strong interest in FDH as catalysts in an electrochemical CCU context.

The prospects of applying FDH electrochemically will be further discussed in Section 5.1.

2.3.3. Kinetic comparison

Through a manually curated literature search, all reaction rates characterized for FDH reducing CO_2 were logged. Enzymes having been characterized with both a reaction rate and CO_2 affinity could then be plotted as seen in Figure 9.

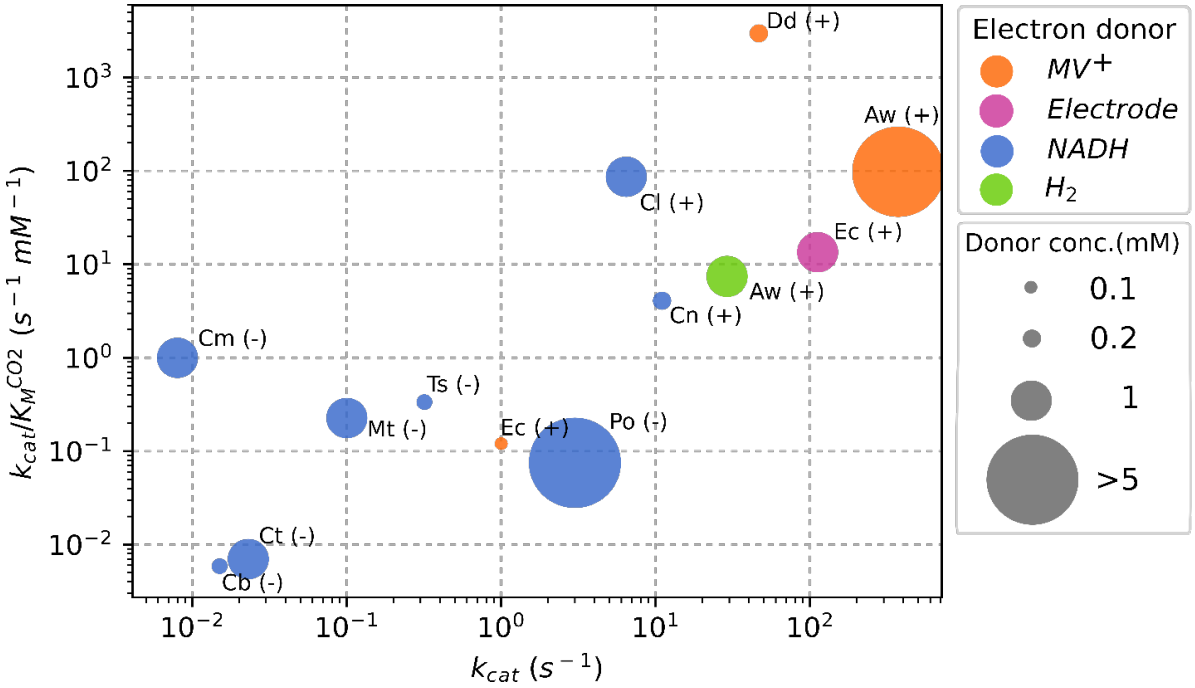

Figure 9: The properties of kinetically characterized FDHs identified from exceptionally thorough manual literature search. These 11 FDH are the only ones to be described both in terms of specificity constant and CO_2 affinity of all known and described FDHs. The properties are visualized as a function of k_{cat} and k_{cat}/K_M with the type and concentration of electron donor visualized by color and size of markers. (-): metal-independent FDH, (+): metal-dependent FDH. Cm: Candida methylica*, Cb:* Candida boidinii*, Ct:* Chaetomium thermophilum*, Mt:* Myceliophthora thermophile*, Ts:* Thiobacillus sp. *KNK65MA, Ec:* Escherichia coli *(Electrode at 150 mV overpotential), Po:* Pseudomonas oxilatus *(100 mM NADH), Cn:* Cupriavidus necator*, Dd:* Desulfovibrio desulfuricans*, Cl:* Clostridium ljungdahlii*, Aw:* Acetobacterium woodii *(5 mM MV^+ and H_2 in head space of reaction bottle). (Figure derived from* (Nielsen et al., 2019)*, see Appendix M).*

Several considerations need to be kept in mind when studying this figure. First of all, although the concentration of electron donor is critical for the rate of the reaction, it is of course, the substrate concentration *relative* to enzyme concentration that matters. However, enzyme concentration is often not listed in the available literature. As such, the only option left is to include the absolute concentration of electron donor, unrelated to enzyme concentration, as an indication of the amount of electron donor.

Additionally, and rather obviously, not only the concentration but also the reduction potential of the electron donor is critical. Formic acid on its own is a relatively strong electron donor (Table 2). In fact, if mixing 1 M CO_2 and with 1 M NADH at pH 7, 25 °C and 1 atm (what is referred to as 'standard conditions') the free energy change of the reaction ($\Delta G°'$) can be calculated to 19.3 kJ mol^{-1} (Berg et al., 2012). In other words, CO_2 reduction at standard conditions with NADH as electron donor is not a favorable reaction.

To complicate matters, as is natural for any reaction involving a free proton, the reduction potential of CO_2 is also pH-dependent (Reda et al., 2008). This creates some confusion since the reduction potential is often reported as the chemical standard of -0.61 V vs. SHE at pH 0. This pH is impractical for most biological systems and the value of -0.61 V is misleading.

Table 2: Standard reduction potential (E'_0) at pH 7, 25 °C, and 1 atm, of relevant electron donors and the main CO_2/formate redox reaction. 'MV': Methyl viologen. 'SHE': Standard hydrogen electrode.

Electron acceptor		*Electron donor*	E'_0 (V) vs SHE	Reference
$MV^{2+} + e^-$	⇌	MV^+	-0.44	(Li et al., 2020)
$2\ H^+ + 2\ e^-$	⇌	H_2	-0.42	(Li et al., 2020)
$CO_2 + 2\ H^+ + 2\ e^-$	⇌	HCOOH	-0.42	(Parkinson and Weaver, 1984)
$NAD^+ + H^+ + 2\ e^-$	⇌	NADH	-0.32	(Li et al., 2020)
$NADP^+ + H^+ + 2\ e^-$	⇌	NADPH	-0.32	(Berg et al., 2012)

Secondly, beyond concentration and reduction potential, other experimental conditions also vary. Again, this creates further bias in Figure 9. However, granted relatively standard methods for quantifying activity, the differences in pH, temperature, and buffer composition can be argued to be small enough to allow indicative comparison.

Thirdly, as an extension of the second point. Substrate concentration is dependent on conditions. FDHs are likely reacting with CO_2 as aqueous CO_2 (Yu et al., 2017), rather than CO_2 as bicarbonate or carbonic acid. As such, Henry's law on gas solubility becomes important for substrate concentration, and as an extension also reaction rate. As will be discussed further in Chapter 3: Temperature, pressure, and pH are in this case influential for both substrate concentration as well as of course enzyme stability and performance.

The above discussed conditional effects are important to keep in mind. Nonetheless, given the magnitude in difference between the best and worst performing enzyme/ED combination, some interesting observations can be made.

Based on Figure 9, it is clear that NADH is poor electron donor. For both metal-dependent and metal-independent FDH, reactions driven by NADH display the lowest catalytic rate for CO_2 reduction. As an indirect consequence, given that metal-independent FDH cannot utilize the electron donors with higher reduction potential, they also generally display by far the lowest catalytic rate.

Unsurprisingly, reactions driven with the strong reduction potential of MV^+ show the highest catalytic rate and catalytic efficiency, with hydrogen as a donor also displaying promising catalytic rate and efficiency. If the hydrogen-driven TkHDCR described in the previous section, with its sensationally higher turnover number of 2650 s^{-1} (Schwarz et al., 2018), had been characterized with a K_M it would have been the enzyme with the highest turnover number in Figure 9.

Finally, use of an electrode proves difficult to compare with chemical electron donors. As discussed above in Section 2.3.2, use of electrodes involves a complex interaction with between protein and electrode. However, if successfully implemented, electrodes are the ultimate electron donors, and in the context of this thesis, the ideal solution.

In conclusion, although the above figure cannot be considered indisputable, it can be considered indicative. In this manner it is possible to conclude that NADH is generally a poor electron donor and in extension that metal-independent FDHs are prohibitively slow and thus irrelevant for application in a CCU context. If using a chemical electron donor, hydrogen or MV^+ is preferred. However, the ideal electron donor is an electrode despite the challenges involved.

2.4. Selection of FDH candidates

Metal-dependent FDHs provided with a sustainable and cheap electron source have great potential to become interesting catalysts for CCU. As presented in this study, metal-dependent FDHs are highly diverse, with abundant room for discovery and learning. Of particular interest is the ability to obtain electron directly from an electrode. In this way, the advantages presented and discussed in Chapter 1 on electrochemical approaches become relevant.

Dauntingly, the inherent oxygen sensitivity of most FDHs and other similar proteins (De Bok et al., 2003; Hille et al., 2014; Schuchmann and Müller, 2014), may infer limits to the applicability. It is very likely that any CO_2 point source will contain O_2 as well. As such, it becomes important to identify candidates that have potential for CO_2 reduction in the presence of oxygen.

Additionally, this thesis focused only on soluble FDH variants, as membrane bound enzymes are often more difficult to handle.

Generally, FDHs from organisms who are known facultative aerobes were considered. Of the metal-dependent FDHs characterized in literature, two variants readily spring to mind. The FDH of *Rhodobacter capsulatus* and FDH of *Cupriavidus necator* (CnFDH) have both been shown to reduce CO_2 in the presence of oxygen (Hartmann and Leimkühler, 2013; Yu et al., 2017).

Rhodobacter spp. are phototrophic purple non-sulfur alpha-proteobacteria, known to be isolated from wet microaerophilic environments (Girija et al., 2010; Ramana et al., 2009). *Rhodobacter sphaeroides* is able to tolerate high oxygen stress, but performs best in microaerophilic environments (Mackenzie et al., 2007) and it is likely a trend for the genus as a whole.

Cupriavidus spp. have a taxonomically turbulent history, only in recently (taxonomically speaking) settled into the current nomenclature (Vandamme and Coenye, 2004). The genus is known to include incredibly versatile beta-proteobacteria able to degrade xenobiotics and toxins (Cserháti et al., 2012; Lal et al., 2013; Sun et al., 2016). Among them *Cupriavidus necator*, previously known as *Ralstonia eutropha*, is an H_2-oxidizing lithoautotrophic 'knallgas' bacterium that is commonly found in periodically anoxic soil and freshwater biotopes (Pohlmann et al., 2006).

The facultative aerobic nature of *R. capsulatus* and *C. necator*, corroborates the oxygen tolerance observed for RcFDH and CnFDH, making them interesting candidates for further study. Additionally, they are known to be soluble, allowing relative ease of expression (Hartmann and Leimkühler, 2013; Yu et al., 2017).

RcFDH and CnFDH were selected as candidates. Additionally, the FDH of *Rhodobacter sphaeroides* (RsFDH) was included due to *R. sphaeroides*' ability to tolerate high levels of oxygen stress.

Additionally, although NADH is poor electron donor, it was decided to apply it as electron donor for this study to be able to compare with previous studies on RcFDH and CnFDH.

Chapter 3. Enzyme production

Please note

This chapter is based on work in preparation for submission in Paper II: Enzyme reaction kinetics and O_2 tolerance of bacterial formate dehydrogenases for CO_2 utilization. See Appendix N for manuscript.

Expression and purification of the candidate FDHs is a necessary step for characterization. The work of this thesis provides valuable insights that can guide future work with metal-dependent FDHs. Throughout this work, FDHs were expressed recombinantly in *E. coli.* This has two major advantages:

1. **Fast turnaround and smaller scale**. As a direct example, CnFDH has been expressed both natively and recombinantly. Native expression required 7 days of culture growth while recombinant expression could be performed in only 2 days. Additionally, biomass yield was significantly higher per liter of culture for recombinant expression, allowing use of smaller scale for a similar yield (Yu et al., 2019). This difference is largely due to fast growth of the heterologous expression strain, combined with the option for overexpression of the FDH genes: Via strong promoters, combined with optimized RNA polymerases and fast translation, much higher expression levels than for any natural FDH promoter is possible (Studier, 2005).
2. **Easy modifications of genes**. Often, native strains lack effective tools for cloning or gene editing. As a result, it is much more troublesome to introduce the desired changes directly in the native genes on the genome. For recombinant expression, the genes are located on an expression plasmid allowing easy transformation and modification.

Although recombinant expression has significant advantages in general, recombinant heterologous expression of FDHs is a surprisingly daunting task (Hartmann et al., 2015; Ihara et al., 2015). As a result, most studies on metal-dependent FDHs are based on enzymes purified from a native culture.

Two of the most successful cases of recombinant FDH expression, are the studies with RcFDH and CnFDH (as discussed in Section 2.4). In 2013, RcFDH was recombinantly expressed in *E. coli* (Hartmann and Leimkühler, 2013) and in 2019, CnFDH was recombinantly expressed in *E. coli* (Yu et al., 2019). For both cases, it was not possible to achieve more than 50% active protein out of the total purified FDH population. In the present study, these yield percentages were deemed too low, and in need of improvement. Several points of interest were identified for this purpose:

- For both studies, the native version of the FDH-encoding operon was used instead of a codon-optimized version for *E. coli.* Additionally, a medium strength pTrc promoter was used.
- In the previous studies, the His-tag used for purification was placed on the smallest subunit, the gamma subunit, instead of the larger alpha subunit.
- Sufficiently slow growth rate has been argued to be important for obtaining a large fraction of active protein, by allowing the expression strain time to fully synthesize the Mo-bis-MGD and [Fe-S] co-factors (Niks and Hille, 2018; Tsai and Tainer, 2018).

- TB medium has been shown to be superior to LB medium for expression of [Fe-S] containing proteins in *E. coli* (Jaganaman et al., 2007).
- The previous studies used either *E. coli* MC1061 or *E. coli* DH5α for expression of RcFDH or CnFDH respectively. Neither of these two *E. coli* strains were originally designed for protein expression (EcoliWiki, 2012; EcoliWiki, 2020).

These observations led to formulation of the following hypotheses and objectives:

Hypotheses:

1. Placement of the His-tag on the alpha subunit, relative to placement on the gamma subunit, will minimize loss of FDH during purification and retain specific activity.
2. The combination of slow growth rates, TB medium, and *E. coli* strains designed for protein expression will result in type 5 FDHs with higher specific activity compared to type 5 FDHs expressed according to methods described in previous work by Hartmann and Leimkühler, 2013 and Yu et al., 2019.

Objectives:

- Design and compare constructs of RcFDH with His-tag placed on the N-terminal of the alpha subunit rather than the N-terminal of the gamma subunit.
- Assess effect of slow growth rates, TB media, and use of *E. coli* protein expression strains on heterologous expression.

Additional objective:

- Demonstrate that the type 5 FDHs derived from purple non-sulfur bacteria *Rhodobacter sphaeroides* (RsFDH) can be heterologously expressed in *E. coli* and purified with comparable activity to RcFDH and CnFDH expressed in a similar manner. Evaluate expression of RsFDH relative to RcFDH and CnFDH.

3.1. Construct design

RcFDH, CnFDH, and RsFDH are all encoded with identical operon gene organization in their native genomes (Figure 10). Based on this assessment, RsFDH can confidently be classified as a type 5 FDH. Each operon contains the genes *fdsG, fdsB,* and *fdsA* encoding the gamma, beta, and alpha subunit respectively. Additionally, the two chaperone genes, *fdsC* and *fdsD*, are also found in the operon. These encode FdsC and FdsD with the latter also known as the delta subunit (Hartmann et al., 2015). The operons were extracted from genome sequences available in the NCBI RefSeq database (O'Leary et al., 2016).

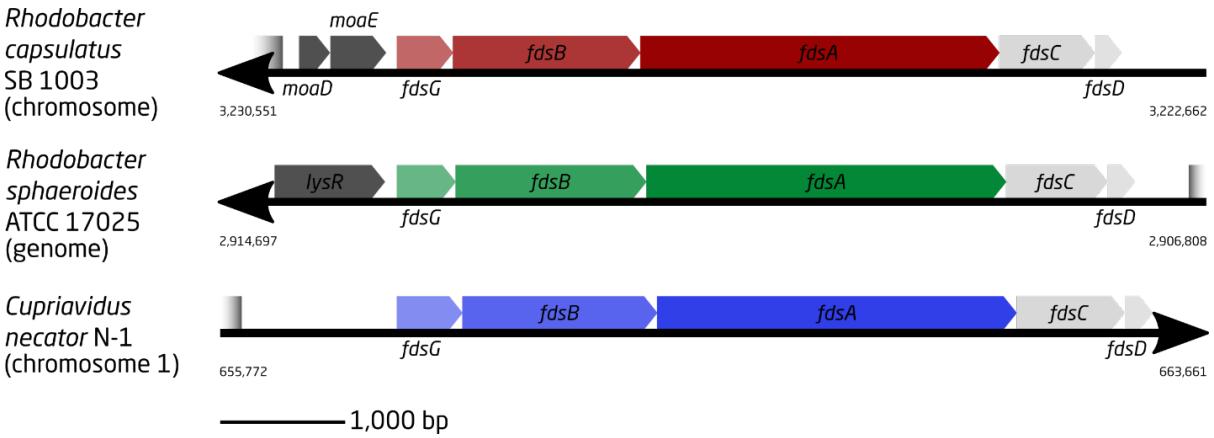

Figure 10: From top to bottom, operons corresponding to RcFDH, RsFDH, and CnFDH respectively. Operon position in genome/chromosome is indicated by values at either end of arrow. The directions of the black arrows indicate if genes are encoded on the complementary strand or not: RcFDH and RsFDH are both encoded on the complementary strand. Please note that fdsC is a homolog to fdhD, and fdsD is unrelated to fdhD or fdhE, as presented in Section 2.1.2.

Based on the observation that native operons had been used for expression without optimization in previous studies with RcFDH and CnFDH, completely synthetic constructs were designed and ordered for this study. The genes were codon-optimized for *E. coli*, a strong T7 promoter was used (compatible with a DE3 system), and artificial RBS sites were introduced. Unfortunately, expression and characterization of protein, produced using these constructs, lead to a series of inconclusive results (data not shown). Although activity was observed, it was much too low, and worryingly difficult to reproduce. Eventually, it was realized that competing false RBS sites likely caused expression of truncated protein.

It is very likely that a synthetic construct in fact could become optimal. In this particular case, it was argued that the risk of introducing another error source was too high relative to time constraints. It was decided to instead use the native operon without any modification beyond an addition of a His-tag as had been demonstrated previously in literature. See illustration of expression construct below (Figure 11).

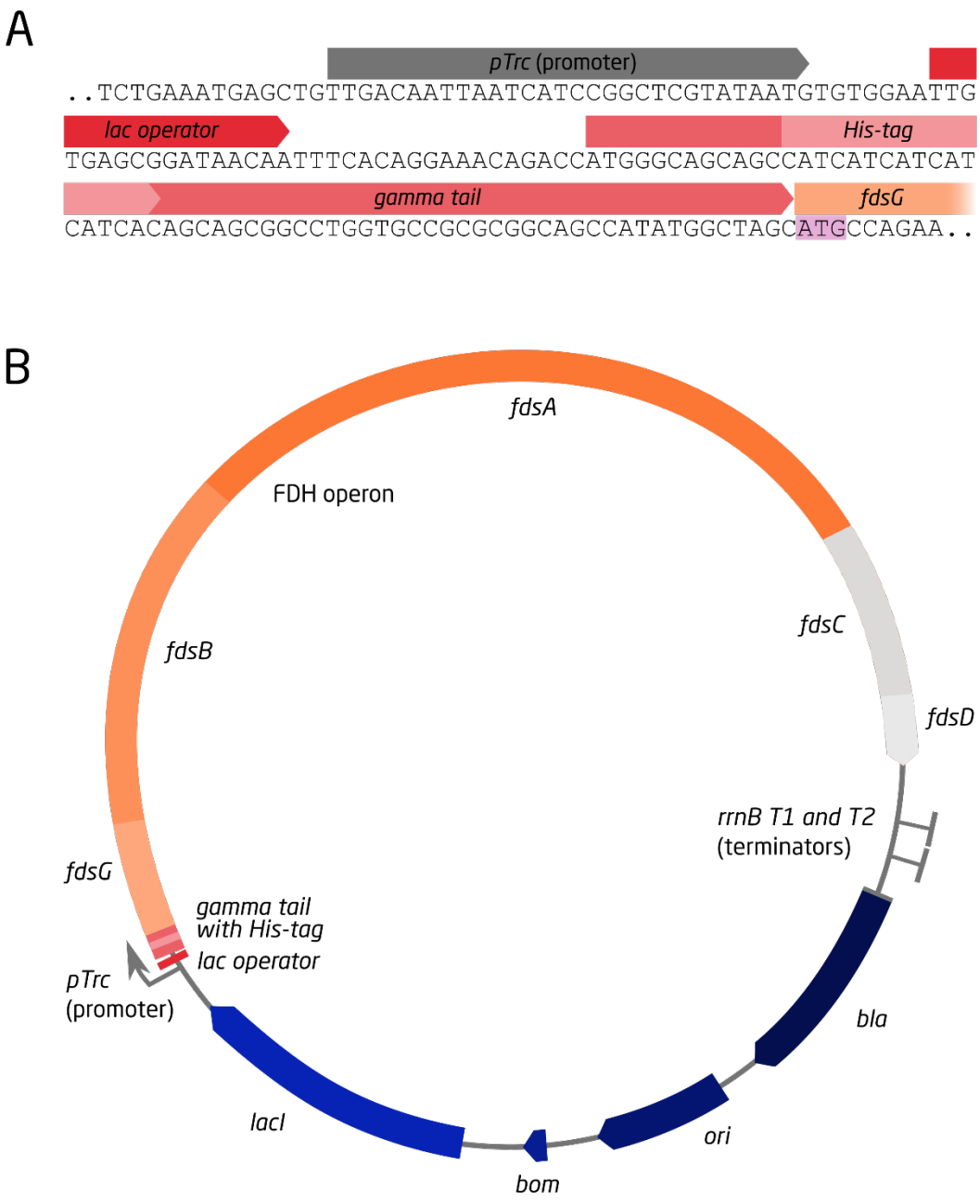

Figure 11: (A) Region immediately upstream of start codon of operon. Region marked as 'gamma tail' encodes 23 amino acid-tail, including a 6-mer His-tag, attached to the N-terminal of the gamma subunit. The region of the gamma-tail between His-tag and fdsG start codon is known to be a flexible linker region. (B) Generalized full expression construct. 'bla' encodes β-lactamase ampicillin resistance. 'ori' encodes a pBR322 low plasmid copy origin of replication. 'bom' encodes the origin of transfer. 'lacI' encodes a strongly expressed Lac repressor protein (Invitrogen, 2008).

This design is identical to the construct employed in the study by Hartmann and Leimkühler on RcFDH. Here, it was reported that a pTrcHis backbone was used for the expression vector (Hartmann and Leimkühler, 2013). The precise sequence for the pTrcHis promoter region was obtained after correspondence with Silke Leimkühler. For a detailed description of materials and methods for cloning, please refer to Appendix G.

3.1.1. Placement of His-tag

For this chapter, the first hypothesis was that placing the His-tag on the alpha subunit, rather than the gamma subunit, would allow for better purification since the alpha subunit is much heavier and thus allow stronger binding to the nickel column. In this way, it was expected to reduce loss of protein during purification.

Expression in different strains of *E. coli* was carried out to qualitatively assess expression levels (Figure 12). The four strains used here were: *E. coli* BL21, *E. coli* BL21 pLysS, *E. coli* C43 and *E. coli* Rossetta2. An SDS-PAGE gel was run on boiled culture samples, followed by a western blot against His-tag.

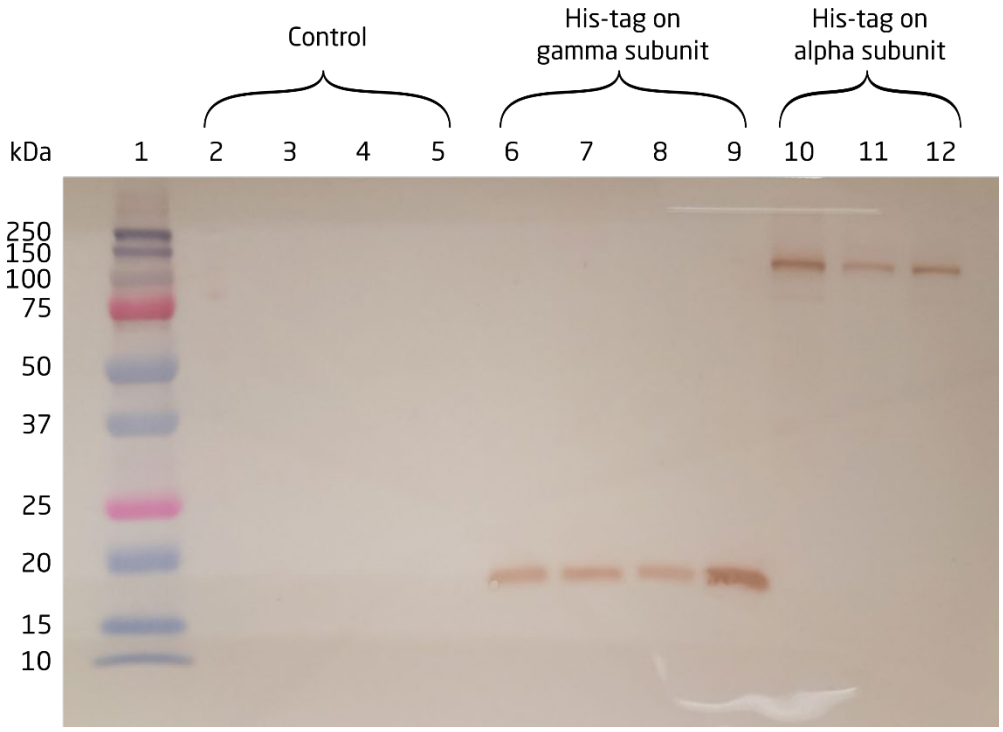

Figure 12: Western blot on His-tag for different cultures of E. coli with or without expression vector. Well 1 contains a size ladder. Well 2-5 contain a negative control without expression vector. Well 6-9 contain cultures expressing gamma-tagged RcFDH. Well 10-12 contain cultures expressing alpha-tagged RcFDH (Only three bands since expression in E. coli BL21 pLysS was omitted due to limited number of wells on gel). The 4 lower bands (~17 kDa) correspond to the gamma subunit. The 3 higher bands (~105 kDa) correspond to the alpha subunit.

This experiment confirmed that it is possible to express a variant of RcFDH with a His-tag on the alpha subunit. A solubility assay was performed that confirmed the solubility of the alpha-tagged FDH (See Appendix E for details).

However, when assayed for formate oxidation activity, a much too low specific activity was observed (Figure 41 in Appendix L). Consequently, hypothesis 1 proposing superiority of His-tag placement on the alpha subunit relative to placement on the gamma subunit became irrelevant. It is possible that placement of His-tag on the alpha subunit could be beneficial, but due to the lost activity the construct became irrelevant in regard to this thesis.

A subsequent similar test of activity of RcFDH with His-tag placed on the gamma-subunit showed increased specific activity. In conclusion, the His-tag should be placed on the N-terminal of the gamma subunit and not on the alpha subunit.

The final constructs were named: pTrc_RcFDH_gamma, pTrc_RsFDH_gamma, and pTrc_CnFDH_gamma, each expressing one of the three candidate type 5 FDHs with a 6-mer His-tag placed on N-terminal of the gamma subunit.

3.2. Expression

3.2.1. Methods and materials for expression

Three different expression protocols were applied and compared. For ease of understanding, a general description of the expression protocol (Figure 13) combined with a table highlighting the differences (Table 3) are presented below. Please refer to Appendix I for presentation and discussion on development of the 'Nielsen protocol' developed for this study.

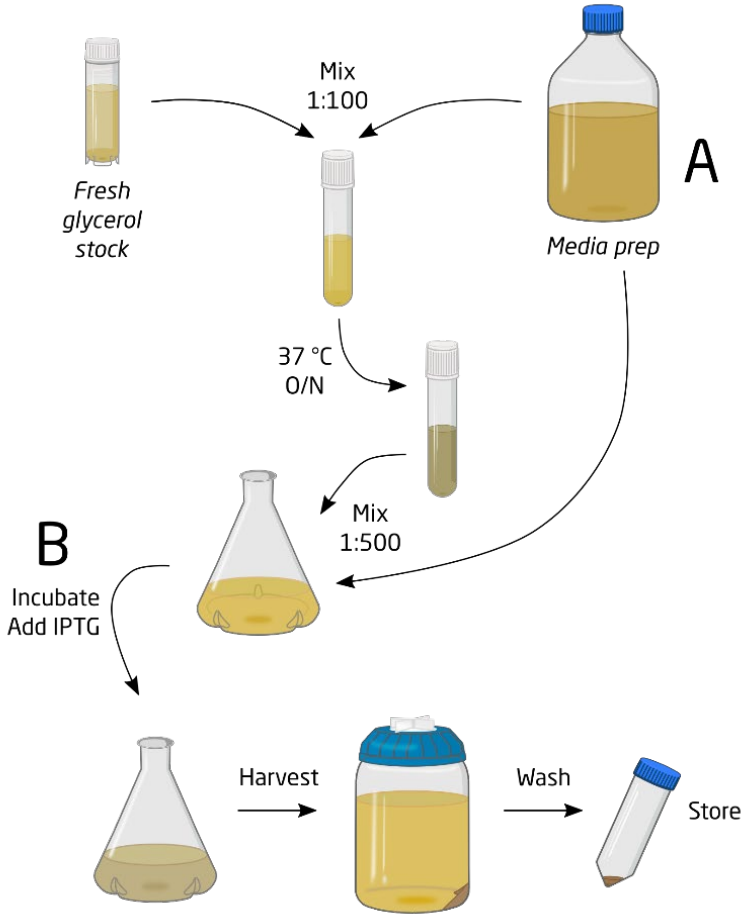

Figure 13: Flow sheet describing generalized expression protocol. For each expression fresh glycerol stock stored at -80 °C was thawed on ice before transferred to pre-culture. The pre-culture was incubated overnight. (A) Either LB or TB medium was used for both pre-culture and expression media. (B) Incubation was started by addition of out-grown pre-culture to 500 ml medium in baffled shake flasks. Depending on method, culture was then either grown for 24 hours with IPTG or grown until OD600 = 0.4-0.8 before addition of IPTG. Shaking speed and culture temperature varied depending on method (Table 3). For all methods, cells were harvested at 5,300 g and washed in buffer with protease inhibitor before being stored at -20 °C.

For all three expression protocols, the same medium was used for both pre-culture and actual expression: Either LB or TB medium with 150 µg/ml ampicillin, 1 mM sodium molybdate, and *with or without* 20 µM isopropyl β-D-1-thiogalactopyranoside (IPTG) (Table 3). For pre-culture 5 ml medium was inoculated with 50 µl of the desired single-use glycerol stock, and then incubated at 37 °C and 130 rpm overnight.

For expression, 2 l baffled Erlenmeyer shake flasks, each containing 500 ml expression medium, were inoculated with 1 ml pre-culture each. For the protocol developed for this study, cultures were grown to OD600 = 0.4-0.8 and then cooled on ice for 10 minutes before induction with 50 µM IPTG. For protocols inspired by literature, cultures were induced with 50 µM IPTG immediately.

Cultures were then incubated for 24 hours at either 18 °C and 30 rpm (Nielsen protocol), 30 °C and 130 rpm (Hartmann protocol), or 28 °C and 160 rpm (Yu protocol). Cells were harvested by centrifuging at 5,300 g for 15 minutes in a precooled (4 °C) centrifuge. From this point onwards, samples were kept at maximum 4 °C or colder. Additionally, procedures were completed as quickly and efficiently as possible. For each gram of cell pellet, 10 ml of 40 mM potassium phosphate buffer, pH 7.5, with 10 mM KNO_3 and EDTA free protease inhibitor (cOmpleteTM Mini from Roche), was used to suspend the pellet. The suspended pellet was centrifuged at 8,000 g for 5 minutes. Discarding the supernatant, the pellet was stored at -20 °C.

Table 3: Differences in expression protocol between (1) method developed for this study, (2) method inspired by Hartmann and Leimkühler, 2013, and (3) method inspired by Yu et al., 2019. 'LB': Lysogeny Broth. 'TB': Terrific Broth. 'Induction at OD600 = 0.4-0.8' entails growing culture at 37 °C and 130 rpm until reaching OD600 = 0.4-0.8 before cooling on ice for 10 minutes and then inducing with IPTG.

Method	**Nielsen protocol**	**Hartmann protocol**	**Yu protocol**
Expression strain	*E. coli* DH5α	*E. coli* DH5α	*E. coli* DH5α
Media	TB	LB	TB
Addition of IPTG to pre-culture	No	Yes	No
Induction at OD600 = 0.4-0.8	Yes	No	No
Temperature	18 °C	30 °C	28 °C
Shaking speed	30 rpm	130 rpm	160 rpm
Literature reference	This study (See Appendix I for development of protocol)	(Hartmann and Leimkühler, 2013)	(Yu et al., 2019)

3.3. Purification

3.3.1. Materials and methods for purification

A flow sheet depicting the individual steps is shown in Figure 14. Frozen cell pellet was thawed on ice in 40 mM potassium phosphate, 10 mM potassium nitrate buffer, pH 8. DNAse and protease inhibitor was added to the suspension. A ratio of 10 ml buffer per 1 g of cell pellet was used to ensure low viscosity and minimum effect of cell lysing on pH.

The cell suspension was lysed at 1.35 bar in a pressure cell homogenizer system (STANSTED SPCH-10), and immediately cooled on ice via a metal spiral submerged in ice-water. The lysed cell solution was centrifuged at 21,000 g in a cooled centrifuge for 60 minutes. The supernatant was kept as the 'soluble fraction' containing the desired soluble FDHs. This solution was kept on ice and transferred to a cold-room (7 °C) for purification.

Immobilized metal affinity chromatography

Two different approaches were used: Gravity flow (Figure 14A) or pre-packed column mounted on ÄKTA pump system (Figure 14B).

For immobilized metal affinity chromatography (IMAC) purification via gravity flow, the supernatant was mixed with 0.2 ml Ni Sepharose™ HP resin per 1 g of lysed cell pellet and allowed to gently mix for 45 minutes. The resin/lysate mixture was then added to an empty gravity 25 ml flow column from BIO-RAD and allowed to settle. The formed nickel resin column should appear dark grey/brown due to high saturation of the [Fe_4-S_4] containing protein. Typically, per 5 g of lysed cell, a 1 ml column volume (CV) was used. The column was washed with 25 CV of first 75 mM potassium phosphate buffer, pH 7.5, with 10 mM KNO_3 and 10 mM imidazole followed by 25 CV 75 mM potassium phosphate buffer, pH 7.5, with 10 mM KNO_3 and 20 mM imidazole. The enzymes were then eluted with 5 CV 75 mM potassium phosphate buffer, pH 7.5, with 10 mM KNO_3 and 250 mM imidazole.

The protein exhibits a dark brown color when [Fe-S] are linked correctly to cysteine. A lighter color is a warning sign of [Fe-S] oxidation or loss (Tsai and Tainer, 2018). As can be seen in the pictures in Appendix K, this is useful visual aid during purification.

For IMAC purification via pre-packed column, the supernatant was loaded onto a 5 ml prepacked HisTrap™ FF column via an ÄKTA prime pump system. The column was washed with minimum 5 CV 75 mM potassium phosphate buffer, pH 7.5, with 10 mM KNO_3 and 10 mM imidazole followed by 5 CV 75 mM potassium phosphate buffer, pH 7.5, with 10 mM KNO_3 and 20 mM imidazole. The enzymes were then eluted with 2 CV 75 mM potassium phosphate buffer, pH 7.5, with 10 mM KNO_3, and 250 mM imidazole in 1 ml fractions. Absorbance of eluate was measured continuously to gauge size and purity.

Immediately following elution, the protein solution was buffer exchanged to 75 mM potassium phosphate buffer, pH 7.5, with 10 mM KNO_3 using PD10 buffer exchange columns (Sephadex™ G-25 M), flash frozen in aliquots in liquid nitrogen with argon gas in the headspace, and stored at -80 °C.

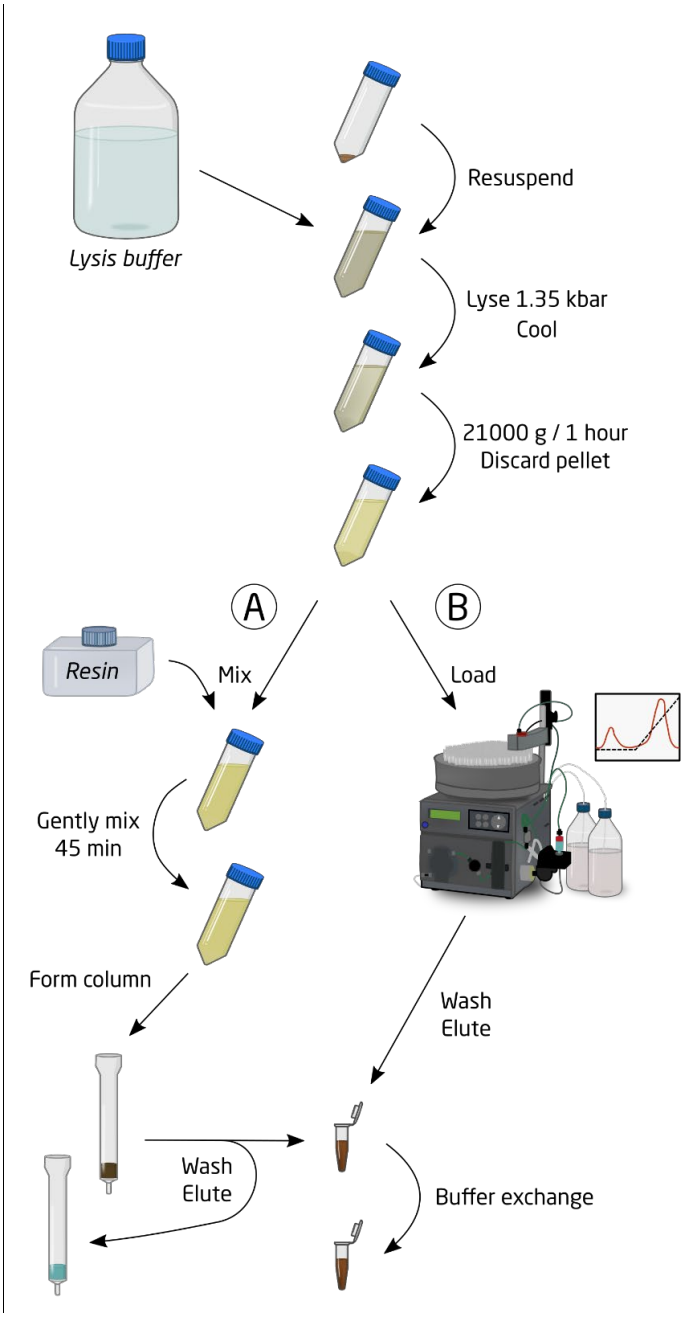

Figure 14: Purification of type 5 FDHs via IMAC. From the top: Cell pellet containing FDH was suspended in lysis buffer (40 mM potassium phosphate, 10 mM potassium nitrate buffer, pH 8) at a ratio of 1 g cell pellet per 10 ml buffer. The suspended cells were lysed at 1.35 bar and immediately cooled before the lysate was spun down at 21,000 g for 1 hour. The FDH-containing supernatant was then purified using one of two methods: (A) Supernatant was mixed with Ni Sepharose HP resin in a ratio of 0.2 ml per 1 g of lysed cell pellet. The supernatant/resin mix was allowed to gently mix for 45 minutes at 7 °C, before poured into empty cylinders to form columns. The columns were washed with buffer (75 mM potassium phosphate, 10 mM potassium nitrate buffer, pH 7.5) contained first 10 mM imidazole, then 20 mM imidazole. FDH was then eluted into 1 ml fractions with buffer containing 250 mM. (B) The alternative to gravity flow was loading the protein containing lysate supernatant onto a HisTrap pre-packed column mounted on an ÄKTA pump system. The column could then subsequently be washed in a comparable manner to gravity flow but with the added advantage of continues monitoring of outflow from column. For both purification methods, the protein was subsequently buffer exchanged to the storage buffer (75 mM potassium phosphate, 10 mM potassium nitrate buffer, pH 7.5).

Size exclusion chromatography

Size exclusion chromatography (SEC) is a standard method in protein research, allowing separation based on protein size. This study employed columns made of a HiLoad™ Superdex™ 200 material. For preparative purification, a larger 120 ml (16/60 prep grade) column was used, and for analytic purposes, a smaller 24 ml column (10/300 increase) was used. The columns were mounted on either an ÄKTA Purifier or ÄKTA Pure system, depending on availability. For each variant a 15-20 mg/ml 2 ml solution was prepared and loaded onto a column equilibrated with the buffer used for storage (75 mM potassium phosphate, 10 mM potassium nitrate, pH 7.5).

SEC-mediated purification was not optimized in this study, but employed conditions were well within the operation recommendations of the employed columns.

The enzyme solutions of all three variants are known or presumed to be comprised a heterogeneous mix of the active heterotrimer-dimer ($(\alpha\beta\gamma)_2$), the heterotrimer-monomer ($\alpha\beta\gamma$), and the incomplete $\beta\gamma$ constellation (Hartmann and Leimkühler, 2013). Fractions were collected conservatively to represent each of the resulting peaks (Peak 1: corresponding to FDH in $(\alpha\beta\gamma)_2$ conformation, peak 2: corresponding to FDH in $\alpha\beta\gamma$ conformation), flash frozen with argon gas headspace and stored at -80 °C. Sample purity was confirmed with SDS-PAGE. Protein fraction molecular weight estimation was performed by correlating to a standard comprised of proteins with known molecular weight.

Routine activity assays were performed by measuring change in absorbance over time at 340 nm (the extinction coefficient for NADH is 6220 M^{-1} cm^{-1} at 340 nm) as described in Section 4.2.1. Protein concentrations were determined at 280 nm using an extinction coefficient based on predictions with the Quest Calculate™ Protein Concentration Calculator (AAT Bioquest, 2017) (Table 4).

Table 4: Predicted weight of representative type 5 FDHs based on protein sequence and co-factor content. The predicted weight is assuming 100% co-factor saturation and includes the His-tag containing 'gamma-tail' described in Figure 11.

FDH variant	Predicted weight (kDa)	Extinction coefficient at 280 nm (M^{-1} cm^{-1})
RcFDH	179,310	167,960
RsFDH	182,380	148,210
CnFDH	185,010	146,260

3.3.2. Background for selection of purification method

During the experiments conducted in relation to this thesis, presence of impurities as well as build-up of pressure was observed when purifying with pre-packed columns. To solve these issues, changes in materials and inclusion of a salt wash step was attempted. This allowed a modicum of success, but ultimately resulted in a shift from pre-packed columns to gravity flow for IMAC assisted purification. See Appendix H for discussion on purification method. In conclusion, purification via gravity flow proved more beneficial for IMAC assisted purification of type 5 FDHs.

3.4. Storage

Severe protein precipitation was observed for RcFDH purified via IMAC when stored at -80 °C. This led to speculations regarding the effect of either imidazole presence, protein concentration, or freeze/thaw cycles. To test this, RcFDH was sampled before and after buffer exchange to gauge effect of imidazole. Each sample was up-concentrated using Vivaspin 20 (30,000 kDa) columns, before protein concentration was measured using absorbance at 280 nm as described in the Section 3.3.1. RcFDH-containing samples were flash frozen and subsequently thawed on ice, before being spun down at 8,000 g for 5 minutes after which protein concentration was measured again (Figure 15).

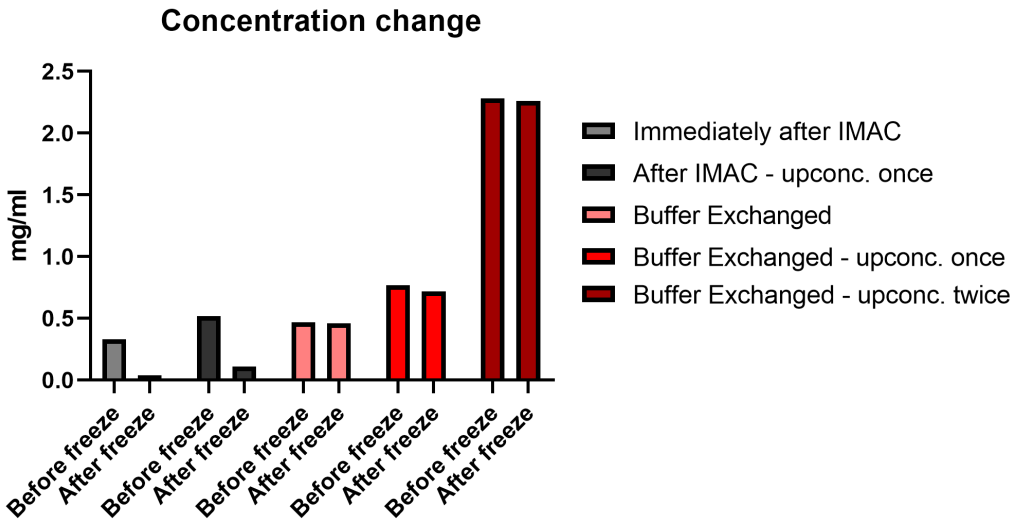

Figure 15: Protein concentrations sampled at two separate steps during purification: after IMAC purification and after buffer exchange of IMAC eluate. For each sample protein concentration was measured at different levels of up-concentration, and the protein was flash frozen and thawed, before protein concentration were measured again.

From Figure 15 it is observed that protein does not precipitate as a result of a freeze/thaw cycle after undergoing buffer exchange. Conversely, samples that are *not* buffer exchanged display distinct precipitation. This trend is even more evident when observing the relative changes in protein concentration before and after one freeze/thaw cycle (Figure 16).

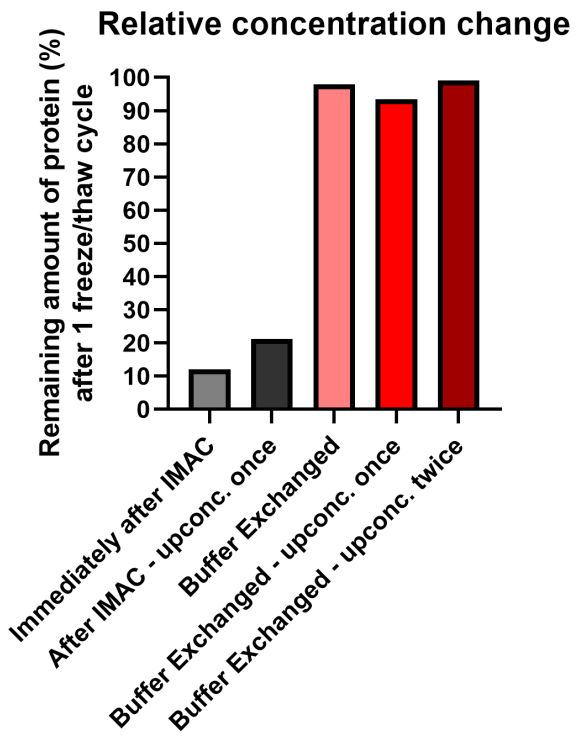

Figure 16: Relative protein concentration change of RcFDH samples as a result of one freeze/thaw cycle. Samples were taken during purification of RcFDH.

In conclusion, RcFDH, and in extension likely also other type 5 FDHs, should not be frozen in the presence of imidazole.

3.5. Comparison of expression protocols

In hypothesis 2 of this chapter, it was hypothesized that slow growth, use of TB medium, and optimized expression strains would result in type 5 FDHs with higher specific activity, compared to enzymes expressed with protocols described in previous work (see Table 3 for differences in protocols).

The optimized (slow growth, TB media, optimized expression strains) protocol developed for this study was denominated: 'Nielsen protocol'. Please refer to Appendix I for a more detailed description of the protocol development. Briefly put, it was observed that when expressing at low temperatures (18 °C), the highest specific activity was achieved when using TB medium and low aeration (30 rpm). Six different expression strains were compared, ultimately revealing that the non-optimized *E. coli* DH5α allowed higher specific activity than the best of the tested optimized expression strains (*E. coli* C43).

Based on the above results it was possible to partially reject hypothesis 2 of this chapter since it was seen that optimized *E. coli* strains did not yield higher specific activity for type 5 FDH, compared to non-optimized strains.

In conclusion, for the optimized Nielsen protocol, expression would be performed with *E. coli* DH5α in TB medium at 18 °C and 30 rpm.

To further test hypothesis 2 of this chapter, RcFDH was expressed using either the optimized Nielsen protocol, the Hartmann protocol, or the Yu protocol as described in Section 3.2.1. For all three protocols, expression was carried out with *E. coli* DH5α as the expression strain. Again, the cell pellets were lysed followed by subsequent IMAC purification of RcFDH as described in Section 3.3.1. The IMAC pure RcFDH could then be assayed for formate oxidation activity as described in Section 4.2.1. This allowed comparison of both specific activity and yield expressed in units (1 U = enzyme to convert 1 µmol formate per minute) (Figure 17).

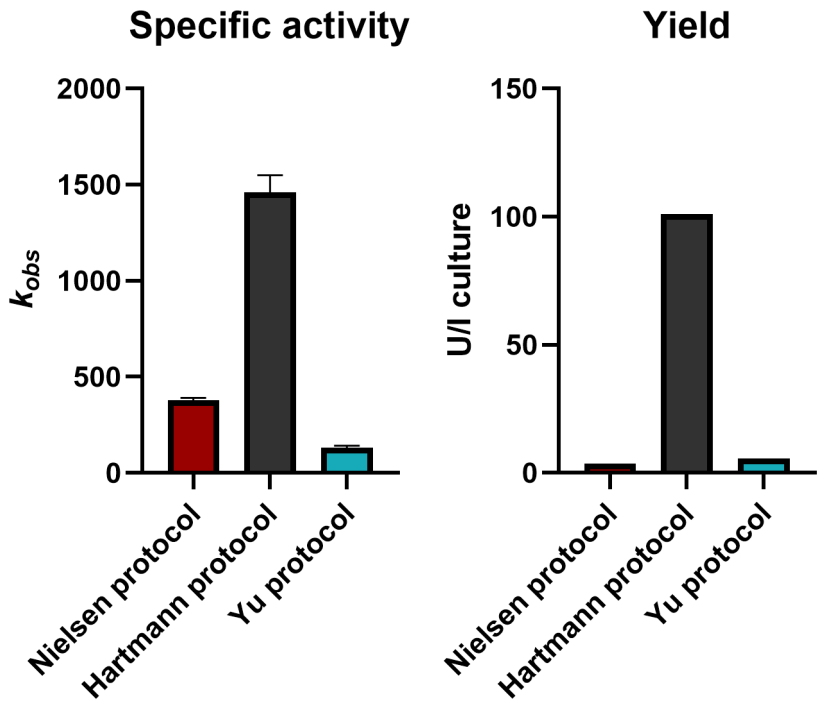

Figure 17: Formate oxidation activity and yield of RcFDH expressed in E. coli DH5α with three different protocols. Yield is given in units purified per liter of expression culture, with a unit (U) defined as the amount of enzyme that can convert 1 µmol of formate per minute.

Surprisingly, the Hartmann protocol, with the highest growth temperature and overall simplest protocol proved to not only allow the highest yields but also allow the highest specific activity. This is especially curious when comparing RcFDH expressed with the Yu protocol with RcFDH expressed with the Hartmann protocol: RcFDH expressed with Yu protocol performs significantly worse despite similar expression conditions. The composition of the IMAC purified protein could be used to investigate the cause of this trend. Using a 24 ml column, SEC was performed on the IMAC purified RcFDH expressed with 3 different protocols (Figure 18).

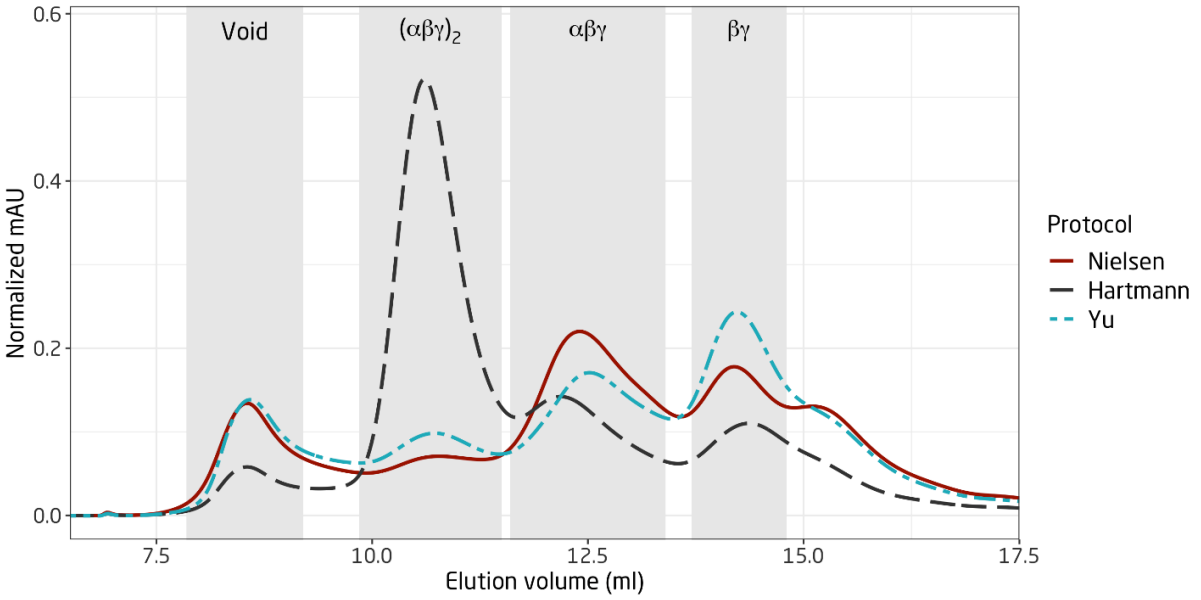

Figure 18: SEC chromatogram on RcFDH expressed with three different protocols. Each peak is marked with grey boxes and predicted subunit composition. SEC was performed on 24 ml Superdex™ 200 10/300 column. Chromatograms are normalized against total area under individual curve. For chromatogram with raw mAU values please refer to Figure 42 in Appendix L.

From Figure 18 it becomes readily apparent that RcFDH expressed with the Hartmann protocol displays a larger fraction of enzyme in the active $(\alpha\beta\gamma)_2$ and αβγ conformations. The relative area under curve (AUC) for peaks containing $(\alpha\beta\gamma)_2$ or αβγ conformation (9.85-11.5 ml for $(\alpha\beta\gamma)_2$, and 11.6-13.4 ml for αβγ) can be estimated to the following values: Nielsen: 40%, Hartmann: 68%, and Yu: 38%.

Both the Nielsen and Yu protocol infer a larger fraction of protein either aggregated in the void fraction or in the inactive βγ conformation. The main similarity of these two protocols, and primary difference to the Hartmann protocol, is the use of TB medium. It can be speculated that the composition of TB medium somehow infers a higher percentage of inactive aggregate and RcFDH in βγ conformation.

Unfortunately, the measured specific activity of the SEC purified type 5 FDH was unreliable. This was likely due inaccurate measurement of the very low protein concentrations and that this error was realized too late. However, as will be demonstrated later in Section 4.3.2, it can be assumed that RcFDH in both $(\alpha\beta\gamma)_2$ and αβγ conformation both display activity. As such, the Hartmann protocol clearly allows the highest fraction of active protein.

In conclusion, the Hartmann protocol is the superior protocol for expression of RcFDH, and in extension likely also other type 5 FDHs. This is in direct contradiction to hypothesis 2 of this chapter, and as such hypothesis 2 can be refuted as valid.

3.6. Comparison of expression of RsFDH, RcFDH, and CnFDH

RcFDH, RsFDH, and CnFDH were expressed using the Hartmann protocol described and discussed in the above sections. All three type 5 FDHs were purified using IMAC via gravity flow, followed by SEC. For SEC the 120 ml column was used. See Sections 3.2.1 and 3.3.1 for a description of the methods. Comparing the chromatograms produced via SEC on the three type 5 FDHs it is possible to gauge differences in enzyme population (Figure 19).

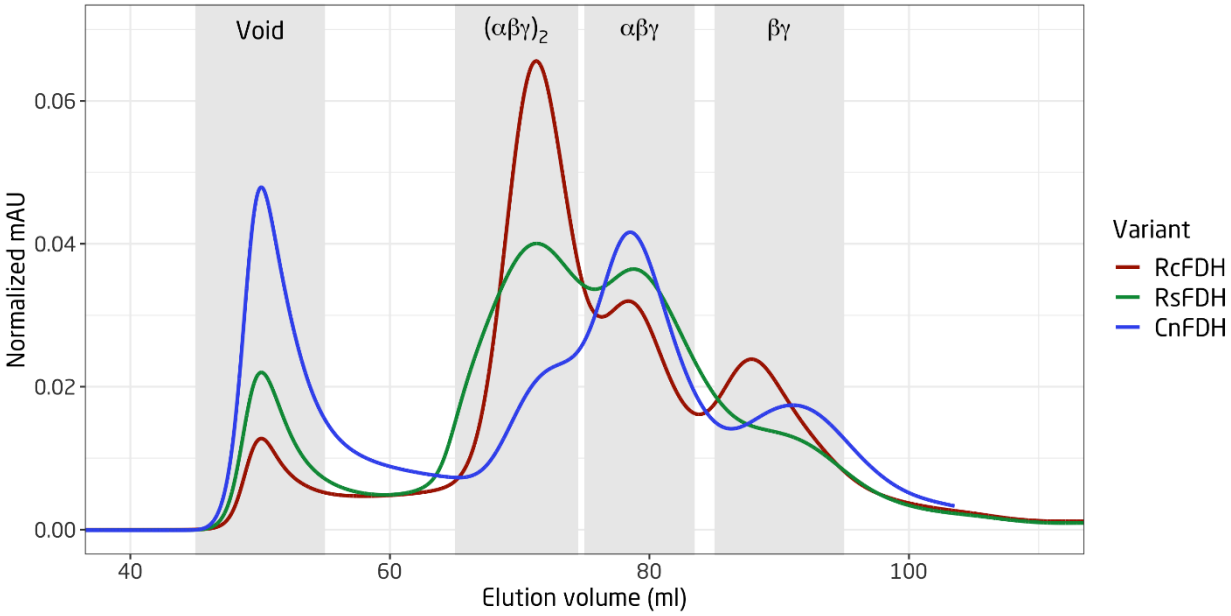

Figure 19: SEC chromatogram on RcFDH, RsFDH, and CnFDH expressed with the Hartmann protocol. Each peak is marked with grey boxes and predicted subunit composition. SEC was performed on 120 ml HiLoad™ Superdex™ 200 16/60 pg column. Chromatograms are normalized against total area under indiviual curve. For chromatogram with raw mAU values please refer to Figure 43 of Appendix L.

Interestingly, RcFDH, RsFDH, and CnFDH display different characteristics in terms of preferred structural composition. In concordance with the results in Section 3.5, RcFDH expressed with Hartmann protocol again shows a high percentage of enzyme in $(\alpha\beta\gamma)_2$ conformation relative to αβγ conformation. RsFDH shows an even distribution between enzyme in $(\alpha\beta\gamma)_2$ conformation and enzyme in αβγ conformation. CnFDH, on the other hand, favors the αβγ conformation over $(\alpha\beta\gamma)_2$ and shows a much larger percentage of protein in the void fraction. A higher percentage of protein in the void fraction, indicates a greater propensity for aggregation, since proteins in the void fraction exceed the size limits of the given column material. For the applied Superdex200 material, the limit is 600 kDa for globular protiens.

In addition, RsFDH was shown to display formate oxidation activity. This will be further detailed in Section 4.5, but signifies that RsFDH is correctly folded and at least partially co-factor saturated.

In conclusion, when expressed using identical methodology, each of the three type 5 FDH demonstrate different characteristics in terms of conformation preference. The dynamics behind this phenomenon are currently not described and would be an interesting topic for further research. With this in mind, it can be concluded that RsFDH displays unique conformation preferences but can be purified using the same protocol as used for other type 5 FDHs.

3.7. Conclusion on expression and purification

It was not possible to conclude on the effect of a synthetic codon-optimized version of the FDH operons. It is likely that a strategy involving a synthetic construct is still viable strategy that should be explored further.

For the first hypothesis that placement of the His-tag on the alpha subunit, relative to placement on the gamma subunit, will minimize loss of FDH during purification and retain specific activity, it is not possible to present a definitive conclusion. The associated experiments showed that RcFDH – and in

extension type 5 FDHs in general – lose nearly all formate oxidation activity when the His-tag is placed on the N-terminal of alpha subunit. It is however possible that placement elsewhere on the alpha subunit would not cause loss of activity.

The second hypothesis of this chapter, that the combination of slow growth rates, TB medium, and *E. coli* strains designed for protein expression will result in type 5 FDHs with higher specific activity compared to expression according to methods described in previous work by Hartmann and Leimkühler, 2013 and Yu et al., 2019, could be refuted. Here, it was shown that RcFDH, expressed with a protocol inspired by the work by Hartmann and Leimkühler, showed vastly higher yields but also higher concentration of active protein in the enzyme population.

It is possible that another method, not involving either slow growth rates, TB medium, and *E. coli* expression strains will prove more beneficial in the future. However, it is recommended that the 'Hartmann protocol' is used for future recombinant expression of type 5 FDHs until a better protocol is developed.

Finally, it was shown that the novel and previously uncharacterized type 5 FDH derived from purple non-sulfur bacteria *Rhodobacter sphaeroides* (RsFDH) can be heterologously expressed and purified *E. coli*. Additionally, it was shown that this RsFDH had similar properties to RcFDH and CnFDH.

In conclusion, development of improved construct design and improved expression protocol proved interesting but ultimately unsuccessful.

Chapter 4. Type 5 formate dehydrogenases as catalysts

Please note

This chapter is based on work in preparation for submission in Paper II: Enzyme reaction kinetics and O_2 tolerance of bacterial formate dehydrogenases for CO_2 utilization. See Appendix N for manuscript.

As discussed in Chapter 1, a cheap CO_2 point source will potentially contain oxygen. For FDH-based CO_2 reduction, the FDHs grouped as 'type 5' according the classification scheme proposed in Section 2.2, are of interest due to their proposed oxygen tolerance. Importantly, the three selected type 5 FDHs are, for the purposes of this thesis, considered to be representative for type 5 FDHs in general.

Expressed and purified as described in the previous chapter, the three candidate type 5 FDHs can be characterized. Here, it can be argued that temperature and pH optima, catalytic rate, and oxygen tolerance form the foundation for characterization.

In this regard, the following hypotheses were formulated and then tested in this chapter:

Hypotheses:

1. Type 5 FDHs show higher pH optima for the forward reaction than the reverse reaction.
2. Type 5 FDHs are oxygen tolerant in the presence of KNO_3.
3. The three candidate FDHs catalyze reduction of CO_2 at a 100-fold slower rate relative to formate oxidation under comparable substrate concentrations.

4.1. Practical considerations regarding substrates

Although metal-dependent FDHs in themselves invoke some practical challenges, the substrates also beseech atypical considerations.

4.1.1. CO_2 as a substrate

Determining and adjusting the substrate concentration of CO_2 is non-trivial. As with any gaseous substrate the concentration is dependent on the solubility of the gas. Here, temperature, pressure, and pH all influence the potential saturation concentration as described by Henry's Law.

Each gas interacts with water in its own manner. This work is based on the understanding that CO_2 concentration in water, at ambient conditions (1 atm pressure, 25 °C, well mixed) can reach 29.5 mM (Hayden, 2003). If creating a reaction buffer saturated with aqueous CO_2 and another saturated with an inert gas, it is possible to mix the two and create substrate concentrations between 0-29.5 mM $CO_{2(aq)}$ (Yu et al., 2017).

However, several considerations further complicate this seemingly trivial matter. CO_2 reacts with water and forms carbonic acid. Depending on pH, carbonic acid then enters an equilibrium with bicarbonate and carbonate. This leads to a fundamental dilemma in regard to the form of CO_2 reacting with FDH.

In 2017, Yu et al. showed that CnFDH in anaerobic conditions only reacts with aqueous CO_2 and not the bicarbonate ions (Yu et al., 2017). Activity was observed with bicarbonate as substrate, but only

in aerobic conditions, leading this group to believe that the activity observed at aerobic conditions was in fact a false positive diaphorase activity where NADH was oxidized with molecular oxygen as electron acceptor. This also makes great sense when considering that CO_2, and not bicarbonate, is the product of the forward reaction, making it more likely that CO_2 is also the substrate of the reverse reaction. In other words, only solubilized CO_2 should be used as substrate. Additionally, the finding underlines the importance of working in an anaerobic setup when studying the reverse reaction to avoid false positive activity measurements.

As a practical consequence of the reaction with CO_2 and water, it is important to note that prolonged exposure to CO_2 acidifies the given buffer dramatically. To ensure a dependable pH while keeping the vial of substrate sealed to avoid oxygen, one must adjust the pH through a septum.

4.1.2. NAD^+/NADH as a substrate

NADH is the natural electron donor of RcFDH, RsFDH, and CnFDH, and holds some practical physicochemical properties that can be exploited for activity assays.

NAD^+ is a colorless chemical that have little to no absorbance above 300 nm. However, the reduced form, NADH, has an absorbance peak around 340 nm. This makes it easy to follow any reaction involving the redox reaction between NAD^+ and NADH (Held, 2007).

For fluorescence, differences between NAD^+ and NADH also allow easy monitoring. When excited at 340 nm, NADH emits at 445 nm. NAD^+ does not. However, unlike NADH absorbance, NADH fluorescence is less trivial. The correlation between fluorescence intensity and NADH concentration is non-linear and requires a standard to correlate against. Additionally, the fluorescence intensity is highly dependent on temperature in an inversely proportional manner (Held, 2007).

Finally, as a practical consideration, pure powdered NADH not only tends to absorb liquid from the air if stored improperly, but it also slowly auto-oxidizes over longer periods of time. In other words, it is essential to measure the concentration of an NADH-containing solution with absorbance prior to using it for experiments to ensure that the reported NADH concentration is dependable. Additionally, NADH solutions should be stored in the fridge and not exposed to sunlight.

4.2. Materials and methods for assessing activity

In general, no matter the reaction, either mono-component or overlapping multi-component buffers were used. These were comprised of acetate buffer, potassium phosphate buffer, and/or Tris/HCl (Trizma) buffer. Buffer concentration were set to 100 mM. For mixed buffers, with wider pH range, 100 mM of each buffer type was used. Common for all buffers was that they were pH-adjusted at the intended reaction temperature.

4.2.1. Assay for the forward reaction

Sodium formate stock solutions were prepared in water and adjusted to intended reaction pH. In an UV-transparent microtiter plate, buffer was mixed with NAD^+ and sodium formate. NAD^+ concentrations ranged from 0-5 mM with 2 mM being standard. Sodium formate concentrations ranged from 0-40 mM with 6 mM being standard. In each well, the volume of reactants was 190 µl. Enzyme stock solutions, 0.5-1.5 mg/ml, were thawed and kept on ice.

The prepared microtiter plate was left in a preheated plate reader and allowed to reach desired temperature. The reaction was started by addition of 10 µl diluted enzyme stock. Absorbance at 340 nm was measured for a minimum of 1 minute. Typically, the first 10 seconds were used to calculate the initial rate (Figure 20).

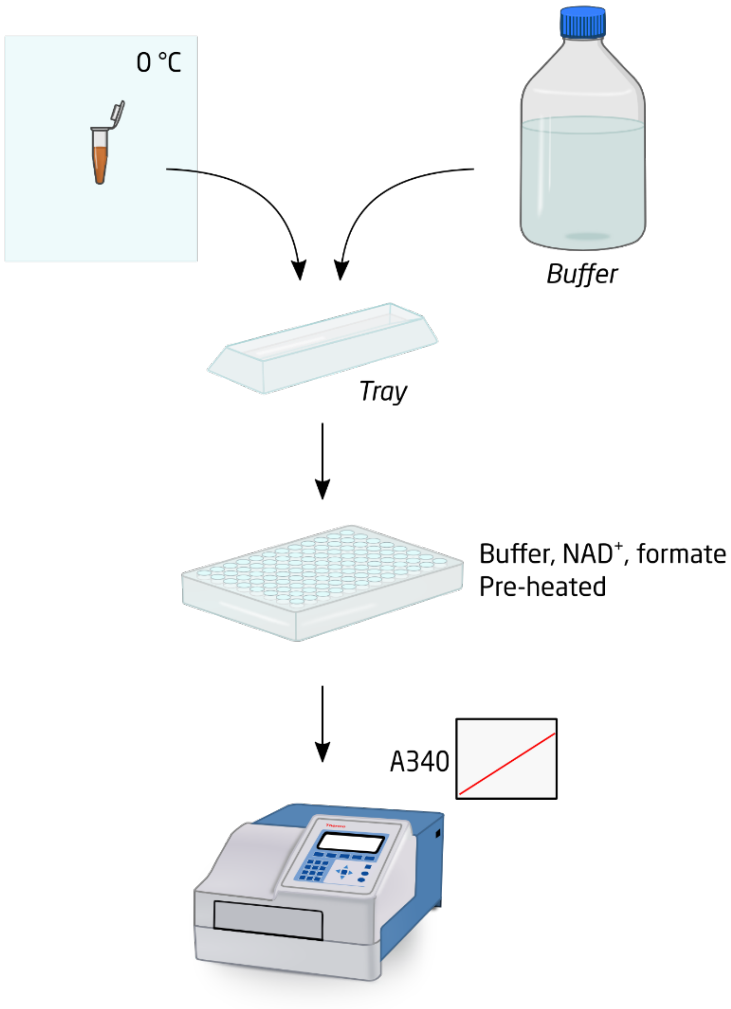

Figure 20: Formate oxidation assay. Enzyme stock of typically 0.5-1.5 mg/ml was thawed and stored on ice throughout the experiment. A microtiter plate was prepared with 190 µl of relevant buffer, formate, and NAD^+ in each well. The microtiter plate was then allowed to reach desired temperature. To initiate the experiment enzyme was mixed with a relevant buffer containing 10 mM KNO_3 in a tray allowing immediate transfer with multichannel pipette to between 1-8 wells in the prepared microtiter plate. The absorbance at 340 nm was measured for a minimum of 1 minute.

4.2.2. Assay for the reverse reaction

For each experimental condition, an identical pair of buffers was prepared in 200 ml volumes in 250 ml blue-cap bottles. These were then degassed with vacuum. Of the pair, one was then bubbled continuously for a minimum of 30 minutes with nitrogen gas and the other likewise but with CO_2. An aquarium ball was used to ensure small high-surface area bubbles.

Immediately after saturating the buffers with either nitrogen or CO_2, the bottles were sealed, leaving the headspace saturated with the intended gas. The pH of the CO_2-saturated buffer was adjusted back to the intended pH with sodium hydroxide. The buffer was then immediately transferred to a glass vial. The vial was flushed with its intended gas, sealed, and then flushed again through the septum seal.

For the assay, a 50 mM NADH stock was added to each vial to reach a concentration of 0.2 mM immediately prior to the experiment. To prepare for the reaction, a 1.4 ml septum-sealed four window quartz cuvette was flushed with nitrogen. Then 950 µl of gas-saturated buffer, was added via gas-tight Hamilton syringes through the septum in the cuvette. Pressure was released and the buffer-containing cuvette was placed in a temperature-regulating spectrofluorometer (JASCO FP-8500). Exciting the NADH in solution with 340 nm and measuring at 445 nm, the buffer was monitored for 7 minutes until a stable baseline had formed. The reaction was then started by addition of 50 µl enzyme stock (0.5-1.5 mg/ml) and followed via fluorescence for 1 minute. Typically, the first 10 seconds were used to calculate initial rate (Figure 21).

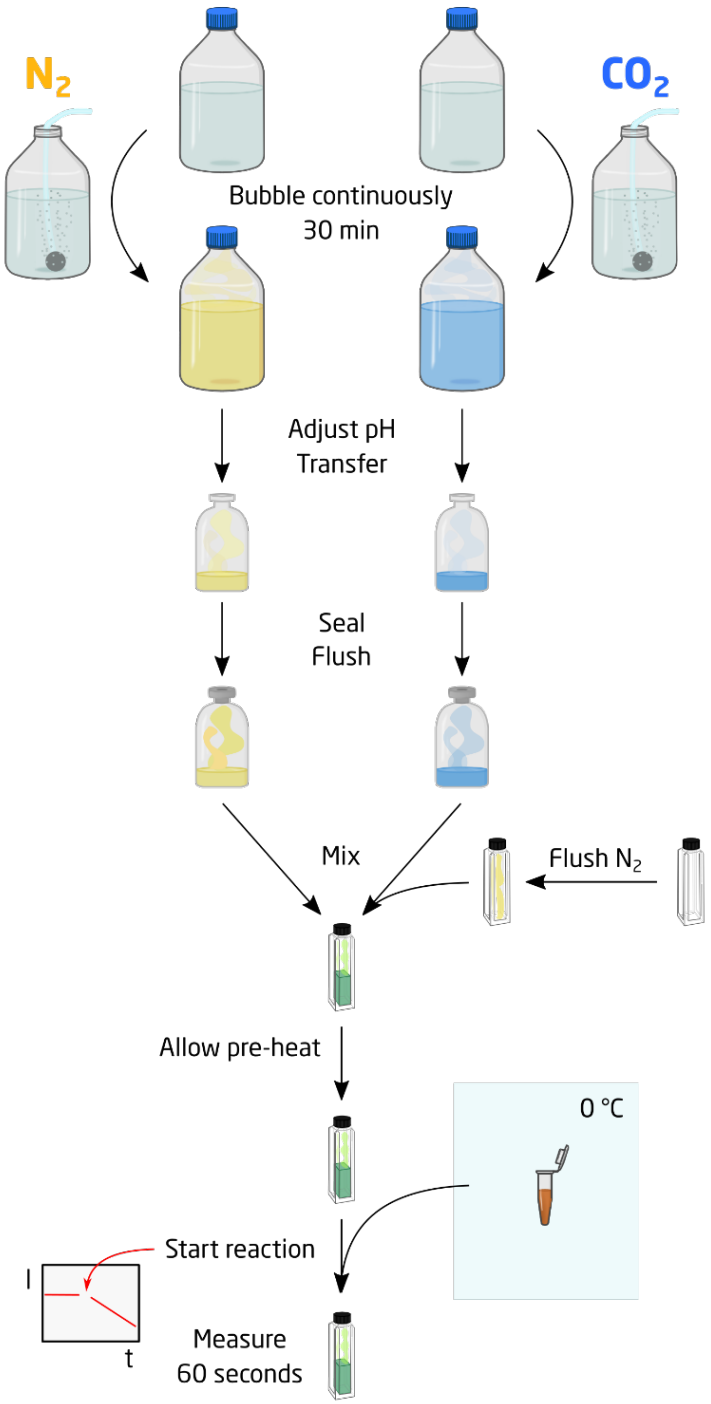

Figure 21: CO_2 reduction assay. Enzyme stock solution (0.5-1.5 mg/ml) was thawed and stored on ice. Reaction buffer was gassed continuously with either N_2 or CO_2 for 30 minutes using high-porosity aquarium ball to generate small bubbles. The pH of the buffer was adjusted to desired pH at desired temperature before transferred to glass vial. The vial was flushed, sealed, and then flushed again. 50 mM NADH stock solution was added to each vial to reach a final concentration of 0.2 mM. The vials with gas-saturated buffer were mixed to a total of volume of 950 µl in ratios allowing 0-95% final CO_2 saturation in an N_2-flushed 4-window septum sealed quartz cuvette. The mixture was allowed to reach desired temperature before the reaction was started by adding 50 µl enzyme stock solution. Fluorescence intensity was measured at 445 nm excited at 340 nm for 60 seconds.

4.3. Evaluation of enzyme population

Despite being of near identical mass, heterogeneity in the enzyme population is still very likely. Here, variation in co-factor saturation is of particular concern.

Additionally, enzymes had previously been observed in both αβγ and $(αβγ)_2$ conformations. It was deemed interesting to test if the conformations display similar catalytic properties.

4.3.1. Co-factor saturation

Synthesis of the molybdenum containing co-factor, bis-MGD, requires a four-step synthesis involving several specialized enzymes (Hartmann et al., 2015). Thankfully, *E. coli* has the complete synthesis pathway, allowing its use as expression strain for RcFDH, RsFDH, and CnFDH (Leimkühler, 2020).

Due to the complexity of the biosynthetic pathways for the bis-MGD pathway, combined with subsequent sulfuration and insertion into the apoprotein, the protein synthesis of the main protein can actually outpace co-factor biosynthesis (Niks and Hille, 2018). This issue, combined with the requirement for the protein to also contain the other eight co-factors to be active, was presumed to be the cause of relatively high percentage of the synthesized protein being incomplete and inactive.

Co-factor saturation can be measured directly via quantification of iron and molybdenum content. The most common technique involves using inductive coupled plasma (ICP) paired with a variant of spectroscopy (Alissandratos et al., 2013; Walker et al., 2019). However, for routine measurements, specific activity (formate oxidation) can be used as an indicator for level of complete expression.

RcFDH and CnFDH have both previously been predicted to contain a total of five [Fe4-S4] and two [Fe2-S2] complexes (Hartmann and Leimkühler, 2013; Yu et al., 2017). Assuming a similar co-factor composition for RsFDH, each mole of enzyme should contain 24 moles of iron and 1 mole of molybdenum. Molybdenum and iron concentrations were quantified with inductive coupled plasma-mass spectrometry (ICP-MS).

Quantification of elemental iron and molybdenum was completed by out-of-house analytic resources at DTU Environment. See Appendix F for details on the applied method. Comparing the concentration of elemental Mo and Fe to protein concentration, the co-factor saturation could be estimated (Table 5).

Table 5: Estimated metal content in percentage of maximum possible metal concentration for the respective enzymes. Uncertainty given as a single standard deviation.

	RcFDH		RsFDH		CnFDH	
	$(αβγ)_2$	αβγ	$(αβγ)_2$	αβγ	$(αβγ)_2$	αβγ
Mo % saturation	**60** ± 1.2	**70** ± 0.5	**43** ± 4.3	**44** ± 1.2	**63** ± 2.4	**87** ± 1.1
Fe % saturation	**65** ± 0.5	**44** ± 0.7	**58** ± 0.9	**50** ± 0.5	**46** ± 1.8	**50** ± 0.5

Hartmann and Leimkühler reported approximately 39% Mo saturation and 48% iron saturation on heterologously expressed RcFDH in $(αβγ)_2$ conformation (Hartmann and Leimkühler, 2013). In this study, aslight increase in co-factor saturation relative to these values was observed. It is observed that the iron content for the three FDH enzyme populations in αβγ conformation is similar. The final, non-metal, co-factor of type 5 FDHs is FMN. This co-factor can be quantified with by denaturing the protein,

purifying the released FMN, and quantifying it photometrically. Due to time constraints it was chosen to rely solely on the metal quantification for comparison between the three enzymes.

It can be concluded that a comparable iron content is observed for all three candidate type 5 FDHs. This indicates that the Hartmann protocol discussed in Section 3.5 allows for iron saturation between 44% and 65%. This is a solid benchmark for future studies to compare against.

4.3.2. Effect of buffer and dimerization

The buffer component of a given reaction is an often-neglected hidden influence within enzyme kinetics. As such, it was tested if the type 5 FDH performed identically in Tris/HCl (Trizma) buffer versus potassium phosphate buffer. Both buffers were equilibrated to pH 7.0 at 30 °C. Additionally, it was tested if FDH in the αβγ versus $(\alpha\beta\gamma)_2$ conformation displayed similar specific activity (Figure 22). For each enzyme, the steady state kinetics were studied on formate oxidation activity for both conformations in both buffers. The assay on the forward reaction was performed as described above with standard NAD^+ concentration and varying formate concentrations.

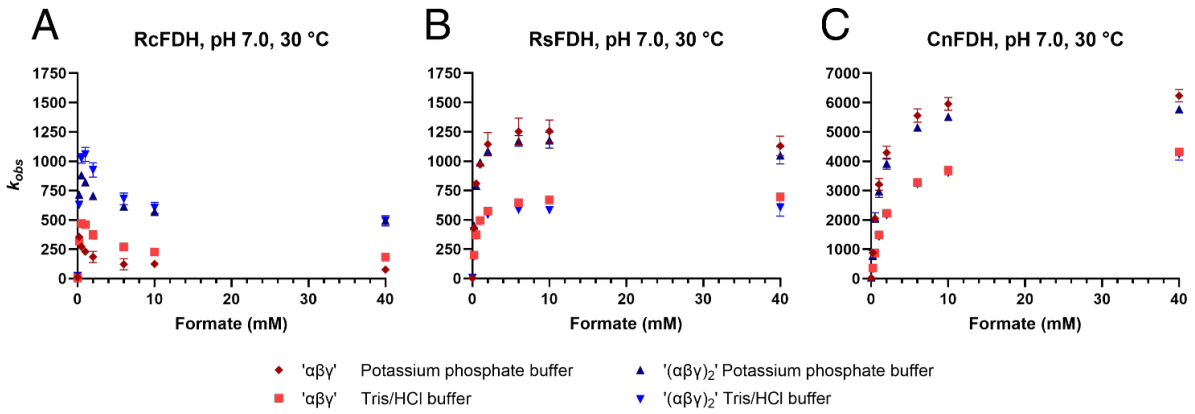

Figure 22: Formate oxidation kinetics of candidate FDHs in both heterotrimer-monomer (αβγ) and heterotrimer-dimer ($(\alpha\beta\gamma)_2$). Assays were performed with 2 mM NAD^+ and 0-40 mM sodium formate in either Tris/HCl (Trizma) buffer or potassium phosphate buffer at pH 7.0 and 30 °C. Initial rate (k_{obs}) is calculated based on the first 10 seconds. Please note that the y-axis in C reaches 4-fold higher values than the y-axes in A and B.

Firstly, from Figure 22 above, it becomes evident that RsFDH and CnFDH perform similarly, independent of dimerization. However, RcFDH shows a clear correlation between dimerization and catalytic rate. Additionally, RcFDH appears severely substrate-inhibited at these conditions (Figure 22A).

In a previous earlier experiment at pH 7.7 and 30 °C in Tris/HCl buffer on a different batch of RcFDH, no apparent effect of dimerization was observed for RcFDH (Figure 23).

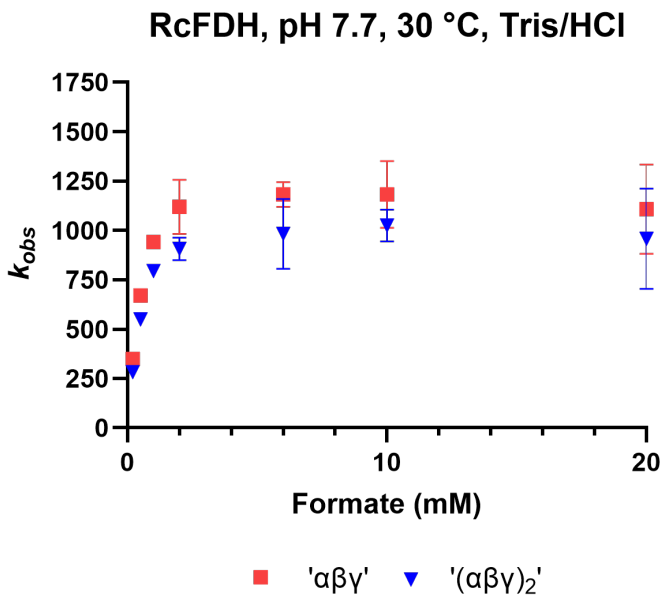

Figure 23: Steady state kinetics of a previous expression and purification batch of RcFDH. RcFDH is represented by both heterotrimer-monomer (αβγ) and heterotrimer-dimer ($(αβγ)_2$). Assays were performed with 2 mM NAD^+ and 0-20 mM sodium formate in Tris/HCl (Trizma) buffer at pH 7.7 and 30 °C.

It is thus likely that also for RcFDH no apparent effect should be observed on the specific activity from dimerization. The curious observation of a dimerization-effect for RcFDH (Figure 22) is likely related to the strong substrate inhibition that is also observed for this FDH variant. This will be discussed further in Section 4.5 on kinetic characterization.

Secondly, a clear tendency of an increased rate of FDH-catalyzed formate oxidation in phosphate buffer was observed (Figure 22). Either Tris/HCl acts as a weak inhibitor or phosphate somehow promotes the catalytic rate of FDHs. In summary, it is clear that phosphate interacts with type 5 FDHs in a previously undescribed manner.

For the purpose of enzyme kinetics study, it was chosen to work with the FDHs in αβγ conformation.

4.4. Temperature and pH optima

To allow comparison of enzymes at their optimum pH and temperature, experiments were designed using a response surface methodology (RSM). The goal was to estimate each enzyme's individual global maximum rate for both the forward and reverse reaction. Additionally, the optimum conditions may reveal interesting insights into the relationship between the forward and reverse reactions.

The experimental design was created with the help of SAS JMP statistical software. A central composite design spanning pH 5 to pH 9 versus 20 °C to 50 °C was created. Default settings were used. A total of 13 measurements were completed per experiment including 5 central measurement points and 4 axial measurement points. An overlapping multi-component buffer consisting of acetate, potassium phosphate and Tris/HCl buffer was applied to cover the full pH range. The assay methods described above in Sections 4.2.1 and 4.2.2 were applied. For the forward reaction, 2 mM NAD^+ and 6 mM sodium formate were applied. For the reverse reaction, 0.2 mM NADH and CO_2-saturated buffer were applied.

A quadratic polynomial model could then be fitted to the observed activity data with a minimum R-squared value of 0.9 and statistically insignificant lack of fit (Figure 24).

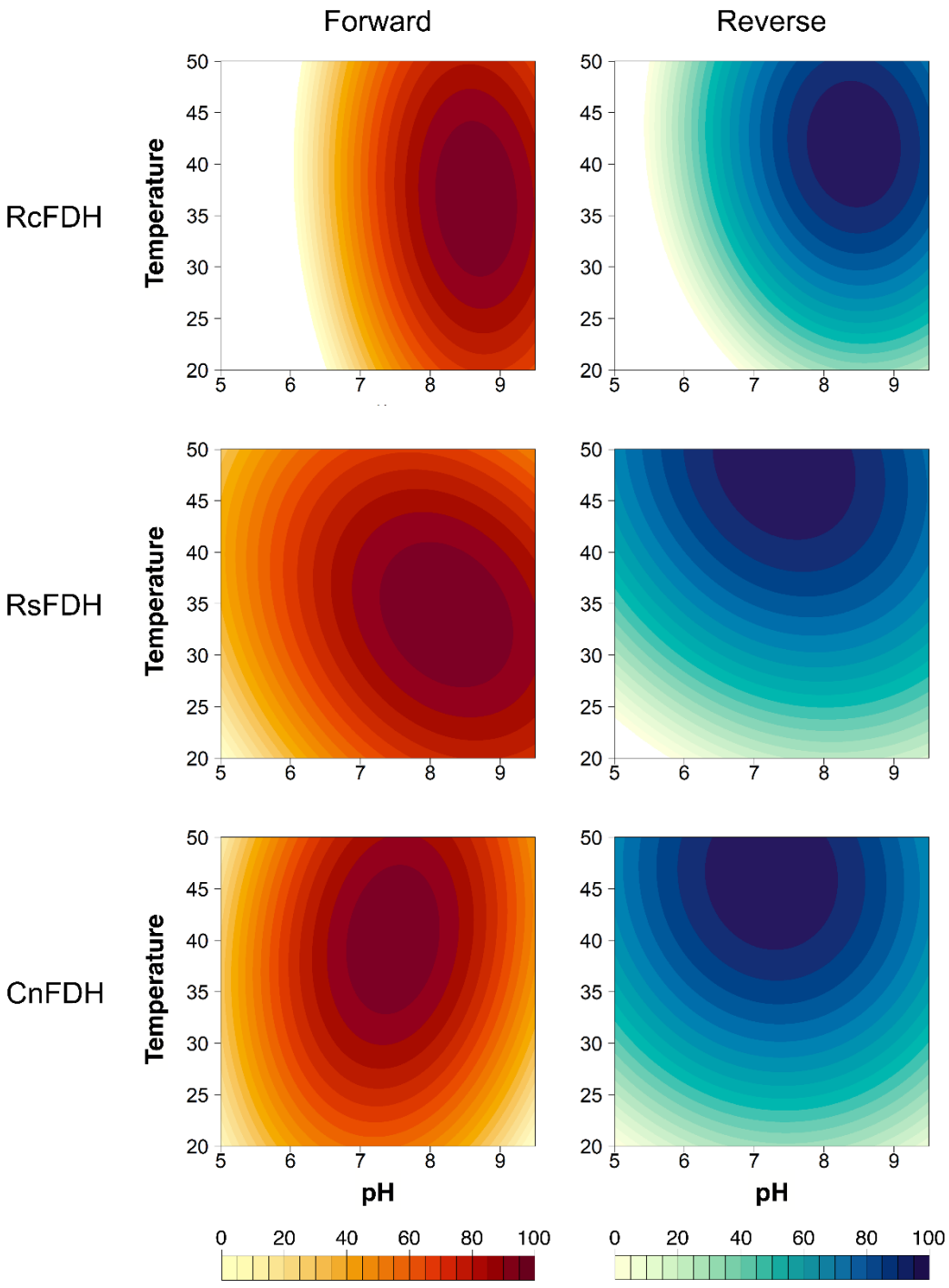

Figure 24: Temperature and pH optima for RcFDH, RsFDH, and CnFDH given in relative activity levels, with 100 being equivalent to the maximum observed activity for the given study.

Based on the fitted model, pH and temperature optima could be predicted by extracting the point of the global maximum (Table 6).

Table 6: Predicted temperature and pH optima for RcFDH, RsFDH, and CnFDH for both the forward and reverse reactions.

	RcFDH		RsFDH		CnFDH	
	Forward	**Reverse**	**Forward**	**Reverse**	**Forward**	**Reverse**
pH (95% CI)	**8.7** (7.8-9.6)	**8.4** (7.8-9.0)	**8.2** (7.2-9.0)	**7.4** (7.0-7.8)	**7.5** (7.1-7.9)	**7.3** (6.6-8.0)
Temperature (°C) (95% CI)	**37** (33-41)	**41** (38-44)	**34** (30-38)	**50** (47-52)	**40** (38-42)	**46** (42-50)

Interestingly, as hypothesized, the optimum pH for the reverse reaction is consistently lower than for the forward reaction. This is most pronounced for RsFDH. However, it is not as strong of a trend as was expected, with overlapping confidence intervals.

The background for the hypothesis was based on the pH dependent equilibrium between carbonic acid, bicarbonate, and carbonate. Acidic conditions favor carbonic acid, physiological pH favors bicarbonate and basic conditions favor carbonates (Andersen, 2002). Knowing that CnFDH is only active on $CO_{2(aq)}$, which again is in equilibrium with carbonic acid, low pH should favor increased CO_2 reduction activity. For all three type 5 FDHs studied here, the optimum pH is indeed lower for the reverse reaction relative to the forward reaction. However, the difference is near negligible and the optimum pH is even slightly basic. As such the hypothesis that the pH optima for the reverse reaction is significantly lower than for the forward reaction is not supported by the data shown here.

4.5. Kinetic characterization

Knowing the pH and temperature optima, it was possible to characterize the enzymes at these conditions. Additionally, conditions to reproduce experiments from literature were included to allow more direct comparisons.

4.5.1. Formate oxidation

Individual assays were completed as described in the methods above. Previously, Hartmann and Leimkühler determined the steady state kinetic parameters of the forward reaction for RcFDH at pH 9.0 and 30 °C in a Tris/HCl buffer. Similarly, Yu et al. characterized CnFDH but at pH 7.7 and 30 °C in a potassium phosphate buffer. Both of these conditions were included for comparison. Additionally, to allow comparison with the reverse reaction, the enzymes were also studied at pH 7.0 and 30 °C in a potassium phosphate buffer.

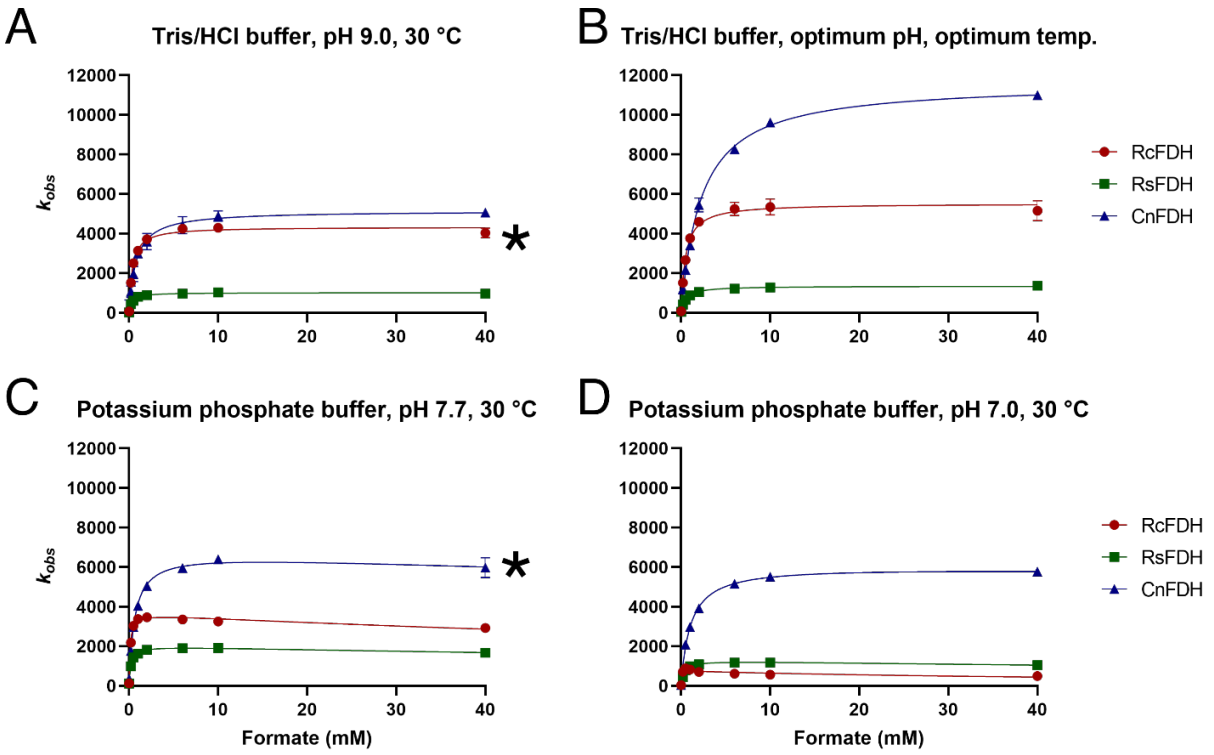

Figure 25: Steady state kinetics with formate saturation on the forward reaction (formate oxidation) for RcFDH, RsFDH, and CnFDH. '': reproduced result from literature* (Hartmann and Leimkühler, 2013; Niks et al., 2016). *NAD^+ concentration was 2 mM and k_{obs} is calculated based on initial rate observed for first 10 seconds.*

Interestingly, it can be observed that CnFDH consistently has a significantly higher formate oxidation rate than RsFDH and RcFDH (Figure 25). Additionally, with the exception of formate oxidation at pH 7.0 in potassium phosphate buffer, RcFDH had a consistently higher formate oxidation rate than RsFDH.

Moreover, particularly RcFDH displays clear indications of substrate inhibition. Curiously, the substrate inhibition is more pronounced in KPO_4 buffer and lower pH. Previously, the RcFDH substrate inhibition was also observed in Tris/HCl buffer at pH 7.0. As such, it is likely the lower pH that causes the increased sensitivity to substrate inhibition by formate.

Previously, a clear trend for KPO_4 buffer to allow a higher activity of RsFDH and CnFDH than Tris/HCl buffer was observed. It is possible that same interaction that causes an increase in activity, also makes particularly RcFDH more prone to substrate inhibition. It would be interesting to further study and elucidate the the interaction between FDH, pH, and phosphate.

Beyond steady state kinetics with formate saturation, steady state kinetics with NAD^+ saturation were also investigated (Figure 44 in Appendix L). Based on the observed steady state kinetics, a standard Michaelis-Menten model, or a model including substrate inhibition when relevant, was fitted. Kinetic parameters could then be extracted (Table 7).

Table 7: Observed forward reaction kinetic parameters. For each value, a confidence interval (CI) at 95% confidence is given. 'ND': Not determined. '-': Not applicable.

		Forward reaction (Formate oxidation)			
		k_{cat} (min^{-1}) (95% CI)	**$K_{M,formate}$ (mM)** (95% CI)	**K_{M,NAD^+} (mM)** (95% CI)	**$K_{i,formate}$ (mM)** (95% CI)
RcFDH	Tris/HCl buffer, Optimum conditions (36. 5 °C, pH 8.7)	**5520** (5300 – 5740)	**0.49** (0.41 – 0.59)	**0.57** (0.47 – 0.68)	-
	Tris/HCl buffer, 30 °C, pH 9.0	**4330** (4200 – 4470)	**0.36** (0.31 – 0.42)	**0.24** (0.29-0.29)	-
	KPO_4 buffer, 30 °C, pH 7.7	**3660** (3480 – 3840)	**0.12** (0.09 – 0.19)	**0.41** (0.31 – 0.54)	**147** (96 – 267)
	KPO_4 buffer, 30 °C, pH 7.0	**760** (710-860)	**0.02** (0.00-0.04)	ND	**56** (29-107)
RsFDH	Tris/HCl buffer, Optimum conditions (33. 8 °C, pH 8.2)	**1350** (1300 -1390)	**0.52** (0.44 – 0.62)	**0.40** (0.28 – 0.57)	-
	Tris/HCl buffer, 30 °C, pH 9.0	**1010** (940 – 1090)	**0.29** (0.19 – 0.42)	**0.18** (0.14 – 0.21)	-
	KPO_4 buffer, 30 °C, pH 7.7	**2030** (1950 – 2110)	**0.21** (0.18 – 0.25)	**0.27** (0.22 – 0.35)	**201** (137 – 345)
	KPO_4 buffer, 30 °C, pH 7.0	**1290** (1240-1340)	**0.33** (0.29-0.39)	ND	**180** (129-278)
CnFDH	Tris/HCl buffer, Optimum conditions (40.1 °C, pH 7.5)	**11640** (11380– 11890)	**2.30** (2.12 – 2.47)	**0.19** (0.15 – 0.23)	-
	Tris/HCl buffer, 30 °C, pH 9.0	**5140** (4880 – 5420)	**0.80** (0.63 – 1.02)	**0.16** (0.13 – 0.19)	-
	KPO_4 buffer, 30 °C, pH 7.7	**6770** (6340 – 7250)	**0.63** (0.51 – 0.78)	**0.13** (0.11 – 0.15)	-
	KPO_4 buffer, 30 °C, pH 7.0	**6110** (5890-6370)	**1.07** (0.95-1.20)	ND	-

Comparing the enzymes at optimum conditions, CnFDH has nearly double turnover number (k_{cat}) relative to RcFDH, and more than 8-fold higher than RsFDH. However, at these higher temperatures, CnFDH is also exhibiting much lower affinity for formate as seen by the more than 4-fold higher $K_{M,formate}$ values relative to RcFDH and RsFDH.

In summary, CnFDH has a significantly higher catalytic activity than RcFDH and RsFDH. Based on the observed kinetic parameters it was possible to compare directly to literature (Table 8).

Table 8: Comparison of kinetic parameters to values listed in literature. 95% confidence intervals (CI) marked with '' are estimated based on error reported in literature and assuming normal distribution. 'ND': Not determined or not reported.*

Reaction	**Study**	**Enzyme**	**Condition**	**k_{cat} (min^{-1})** (95% CI)	**$K_{M,formate}$ (mM)** (95% CI)	**K_{M,NAD^+} (mM)** (95% CI)
Forward	This study	RcFDH	Tris/HCl buffer, pH 9.0, 30 °C	**4330** (4200 – 4470)	**0.36** (0.31 – 0.42)	**0.24** (0.29-0.29)
	(Hartmann and Leimkühler, 2013)			**2189** (2110 – 2270)*	**0.28** (0.26 – 0.30)*	**0.17** (0.13 – 0.21)*
Forward	This study	CnFDH	KPO_4 buffer, pH 7.7, 30 °C	**6770** (6340 – 7250)	**0.63** (0.51 – 0.78)	**0.13** (0.11 – 0.15)
	(Yu et al., 2019)			**5940** (ND)	**0.26** (ND)	**0.11** (ND)
	(Niks et al., 2016)			**12060** (11330 - 12790)*	**0.31** (0.30 – 0.32)*	**0.13** (0.12 - 0.14)*
	(Friedebold and Bowien, 1993)			**-**	**3.3** (ND)	**0.09** (ND)

Benchmarking the activity, a turnover number for RcFDH of 4330 min^{-1} at conditions identical to the ones reported by Hartmann and Leimkühler in 2013 is observed. Here, Hartmann and Leimkühler reported an activity of 2189 min^{-1} with an approximate saturation of 39% Mo and 48% Fe (Hartmann and Leimkühler, 2013). For this study, a higher Mo saturation and comparable Fe saturation was observed. The higher Mo saturation may partially explain the nearly double k_{cat} observed in this study relative to literature, but it may not paint the full picture. The K_M values for both formate and NAD^+ are slightly higher for this study, indicating a lower binding affinity towards the substrates for the enzyme produced in this study. This could add to a story of an enzyme population that catalyses a faster reaction but somehow also interacts with phosphate and is substrate-inhibited at pH 7.

Similarly, it is possible to benchmark the results for CnFDH. Yu et al. recombinantly expressed and characterized CnFDH in 2019 and reported an observed turnover number of 5940 min^{-1} with a co-factor saturation of approximately 50%. This co-factor saturation was estimated based on a comparison between the observed turnover number for natively expressed CnFDH of 12060 min^{-1} (Niks et al., 2016) and the turnover number of the recombinantly expressed CnFDH. Assuming that native expression allows complete co-factor saturation, 50% turnover number for recombinantly expressed CnFDH relative to natively expressed CnFDH, means 50% co-factor saturation (Yu et al., 2019). If one were to do the same calculation for this study, the observed k_{cat} of 6770 min^{-1} corresponds to general co-factor saturation of 56%. This value corresponds reasonably well with the calculated metal saturation of 50% Fe and 87% Mo observed for CnFDH of this study.

In conclusion, high formate oxidation activities were observed and these correlated well with kinetic parameters reported for previous studies when taking co-factor saturation into account. This is an important observation as it demonstrates a reasonable reproduction of previous results, corroborating the validity of both the kinetic parameters reported in this thesis, but also the kinetic parameters reported previously. Additionally, the substrate inhibition observed for the dimerization experiments described in Section 4.3.2 was observed again, albeit at a less pronounced extent.

4.5.2. CO_2 reduction

CO_2 reduction assays were performed significantly differently than formate oxidation. The main differentiator is the requirement of anaerobic reaction conditions to avoid false positive signals. Applying saturated buffers, as described in method Section 4.2.2, steady state kinetics on the three FDHs were performed (Figure 26).

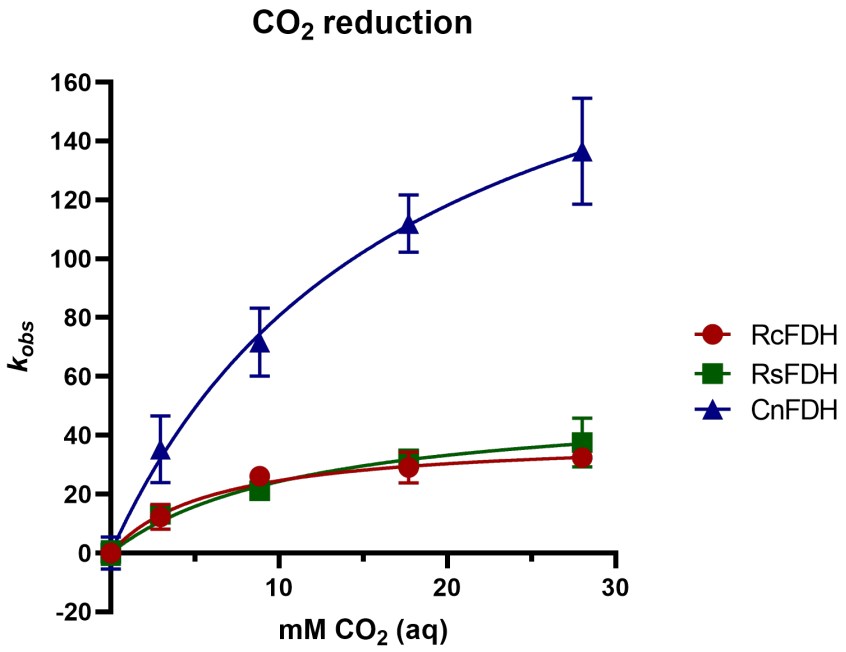

Figure 26: Comparison of steady state kinetics of CO_2 reduction for recombinantly expressed type 5 FDHs. Reactions were completed at optimum pH and optimum temperature determined in this study. All reactions were completed in 100 mM potassium phosphate, 100 mM Tris/HCl buffer with 0.2 mM NADH, at ambient pressure and in anaerobic conditions. The range of CO_2 substrate concentrations was achieved by mixing buffer saturated with either nitrogen or CO_2.

Here, it is evident that CnFDH again catalyzes the measured reaction at significantly higher rates than RcFDH and RsFDH. It is simply a much faster enzyme.

Another, more troubling observation, is that a complete saturation is not observed as expected. This is also evident when fitting the observed values to a Michaelis-Menten model and seeing the rather high $K_{M,CO2}$ values derived from the fit (Table 9).

Table 9: Observed reverse reaction kinetic parameters from a fitted Michaelis-Menten model. For each value a confidence interval (CI) at 95% confidence is given when possible. (-): Not applicable.

		Reverse reaction (CO_2 reduction)	
		k_{cat} (min^{-1}) (95% CI)	**$K_{M,CO2}$ (mM)** (95% CI)
RcFDH	Tris/HCl buffer, Optimum conditions, (41.4 °C, pH 8.4)	**39.5** (33.0-50.0)	**6.1** (3.1-12.4)
	KPO_4 buffer, 30 °C, pH 7.0	**36.1** (29.1 – 43.1)	**-**
RsFDH	Tris/HCl buffer, Optimum conditions, (49.9 °C, pH 7.4)	**52.5** (39.4-80.4)	**11.6** (5.3-27.4)
	KPO_4 buffer, 30 °C, pH 7.0	**43.6** (38.0 – 49.2)	**-**
CnFDH	Tris/HCl buffer, Optimum conditions, (45.7 °C, pH 7.3)	**221** (172-320)	**17.5** (9.9-34.2)
	KPO_4 buffer, 30 °C, pH 7.0	**127** (92.5 – 167)	**-**

The kinetic parameters observed for this study could then be compared to kinetic parameters described in previous studies (Table 10).

Table 10: Comparison of kinetic parameters with kinetic parameters described in previous studies. '': Not able to determine.*

Reaction	**Study**	**Enzyme**	**Condition**	**k_{cat} (min^{-1})**	**$K_{M,CO2}$ (mM)**	**$K_{M,NADH}$ (mM)**
Reverse	This study	RcFDH	KPO_4 buffer, pH 7.0, 30 °C, $CO_{2(aq)}$	**36.1** (29.1 – 43.1)	**-**	**-**
	(Hartmann and Leimkühler, 2013)		KPO_4 buffer, pH 6.8, 30 °C, HCO_3^-	**89** (87 – 91)	**-**	**-**
Reverse	This study	CnFDH	KPO_4 buffer, pH 7.0, 30 °C	**127** (92.5 – 167)	**-**	**-**
	(Yu et al., 2017)			**660** (612 – 708)	**2.7** (2.1 – 3.3)	**0.046** (0.045 – 0.047)

CnFDH has been studied with aqueous CO_2 as substrate (Yu et al., 2017). The variant of CnFDH in this study was purified from a native culture of *C. necator* and as a result likely to be composed of close to 100% active protein. Here, they achieved a k_{cat} of 660 min^{-1}. This is more than 4-fold higher than the k_{cat} of 127 min^{-1} that was observed for CnFDH produced for this study characterized under identical conditions to those reported by Yu et al. For formate oxidation, it was observed that the CnFDH produced for this study had a similar, even slightly higher, catalytic rate than CnFDH characterized in literature by Yu et al. However, it now appears to be the opposite trend for CO_2 reduction. If the

enzyme produced for this study displays 56% catalytic rate relative to natively produced CnFDH as calculated in Section 4.5.1, then a CO_2 reduction k_{cat} of approximately 370 min^{-1} should have been observed – almost 3-fold higher than the actually observed k_{cat} of only 127 min^{-1}. This further corroborates the suspicion that CO_2 saturation was not achieved.

RcFDH has previously been studied with 100 mM bicarbonate as a substitute CO_2 substrate. However, the actual aqueous CO_2 concentration of this study is unknown. Nonetheless, a k_{cat} of 89 min^{-1} was achieved indicating either a high level of bicarbonate shifting to CO_2 or false positive measurements. In comparison, the RcFDH produced for this study achieved a k_{cat} of 36 min^{-1}. Without clear saturation it is unknown if this value corresponds to the actual k_{cat} for CO_2 reduction, and as it was observed for CnFDH the value for RcFDH is likely biased by the assay.

In conclusion, although it can be confirmed that CnFDH has a significantly higher catalytic rate also for the reverse reaction relative to RcFDH and RsFDH, it must also be concluded that the observed activities are too low compared to expected values. It is suspected that the applied method does not allow for complete saturation of substrate or inhibits the FDHs in another way.

4.5.3. Ratio of forward and reverse reaction rates

As mentioned above, it is suspected that the catalytic rates observed for the reverse reactions are below the potentially achieved rates. Nonetheless, the ratio between the forward and reverse reaction may provide insight into the three enzymes' suitability to perform in a CCU setting when compared to one another (Table 11). This is assuming that all three enzymes are equally inhibited by the method for the reverse reaction.

Table 11: Ratio of k_{cat} for the forward reaction over the k_{cat} of the reverse reaction for each of the three type 5 FDHs. Values are given as percentage relative rate of the reverse reaction compared to the forward reaction. E.g. for CnFDH a reverse reaction rate of 127 min^{-1} corresponds to 1.9% of the forward reaction rate of 6770 min^{-1}.

	Relative rate (%)		
Condition	RcFDH	RsFDH	CnFDH
Tris/HCl buffer, optimum pH, optimum temp.	0.7	3.8	1.9
Potassium phosphate buffer, pH 7.0, 30 °C	4.7	3.4	2.0

Again, RcFDH stands out by having a large difference between the ratios calculated for the optimum condition compared to those for pH 7.0 and 30 °C in KPO_4 buffer. However, previously it was observed that RcFDH was strongly substrate-inhibited at pH 7.0 in KPO_4 buffer. As such, the ratio at this condition becomes biased.

In contrast, both RsFDH and CnFDH display similar ratios for both conditions. Interestingly, despite CnFDH being a faster enzyme, it appears that RsFDH is more prone to catalyze the reverse reaction. This is an interesting observation, in regard to future studies. Should a structural model of the two enzymes be presented, it would be interesting to look into the differences in structure in an attempt to explain why RsFDH is more prone to CO_2 reduction than CnFDH. It is possible that the very structure that allows CnFDH to achieve higher catalytic rates, is also a structure that favors formate oxidation.

In conclusion, although RsFDH displays lower catalytic rates, the increased propensity for CO_2 reduction is of interest.

4.6. Oxygen tolerance

As discussed in Chapter 1, CO_2 as a resource is fairly diverse concept. The cheapest sources of CO_2 are the least processed. This means that other gasses and vapors will be present in a scenario where a cheap CO_2 source is used as substrate. Of the many impurities, oxygen is likely significantly represented. Additionally, a completely anaerobic conversion unit is, under any earthly circumstances, significantly more expensive to operate than a one where oxygen is present in small quantities.

Other impurities to consider would NO_x gasses from impure combustion, or H_2S from biogas. While interesting, these gasses were not studied due to challenges with toxicity and time constraints.

4.6.1. Oxygen tolerance of candidate FDH

As mentioned several times in this thesis, CnFDH and RcFDH have been claimed to be oxygen tolerant. Or rather, more specifically, they have been claimed to be oxygen tolerant in the presence of KNO_3. (Friedebold and Bowien, 1993; Hartmann and Leimkühler, 2013; Niks et al., 2016; Yu et al., 2017).

Both azide and nitrate ions have been shown to stabilize CnFDH under aerobic conditions. However, both azide and nitrate acts as a competitive inhibitors, with 5 mM NaN_3 reducing formate oxidation activity of CnFDH by 86% and 10 mM KNO_3 reducing formate oxidation activity of CnFDH by 38% (Friedebold and Bowien, 1993). In this regard, it can be speculated that the manner with which nitrate and azide ions inhibit the type 5 FDHs is by interacting with the same domain on the protein as the oxygen. And since a inhibitory effect is observed, it is likely that this interaction involves the active site.

To test the extent of oxygen tolerance of type 5 FDHs, an experiment was devised. Here the enzymes were incubated with either 0.5 mM KNO_3 or 10 mM_3 KNO_3 at room temperature in Tris/HCl buffer, pH 8 that was allowed to be saturated with ambient air for 10 minutes. This should allow an approximate concentration of O_2 of 0.25 mM and be representative of practical oxygen concentration to be expected in an actual application. Additionally, it was tested if any significant difference between FDH in either αβγ or $(αβγ)_2$ conformation was observed. Formate oxidation activity was measured was measured as described previously in Section 4.2.1 every two minutes for a total of six measurements (t=0, 2, 4, 6, 8, and 10 minutes).

The experiment was started by addition of 50 µl enzyme stock, containing 10 mM KNO_3, to 950 µl of either of the two prepared buffers. The buffer and enzyme were briefly mixed, before 10 µl of the buffer/enzyme mix were used to measure formate oxidation activity was measured as described previously in Section 4.2.1. From addition of enzyme to the buffer to initiating the activity assay, approximately 15 seconds transpired. The experiments were repeated in duplicates.

The observed catalytic rates at each time-point could then be plotted for comparison (Figure 27).

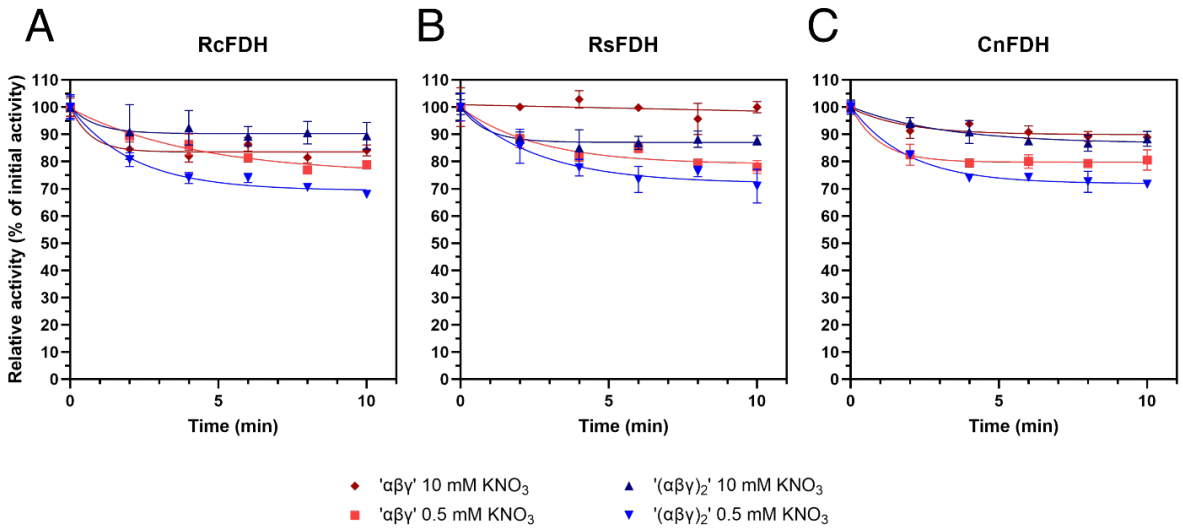

Figure 27: Time decay study of type 5 FDHs in either the heterotrimer-monomer (αβγ) or heterotrimer-dimer ((αβγ)$_2$) conformation in the presence of either 0.5 mM or 10 mM KNO_3. Formate oxidation activity was measured on enzyme incubated in 25 °C Tris/HCl buffer, pH 8. Importantly the buffer was prepared and stored at aerobic conditions prior to introduction of enzyme. FDHs in either αβγ (circle and square) or (αβγ)$_2$ (triangles) conformation were studied.

From Figure 27, it can be seen that even at 10 mM KNO_3 a slight decay trend for all but RsFDH in αβγ conformation was observed. This is in contradiction with the previous notion of complete oxygen tolerance in the presence of KNO_3. It should be noted that the initial activity (at t = 0) for all enzymes did not change over time between replicates on the same enzyme stock sample. When stored on ice at 10 mM KNO_3 no obvious or large change in activity was observed over an 8-hour period. It is however likely that a similar decay is observed, albeit at a much slower rate.

The activity change over time could be fitted to a one-phase decay model. For FDHs at 10 mM KNO_3 the model was mostly unable to predict half-lives due to the relatively limited drop in activity over time (Table 12).

Table 12: Predicted plateaus and half-lives of type 5 FDHs based on a one-phase decay model. '-': The model was unable to dependably predict this value.

		RcFDH		**RsFDH**		**CnFDH**	
		$(\alpha\beta\gamma)_2$	αβγ	$(\alpha\beta\gamma)_2$	αβγ	$(\alpha\beta\gamma)_2$	αβγ
0.5 mM KNO_3	Plateau (% activity) (95% CI)	69 (66-72)	75 (64-80)	72 (64-76)	79 (65-83)	72 (70-74)	80 (78-81)
	Half-life (min) (95% CI)	1.5 (1.0-2.3)	2.9 (1.7-6.7)	1.8 (1.0-3.9)	1.8 (0.7-6.8)	1.3 (0.9-1.7)	-
10 mM KNO_3	Plateau (% activity) (95% CI)	90 (88-92)	84 (82-85)	87 (85-89)	-	87 (77-89)	90 (89-92)
	Half-life (min) (95% CI)	-	-	-	-	2.1 (0.9-7.4)	-

From Figure 27 as well as the predicted plateaus and half-life values, it is evident that 10 mM KNO_3 stabilizes the FDHs to larger extent when compared to 0.5 mM KNO_3. For all three candidate enzymes a 20-31% drop in activity relative to initial activity (t = 0) is observed at 0.5 mM KNO_3. In comparison at 10 mM KNO_3 only a 10-14% reduction is observed. This clearly confirms that nitrate has a stabilizing effect as expected.

However, despite the reduction in activity being lower at 10 mM KNO_3, the reduction is still significant. It is interesting that the relative activity reaches a plateau. The plateau suggests one of two potential dynamics at play: Either the FDH population is heterogeneous, with a fraction of the enzymes being more oxygen sensitive than the rest, or an equilibrium between FDH-oxygen affinity and FDH-nitrate affinity is reached.

In summary, it was not possible to confirm the hypothesis that the type 5 FDHs are fully oxygen tolerant in the presence of KNO_3. Only RsFDH displayed no significant reduction in activity (Figure 27B).

4.7. Synthesis with FDHs

As presented in Chapter 1 of this thesis, ideal enzymatic candidates to operate in a CCU context are both fast and robust. An addendum to this rationalization would be, that the ideal enzyme would also favor CO_2 conversion over the opposite reaction. In this regard the third hypothesis, that type 5 FDH catalyze the reverse reaction a 100-fold faster than the forward reaction, can be refuted given that much fold changes are observed.

Furthermore, it can be observed that the first hypothesis of this chapter on pH optima being higher for the forward reaction, cannot be supported by the data presented for this thesis.

However, when comparing RcFDH, RsFDH, and CnFDH, it is readily apparent that CnFDH is a much more active protein than RcFDH and RsFDH. Interestingly, RsFDH shows a higher propensity for catalyzing the reverse reaction. Furthermore, it can be argued that RsFDH are less prone to inactivation with oxygen. Although the second hypothesis of this chapter, that type 5 FDHs are oxygen tolerant could be partially refuted given that complete enzyme population is not oxygen tolerant, a major fraction reaches a stable plateau depending on nitrate concentration. And here RsFDH distinguishes itself via minimum effect of oxygen when in αβγ confirmation with 10 mM KNO_3.

In a study by Min et al. from 2020, catalytic parameters of select FDHs are compared to catalytic parameters of the FDH of *Rhodobacter aestuarii* (RaFDH). RaFDH showed a k_{cat} for CO_2 reduction of 48.3 min^{-1}. This in itself is not remarkable, however, RaFDH also demonstrated a k_{cat} for formate oxidation of just 15.6 min^{-1} (Min et al., 2020). In other words, the catalytic rate of the reverse reaction is 309% of the catalytic rate of the forward reaction. In other words, the enzyme appears more prone to reduce CO_2 than to oxidize formate.

It would be interesting to compare the structural differences of the fast CnFDH with the slower, but more CO_2 reduction prone, RsFDH and RaFDH. For now, although CnFDH is less prone to CO_2 reduction than RsFDH, it displays several-fold higher turnover numbers. In terms of oxygen sensitivity, both enzymes reach a plateau of approximately 90% remaining activity when in $(\alpha\beta\gamma)_2$ conformation. However, interestingly, as the only variant, RsFDH in αβγ conformation show very slow decay relative to RcFDH and CnFDH in the presence of 10 mM KNO_3. It is possible that RsFDH not only is more prone for CO_2 reduction but also more oxygen tolerant.

In conclusion, type 5 FDHs are not completely oxygen tolerant, but display higher preference for CO_2 reduction than expected. CnFDH in conjunction with more oxygen tolerant FDH variants such as RsFDH, are interesting candidates for further study in a CCU context.

In parallel, of more scientific interest, particularly RcFDH has displayed some interesting kinetic phenomena. It appears that the enzyme is particularly substrate-inhibited at pH 7, and less at pH 7.7 and higher. Additionally, it appears that phosphate somehow also interacts with the FDHs.

In summary, indications of an intricate interplay between the following were observed:

- Oxygen appears to irreversible inhibit part of the enzyme population.
- Nitrate ions stabilize and protect the enzyme from oxygen, potentially by interacting with the same domains that are vulnerable to oxygen damage. However, it also acts as a competitive inhibitor.
- Oxygen inhibition appears to also be dependent on temperature. Enzymes stored on ice under aerobic conditions for a full day are not observed to lose specific activity. Enzymes stored at room temperature (25 °C), however, did decay to a stable plateau over a short period of time.
- Phosphate also interacts with type 5 FDHs, causing the maximum turnover rate to increase. However, presence of phosphate also amplifies substrate inhibition.
- Particularly RcFDH, but also RsFDH, displays full or partial substrate inhibition (forward reaction only) at pH 7.0 and pH 7.7. This effect seems amplified by presence of phosphate.
- The substrates, particularly CO_2, are highly dependent on pressure, temperature and pH. CO_2 is in a constant equilibrium between its gaseous and aqueous states. Additionally, it reacts with water to form bicarbonate.
- The enzyme population itself is likely not completely homogenous. When expressed recombinantly, the enzymes are not fully saturated with co-factor. It is unknown how the distribution of co-factors is among the enzyme population.

All of the above form a delicate equilibrium that does not settle immediately. As such, timing become another significant factor when studying these enzymes. The interplay between the many factors that govern FDH stability and turnover number is dynamic. Whether 1 mM KNO_3 or 2 mM KNO_3 is present matters. If the enzymes are stored at 0 °C or at room temperature matters. The reaction buffer concentration matters. It is an incredibly intricate system with a host of known, and unknown, parameters.

Chapter 5. Perspectives on application

With an understanding of the CCU-relevant catalytic properties of the oxygen pseudo-tolerant type 5 FDHs the obvious next step for this thesis is to assess the manner of application of these enzymes. Additionally, in the interest of gauging the potential of FDHs for CCU, the application potential of the reaction product, formate, is evaluated.

5.1. Application of FDHs for enzymatic electrosynthesis

As presented in Chapter 2, metal-dependent FDHs are able to interact with range of different electron carriers. This also includes electrodes. As argued in Chapter 1, electrochemical approaches have a great potential for replacing existing petrochemical production methods. In this context it is interesting to study the current knowledge and perspectives for FDHs as catalysts for enzymatic electrosynthesis (EES).

5.1.1. General design considerations

Electrosynthesis in general is a recently emerging field of study, with the majority of research revolving around fundamental and mechanistic understanding of the core CO_2 reduction reaction as well as development of catalysts. Even within more established non-biological systems, the primary challenge is up-scaling and implementation (Sánchez et al., 2019). This thesis will briefly discuss the most general considerations and possibilities for a device design that includes an FDH in a CO_2 reduction EES-setup. Four areas of considerations are presented below.

First of all, are considerations on electrode-enzyme interactions. The manner and efficiency with which electrons are transferred between electrode and enzyme is critical for performance. As mentioned in Section 2.3.2, the interactions are typically divided into mediated electron transfer (MET) and direct electron transfer (DET). MET is the simplest and most common method for transferring electrons. Here, a small redox active molecule (mediator) shuttles the electrons between electrode and an enzyme's co-factor. In DET, electrons are transferred directly from the electrode surface to the enzyme co-factor (Cadoux and Milton, 2020). MET is generally not considered scalable, as the mediator is expensive to replace when flushed away. Resultingly, DET in general or a MET system with a mediator stabilized in solid matrix are viewed as more feasible (Milton and Minteer, 2017).

For systems with either DET or solid matrix-MET, considerations on surface morphology become relevant. As an example, if an enzyme is immobilized on a planar surface, the orientation of the enzyme may be wrong, resulting in too large distance from the electrode to the electroactive co-factor (Sakai et al., 2018). This essentially renders a large part of the immobilized enzyme population inactive. In other words, the enzymes become inefficiently wired. If enzymes are immobilized in a 3D matrix, it increases the chances of having a contact point where electrons can transfer between electrode and electroactive co-factor, but introduces problems with mass transfer (Xiao et al., 2019). In summary, the options for both MET and DET are presently not explored to any great extent, and a significant gap still exists between studies on purified protein and actual application (Yuan et al., 2019).

Secondly, stability must be considered. In a recent review, Bernal et al. argue that combining protein engineering and immobilization of enzymes allows for an increase in overall performance. Enzymes are often stabilized after undergoing immobilization (Marpani et al., 2017). In the context of this thesis, it is important to emphasize that enzymes can be engineered both to be more suited for

immobilization (Bernal et al., 2018b), *and* to be more stable in general (Bommarius et al., 2010; Chen and Zeng, 2016). A good example is a carbonic anhydrase that was engineered to tolerate temperatures up 107 °C and extreme solvent conditions (Alvizo et al., 2014). Additionally, the electrode may be adjusted as well. One can alter the porosity and modify the surface chemically, resulting in an altered interaction between electrode and enzyme (Sakai et al., 2018). In summary, methods for stabilizing enzyme/electrode conformations are theoretically possible and under development.

Third are considerations on mass transfer for both substrate and product. Here, membrane diffusion systems or continuous flow are commonly considered the two most scalable solutions (Sánchez et al., 2019). In the context of CCU, electrodes allowing gas diffusion have been employed with success for circumventing mass transfer issues with the CO_2 substrate (Sakai et al., 2016; Szczesny et al., 2020). Beyond substrate supply, product removal is also a concern given the enzymes' propensity for formate oxidation. In a recent study, Szczesny and coworkers experimented with longer term CO_2 reduction and experienced that the formate product disappeared (Szczesny et al., 2020). They suspected that the product simply evaporated given its volatility. If true, this would be a simple mechanism to exploit for product removal, but in conclusion, mass transfer remains another parameter for optimization.

Finally, beyond the considerations of the electrochemical FDH catalyst design, it is worth mentioning that a host of other considerations must also be taken into account. In general, to implement the electrochemical technologies, an extremely large optimization problem must first be tackled. Like the existing and very well-established petrochemical industry, the electrochemical equivalent first needs to be fully developed. This means dealing with supply chains and logistics, and matching point sources to manufacturing scales. Combine this with the unpredictability of sustainable electricity production and a requirement to be profitable, and you have truly massive logistic problem to solve (De Luna et al., 2019).

In conclusion, although EES is being actively developed and studied, the technology as whole is still at a low technology readiness level (TRL) with significant design challenges that have yet to be optimized.

5.1.2. FDHs as electrochemical catalysts

Briefly looking at non-biological systems, formate can be produced electrochemically with faradaic activities at 95% with a current density of 50 mA/cm^2 with a lead catalyst (Lu et al., 2017), or at 84% with a current density of 133 mA/cm^2 (Li and Oloman, 2006). This is compared to FDH of *Syntrophobacter fumaroxidans* (SfFDH) immobilized on a graphite electrode with current density of only 0.08 mA/cm^2 but almost perfect faradaic efficiency (Reda et al., 2008). As a reminder, for electrochemistry, current density is a direct representation of catalytic rate, and faradaic efficiency represents the percentage of electrons used for the desired reaction.

To limit the scope of this thesis, non-biological systems will not be discussed further, but it is worth noting that the scientific community is working on developing and scaling viable solutions for electrochemical synthesis with CO_2 as substrate.

Since 2008, when the cornerstone study of SfFDH by Reda et al. was published, several other studies with FDH in an EES context have been published. FDH of *Clostridium ljugdahlii* (ClFDH) was immobilized on a conductive polymer hydrogel electrode resulting in a 92.7% faradaic efficiency. The current density was not reported (Kuk et al., 2019). FDH-H of *E. coli* was immobilized in a cobaltocene containing redox polymer achieving peak current densities of 0.06 mA/cm^2 and faradaic efficiencies

of 99% (Yuan et al., 2018). As a final example, DvFDH was immobilized in another redox active polymer achieving current densities of 0.33 mA/cm^2 with unreported faradaic efficiencies (Szczesny et al., 2020).

These studies are representative of the current state of the art with FDH in an EES context. Additionally, it should be mentioned that the above three studies were affected by very large uncertainties and challenges with reproducibility. Furthermore, since the enzymes were in fact immobilized in a 3D structure, this allowed several layers of enzymes to be present per cm^2. The higher current density observed for DvFDH of 0.33 mA/cm^2 can likely partially be contributed to multilayer structure. Additionally, for this particular study, gas diffusion was introduced which could have also contributed to increased rate.

Within EES, a recurring argument against the use of FDH is oxygen sensitivity (Cadoux and Milton, 2020). Introduction of circumstantially oxygen tolerant type 5 FDHs addresses some of these concerns. In this regard it is interesting that both RcFDH and CnFDH have been studied in electrochemical settings. However, both of these studies applied a MET method. RcFDH was shown to reduce CO_2 with methyl viologen as electron shuffle (Choi et al., 2018). For CnFDH, neutral red was used to regenerate NADH, which was then used as electron donor to reduce CO_2 as seen previously (Chen et al., 2018). For a discussion on application, it would interesting to study type 5 FDHs in a DET system.

Looking even further ahead than simply immobilizing whole enzymes on electrodes, one could look into only applying the relevant domain/subunit/truncated enzyme to reduce the complexity even further. For this study, a significant loss of activity was experienced when expressing RcFDH with the His-tag placed on FdsA, the α-subunit, was experienced, relative to His-tag placement on FdsG, the γ-subunit. It may be speculated that this could be due to a structural interference with FdsB, the β-subunit, resulting in a lack of the secondary NADH-oxidizing active site. However, a relatively high protein concentration was also observed, clearly identified via Western blot as the His-tagged FdsA. In other words, although unable to receive electron from oxidation of NADH, resulting in low activity, the protein was still soluble.

Interestingly, FdsA of CnFDH was recently studied in an electrochemical setting by Walker et. at (Walker et al., 2019). Here, it was shown that it is possible to immobilize FdsA on an planar surface electrode and catalyze formate oxidation. Personal correspondence with the corresponding author revealed that the expression and purification of the FdsA from CnFDH had not been trivial at all. Nonetheless, it is still an interesting path for further study. For the study, Walker et al. discussed the reduction potentials of the individual co-factors. They did not discuss application or observed rates. However, it is a promising demonstration of the possibility to apply truncated single subunit FDHs in an electrochemical setting.

In summary, FDH immobilized as a protein film on an electrode is not directly competitive with existing non-biological systems. However, EES in a CCU context demonstrates high selectivity and faradaic efficiency. Additionally, the methods are in the very early stages of development and major challenges in efficiency and electron transfer remain to be solved. If further studied, the use of FDH-based EES in the context of CCU holds some very exciting prospects for sustainable formate production (P. Chiranjeevi et al., 2019; Wu et al., 2020).

5.2. Downstream processing of formate

To discuss the relevance of FDHs, one has to discuss the relevance of formate. As presented in Section 1.2, formate and formic acid have a range of existing applications. In these, formate produced from CO_2 can directly substitute petrochemically-produced formate. However, the truly exciting promises of formate production lie in novel applications: Formate has been argued to be strong candidate for hydrogen storage or to be used directly in formate fuel cells (An and Chen, 2017, 2016; Enthaler et al., 2010; Mellmann et al., 2016; Singh et al., 2015). Simply put, formate would act as a fuel for personal transportation in place of gasoline and diesel.

However, both the hydrogen economy, and certainly also formate fuel cells, lack implementation. Whether the future of personal transport is based on fuel cells, batteries, or internal combustion engines is up for debate and falls outside of the scope of this thesis.

However, apart from producing formate for hydrogen storage or fuel cells, formate also holds other promises. As will be discussed below, formate may become a foundational building block or substrate to be used in industrially relevant chemical and biological reactions.

5.2.1. Formate to other chemicals

In an enzymatic context, the cascade reaction from CO_2 to methanol has received a great deal of attention. Already in 1999, the first cascade reaction with FDH, formaldehyde dehydrogenase (FaldDH), and alcohol dehydrogenase (ADH) converting CO_2 via formaldehyde to methanol was demonstrated (Obert and Dave, 1999) (Figure 28).

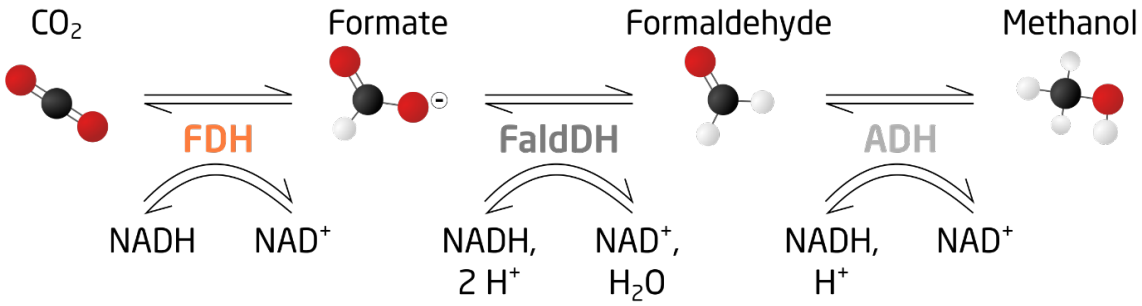

Figure 28: Cascade reaction from CO_2 to methanol via formate and formaldehyde. The cascade reaction is catalyzed by formate dehydrogenase (FDH), formaldehyde dehydrogenase (FaldDH), and alcohol dehydrogenase (ADH) with NADH as electron donor for all three reactions.

This cascade reaction has since been studied extensively. For the cascade reaction, most commonly the metal-independent CbFDH (FDH of *Candida boidinii*) was used in conjunction with a FaldDH of *Pseudomonas putida* (PpFaldDH) and an ADH of *Saccharomyces cerevisiae* (ScADH) (Cazelles et al., 2013; Luo et al., 2015; Wang et al., 2014). All of these enzymes are commercially available, allowing easy execution of enzymatic experiments, but hindering quantification of turnover number since the concentration of enzyme molecules is unknown (Cazelles et al., 2013). This also makes it difficult to compare experiments.

The current state of the art for this cascade reaction is now claiming to be 81-fold faster than the best version of the original CbFDH-PpFaldDH-ScADH cascade. The primary contributor to this increase is a much faster zinc-containing FaldDH of *Burkholderia multivorans* (BmFaldDH) as well as the slightly faster FDH of *Clostridium ljungdahlii* (ClFDH) (Singh et al., 2018). In absolute numbers, the 81-fold increase is an increase from 0.014 mM methanol/hr to 1.13 mM methanol/hr. This maximum rate is

corresponding to 35.2 mg/L hr^{-1}. Formaldehyde production without ADH was slower at approximately 0.5 mM/hr. This slower reaction rate is likely due to lack of product removal as the enzymes were added in a ratio of 2.5 U FDH, 2.5 U FaldDH, and 50 U ADH for the full cascade (Singh et al., 2018).

The low production rate, even with the massive optimization effort achieved in the last two decades, is due to the reaction still depending on NADH (regenerated or not) to drive the reaction. As shown in Chapter 2, this induces very low rates. If this reaction were to be scaled, a 1000 L reaction volume would produce only 845 g methanol per day. This is equivalent to 1.07 L of pure methanol worth approximately 0.3 €. At such a low economic gain, it is highly unlikely that the cascade reaction, in its current form, will ever become industrially relevant.

If the above cascade pathway is to ever become viable, a solution without NADH will need to be developed. Electrochemical production of formate, with inspiration or application of FDH, may potentially prove a viable pathway. It is possible that a bio-electrochemical solution could also be found for reducing formate to formaldehyde and converting formaldehyde to methanol.

In summary, to the best of our understanding, formate is not an intermediate in any established chemical production. Nor do we know of any promising developing enzymatic methods for upgrading formate.

5.2.2. Formate as a feedstock for fermentation

Unlike the prospects as a chemical feedstock, using formate as a biological feedstock is incredibly exciting. Formate is preferable to other C1 feedstocks that can be produced from CO_2 (CO, methanol, methane, H_2/CO_2) in the sense that it is easy to store, completely water miscible, and supports up to 90% energy efficiency in microbial conversion (Claassens et al., 2019).

Additionally, since electrochemical formate production, e.g. using EES with FDHs, is very selective, it allows for implementation of defined culture media. This is oftentimes advantageous in large productions where predictability is a quality (Hahn-Hägerdal et al., 2005).

Formate has traditionally been neglected as a substrate since it has been more expensive than for instance H_2/CO_2 or CO. Another reason has been that formate is toxic to some, but not all, organisms. *E. coli* shows severe impairment (Zaldivar and Ingram, 1999) while acetogens like *Acetobacterium woodii* do not (Genthner and Bryant, 1987). This is generally limiting, but if using a tolerant strain, it could also be considered beneficial due to the reduced risk of contamination.

Formate can be incorporated into metabolites via several natural and synthetic pathways, under both aerobic and anaerobic conditions. Particularly, anaerobic bioproduction of ethanol, acetone, isopropanol, fatty acids, and fatty alcohols are currently neglected but promising production pathways (Cotton et al., 2020). In fact, if employing both natural and synthetic pathways just right, formate may become the ideal mediator between electricity-driven CCU and the biological realm (Bar-Even, 2016).

In summary, although no large-scale fermentation on formate has been implemented, it could very well become an extremely interesting venture for production of several in-demand chemical products and fuels.

5.3. Impact on CO_2 emissions

Due to the range of inherent uncertainties, it is rather daunting to estimate the impact of implementing a novel undeveloped technology on climate change. Essentially, large uncertainties are to be expected and as a result, the estimation of impact on CO_2 emissions will be ballpark estimates.

Here, it is important to clarify that the potential of FDH-mediated CCU is based on the substitution of existing *net-positive* production pathways with new CO_2- and electricity-based *net-neutral* production pathways.

As presented in Chapter 1, the current demand of formate/formic acid is approximately 0.85 Mt/yr. Current formate production is almost completely based on petrochemical processes (Hietala et al., 2016). With the knowledge that formate/formic acid readily degrades in nature releasing CO_2, disregarding the CO_2 emitted for the energy to drive the production, it can be conservatively estimated that 0.8 Mt/yr of net-positive CO_2 emission is due to formate production per year. This is of course a rough estimate. In other words, the impact of replacing unsustainable petrochemical production of formate causing net-positive CO_2 emission, with sustainable production with net-neutral emissions, is approximately 0.8 Mt of CO_2 per year.

In comparison, a large modern state-of-the-art 750 MW supercritical pulverized coal power plant, assuming it runs at 100% capacity, will generate 6.5 Mt CO_2/yr (Carlsson, 2014). The energy production corresponding to this emission is enough to provide the energy for 4.1 million average Danish people (Jyllandsposten, 2013). As such, the entire global formate production only contributes an eighth of the CO_2 emission of a single (albeit large) coal power plant.

However, as argued above, the potential of formate is not limited to its current uses. In a European Commission Joint Research Centre report from 2016, calculations on the potential of formic acid applied as hydrogen storage and used for fuel cells were presented. Here, depending on the scenario, reduction of CO_2 emissions between 12 and 57 Mt CO_2/yr would be possible. These numbers are for the EU alone, and based upon the broad introduction of hydrogen and formate fuel cells (Pérez-Fortes and Tzimas, 2016). A worldwide implementation would obviously cause a reduction in CO_2 emission that would be several times larger.

Apart from using formate for hydrogen storage, the exciting prospect of using formate as bulk substrate for fermentation also holds tremendous potential. It is difficult to gauge the realistic size that chemical production based on formatotrophs could reach, but the demand for the potential products produced with formatotrophs amounts to several hundreds of Mt/yr, with particularly fuel ethanol being a high impact chemical if implemented (Munkajohnpong et al., 2020; Panjapakkul and El-Halwagi, 2018, Renewable Fuels Association, 2019).

To summarize, a total yearly CO_2 emission of 41.000 Mt CO_2/yr needs to be replaced with sustainable alternatives, as presented in Chapter 1. In this regard the 0.81 Mt CO_2/yr emission related to formate is relatively negligible. However, formate has the potential to become a foundational compound in two separate sustainable solutions: formate as hydrogen storage, and formate as bulk substrate for fermentation. If either of these solutions will be implemented at worldwide scale, the potential reduction in CO_2 emission could reach several hundreds of Mt CO_2/yr.

Conclusion

This thesis represents a consolidation and expansion of the existing knowledge on the application of FDHs in the context of CCU.

Specifically, this thesis presents a novel classification scheme for metal-dependent FDHs. This provides terminology to describe the inherent diversity of these remarkable enzymes allowing for improved discussions. Additionally, via this classification scheme, it was possible to demonstrate how proposed oxygen tolerant FDHs group into a single sub-type: The type 5 FDHs. As representatives of type 5 FDHs, RcFDH, RsFDH, and CnFDH were studied and compared to previously reported results.

It can be concluded, contrary to previously discussed recommendations on expression that the current best method for expression of type 5 FDHs includes LB media and high growth rates. However, co-factor saturation with this method is still approximately only half of full saturation beckoning further improvements to be made.

This thesis constitutes the first study where multiple metal-dependent FDHs, previously described in separate studies, have been expressed and characterized in parallel. In this manner, this thesis actively contributes to the consolidation of existing literature.

The type 5 FDHs display high formate oxidation rates with 20-50 times lower CO_2 reduction rates. Interestingly, although CnFDH displays the highest catalytic rate for both the forward and reverse reaction, RsFDH displays a higher preference for CO_2 reduction as well as potential for increased oxygen tolerance. Additionally, the enzymes display complex interactions with nitrate, phosphate, and molecular oxygen in conjunction with the intended substrates. In conclusion, although further research is warranted, type 5 FDHs are interesting candidates to study as model enzymes for CO_2 reduction.

Furthermore, the advent of EES reveals new opportunities. The combination of EES with type 5 FDHs could prove extremely interesting for efficient and selective production of formate. However, low TRLs for both EES and FDH application currently prevent the technology from being implemented. Nonetheless, the potential of a formate-based chemical industry represents an impactful alternative to current petrochemical production.

By describing the diversity, nuances, and characteristics of the metal-dependent type 5 FDHs, this thesis supports and expands the knowledgebase that could lead to large-scale use of type 5 FDH-based catalysts as part of a sustainable future.

References

Adnan, Ong, Nomanbhay, Chew, Show, 2019. Technologies for Biogas Upgrading to Biomethane: A Review. Bioengineering 6, 92. https://doi.org/10.3390/bioengineering6040092

Afshar, A.A.N., 2014. Chemical profile: Formic acid, TranTech Consultants, Inc.

Al-Mamoori, A., Krishnamurthy, A., Rownaghi, A.A., Rezaei, F., 2017. Carbon Capture and Utilization Update. Energy Technol. 65409, 834–849. https://doi.org/10.1002/ente.201600747

Alissandratos, A., Kim, H.-K., Matthews, H., Hennessy, J.E., Philbrook, A., Easton, C.J., 2013. Clostridium carboxidivorans Strain P7T Recombinant Formate Dehydrogenase Catalyzes Reduction of CO 2 to Formate. Appl. Environ. Microbiol. 79, 741–744. https://doi.org/10.1128/AEM.02886-12

Alpdağtaş, S., Yücel, S., Kapkaç, H.A., Liu, S., Binay, B., 2018. Discovery of an acidic, thermostable and highly NADP+ dependent formate dehydrogenase from Lactobacillus buchneri NRRL B-30929. Biotechnol. Lett. 40, 1135–1147. https://doi.org/10.1007/s10529-018-2568-6

Alvizo, O., Nguyen, L.J., Savile, C.K., Bresson, J. a, Lakhapatri, S.L., Solis, E.O.P., Fox, R.J., Broering, J.M., Benoit, M.R., Zimmerman, S. a, Novick, S.J., Liang, J., Lalonde, J.J., 2014. Directed evolution of an ultrastable carbonic anhydrase for highly efficient carbon capture from flue gas. Proc. Natl. Acad. Sci. U. S. A. 111, 16436–41. https://doi.org/10.1073/pnas.1411461111

Amao, Y., 2018. Formate dehydrogenase for CO2utilization and its application. J. CO2 Util. https://doi.org/10.1016/j.jcou.2018.06.022

An, L., Chen, R., 2017. Mathematical modeling of direct formate fuel cells. Appl. Therm. Eng. 124, 232–240. https://doi.org/10.1016/j.applthermaleng.2017.06.020

An, L., Chen, R., 2016. Direct formate fuel cells: A review. J. Power Sources 320, 127–139. https://doi.org/10.1016/j.jpowsour.2016.04.082

Andersen, C.B., 2002. Understanding carbonate equilibria by measuring alkalinity in experimental and natural systems. J. Geosci. Educ. 50, 389–403. https://doi.org/10.5408/1089-9995-50.4.389

Aouini, I., Ledoux, A., Estel, L., Mary, S., 2014. É tude du captage du CO2dans des gaz de combustion d'un incinérateur de déchets à l'aide d'un pilote utilisant un solvant à base de MEA. Oil Gas Sci. Technol. 69, 1091–1104. https://doi.org/10.2516/ogst/2013205

Apaydin, D.H., Schlager, S., Portenkirchner, E., Sariciftci, N.S., 2017. Organic, Organometallic and Bioorganic Catalysts for Electrochemical Reduction of CO2. ChemPhysChem 18, 3094–3116. https://doi.org/10.1002/cphc.201700148

Arachchige, U.S.P.R., Melaaen, M.C., 2012. Aspen plus simulation of CO2 removal from coal and gas fired power plants. Energy Procedia 23, 391–399. https://doi.org/10.1016/j.egypro.2012.06.060

Aresta, M., Dibenedetto, A., Angelini, A., 2014. Catalysis for the valorization of exhaust carbon: From CO2 to chemicals, materials, and fuels. technological use of CO2. Chem. Rev. https://doi.org/10.1021/cr4002758

Aresta, M., Dibenedetto, A., Quaranta, E., 2016. State of the art and perspectives in catalytic processes for CO2 conversion into chemicals and fuels: The distinctive contribution of chemical catalysis and biotechnology. J. Catal. 343, 2–45. https://doi.org/10.1016/j.jcat.2016.04.003

Artz, J., Müller, T.E., Thenert, K., Kleinekorte, J., Meys, R., Sternberg, A., Bardow, A., Leitner, W., 2018. Sustainable Conversion of Carbon Dioxide: An Integrated Review of Catalysis and Life Cycle Assessment. Chem. Rev. https://doi.org/10.1021/acs.chemrev.7b00435

Aryal, N., Kvist, T., Ammam, F., Pant, D., Ottosen, L.D.M., 2018. An overview of microbial biogas enrichment. Bioresour. Technol. 264, 359–369. https://doi.org/10.1016/j.biortech.2018.06.013

Bailey, K.J., Gray, J.E., Walker, R.P., Leegood, R.C., 2007. Coordinate regulation of phosphoenolpyruvate carboxylase and phosphoenolpyruvate carboxykinase by light and CO2 during C 4 photosynthesis. Plant Physiol. 144, 479–486. https://doi.org/10.1104/pp.106.093013

Bajracharya, S., Sharma, M., Mohanakrishna, G., Dominguez Benneton, X., Strik, D.P.B.T.B., Sarma, P.M., Pant, D., 2016. An overview on emerging bioelectrochemical systems (BESs): Technology for sustainable electricity, waste remediation, resource recovery, chemical production and beyond. Renew. Energy 98, 153–170. https://doi.org/10.1016/j.renene.2016.03.002

Bar-Even, A., 2016. Formate Assimilation: The Metabolic Architecture of Natural and Synthetic Pathways. Biochemistry 55, 3851–3863. https://doi.org/10.1021/acs.biochem.6b00495

Barrett, K., Lange, L., 2019. Peptide-based functional annotation of carbohydrate-active enzymes by conserved unique peptide patterns (CUPP). Biotechnol. Biofuels 12, 102. https://doi.org/10.1186/s13068-019-1436-5

Berg, I.A., Kockelkorn, D., Ramos-Vera, W.H., Say, R.F., Zarzycki, J., Hügler, M., Alber, B.E., Fuchs, G., 2010. Autotrophic carbon fixation in archaea. Nat. Rev. Microbiol. https://doi.org/10.1038/nrmicro2365

Bernal, C., Rodríguez, K., Martínez, R., 2018a. Integrating enzyme immobilization and protein engineering: An alternative path for the development of novel and improved industrial biocatalysts. Biotechnol. Adv. https://doi.org/10.1016/j.biotechadv.2018.06.002

Bernal, C., Rodríguez, K., Martínez, R., 2018b. Integrating enzyme immobilization and protein engineering: An alternative path for the development of novel and improved industrial biocatalysts. Biotechnol. Adv. https://doi.org/10.1016/j.biotechadv.2018.06.002

Böhmer, N., Hartmann, T., Leimkühler, S., 2014. The chaperone FdsC for Rhodobacter capsulatus formate dehydrogenase binds the bis-molybdopterin guanine dinucleotide cofactor. FEBS Lett. 588, 531–537. https://doi.org/10.1016/j.febslet.2013.12.033

Bommarius, A.S., Blum, J.K., Abrahamson, M.J., 2010. Status of protein engineering for biocatalysts: how to design an industrially useful biocatalyst. Curr. Opin. Chem. Biol. 15, 194–200. https://doi.org/10.1016/j.cbpa.2010.11.011

Boyd, J.M., Ellsworth, H., Ensign, S.A., 2004. Bacterial acetone carboxylase is a manganese-dependent metalloenzyme. J. Biol. Chem. 279, 46644–46651. https://doi.org/10.1074/jbc.M407177200

Broussard, T.C., Price, A.E., Laborde, S.M., Waldrop, G.L., 2013. Complex formation and regulation of

escherichia coli acetyl-CoA carboxylase. Biochemistry 52, 3346–3357. https://doi.org/10.1021/bi4000707

Cadoux, C., Milton, R.D., 2020. Recent Enzymatic Electrochemistry for Reductive Reactions. ChemElectroChem 7, 1974–1986. https://doi.org/10.1002/celc.202000282

Canadell, J.G., Schulze, E.D., 2014. Global potential of biospheric carbon management for climate mitigation. Nat. Commun. 5. https://doi.org/10.1038/ncomms6282

Carlsson, J.E. Al, 2014. ETRI 2014. https://doi.org/10.2790/057687

Castillo, R., Oliva, M., Martí, S., Moliner, V., 2008. A Theoretical Study of the Catalytic Mechanism of Formate Dehydrogenase. J. Phys. Chem. B 112, 10012–10022. https://doi.org/10.1021/jp8025896

Cazelles, R., Drone, J., Fajula, F., Ersen, O., Moldovan, S., Galarneau, A., 2013. Reduction of CO2 to methanol by a polyenzymatic system encapsulated in phospholipids–silica nanocapsules. New J. Chem. 37, 3721. https://doi.org/10.1039/c3nj00688c

Chen, X., Cao, Y., Li, F., Tian, Y., Song, H., 2018. Enzyme-Assisted Microbial Electrosynthesis of Poly(3-hydroxybutyrate) via CO 2 Bioreduction by Engineered Ralstonia eutropha. ACS Catal. 8, 4429–4437. https://doi.org/10.1021/acscatal.8b00226

Chen, Y., Li, P., Noh, H., Kung, C.W., Buru, C.T., Wang, X., Zhang, X., Farha, O.K., 2019. Stabilization of Formate Dehydrogenase in a Metal–Organic Framework for Bioelectrocatalytic Reduction of CO2. Angew. Chemie - Int. Ed. 58, 7682–7686. https://doi.org/10.1002/anie.201901981

Chen, Z., Zeng, A.P., 2016. Protein engineering approaches to chemical biotechnology. Curr. Opin. Biotechnol. https://doi.org/10.1016/j.copbio.2016.07.007

Chiranjeevi, P, Bulut, M., Breugelmans, T., Patil, S.A., Pant, D., 2019. Current trends in enzymatic electrosynthesis for CO 2 reduction. Curr. Opin. Green Sustain. Chem. https://doi.org/10.1016/j.cogsc.2019.02.007

Chiranjeevi, P., Bulut, M., Breugelmans, T., Patil, S.A., Pant, D., 2019. Current trends in enzymatic electrosynthesis for CO 2 reduction. Curr. Opin. Green Sustain. Chem. https://doi.org/10.1016/j.cogsc.2019.02.007

Choe, H., Joo, J.C., Cho, D.H., Kim, M.H., Lee, S.H., Jung, K.D., Kim, Y.H., 2014. Efficient CO2-reducing activity of NAD-dependent formate dehydrogenase from Thiobacillus sp. KNK65MA for formate production from CO 2 gas. PLoS One 9. https://doi.org/10.1371/journal.pone.0103111

Chohan, U.W., 2018. The Double Spending Problem and Cryptocurrencies. SSRN Electron. J. https://doi.org/10.2139/ssrn.3090174

Choi, E., Yeon, Y.J., Min, K., Kim, Y.H., 2018. Communication—CO 2 Reduction to Formate: An Electro-Enzymatic Approach Using a Formate Dehydrogenase from Rhodobacter capsulatus. J. Electrochem. Soc. 165, H446–H448. https://doi.org/10.1149/2.0531809jes

Claassens, N.J., Cotton, C.A.R., Kopljar, D., Bar-Even, A., 2019. Making quantitative sense of electromicrobial production. Nat. Catal. 2, 437–447. https://doi.org/10.1038/s41929-019-0272-0

Claassens, N.J., Sousa, D.Z., dos Santos, V.A.P.M., de Vos, W.M., van der Oost, J., 2016. Harnessing the power of microbial autotrophy. Nat. Rev. Microbiol. 14, 692–706. https://doi.org/10.1038/nrmicro.2016.130

Cordas, C.M., Campaniço, M., Baptista, R., Maia, L.B., Moura, I., Moura, J.J.G., 2019. Direct electrochemical reduction of carbon dioxide by a molybdenum-containing formate dehydrogenase. J. Inorg. Biochem. 196, 110694. https://doi.org/10.1016/j.jinorgbio.2019.110694

Costa, K.C., Wong, P.M., Wang, T., Lie, T.J., Dodsworth, J.A., Swanson, I., Burn, J.A., Hackett, M., Leigh, J.A., 2010. Protein complexing in a methanogen suggests electron bifurcation and electron delivery from formate to heterodisulfide reductase. Proc. Natl. Acad. Sci. U. S. A. 107, 11050–11055. https://doi.org/10.1073/pnas.1003653107

Cotton, C.A., Claassens, N.J., Benito-Vaquerizo, S., Bar-Even, A., 2020. Renewable methanol and formate as microbial feedstocks. Curr. Opin. Biotechnol. 62, 168–180. https://doi.org/10.1016/j.copbio.2019.10.002

Cotton, C.A., Edlich-Muth, C., Bar-Even, A., 2018. Reinforcing carbon fixation: CO 2 reduction replacing and supporting carboxylation. Curr. Opin. Biotechnol. 49, 49–56. https://doi.org/10.1016/j.copbio.2017.07.014

Cserháti, M., Kriszt, B., Szoboszlay, S., Tóth, Á., Szabó, I., Táncsics, A., Nagy, I., Horváth, B., Nagy, I., Kukolya, J., 2012. De novo genome project of Cupriavidus basilensis OR16. J. Bacteriol. https://doi.org/10.1128/JB.06752-11

da Silva, S.M., Pimentel, C., Valente, F.M.A., Rodrigues-Pousada, C., Pereira, I.A.C., 2011. Tungsten and molybdenum regulation of formate dehydrogenase expression in Desulfovibrio vulgaris Hildenborough. J. Bacteriol. 193, 2909–2916. https://doi.org/10.1128/JB.00042-11

De Bok, F.A.M., Hagedoorn, P.L., Silva, P.J., Hagen, W.R., Schiltz, E., Fritsche, K., Stams, A.J.M., 2003. Two W-containing formate dehydrogenases (CO2-reductases) involved in syntrophic propionate oxidation by Syntrophobacter fumaroxidans. Eur. J. Biochem. 270, 2476–2485. https://doi.org/10.1046/j.1432-1033.2003.03619.x

De Luna, P., Hahn, C., Higgins, D., Jaffer, S.A., Jaramillo, T.F., Sargent, E.H., 2019. What would it take for renewably powered electrosynthesis to displace petrochemical processes? Science (80-.). 364. https://doi.org/10.1126/science.aav3506

Drake, H.L., Gößner, A.S., Daniel, S.L., 2008. Old acetogens, new light. Ann. N. Y. Acad. Sci. 1125, 100–128. https://doi.org/10.1196/annals.1419.016

Energinet Elsystemansvar, 2020. MILJØRAPPORT 2020: Redegørelse for miljøpåvirkning fra dansk el- og kraftvarmeproduktion for statusåret 2019.

Enthaler, S., von Langermann, J., Schmidt, T., 2010. Carbon dioxide and formic acid—the couple for environmental-friendly hydrogen storage? Energy Environ. Sci. 3, 1207. https://doi.org/10.1039/b907569k

Filippova, E.V., Polyakov, K.M., Tikhonova, T.V., Stekhanova, T.N., Boiko, K.M., Popov, V.O., 2005. Structure of a new crystal modification of the bacterial NAD-dependent formate dehydrogenase with a resolution of 2.1 A. Crystallogr. reports 50, 796–800. https://doi.org/10.2210/PDB2GO1/PDB

Fogal, S., Beneventi, E., Cendron, L., Bergantino, E., 2015. Structural basis for double cofactor specificity in a new formate dehydrogenase from the acidobacterium Granulicella mallensis MP5ACTX8. Appl. Microbiol. Biotechnol. 99, 9541–9554. https://doi.org/10.1007/s00253-015-6695-x

Friedebold, J., Bowien, B., 1993. Physiological and biochemical characterization of the soluble formate dehydrogenase, a molybdoenzyme from Alcaligenes eutrophus. J. Bacteriol. 175, 4719–4728. https://doi.org/10.1128/jb.175.15.4719-4728.1993

Fuchs, G., 2011. Alternative Pathways of Carbon Dioxide Fixation: Insights into the Early Evolution of Life? Annu. Rev. Microbiol. 65, 631–658. https://doi.org/10.1146/annurev-micro-090110-102801

Genthner, B.R.S., Bryant, M.P., 1987. Additional characteristics of one-carbon-compound utilization by Eubacterium limosum and Acetobacterium woodii. Appl. Environ. Microbiol. 53, 471–476. https://doi.org/10.1128/aem.53.3.471-476.1987

Girija, K.R., Sasikala, C., Ramana, C. V, Spröer, C., Takaichi, S., Thiel, V., Imhoff, J.F., 2010. Rhodobacter johrii sp. nov., an endospore-producing cryptic species isolated from semi-arid tropical soils. Int. J. Syst. Evol. Microbiol. https://doi.org/10.1099/ijs.0.011718-0

Goeppert, A., Czaun, M., Jones, J.P., Surya Prakash, G.K., Olah, G.A., 2014. Recycling of carbon dioxide to methanol and derived products-closing the loop. Chem. Soc. Rev. 43, 7995–8048. https://doi.org/10.1039/c4cs00122b

Granjon, T., Maniti, O., Auchli, Y., Dahinden, P., Buchet, R., Marcillat, O., Dimroth, P., 2010. Structure-function relations in oxaloacetate decarboxylase complex. Fluorescence and infrared approaches to monitor oxomalonate and Na+ binding effect. PLoS One 5, 1–10. https://doi.org/10.1371/journal.pone.0010935

Grimaldi, S., Schoepp-Cothenet, B., Ceccaldi, P., Guigliarelli, B., Magalon, A., 2013. The prokaryotic Mo/W-bisPGD enzymes family: A catalytic workhorse in bioenergetic. Biochim. Biophys. Acta - Bioenerg. 1827, 1048–1085. https://doi.org/10.1016/j.bbabio.2013.01.011

Guo, Q., Gakhar, L., Wickersham, K., Francis, K., Vardi-Kilshtain, A., Major, D.T., Cheatum, C.M., Kohen, A., 2016. Structural and Kinetic Studies of Formate Dehydrogenase from Candida boidinii. Biochemistry 55, 2760–2771. https://doi.org/10.1021/acs.biochem.6b00181

Hahn-Hägerdal, B., Karhumaa, K., Larsson, C.U., Gorwa-Grauslund, M., Görgens, J., van Zyl, W.H., 2005. Role of cultivation media in the development of yeast strains for large scale industrial use. Microb. Cell Fact. 4. https://doi.org/10.1186/1475-2859-4-31

Hartmann, T., Leimkühler, S., 2013. The oxygen-tolerant and NAD+-dependent formate dehydrogenase from Rhodobacter capsulatus is able to catalyze the reduction of CO2 to formate. FEBS J. 280, 6083–6096. https://doi.org/10.1111/febs.12528

Hartmann, T., Schwanhold, N., Leimkühler, S., 2015. Assembly and catalysis of molybdenum or tungsten-containing formate dehydrogenases from bacteria. Biochim. Biophys. Acta - Proteins Proteomics 1854, 1090–1100. https://doi.org/10.1016/j.bbapap.2014.12.006

Hayden, P.L., 2003. Carbonate Chemistry Applied to the Beverage Production of Still Water 1–12.

Held, P., 2007. Determination of NADH Concentrations with the Synergy ™ 2 Multi-Detection

Microplate Reader using Fluorescence or Absorbance. BioTek 6.

Hepburn, C., Adlen, E., Beddington, J., Carter, E.A., Fuss, S., Mac Dowell, N., Minx, J.C., Smith, P., Williams, C.K., 2019. The technological and economic prospects for CO2 utilization and removal. Nature 575, 87–97. https://doi.org/10.1038/s41586-019-1681-6

Hietala, J., Vuori, A., Johnsson, P., Pollari, I., Reutemann, W., Kieczka, H., 2016. Formic Acid, in: Ullmann's Encyclopedia of Industrial Chemistry. Wiley-VCH Verlag GmbH & Co. KGaA, Weinheim, Germany, pp. 1–22. https://doi.org/10.1002/14356007.a12_013.pub3

Hille, R., Hall, J., Basu, P., 2014. The mononuclear molybdenum enzymes. Chem. Rev. 114, 3963–4038. https://doi.org/10.1021/cr400443z

Hu, B., Harris, D.F., Dean, D.R., Liu, T.L., Yang, Z.Y., Seefeldt, L.C., 2018. Electrocatalytic CO2reduction catalyzed by nitrogenase MoFe and FeFe proteins. Bioelectrochemistry 120, 104–109. https://doi.org/10.1016/j.bioelechem.2017.12.002

Hügler, M., Sievert, S.M., 2011. Beyond the Calvin Cycle: Autotrophic Carbon Fixation in the Ocean. Ann. Rev. Mar. Sci. 3, 261–289. https://doi.org/10.1146/annurev-marine-120709-142712

Humphreys, C.M., Minton, N.P., 2018. Advances in metabolic engineering in the microbial production of fuels and chemicals from C1 gas. Curr. Opin. Biotechnol. 50, 174–181. https://doi.org/10.1016/j.copbio.2017.12.023

Ihara, M., Kawano, Y., Fujiwara, Y., Kodo, T., Mizuguchi, M., Mochiduki, Y., Kodoh, K., Okabe, A., Matsuno, I., 2015. Expression systems for soluble metal-dependent formate dehydrogenase. J. Photochem. Photobiol. A Chem. 313, 154–162. https://doi.org/10.1016/j.jphotochem.2015.06.028

IHS, 2016. Formic acid, Chemical Economics Handbook.

Intergovernmental Panel on Clima Change, 2013. Climate Change 2013. https://doi.org/10.1017/CBO9781107415324.Summary

Invitrogen, 2008. pTrcHis A, B, and C, Catalog no. V360-20.

Iobbi-Nivol, C., Leimkühler, S., 2013. Molybdenum enzymes, their maturation and molybdenum cofactor biosynthesis in Escherichia coli. Biochim. Biophys. Acta - Bioenerg. https://doi.org/10.1016/j.bbabio.2012.11.007

Jaganaman, S., Pinto, A., Tarasev, M., Ballou, D.P., 2007. High levels of expression of the iron-sulfur proteins phthalate dioxygenase and phthalate dioxygenase reductase in Escherichia coli. Protein Expr. Purif. 52, 273–279. https://doi.org/10.1016/j.pep.2006.09.004

Jenner, L.P., Butt, J.N., 2018. Electrochemistry of surface-confined enzymes: Inspiration, insight and opportunity for sustainable biotechnology. Curr. Opin. Electrochem. 8, 81–88. https://doi.org/10.1016/j.coelec.2018.03.021

Jeske, L., Placzek, S., Schomburg, I., Chang, A., Schomburg, D., 2019. BRENDA in 2019: a European ELIXIR core data resource. Nucleic Acids Res. 47, D542–D549. https://doi.org/10.1093/nar/gky1048

Johnke, B., 1996. Emissions From Waste Incineration. Intergov. Panel Clim. Chang. 455–468.

Joos, F., Spahni, R., 2008. Rates of change in natural and anthropogenic radiative forcing over the past 20,000 years. Proc. Natl. Acad. Sci. U. S. A. 105, 1425–1430. https://doi.org/10.1073/pnas.0707386105

Jormakka, M., Byrne, B., Iwata, S., 2003. Formate dehydrogenase - A versatile enzyme in changing environments. Curr. Opin. Struct. Biol. 13, 418–423. https://doi.org/10.1016/S0959-440X(03)00098-8

Jormakka, M., Törnroth, S., Byrne, B., Iwata, S., 2002. Molecular Basis of Proton Motive Force Generation: Structure of Formate Dehydrogenase. Science (80-.). 295, 1863–1868.

Kanamori, T., Kanou, N., Atomi, H., Imanaka, T., 2004. Enzymatic Characterization of a Prokaryotic Urea Carboxylase. J. Bacteriol. 186, 2532–2539. https://doi.org/10.1128/JB.186.9.2532-2539.2004

Katoh, K., Rozewicki, J., Yamada, K.D., 2017. MAFFT online service: multiple sequence alignment, interactive sequence choice and visualization. Brief. Bioinform. 1–7. https://doi.org/10.1093/bib/bbx108

Katoh, K., Standley, D.M., 2013. MAFFT multiple sequence alignment software version 7: Improvements in performance and usability. Mol. Biol. Evol. 30, 772–780. https://doi.org/10.1093/molbev/mst010

Keith, D.W., Holmes, G., St Angelo, D., Heidel, K., 2018. A Process for Capturing CO 2 from the Atmosphere. Joule 2, 1573–1594. https://doi.org/10.1016/j.joule.2018.05.006

Kuk, S.K., Gopinath, K., Singh, R.K., Kim, T.D., Lee, Y., Choi, W.S., Lee, J.K., Park, C.B., 2019. NADH-Free Electroenzymatic Reduction of CO2 by Conductive Hydrogel-Conjugated Formate Dehydrogenase. ACS Catal. 9, 5584–5589. https://doi.org/10.1021/acscatal.9b00127

Lal, D., Nayyar, N., Kohli, P., Lal, R., 2013. Cupriavidus metallidurans: A Modern Alchemist. Indian J. Microbiol. 53, 114–115. https://doi.org/10.1007/s12088-013-0355-6

Le, S.Q., Gascuel, O., 2008. An improved general amino acid replacement matrix. Mol. Biol. Evol. 25, 1307–1320. https://doi.org/10.1093/molbev/msn067

Leimkühler, S., 2020. The biosynthesis of the molybdenum cofactors in Escherichia coli. Environ. Microbiol. 22, 2007–2026. https://doi.org/10.1111/1462-2920.15003

Lemaire, O.N., Jespersen, M., Wagner, T., 2020. CO2-Fixation Strategies in Energy Extremophiles: What Can We Learn From Acetogens? Front. Microbiol. 11, 1–8. https://doi.org/10.3389/fmicb.2020.00486

Lenger, R., Herrmann, U., Gross, R., Simon, J., Kroger, A., 1997. Structure and function of a second gene cluster encoding the formate dehydrogenase of Wolinella succinogenes. Eur. J. Biochem. 246, 646–651.

Lennon, J.T., Locey, K.J., 2016. The underestimation of global microbial diversity. MBio 7, 2016. https://doi.org/10.1128/mBio.01298-16

Li, H., Oloman, C., 2006. Development of a continuous reactor for the electro-reduction of carbon dioxide to formate - Part 1: Process variables. J. Appl. Electrochem. 36, 1105–1115. https://doi.org/10.1007/s10800-006-9194-z

Li, S., Song, Y.E., Baek, J., Im, H.S., Sakuntala, M., Kim, M., Park, C., Min, B., Kim, J.R., 2020. Bioelectrosynthetic conversion of CO2 using different redox mediators: Electron and carbon balances in a bioelectrochemical system. Energies 13. https://doi.org/10.3390/en13102572

Li, W., Godzik, A., 2006. Cd-hit: a fast program for clustering and comparing large sets of protein or nucleotide sequences 22, 1658–1659. https://doi.org/10.1093/bioinformatics/btl158

Lienemann, M., Deutzmann, J.S., Milton, R.D., Sahin, M., Spormann, A.M., 2018. Mediator-free enzymatic electrosynthesis of formate by the Methanococcus maripaludis heterodisulfide reductase supercomplex. Bioresour. Technol. 254, 278–283. https://doi.org/10.1016/j.biortech.2018.01.036

Ljungdahl, L.G., 1986. The autotrophic pathway of acetate synthesis in acetogenic bacteria. Annu. Rev. Microbiol. https://doi.org/10.1146/annurev.micro.40.1.415

Lu, X., Leung, D.Y.C., Wang, H., Xuan, J., 2017. A high performance dual electrolyte microfluidic reactor for the utilization of CO 2. Appl. Energy 194, 549–559. https://doi.org/10.1016/j.apenergy.2016.05.091

Luo, J., Meyer, A.S., Mateiu, R. V, Pinelo, M., 2015. Cascade catalysis in membranes with enzyme immobilization for multi-enzymatic conversion of CO2 to methanol. N. Biotechnol. 32, 319–327. https://doi.org/10.1016/j.nbt.2015.02.006

Mackenzie, C., Eraso, J.M., Choudhary, M., Jung, H.R., Zeng, X., Bruscella, P., Puskás, Á., Kaplan, S., 2007. Postgenomic adventures with Rhodobacter sphaeroides. Annu. Rev. Microbiol. https://doi.org/10.1146/annurev.micro.61.080706.093402

Maia, L.B., Moura, I., Moura, J.J.G., 2017. Molybdenum and tungsten-containing formate dehydrogenases: Aiming to inspire a catalyst for carbon dioxide utilization. Inorganica Chim. Acta 455, 350–363. https://doi.org/10.1016/j.ica.2016.07.010

Maia, L.B., Moura, J.J.G., Moura, I., 2015. Molybdenum and tungsten-dependent formate dehydrogenases. JBIC J. Biol. Inorg. Chem. 20, 287–309. https://doi.org/10.1007/s00775-014-1218-2

Marpani, F., Pinelo, M., Meyer, A.S., 2017. Enzymatic conversion of CO2to CH3OH via reverse dehydrogenase cascade biocatalysis: Quantitative comparison of efficiencies of immobilized enzyme systems. Biochem. Eng. J. 127, 217–228. https://doi.org/10.1016/j.bej.2017.08.011

Masson-Delmotte, V., Zhai, P., Pörtner, H.-O., Roberts, D., Skea, J., Shukla, P.R., Pirani, A., Moufouma-Okia, W., Clotilde, P., Pidcock, R., Connors, S., Matthews, J.B.R., Chen, Y., Zhou, X., Gomis, M.I., Lonnoy, E., Maycock, T., Tignor, M., Waterfield, T., 2018. Global warming of 1.5°C, IPCC - SR15.

Mateo, C., Palomo, J.M., Fernandez-Lorente, G., Guisan, J.M., Fernandez-Lafuente, R., 2007. Improvement of enzyme activity, stability and selectivity via immobilization techniques. Enzyme Microb. Technol. https://doi.org/10.1016/j.enzmictec.2007.01.018

McDowall, J.S., Murphy, B.J., Haumann, M., Palmer, T., Armstrong, F.A., Sargent, F., 2014. Bacterial formate hydrogenlyase complex. Proc. Natl. Acad. Sci. 111, E3948–E3956. https://doi.org/10.1073/pnas.1407927111

Mellmann, D., Sponholz, P., Junge, H., Beller, M., 2016. Formic acid as a hydrogen storage material –

development of homogeneous catalysts for selective hydrogen release. Chem. Soc. Rev. 45, 3954–3988. https://doi.org/10.1039/C5CS00618J

Miller, M., Robinson, W.E., Oliveira, A.R., Heidary, N., Kornienko, N., Warnan, J., Pereira, I.A.C., Reisner, E., 2019. Interfacing Formate Dehydrogenase with Metal Oxides for the Reversible Electrocatalysis and Solar-Driven Reduction of Carbon Dioxide. Angew. Chemie Int. Ed. 58, 4601–4605. https://doi.org/10.1002/anie.201814419

Miller, M.A., Pfeiffer, W., Schwartz, T., 2010. Creating the CIPRES Science Gateway for inference of large phylogenetic trees, in: 2010 Gateway Computing Environments Workshop (GCE). IEEE, pp. 1–8. https://doi.org/10.1109/GCE.2010.5676129

Milton, R.D., Minteer, S.D., 2017. Direct enzymatic bioelectrocatalysis: differentiating between myth and reality. J. R. Soc. Interface 14, 20170253. https://doi.org/10.1098/rsif.2017.0253

Min, K., Park, Y.S., Park, G.W., Lee, J. pyo, Moon, M., Ko, C.H., Lee, J.S., 2020. Elevated conversion of CO2 to versatile formate by a newly discovered formate dehydrogenase from Rhodobacter aestuarii. Bioresour. Technol. 305, 123155. https://doi.org/10.1016/j.biortech.2020.123155

Moura, J.J.G., Brondino, C.D., Trincão, J., Romão, M.J., 2004. Mo and W bis-MGD enzymes: Nitrate reductases and formate dehydrogenases. J. Biol. Inorg. Chem. 9, 791–799. https://doi.org/10.1007/s00775-004-0573-9

Müller, V., 2019. New Horizons in Acetogenic Conversion of One-Carbon Substrates and Biological Hydrogen Storage. Trends Biotechnol. https://doi.org/10.1016/j.tibtech.2019.05.008

Munkajohnpong, P., Kesornpun, C., Buttranon, S., Jaroensuk, J., Weeranoppanant, N., Chaiyen, P., 2020. Fatty alcohol production: an opportunity of bioprocess. Biofuels, Bioprod. Biorefining 14, 986–1009. https://doi.org/10.1002/bbb.2112

Naims, H., 2016. Economics of carbon dioxide capture and utilization—a supply and demand perspective. Environ. Sci. Pollut. Res. 23, 22226–22241. https://doi.org/10.1007/s11356-016-6810-2

Nielsen, C.F., Lange, L., Meyer, A.S., 2019. Classification and enzyme kinetics of formate dehydrogenases for biomanufacturing via CO2 utilization. Biotechnol. Adv. https://doi.org/10.1016/j.biotechadv.2019.06.007

Niks, D., Duvvuru, J., Escalona, M., Hille, R., 2016. Spectroscopic and kinetic properties of the molybdenum-containing, NAD+-dependent formate dehydrogenase from Ralstonia eutropha. J. Biol. Chem. 291, 1162–1174. https://doi.org/10.1074/jbc.M115.688457

Niks, D., Hille, R., 2019. Molybdenum- and tungsten-containing formate dehydrogenases and formylmethanofuran dehydrogenases: Structure, mechanism, and cofactor insertion. Protein Sci. 28, 111–122. https://doi.org/10.1002/pro.3498

Niks, D., Hille, R., 2018. Reductive activation of CO2 by formate dehydrogenases, 1st ed, Methods in Enzymology. Elsevier Inc. https://doi.org/10.1016/bs.mie.2018.10.013

NREL, 2020. Today's Energy Challenges, Tomorrow's Solutions.

O'Leary, N.A., Wright, M.W., Brister, J.R., Ciufo, S., Haddad, D., McVeigh, R., Rajput, B., Robbertse, B., Smith-White, B., Ako-Adjei, D., Astashyn, A., Badretdin, A., Bao, Y., Blinkova, O., Brover, V.,

Chetvernin, V., Choi, J., Cox, E., Ermolaeva, O., Farrell, C.M., Goldfarb, T., Gupta, T., Haft, D., Hatcher, E., Hlavina, W., Joardar, V.S., Kodali, V.K., Li, W., Maglott, D., Masterson, P., McGarvey, K.M., Murphy, M.R., O'Neill, K., Pujar, S., Rangwala, S.H., Rausch, D., Riddick, L.D., Schoch, C., Shkeda, A., Storz, S.S., Sun, H., Thibaud-Nissen, F., Tolstoy, I., Tully, R.E., Vatsan, A.R., Wallin, C., Webb, D., Wu, W., Landrum, M.J., Kimchi, A., Tatusova, T., DiCuccio, M., Kitts, P., Murphy, T.D., Pruitt, K.D., 2016. Reference sequence (RefSeq) database at NCBI: current status, taxonomic expansion, and functional annotation. Nucleic Acids Res. 44, D733–D745. https://doi.org/10.1093/nar/gkv1189

Obert, R., Dave, B.C., 1999. Enzymatic Conversion of Carbon Dioxide to Methanol: Enhanced Methanol Production in Silica Sol−Gel Matrices. J. Am. Chem. Soc. 121, 12192–12193. https://doi.org/10.1021/ja991899r

Panjapakkul, W., El-Halwagi, M.M., 2018. Technoeconomic Analysis of Alternative Pathways of Isopropanol Production. ACS Sustain. Chem. Eng. 6, 10260–10272. https://doi.org/10.1021/acssuschemeng.8b01606

Parkinson, B.A., Weaver, P.F., 1984. Photoelectrochemical pumping of enzymatic CO2reduction. Nature 309, 148–149. https://doi.org/10.1038/309148a0

Patricio, J., Angelis-Dimakis, A., Castillo-Castillo, A., Kalmykova, Y., Rosado, L., 2017. Region prioritization for the development of carbon capture and utilization technologies. J. CO2 Util. 17, 50–59. https://doi.org/10.1016/j.jcou.2016.10.002

Pérez-Fortes, M., Tzimas, E., 2016. Techno-economic and environmental evaluation of CO2 utilisation for fuel production. Synthesis of methanol and formic acid, Scientific and Technical Research Series. https://doi.org/10.2790/31552

Pierre, A.C., 2012. Enzymatic Carbon Dioxide Capture. ISRN Chem. Eng. 2012, 1–22. https://doi.org/10.5402/2012/753687

Pohlmann, A., Fricke, W.F., Reinecke, F., Kusian, B., Liesegang, H., Cramm, R., Eitinger, T., Ewering, C., Pötter, M., Schwartz, E., Strittmatter, A., Voß, I., Gottschalk, G., Steinbüchel, A., Friedrich, B., Bowien, B., 2006. Genome sequence of the bioplastic-producing "Knallgas" bacterium Ralstonia eutropha H16. Nat. Biotechnol. 24, 1257–1262. https://doi.org/10.1038/nbt1244

Quéré, C., Andrew, R., Friedlingstein, P., Sitch, S., Hauck, J., Pongratz, J., Pickers, P., Ivar Korsbakken, J., Peters, G., Canadell, J., Arneth, A., Arora, V., Barbero, L., Bastos, A., Bopp, L., Ciais, P., Chini, L., Ciais, P., Doney, S., Gkritzalis, T., Goll, D., Harris, I., Haverd, V., Hoffman, F., Hoppema, M., Houghton, R., Hurtt, G., Ilyina, T., Jain, A., Johannessen, T., Jones, C., Kato, E., Keeling, R., Klein Goldewijk, K., Landschützer, P., Lefèvre, N., Lienert, S., Liu, Z., Lombardozzi, D., Metzl, N., Munro, D., Nabel, J., Nakaoka, S.I., Neill, C., Olsen, A., Ono, T., Patra, P., Peregon, A., Peters, W., Peylin, P., Pfeil, B., Pierrot, D., Poulter, B., Rehder, G., Resplandy, L., Robertson, E., Rocher, M., Rödenbeck, C., Schuster, U., Skjelvan, I., Séférian, R., Skjelvan, I., Steinhoff, T., Sutton, A., Tans, P., Tian, H., Tilbrook, B., Tubiello, F., Van Der Laan-Luijkx, I., Van Der Werf, G., Viovy, N., Walker, A., Wiltshire, A., Wright, R., Zaehle, S., Zheng, B., 2018. Global Carbon Budget 2018. Earth Syst. Sci. Data 10, 2141–2194. https://doi.org/10.5194/essd-10-2141-2018

Raaijmakers, H., Macieira, S., Dias, J.M., Teixeira, S., Bursakov, S., Huber, R., Moura, J.J.G., Moura, I., Romão, M.J., Dias, M., Teixeira, S., Bursakov, S., Huber, R., Moura, J.J.G., Moura, I., Roma, M.J., Quı, D. De, 2002. Gene Sequence and the 1.8 A Crystal Structure Gene Sequence and the 1 . 8 A of the Tungsten-Containing Formate Dehydrogenase from Desulfovibrio gigas. Structure 10,

1261–1272. https://doi.org/http://dx.doi.org/10.1016/S0969-2126(02)00826-2

Raaijmakers, H.C.A., Romão, M.J., 2006. Formate-reduced E. coli formate dehydrogenase H: The reinterpretation of the crystal structure suggests a new reaction mechanism. J. Biol. Inorg. Chem. 11, 849–854. https://doi.org/10.1007/s00775-006-0129-2

Ragsdale, S.W., 2008. Enzymology of the Woods-Ljundahl Pathway of Acetogenesis. Ann. N. Y. Acad. Sci. 1125, 129–136. https://doi.org/10.1196/annals.1419.015.Enzymology

Ramana, V.V., Kumar, P.A., Srinivas, T.N.R., Sasikala, C., Ramana, C. V, 2009. Rhodobacter aestuarii sp. nov., a phototrophic alphaproteobacterium isolated from an estuarine environment. Int. J. Syst. Evol. Microbiol. 59, 1133–1136. https://doi.org/10.1099/ijs.0.004507-0

Raven, J.A., 2013. Rubisco: Still the most abundant protein of Earth? New Phytol. 198, 1–3. https://doi.org/10.1111/nph.12197

Rebelein, J.G., Stiebritz, M.T., Lee, C.C., Hu, Y., 2017. Activation and reduction of carbon dioxide by nitrogenase iron proteins. Nat. Chem. Biol. 13, 147–149. https://doi.org/10.1038/nchembio.2245

Reda, T., Plugge, C.M., Abram, N.J., Hirst, J., 2008. Reversible interconversion of carbon dioxide and formate by an electroactive enzyme. Proc. Natl. Acad. Sci. 105, 10654–10658. https://doi.org/10.1073/pnas.0801290105

Rothery, R.A., Workun, G.J., Weiner, J.H., 2008. The prokaryotic complex iron-sulfur molybdoenzyme family. Biochim. Biophys. Acta - Biomembr. https://doi.org/10.1016/j.bbamem.2007.09.002

Sakai, K., Kitazumi, Y., Shirai, O., Takagi, K., Kano, K., 2016. Efficient bioelectrocatalytic CO2 reduction on gas-diffusion-type biocathode with tungsten-containing formate dehydrogenase. Electrochem. commun. 73, 85–88. https://doi.org/10.1016/j.elecom.2016.11.008

Sakai, K., Sugimoto, Y., Kitazumi, Y., Shirai, O., Takagi, K., Kano, K., 2017. Direct electron transfer-type bioelectrocatalytic interconversion of carbon dioxide/formate and NAD+/NADH redox couples with tungsten-containing formate dehydrogenase. Electrochim. Acta 228, 537–544. https://doi.org/10.1016/j.electacta.2017.01.112

Sakai, K., Xia, H. qi, Kitazumi, Y., Shirai, O., Kano, K., 2018. Assembly of direct-electron-transfer-type bioelectrodes with high performance. Electrochim. Acta 271, 305–311. https://doi.org/10.1016/j.electacta.2018.03.163

Sánchez, O.G., Birdja, Y.Y., Bulut, M., Vaes, J., Breugelmans, T., Pant, D., 2019. Recent advances in industrial CO 2 electroreduction. Curr. Opin. Green Sustain. Chem. https://doi.org/10.1016/j.cogsc.2019.01.005

Schloss, P.D., Girard, R.A., Martin, T., Edwards, J., Thrash, J.C., 2016. Status of the archaeal and bacterial census: An update. MBio 7. https://doi.org/10.1128/mBio.00201-16

Schneider, F., Lö We, J., Huber, R., Schindelin, H., Kisker, C., Rg, J., Blein, K., 1996. Crystal Structure of Dimethyl Sulfoxide Reductase from Rhodobacter capsulatus at 1.88 Å Resolution. J. Mol. Biol 263, 53–69.

Schomburg, I., Jeske, L., Ulbrich, M., Placzek, S., Chang, A., Schomburg, D., 2017. The BRENDA enzyme information system–From a database to an expert system. J. Biotechnol.

https://doi.org/10.1016/j.jbiotec.2017.04.020

Schuchmann, K., Muller, V., 2013. Direct and Reversible Hydrogenation of CO2 to Formate by a Bacterial Carbon Dioxide Reductase. Science (80-.). 342, 1382–1385. https://doi.org/10.1126/science.1244758

Schuchmann, K., Müller, V., 2014. Autotrophy at the thermodynamic limit of life: a model for energy conservation in acetogenic bacteria. Nat. Rev. Microbiol. 12, 809–821. https://doi.org/10.1038/nrmicro3365

Schwarz, F.M., Schuchmann, K., Müller, V., 2018. Hydrogenation of CO2 at ambient pressure catalyzed by a highly active thermostable biocatalyst. Biotechnol. Biofuels 11, 237. https://doi.org/10.1186/s13068-018-1236-3

Self, W., 2013. Formate Dehydrogenase, Encyclopedia of Metalloproteins. Springer New York, New York, NY. https://doi.org/10.1007/978-1-4614-1533-6

Shabalin, I.G., Serov, A.E., Skirgello, O.E., Timofeev, V.I., Samygina, V.R., Popov, V.O., Tishkov, V.I., Kuranova, I.P., 2010. Recombinant formate dehydrogenase from Arabidopsis thaliana: Preparation, crystal growth in microgravity, and preliminary X-ray diffraction study. Crystallogr. Reports 55, 806–810. https://doi.org/10.1134/S1063774510050159

Shi, J., Jiang, Y., Jiang, Z., Wang, Xueyan, Wang, Xiaoli, Zhang, S., Han, P., Yang, C., 2015. Enzymatic conversion of carbon dioxide. Chem. Soc. Rev. Chem. Soc. Rev 44, 5981–6000. https://doi.org/10.1039/c5cs00182j

Simon, J., 2002. Enzymology and bioenergetics of respiratory nitrite ammonification. FEMS Microbiol. Rev. 26, 285–309. https://doi.org/10.1111/j.1574-6976.2002.tb00616.x

Singh, A.K., Singh, S., Kumar, A., 2015. Hydrogen energy future with formic acid: a renewable chemical hydrogen storage system. Catal. Sci. Technol. 6, 12–40. https://doi.org/10.1039/C5CY01276G

Singh, R.K., Singh, R., Sivakumar, D., Kondaveeti, S., Kim, T., Li, J., Sung, B.H., Cho, B.K., Kim, D.R., Kim, S.C., Kalia, V.C., Zhang, Y.H.P.J., Zhao, H., Kang, Y.C., Lee, J.K., 2018. Insights into Cell-Free Conversion of CO2 to Chemicals by a Multienzyme Cascade Reaction. ACS Catal. 8, 11085–11093. https://doi.org/10.1021/acscatal.8b02646

Sluis, M.K., Small, F.J., Allen, J.R., Ensign, S.A., 1996. Involvement of an ATP-Dependent Carboxylase in a CO 2-Dependent Pathway of Acetone Metabolism by Xanthobacter Strain Py2, JOURNAL OF BACTERIOLOGY.

Song, Q.-W., Zhou, Z.-H., He, L.-N., 2017. Efficient, selective and sustainable catalysis of carbon dioxide. Green Chem. 19, 3707–3728. https://doi.org/10.1039/C7GC00199A

Stamatakis, A., 2014. RAxML version 8: A tool for phylogenetic analysis and post-analysis of large phylogenies. Bioinformatics 30, 1312–1313. https://doi.org/10.1093/bioinformatics/btu033

Studier, F.W., 2005. Protein production by auto-induction in high density shaking cultures. Protein Expr. Purif. 41, 207–234. https://doi.org/10.1016/j.pep.2005.01.016

Sultana, S., Chandra Sahoo, P., Martha, S., Parida, K., 2016. A review of harvesting clean fuels from enzymatic CO_2 reduction. RSC Adv. 6, 44170–44194. https://doi.org/10.1039/C6RA05472B

Sun, L.N., Wang, D.S., Yang, E.D., Fang, L.C., Chen, Y.F., Tang, X.Y., Hua, R.M., 2016. Cupriavidus nantongensis sp. nov., a novel chlorpyrifos-degrading bacterium isolated from sludge. Int. J. Syst. Evol. Microbiol. 66, 2335–2341. https://doi.org/10.1099/ijsem.0.001034

Supuran, C.T., 2016. Structure and function of carbonic anhydrases. Biochem. J. https://doi.org/10.1042/BCJ20160115

Szczesny, J., Ruff, A., Oliveira, A.R., Pita, M., Pereira, I.A.C., De Lacey, A.L., Schuhmann, W., 2020. Electroenzymatic CO2 Fixation Using Redox Polymer/Enzyme-Modified Gas Diffusion Electrodes. ACS Energy Lett. 5, 321–327. https://doi.org/10.1021/acsenergylett.9b02436

Takacs, M., Makhlynets, O. V, Tolbert, P.L., Korendovych, I. V, 2017. Secretion of functional formate dehydrogenase in Pichia pastoris. Protein Eng. Des. Sel. 30, 381–386. https://doi.org/10.1093/protein/gzx010

Tan, Z., Zhu, X., Chen, J., Li, Q., Zhanga, X., 2013. Activating phosphoenolpyruvate carboxylase and phosphoenolpyruvate carboxykinase in combination for improvement of succinate production. Appl. Environ. Microbiol. 79, 4838–4844. https://doi.org/10.1128/AEM.00826-13

Tatusova, T., DiCuccio, M., Badretdin, A., Chetvernin, V., Nawrocki, E.P., Zaslavsky, L., Lomsadze, A., Pruitt, K.D., Borodovsky, M., Ostell, J., 2016. NCBI prokaryotic genome annotation pipeline. Nucleic Acids Res. 44, 6614–6624. https://doi.org/10.1093/nar/gkw569

Tishkov, V.I., Popov, V.O., 2006. Protein engineering of formate dehydrogenase. Biomol. Eng. 23, 89–110. https://doi.org/10.1016/j.bioeng.2006.02.003

Trachtenberg, M.C., 2006. Efficient flue gas CO2 capture by a biomimetic facilitated transport membrane. 2006 AFS Fall Top. Conf. Sep. Process. Power Gener. Ind.

Tsai, C.L., Tainer, J.A., 2018. Robust Production, Crystallization, Structure Determination, and Analysis of [Fe–S] Proteins: Uncovering Control of Electron Shuttling and Gating in the Respiratory Metabolism of Molybdopterin Guanine Dinucleotide Enzymes, in: Methods in Enzymology. pp. 157–196. https://doi.org/10.1016/bs.mie.2017.11.006

van Ruijven, B.J., van Vuuren, D.P., Boskaljon, W., Neelis, M.L., Saygin, D., Patel, M.K., 2016. Long-term model-based projections of energy use and CO2 emissions from the global steel and cement industries. Resour. Conserv. Recycl. 112, 15–36. https://doi.org/10.1016/j.resconrec.2016.04.016

Vandamme, P., Coenye, T., 2004. Taxonomy of the genus Cupriavidus: A tale of lost and found. Int. J. Syst. Evol. Microbiol. 54, 2285–2289. https://doi.org/10.1099/ijs.0.63247-0

Vorholt, J.A., 2002. Cofactor-dependent pathways of formaldehyde oxidation in methylotrophic bacteria. Arch. Microbiol. 178, 239–249. https://doi.org/10.1007/s00203-002-0450-2

Walker, L.M., Li, B., Niks, D., Hille, R., Elliott, S.J., 2019. Deconvolution of reduction potentials of formate dehydrogenase from Cupriavidus necator. J. Biol. Inorg. Chem. 24, 889–898. https://doi.org/10.1007/s00775-019-01701-1

Wang, X., Li, Z., Shi, J., Wu, H., Jiang, Z., Zhang, W., Song, X., Ai, Q., 2014. Bioinspired approach to multienzyme cascade system construction for efficient carbon dioxide reduction. ACS Catal. 4, 962–972. https://doi.org/10.1021/cs401096c

Wray, J., 1670. Concerning some un-common observations and experiments made with an Acid juyce to be found in Ants. Philos. Trans. R. Soc. London 5, 2163–2166. https://doi.org/10.1098/rstl.1670.0052

Wu, J., Huang, Y., Ye, W., Li, Y., 2017. CO2 Reduction: From the Electrochemical to Photochemical Approach. Adv. Sci. 4, 1–29. https://doi.org/10.1002/advs.201700194

Wu, R., Ma, C., Zhu, Z., 2020. Enzymatic electrosynthesis as an emerging electrochemical synthesis platform. Curr. Opin. Electrochem. https://doi.org/10.1016/j.coelec.2019.08.004

Xiao, X., Xia, H., Wu, R., Bai, L., Yan, L., Magner, E., Cosnier, S., Lojou, E., Zhu, Z., Liu, A., 2019. Tackling the Challenges of Enzymatic (Bio)Fuel Cells. Chem. Rev. 119, 9509–9558. https://doi.org/10.1021/acs.chemrev.9b00115

Yang, N., Waldvogel, S.R., Jiang, X., 2016. Electrochemistry of Carbon Dioxide on Carbon Electrodes. ACS Appl. Mater. Interfaces. https://doi.org/10.1021/acsami.5b09825

Yu, X., Niks, D., Ge, X., Liu, H., Hille, R., Mulchandani, A., 2019. Synthesis of Formate from CO2 Gas Catalyzed by an O2-Tolerant NAD-Dependent Formate Dehydrogenase and Glucose Dehydrogenase. Biochemistry 58, 1861–1868. https://doi.org/10.1021/acs.biochem.8b01301

Yu, X., Niks, D., Mulchandani, A., Hille, R., 2017. Efficient reduction of CO 2 by the molybdenum-containing formate dehydrogenase from Cupriavidus necator (Ralstonia eutropha). J. Biol. Chem. 292, 16872–16879. https://doi.org/10.1074/jbc.M117.785576

Yuan, M., Kummer, M.J., Minteer, S.D., 2019. Strategies for Bioelectrochemical CO 2 Reduction. Chem. – A Eur. J. 25, 14258–14266. https://doi.org/10.1002/chem.201902880

Yuan, M., Sahin, S., Cai, R., Abdellaoui, S., Hickey, D.P., Minteer, S.D., Milton, R.D., 2018. Creating a Low-Potential Redox Polymer for Efficient Electroenzymatic CO 2 Reduction. Angew. Chemie - Int. Ed. 57, 6582–6586. https://doi.org/10.1002/anie.201803397

Yuan, Z., Eden, M.R., Gani, R., 2016. Toward the Development and Deployment of Large-Scale Carbon Dioxide Capture and Conversion Processes. Ind. Eng. Chem. Res. 55, 3383–3419. https://doi.org/10.1021/acs.iecr.5b03277

Zaldivar, J., Ingram, L.O., 1999. Effect of organic acids on the growth and fermentation of ethanologenic Escherichia coli LY01. Biotechnol. Bioeng. 66, 203–210. https://doi.org/10.1002/(sici)1097-0290(1999)66:4<203::aid-bit1>3.0.co;2-#

Website references:

The Danish Energy Agency, 16th of August, 2017. *Biogas in Denmark.* Retrieved from: https://ens.dk/en/our-responsibilities/bioenergy/biogas-denmark on 2nd of November, 2020.

Jyllandsposten, 1st of December, 2013. *Så meget el, vand og varme bruger en gennemsnitsfamilie.* Retrieved from: https://jyllands-posten.dk/bolig/tips/ECE6289428/saa-meget-el-vand-og-varme-bruger-en-gennemsnitsfamilie/ on 3rd of November, 2020. (Article is in Danish)

AAT Bioquest, Inc, 23rd of November, 2017. *Quest Calculate™ Protein Concentration Calculator.* Retrieved from https://www.aatbio.com/tools/calculate-protein-concentration on 6th of November, 2020.

IndustryARC, 3rd of April, 2019. *Formic Acid Market Driven by Rubber Plantations and Production in APAC.* Retrieved from: https://www.industryarc.com/PressRelease/747/Formic-Acid-Market-Research.html on 9th of November, 2020.

Renewable Fuels Association, 12th of May, 2019. *Annual Fuel Ethanol Production.* Retrieved from: https://ethanolrfa.org/statistics/annual-ethanol-production/ on 10th of November, 2020.

EcoliWiki, 20th of December, 2012. *DH5 alpha.* Retrieved from: https://ecoliwiki.org/colipedia/index.php/DH5_alpha on 10th of November, 2020

EcoliWiki, 16th of October, 2020. *MC1061.* Retrieved from: https://ecoliwiki.org/colipedia/index.php/Category:Strain:MC1061 on 10th of November, 2020

Physical book reference:

Berg, J.M., Tymoczko, J.L., Stryer, L., 2012. *Biochemistry 7th Ed.* New York: W.H. Freeman.

Appendix A. Common gene product annotations

Table 13: When annotating metal-dependent FDHs according to the classification scheme presented for this thesis, the genes directly upstream and downstream of the gene encoding the alpha subunit were logged and used to create a profile for the given FDH. In this table the most common gene products, as predicted by RefSeq, are listed along with the search terms used to find them. Additionally, the one-letter abbreviation for the given gene product is given (E.g. 'X' for gene only annotated as 'formate dehydrogenase' and 'B' for genes annotated as both 'beta' and 'formate dehydrogenase'). Furthermore, gene products observed less frequently are listed under 'Not included less common gene products'.

Included common gene products	**Search term**	**Letter**
formate dehydrogenase-N subunit alpha	"alpha" AND "formate dehydrogenase"	A
formate dehydrogenase subunit alpha	"alpha" AND "formate dehydrogenase"	A
formate dehydrogenase subunit beta	"beta" AND "formate dehydrogenase"	B
formate dehydrogenase subunit gamma	"gamma" AND "formate dehydrogenase"	C
formate dehydrogenase accessory sulfurtransferase FdhD	"accessory sulfurtransferase" AND "formate dehydrogenase"	D
NAD-dependent formate dehydrogenase subunit delta	"delta" AND "formate dehydrogenase"	S
formate dehydrogenase	"formate dehydrogenase"	X
formate dehydrogenase accessory protein FdhE	"accessory protein FdhE" AND "formate dehydrogenase"	E
NADH-quinone oxidoreductase subunit E	"NAD" AND "oxidoreductase"	O
NADH-quinone oxidoreductase subunit NuoF	"NAD" AND "oxidoreductase"	O
NADH-quinone oxidoreductase subunit NuoE	"NAD" AND "oxidoreductase"	O
NADH-quinone oxidoreductase subunit F	"NAD" AND "oxidoreductase"	O
NAD(P)-dependent oxidoreductase	"NAD" AND "oxidoreductase"	O
4Fe-4S dicluster domain-containing protein	"4Fe-4S dicluster domain"	F
formate dehydrogenase cytochrome b556	"cytochrome"	P
Not included less common gene products	-	-
LysR family transcriptional regulator	-	-
LytR family transcriptional regulator	-	-
hydrogenase iron-sulfur subunit	-	-
formate/nitrite transporter family protein	-	-
ABC transporter	-	-
ABC transporter permease	-	-
sulfate ABC transporter substrate-binding protein	-	-
TetR/AcrR family transcriptional regulator	-	-
molybdenum cofactor biosynthesis protein MoaE	-	-
molybdopterin converting factor subunit 1	-	-
colanic acid biosynthesis glycosyltransferase	-	-
AEC family transporter	-	-
ModE family transcriptional regulator	-	-
trehalose-binding protein	-	-
ABC transporter substrate-binding protein	-	-
ModE family transcriptional regulator	-	-
carbon-monoxide dehydrogenase catalytic subunit	-	-

Appendix B. Reactions involving CO_2 by EC number

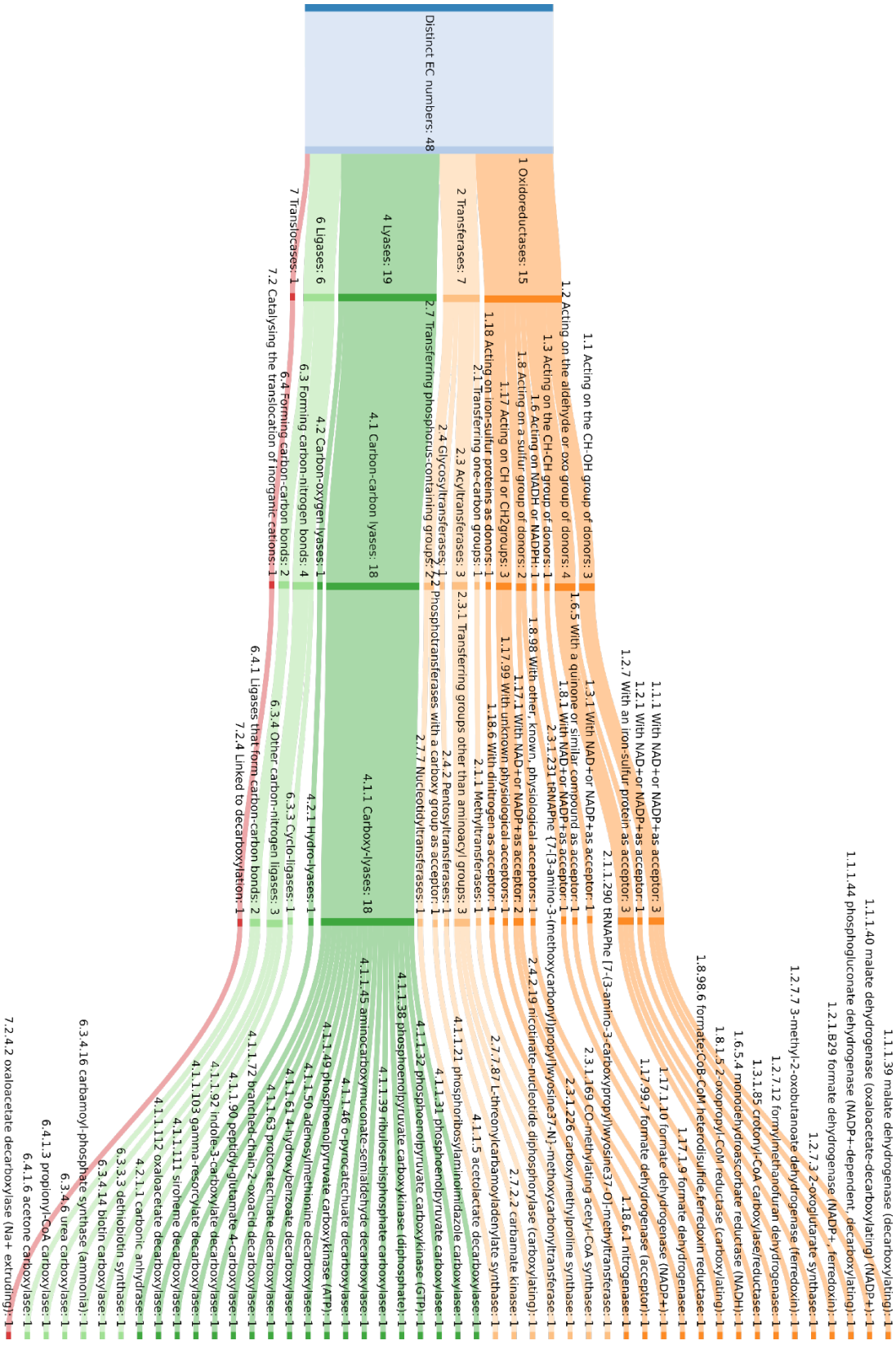

Figure 29: Overview of EC numbers for enzymes registered in BRENDA as utilizing CO_2 as substrate.

Appendix C. Enzymes catalyzing reactions involving CO_2

Examining the list depicted in Appendix B (above), unsurprisingly, a major fraction of the reactions involving CO_2 as a substrate are carboxylations catalyzed by carboxylases or decarboxylases (reversible reactions) is seen. Carboxylation is the main way for carbon to be incorporated into biomass. As such, enzymes catalyzing carboxylation are incredibly prominent, with ribulose-1,5-bisphosphate carboxylase/oxygenase (RuBisCO) quite literally being the most abundant protein on Earth (Raven, 2013). RuBisCO is a lyase. Lyases are listed in the figure of Appendix B among the most diverse known enzymes that able to catalyze reactions with CO_2. However, unsurprisingly, many of these lyases are in fact decarboxylases prone to the reverse CO_2-emitting reaction, rather than the CO_2-consuming. Lyases that are prone to catalyze CO_2-consuming reactions include the aforementioned RuBisCO (Pierre, 2012; Shi et al., 2015), oxaloacetate decarboxylase (ODC) (Granjon et al., 2010), phosphoenolpyruvate carboxykinase (PEPC) (Bailey et al., 2007; Tan et al., 2013), and carbonic anhydrase (CA) (Alvizo et al., 2014) (Figure 30).

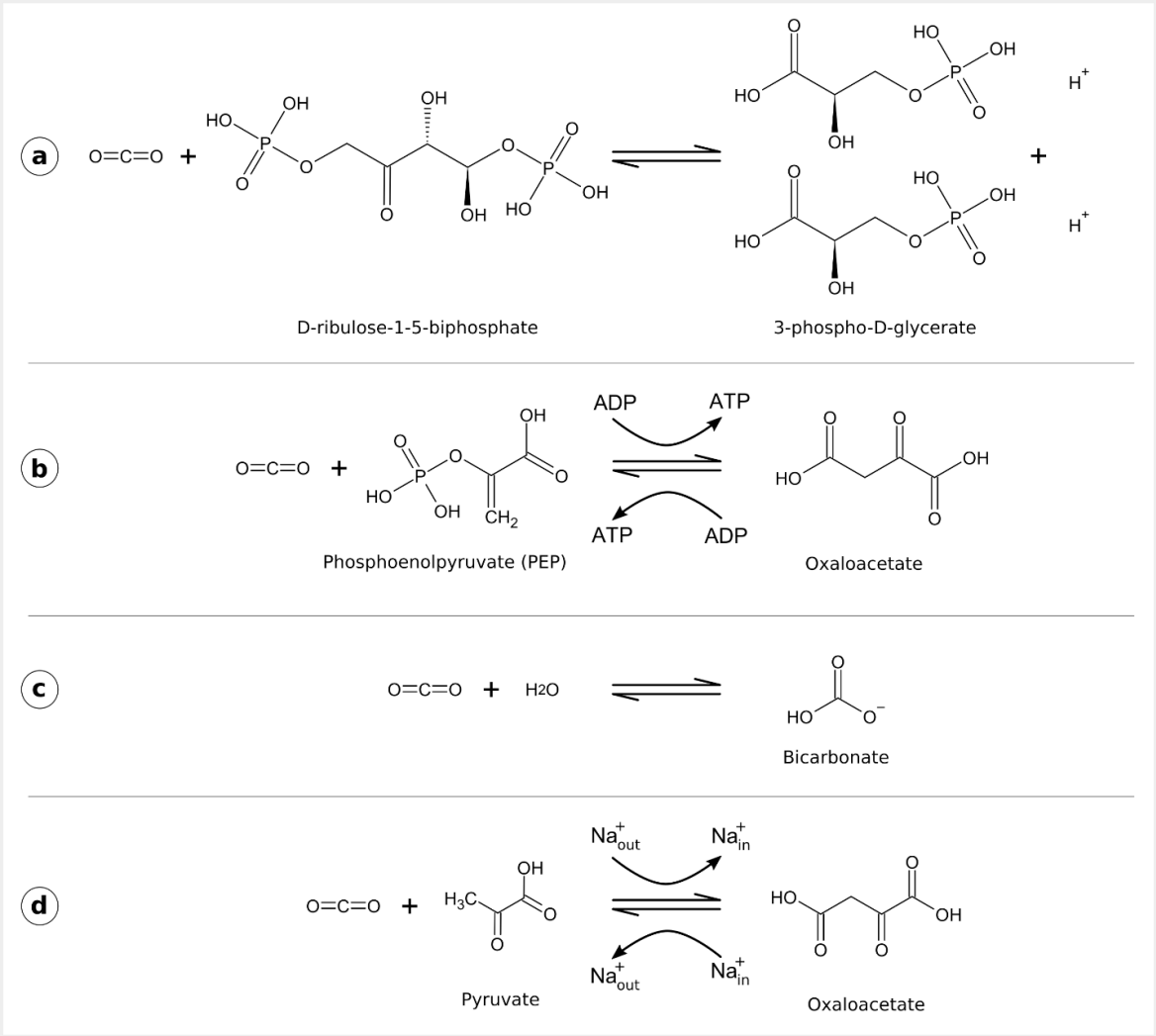

Figure 30: Lyase reactions involving CO_2. Reactions of a) RuBisCO, b) phosphoenolpyruvate carboxykinase (PEPC), c) carbonic anhydrase (CA), and d) oxaloacetate decarboxylase (ODC).

Interestingly, these four lyases function very differently in terms of the driving force for their respective reactions. RuBisCO employs the inherent high energy density of its substrate, PEPC drives its reaction though hydrolysis of ATP (or a similar tri-phosphate molecule), and CA catalyzes a pH driven equilibrium (Supuran, 2016). ODC can be coupled to a translocase, allowing an ion gradient to drive the reaction. Which is also why a translocase EC number is found in the list from BRENDA.

Also, enzymes classified with EC numbers denominating them as ligases or transferases are able to utilize CO_2 as substrate. Transferases are predominantly found described with EC numbers related to tRNA synthesis or other highly complex molecules. Examples of ligases include acetyl-CoA carboxylase (Broussard et al., 2013), urea carboxylase (Kanamori et al., 2004), and acetone carboxylase (Boyd et al., 2004; Sluis et al., 1996) (Figure 31).

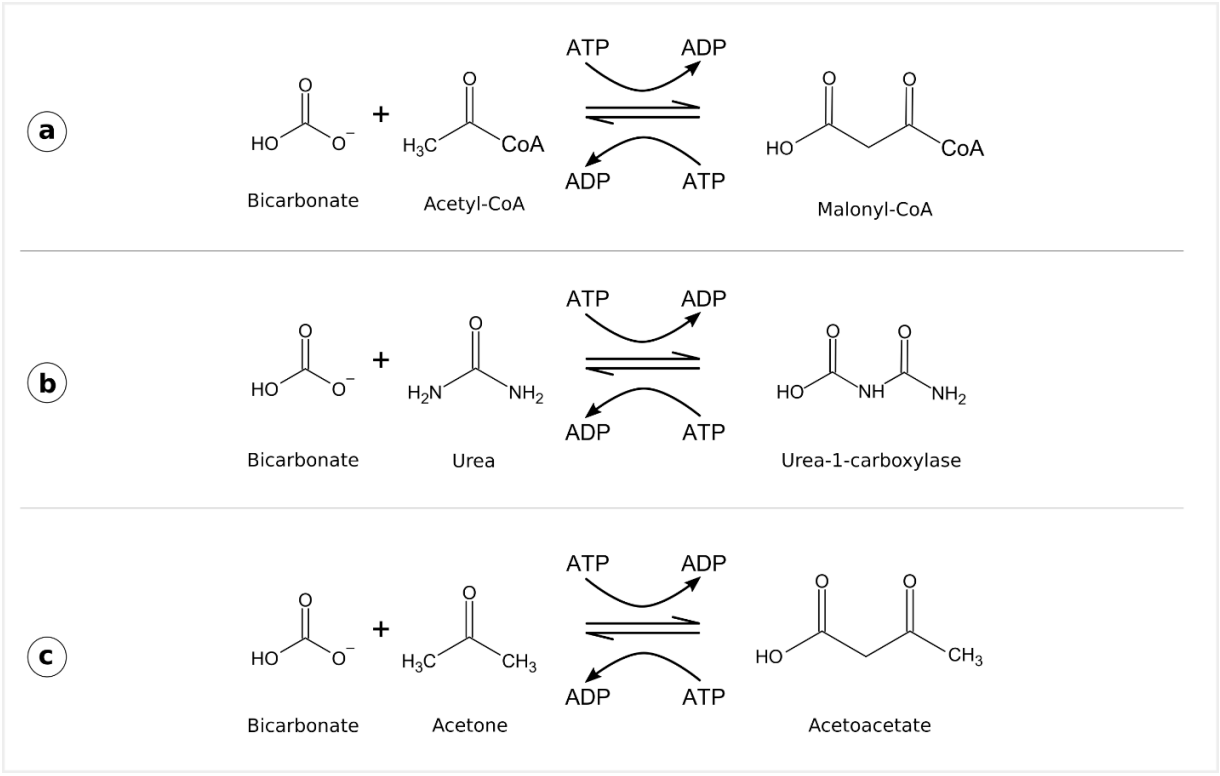

Figure 31: Ligase reactions involving CO_2. Reactions of a) acetyl-CoA carboxylase, b) urea carboxylase, and c) acetone carboxylase.

As for the lyases again the reactions driven by energy dense co-substrates such as ATP is seen. Interestingly, for the ligases presented here, carbon dioxide is often metabolized in the form of bicarbonate.

Looking closer at the oxidoreductases it is observed that they are primarily comprised of dehydrogenase and reductases. A single synthase and nitrogenase also included. The nitrogenase is included because they have been shown to be promiscuous redox proteins that in the context of CCU have been studied for their potential to reduce other chemicals than molecular nitrogen to ammonia (Rebelein et al., 2017). The six EC numbers described as dehydrogenases are in fact four different definitions of formate dehydrogenase and two other dehydrogenases. Strong examples of oxidoreductases able to use CO_2 as a substrate include FDHs (Rothery et al., 2008), carbon monoxide dehydrogenase (Hu et al., 2018; Ragsdale, 2008), and 2-oxogluterate synthase (Figure 32).

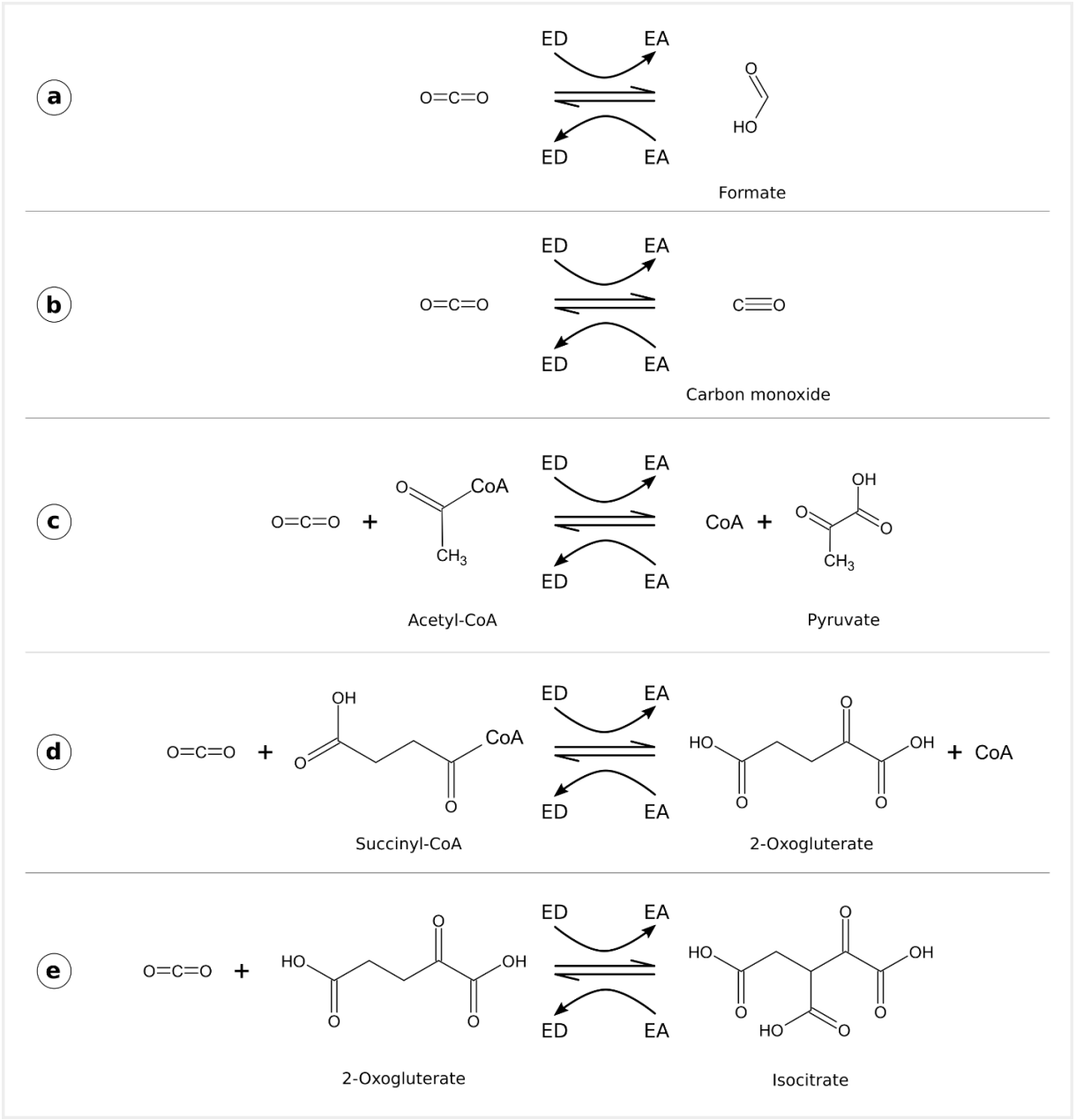

Figure 32: Oxidoreductase reactions involving CO_2. Reactions of a) formate dehydrogenase, b) carbon monoxide dehydrogenase, c) pyruvate synthase, d) 2-oxogluterate synthase, and e) isocitrate dehydrogenase.

Conversely to the lyases, transferases and ligases, the oxidoreductases catalyze CO_2 conversion driven by electron donors (EDs), such as NADH, NADPH, and ferrodoxin. Electrodes directly can be applied as ED. Depending on the reduction potential and concentration of the given ED, a reaction may occur to a faster or slower extent (Nielsen et al., 2019).

Appendix D. FDH sequence analysis (Large figure)

Figure 33: Phylogenetic tree generated based on alignment of 965 metal-dependent FDH alpha subunit sequences. Inter-sequence identity was reduced to a maximum of 90% between any two sequences. Each branch tip represents a single sequence. Each sequence is annotated with an FDH type based on gene segment organization. Gene segment organization is defined as the genetic makeup of the surrounding genes of a given FDH alpha subunit sequence. Here 'A': alpha (α) subunit, 'B': beta (β) subunit, 'C': gamma (γ) subunit, 'D': accessory sulfurtranferase fdhD, 'E': accessory protein fdhE, 'S': delta subunit, 'X': unspecified formate dehydrogenase subunit, 'O': NADH-quinone oxidoreductase related subunit, 'F': 4Fe-4S containing protein, and 'P': cytochrome formate dehydrogenase subunit.

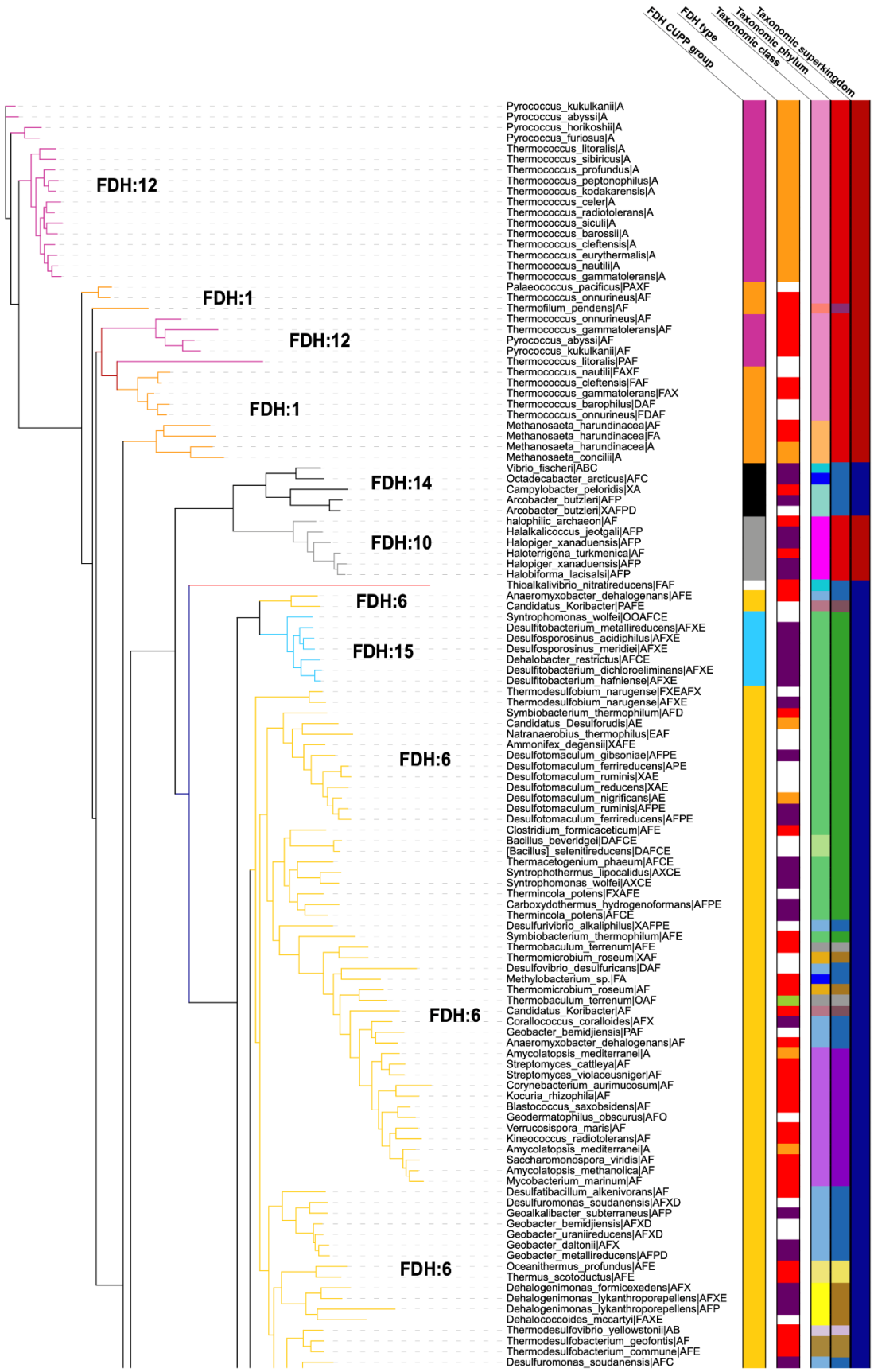
FDH CUPP group
FDH type
Taxonomic class
Taxonomic phylum
Taxonomic superkingdom
FDH:12
FDH:1
FDH:12
FDH:1
FDH:14
FDH:10
FDH:6
FDH:15
FDH:6
FDH:6
FDH:6
Pyrococcus_kukulkanii|A
Pyrococcus_abyssi|A
Pyrococcus_horikoshii|A
Pyrococcus_furiosus|A
Thermococcus_litoralis|A
Thermococcus_sibiricus|A
Thermococcus_profundus|A
Thermococcus_peptonophilus|A
Thermococcus_kodakarensis|A
Thermococcus_celer|A
Thermococcus_radiotolerans|A
Thermococcus_siculi|A
Thermococcus_barossii|A
Thermococcus_cleftensis|A
Thermococcus_eurythermalis|A
Thermococcus_nautilii|A
Thermococcus_gammatolerans|A
Palaeococcus_pacificus|PAXF
Thermococcus_onnurineus|AF
Thermofilum_pendens|AF
Thermococcus_onnurineus|AF
Thermococcus_gammatolerans|AF
Pyrococcus_abyssi|AF
Pyrococcus_kukulkanii|AF
Thermococcus_litoralis|PAF
Thermococcus_nautilii|FAXF
Thermococcus_cleftensis|FAF
Thermococcus_gammatolerans|FAX
Thermococcus_barophilus|DAF
Thermococcus_onnurineus|FDAF
Methanosaeta_harundinacea|AF
Methanosaeta_harundinacea|FA
Methanosaeta_harundinacea|A
Methanosaeta_concilii|A
Vibrio_fischeri|ABC
Octadecabacter_arcticus|AFC
Campylobacter_peloridis|XA
Arcobacter_butzleri|AFP
Arcobacter_butzleri|XAFPD
halophilic_archaeon|AF
Halalkalicoccus_jeotgali|AFP
Halopiger_xanaduensis|AFP
Halterrigena_turkmenica|AF
Halopiger_xanaduensis|AFP
Halobiforma_lacisalsi|AFP
Thioalkalivibrio_nitratireducens|FAF
Anaeromyxobacter_dehalogenans|AFE
Candidatus_Koribacter|PAFE
Syntrophomonas_wolfei|OOAFCE
Desulfitobacterium_metallireducens|AFXE
Desulfosporosinus_acidiphilus|AFXE
Desulfosporosinus_meridiei|AFXE
Dehalobacter_restrictus|AFCE
Desulfitobacterium_dichloroeliminans|AFXE
Desulfitobacterium_hafniense|AFXE
Thermodesulfobium_narugense|FXEAFX
Thermodesulfobium_narugense|AFXE
Symbiobacterium_thermophilum|AFD
Candidatus_Desulforudis|AE
Natranaerobius_thermophilus|EAF
Ammonifex_degensii|XAFE
Desulfotomaculum_gibsoniae|AFPE
Desulfotomaculum_ferrireducens|APE
Desulfotomaculum_ruminis|XAE
Desulfotomaculum_reducens|XAE
Desulfotomaculum_nigrificans|AE
Desulfotomaculum_ruminis|AFPE
Desulfotomaculum_ferrireducens|AFPE
Clostridium_formicaceticum|AFE
Bacillus_beveridgei|DAFCE
[Bacillus]_selenitireducens|DAFCE
Thermacetogenium_phaeum|AFCE
Syntrophothermus_lipocalidus|AXCE
Syntrophomonas_wolfei|AXCE
Thermincola_potens|FXAFE
Carboxydothermus_hydrogenoformans|AFPE
Thermincola_potens|AFCE
Desulfurivibrio_alkaliphilus|XAFPE
Symbiobacterium_thermophilum|AFE
Thermobaculum_terrenum|AFE
Thermomicrobium_roseum|XAF
Desulfovibrio_desulfuricans|DAF
Methylobacterium_sp.|FA
Thermomicrobium_roseum|AF
Thermobaculum_terrenum|OAF
Candidatus_Koribacter|AF
Corallococcus_coralloides|AFX
Geobacter_bemidjiensis|PAF
Anaeromyxobacter_dehalogenans|AF
Amycolatopsis_mediterranei|A
Streptomyces_cattleya|AF
Streptomyces_violaceusniger|AF
Corynebacterium_aurimucosum|AF
Kocuria_rhizophila|AF
Blastococcus_saxobsidens|AF
Geodermatophilus_obscurus|AFO
Verrucosispora_maris|AF
Kineococcus_radiotolerans|AF
Amycolatopsis_mediterranei|A
Saccharomonospora_viridis|AF
Amycolatopsis_methanolica|AF
Mycobacterium_marinum|AF
Desulfatibacillum_alkenivorans|AF
Desulfuromonas_soudanensis|AFXD
Geoalkalibacter_subterraneus|AFP
Geobacter_bemidjiensis|AFXD
Geobacter_uraniireducens|AFXD
Geobacter_daltonii|AFX
Geobacter_metallireducens|AFPD
Oceanithermus_profundus|AFE
Thermus_scotoductus|AFE
Dehalogenimonas_formicexedens|AFX
Dehalogenimonas_lykanthroporepellens|AFXE
Dehalogenimonas_lykanthroporepellens|AFP
Dehalococcoides_mccartyi|FAXE
Thermodesulfovibrio_yellowstonii|AB
Thermodesulfobacterium_geofontis|AF
Thermodesulfobacterium_commune|AFE
Desulfuromonas_soudanensis|AFC

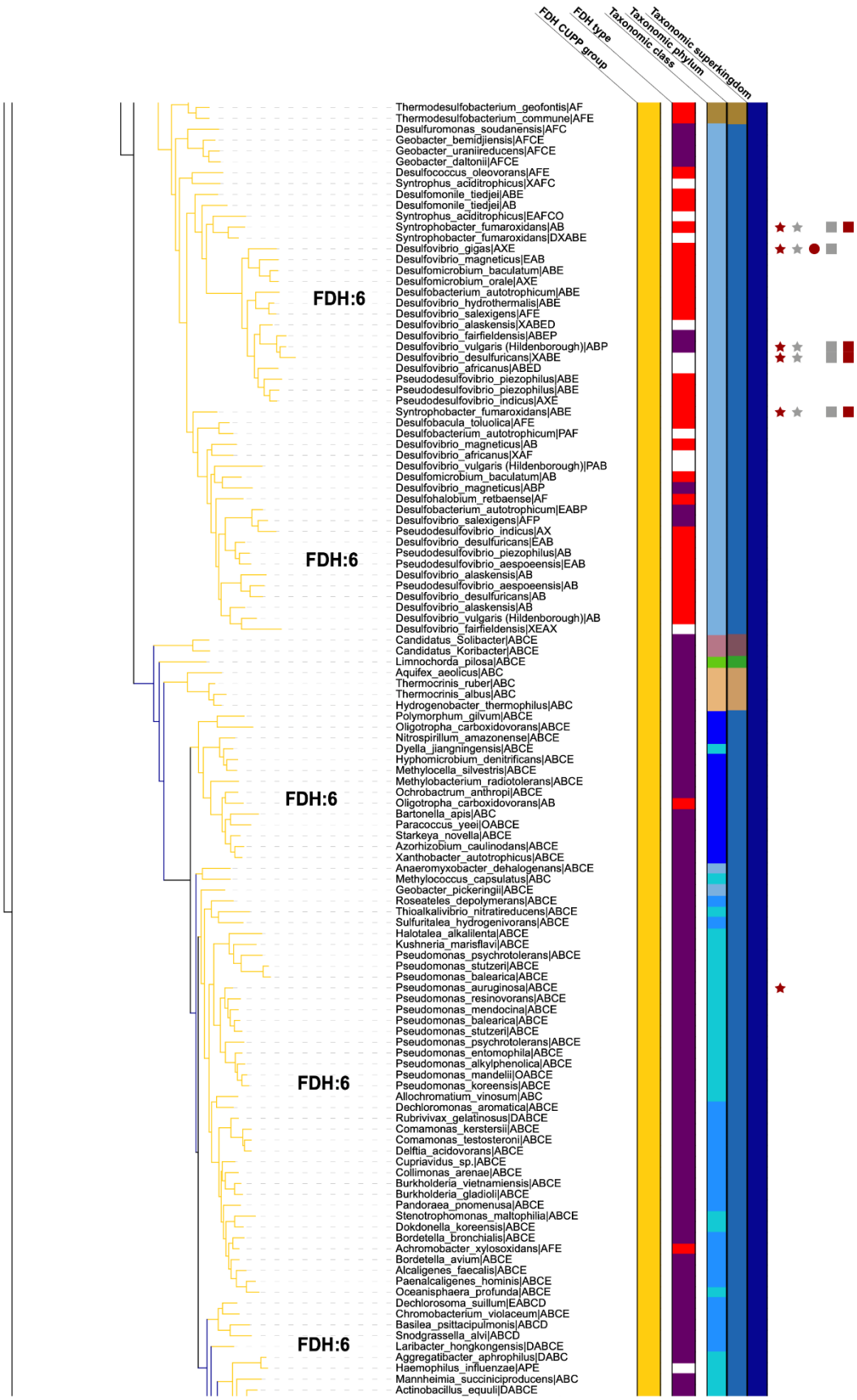
FDH CUPP group
FDH type
Taxonomic class
Taxonomic phylum
Taxonomic superkingdom
Thermodesulfobacterium_geofontis|AF
Thermodesulfobacterium_commune|AFE
Desulfuromonas_soudanensis|AFC
Geobacter_bemidjiensis|AFCE
Geobacter_uraniireducens|AFCE
Geobacter_daltonii|AFCE
Desulfococcus_oleovorans|AFE
Syntrophus_aciditrophicus|XAFC
Desulfomonile_tiedjei|ABE
Desulfomonile_tiedjei|AB
Syntrophus_aciditrophicus|EAFCO
Syntrophobacter_fumaroxidans|AB
Syntrophobacter_fumaroxidans|DXABE
Desulfovibrio_gigas|AXE
Desulfovibrio_magneticus|EAB
Desulfomicrobium_baculatum|ABE
Desulfomicrobium_orale|AXE
Desulfobacterium_autotrophicum|ABE
Desulfovibrio_hydrothermalis|ABE
Desulfovibrio_salexigens|AFE
Desulfovibrio_alaskensis|XABED
Desulfovibrio_fairfieldensis|ABEP
Desulfovibrio_vulgaris (Hildenborough)|ABP
Desulfovibrio_desulfuricans|XABE
Desulfovibrio_africanus|ABED
Pseudodesulfovibrio_piezophilus|ABE
Pseudodesulfovibrio_piezophilus|ABE
Pseudodesulfovibrio_indicus|AXE
Syntrophobacter_fumaroxidans|ABE
Desulfobacula_toluolica|AFE
Desulfobacterium_autotrophicum|PAF
Desulfovibrio_magneticus|AB
Desulfovibrio_africanus|XAF
Desulfovibrio_vulgaris (Hildenborough)|PAB
Desulfomicrobium_baculatum|AB
Desulfovibrio_magneticus|ABP
Desulfohalobium_retbaense|AF
Desulfobacterium_autotrophicum|EABP
Desulfovibrio_salexigens|AFP
Pseudodesulfovibrio_indicus|AX
Desulfovibrio_desulfuricans|EAB
Pseudodesulfovibrio_piezophilus|AB
Pseudodesulfovibrio_aespoeensis|EAB
Desulfovibrio_alaskensis|AB
Pseudodesulfovibrio_aespoeensis|AB
Desulfovibrio_desulfuricans|AB
Desulfovibrio_alaskensis|AB
Desulfovibrio_vulgaris (Hildenborough)|AB
Desulfovibrio_fairfieldensis|XEAX
Candidatus_Solibacter|ABCE
Candidatus_Koribacter|ABCE
Limnochorda_pilosa|ABCE
Aquifex_aeolicus|ABC
Thermocrinis_ruber|ABC
Thermocrinis_albus|ABC
Hydrogenobacter_thermophilus|ABC
Polymorphum_gilvum|ABCE
Oligotropha_carboxidovorans|ABCE
Nitrospirillum_amazonense|ABCE
Dyella_jiangningensis|ABCE
Hyphomicrobium_denitrificans|ABCE
Methylocella_silvestris|ABCE
Methylobacterium_radiotolerans|ABCE
Ochrobactrum_anthropi|ABCE
Oligotropha_carboxidovorans|AB
Bartonella_apis|ABC
Paracoccus_yeei|OABCE
Starkeya_novella|ABCE
Azorhizobium_caulinodans|ABCE
Xanthobacter_autotrophicus|ABCE
Anaeromyxobacter_dehalogenans|ABCE
Methylococcus_capsulatus|ABC
Geobacter_pickeringii|ABCE
Roseateles_depolymerans|ABCE
Thioalkalivibrio_nitratireducens|ABCE
Sulfuritalea_hydrogenivorans|ABCE
Halotalea_alkalilenta|ABCE
Kushneria_marisflavi|ABCE
Pseudomonas_psychrotolerans|ABCE
Pseudomonas_stutzeri|ABCE
Pseudomonas_balearica|ABCE
Pseudomonas_auruginosa|ABCE
Pseudomonas_resinovorans|ABCE
Pseudomonas_mendocina|ABCE
Pseudomonas_balearica|ABCE
Pseudomonas_stutzeri|ABCE
Pseudomonas_psychrotolerans|ABCE
Pseudomonas_entomophila|ABCE
Pseudomonas_alkylphenolica|ABCE
Pseudomonas_mandelii|OABCE
Pseudomonas_koreensis|ABCE
Allochromatium_vinosum|ABC
Dechloromonas_aromatica|ABCE
Rubrivivax_gelatinosus|DABCE
Comamonas_kerstersii|ABCE
Comamonas_testosteroni|ABCE
Delftia_acidovorans|ABCE
Cupriavidus_sp.|ABCE
Collimonas_arenae|ABCE
Burkholderia_vietnamiensis|ABCE
Burkholderia_gladioli|ABCE
Pandoraea_pnomenusa|ABCE
Stenotrophomonas_maltophilia|ABCE
Dokdonella_koreensis|ABCE
Bordetella_bronchialis|ABCE
Achromobacter_xylosoxidans|AFE
Bordetella_avium|ABCE
Alcaligenes_faecalis|ABCE
Paenalcaligenes_hominis|ABCE
Oceanisphaera_profunda|ABCE
Dechlorosoma_suillum|EABCD
Chromobacterium_violaceum|ABCE
Basilea_psittacipulmonis|ABCD
Snodgrassella_alvi|ABCD
Laribacter_hongkongensis|DABCE
Aggregatibacter_aphrophilus|DABC
Haemophilus_influenzae|APE
Mannheimia_succiniciproducens|ABC
Actinobacillus_equuli|DABCE
FDH:6
FDH:6
FDH:6
FDH:6

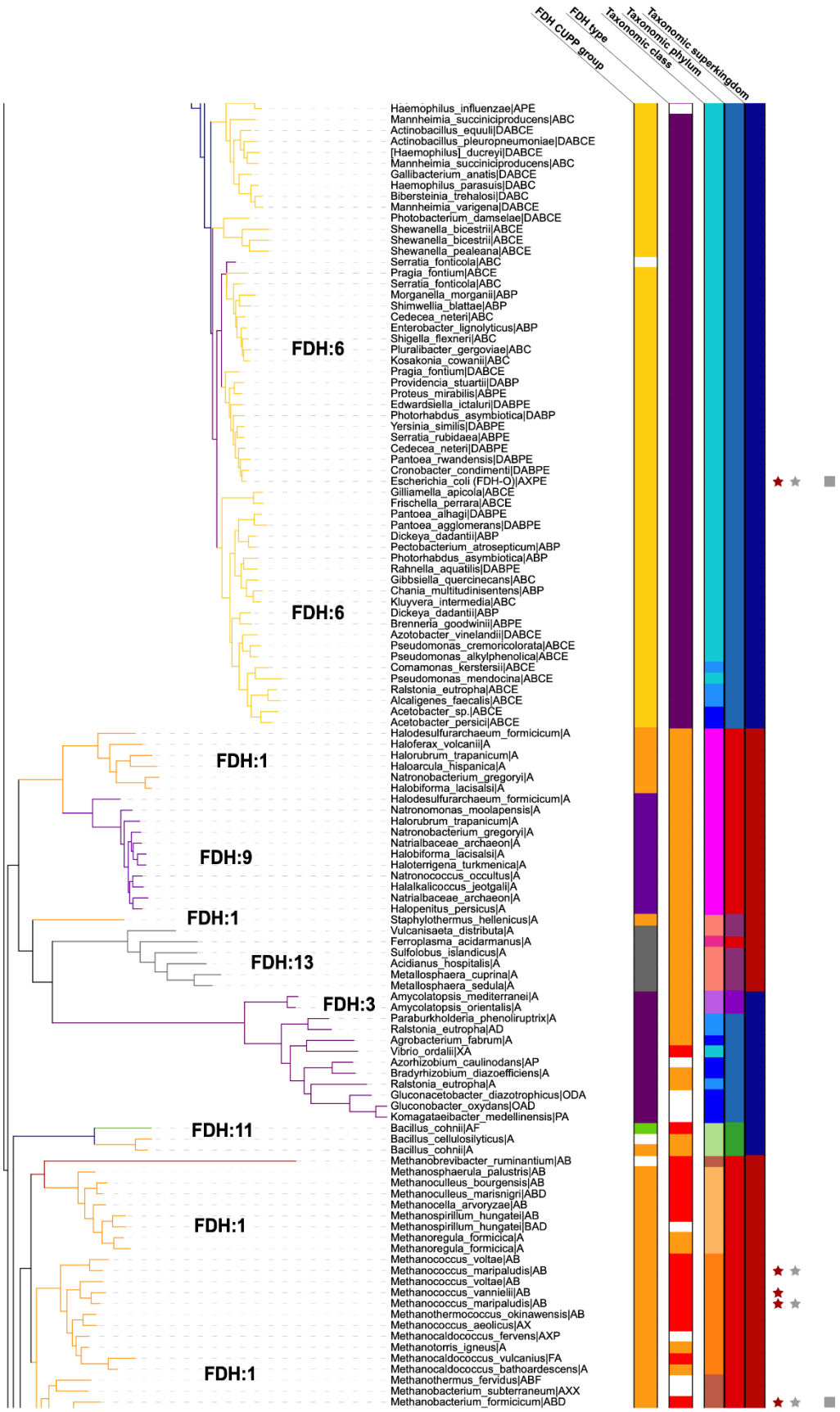
FDH CUPP group
FDH type
Taxonomic class
Taxonomic phylum
Taxonomic superkingdom
Haemophilus_influenzae|APE
Mannheimia_succiniciproducens|ABC
Actinobacillus_equuli|DABCE
Actinobacillus_pleuropneumoniae|DABCE
[Haemophilus]_ducreyi|DABCE
Mannheimia_succiniciproducens|ABC
Gallibacterium_anatis|DABCE
Haemophilus_parasuis|DABC
Bibersteinia_trehalosi|DABC
Mannheimia_varigena|DABCE
Photobacterium_damselae|DABCE
Shewanella_bicestrii|ABCE
Shewanella_bicestrii|ABCE
Shewanella_pealeana|ABCE
Serratia_fonticola|ABC
Pragia_fontium|ABCE
Serratia_fonticola|ABC
Morganella_morganii|ABP
Shimwellia_blattae|ABP
Cedecea_neteri|ABC
Enterobacter_lignolyticus|ABP
Shigella_flexneri|ABC
FDH:6
Pluralibacter_gergoviae|ABC
Kosakonia_cowanii|ABC
Pragia_fontium|DABCE
Providencia_stuartii|DABP
Proteus_mirabilis|ABPE
Edwardsiella_ictaluri|DABPE
Photorhabdus_asymbiotica|DABP
Yersinia_similis|DABPE
Serratia_rubidaea|ABPE
Cedecea_neteri|DABPE
Pantoea_rwandensis|DABPE
Cronobacter_condimenti|DABPE
Escherichia_coli (FDH-O)|AXPE
Gilliamella_apicola|ABCE
Frischella_perrara|ABCE
Pantoea_alhagi|DABPE
Pantoea_agglomerans|DABPE
Dickeya_dadantii|ABP
Pectobacterium_atrosepticum|ABP
Photorhabdus_asymbiotica|ABP
Rahnella_aquatilis|DABPE
Gibbsiella_quercinecans|ABC
Chania_multitudinisentens|ABP
Kluyvera_intermedia|ABC
FDH:6
Dickeya_dadantii|ABP
Brenneria_goodwinii|ABPE
Azotobacter_vinelandii|DABCE
Pseudomonas_cremoricolorata|ABCE
Pseudomonas_alkylphenolica|ABCE
Comamonas_kerstersii|ABCE
Pseudomonas_mendocina|ABCE
Ralstonia_eutropha|ABCE
Alcaligenes_faecalis|ABCE
Acetobacter_sp.|ABCE
Acetobacter_persici|ABCE
Halodesulfurarchaeum_formicicum|A
Haloferax_volcanii|A
FDH:1
Halorubrum_trapanicum|A
Haloarcula_hispanica|A
Natronobacterium_gregoryi|A
Halobiforma_lacisalsi|A
Halodesulfurarchaeum_formicicum|A
Natronomonas_moolapensis|A
Halorubrum_trapanicum|A
Natronobacterium_gregoryi|A
Natrialbaceae_archaeon|A
FDH:9
Halobiforma_lacisalsi|A
Haloterrigena_turkmenica|A
Natronococcus_occultus|A
Halalkalicoccus_jeotgali|A
Natrialbaceae_archaeon|A
Halopenitus_persicus|A
FDH:1
Staphylothermus_hellenicus|A
Vulcanisaeta_distributa|A
Ferroplasma_acidarmanus|A
Sulfolobus_islandicus|A
FDH:13
Acidianus_hospitalis|A
Metallosphaera_cuprina|A
Metallosphaera_sedula|A
FDH:3
Amycolatopsis_mediterranei|A
Amycolatopsis_orientalis|A
Paraburkholderia_phenoliruptrix|A
Ralstonia_eutropha|AD
Agrobacterium_fabrum|A
Vibrio_ordalii|XA
Azorhizobium_caulinodans|AP
Bradyrhizobium_diazoefficiens|A
Ralstonia_eutropha|A
Gluconacetobacter_diazotrophicus|ODA
Gluconobacter_oxydans|OAD
Komagataeibacter_medellinensis|PA
FDH:11
Bacillus_cohnii|AF
Bacillus_cellulosilyticus|A
Bacillus_cohnii|A
Methanobrevibacter_ruminantium|AB
Methanosphaerula_palustris|AB
Methanoculleus_bourgensis|AB
Methanoculleus_marisnigri|ABD
Methanocella_arvoryzae|AB
FDH:1
Methanospirillum_hungatei|AB
Methanospirillum_hungatei|BAD
Methanoregula_formicica|A
Methanoregula_formicica|A
Methanococcus_voltae|AB
Methanococcus_maripaludis|AB
Methanococcus_voltae|AB
Methanococcus_vannielii|AB
Methanococcus_maripaludis|AB
Methanothermococcus_okinawensis|AB
Methanococcus_aeolicus|AX
Methanocaldococcus_fervens|AXP
Methanotorris_igneus|A
Methanocaldococcus_vulcanius|FA
FDH:1
Methanocaldococcus_bathoardescens|A
Methanothermus_fervidus|ABF
Methanobacterium_subterraneum|AXX
Methanobacterium_formicicum|ABD

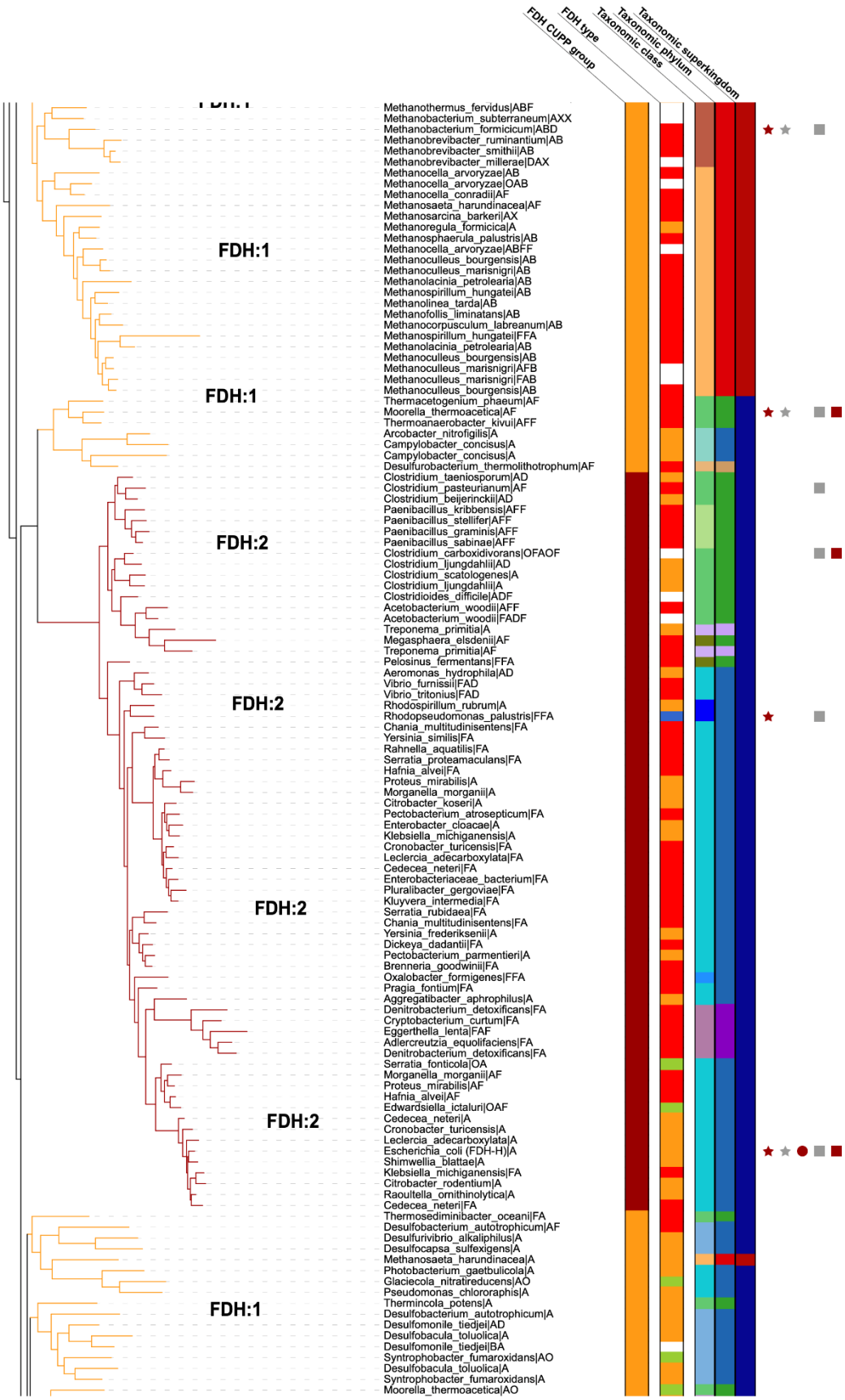
FDH CUPP group
FDH type
Taxonomic class
Taxonomic phylum
Taxonomic superkingdom
FDH:1
FDH:1
FDH:2
FDH:2
FDH:2
FDH:1
Methanothermus_fervidus|ABF
Methanobacterium_subterraneum|AXX
Methanobacterium_formicicum|ABD
Methanobrevibacter_ruminantium|AB
Methanobrevibacter_smithii|AB
Methanobrevibacter_millerae|DAX
Methanocella_arvoryzae|AB
Methanocella_arvoryzae|OAB
Methanocella_conradii|AF
Methanosaeta_harundinacea|AF
Methanosarcina_barkeri|AX
Methanoregula_formicica|A
Methanosphaerula_palustris|AB
Methanocella_arvoryzae|ABFF
Methanoculleus_bourgensis|AB
Methanoculleus_marisnigri|AB
Methanolacinia_petrolearia|AB
Methanospirillum_hungatei|AB
Methanolinea_tarda|AB
Methanofollis_liminatans|AB
Methanocorpusculum_labreanum|AB
Methanospirillum_hungatei|FFA
Methanolacinia_petrolearia|AB
Methanoculleus_bourgensis|AB
Methanoculleus_marisnigri|AFB
Methanoculleus_marisnigri|FAB
Methanoculleus_bourgensis|AB
Thermacetogenium_phaeum|AF
Moorella_thermoacetica|AF
Thermoanaerobacter_kivui|AFF
Arcobacter_nitrofigilis|A
Campylobacter_concisus|A
Campylobacter_concisus|A
Desulfurobacterium_thermolithotrophum|AF
Clostridium_taeniosporum|AD
Clostridium_pasteurianum|AF
Clostridium_beijerinckii|AD
Paenibacillus_kribbensis|AFF
Paenibacillus_stellifer|AFF
Paenibacillus_graminis|AFF
Paenibacillus_sabinae|AFF
Clostridium_carboxidivorans|OFAOF
Clostridium_ljungdahlii|AD
Clostridium_scatologenes|A
Clostridium_ljungdahlii|A
Clostridioides_difficile|ADF
Acetobacterium_woodii|AFF
Acetobacterium_woodii|FADF
Treponema_primitia|A
Megasphaera_elsdenii|AF
Treponema_primitia|AF
Pelosinus_fermentans|FFA
Aeromonas_hydrophila|AD
Vibrio_furnissii|FAD
Vibrio_tritonius|FAD
Rhodospirillum_rubrum|A
Rhodopseudomonas_palustris|FFA
Chania_multitudinisentens|FA
Yersinia_similis|FA
Rahnella_aquatilis|FA
Serratia_proteamaculans|FA
Hafnia_alvei|FA
Proteus_mirabilis|A
Morganella_morganii|A
Citrobacter_koseri|A
Pectobacterium_atrosepticum|FA
Enterobacter_cloacae|A
Klebsiella_michiganensis|A
Cronobacter_turicensis|FA
Leclercia_adecarboxylata|FA
Cedecea_neteri|FA
Enterobacteriaceae_bacterium|FA
Pluralibacter_gergoviae|FA
Kluyvera_intermedia|FA
Serratia_rubidaea|FA
Chania_multitudinisentens|FA
Yersinia_frederiksenii|A
Dickeya_dadantii|FA
Pectobacterium_parmentieri|A
Brenneria_goodwinii|FA
Oxalobacter_formigenes|FFA
Pragia_fontium|FA
Aggregatibacter_aphrophilus|A
Denitrobacterium_detoxificans|FA
Cryptobacterium_curtum|FA
Eggerthella_lenta|FAF
Adlercreutzia_equolifaciens|FA
Denitrobacterium_detoxificans|FA
Serratia_fonticola|OA
Morganella_morganii|AF
Proteus_mirabilis|AF
Hafnia_alvei|AF
Edwardsiella_ictaluri|OAF
Cedecea_neteri|A
Cronobacter_turicensis|A
Leclercia_adecarboxylata|A
Escherichia_coli (FDH-H)|A
Shimwellia_blattae|A
Klebsiella_michiganensis|FA
Citrobacter_rodentium|A
Raoultella_ornithinolytica|A
Cedecea_neteri|FA
Thermosediminibacter_oceani|FA
Desulfobacterium_autotrophicum|AF
Desulfurivibrio_alkaliphilus|A
Desulfocapsa_sulfexigens|A
Methanosaeta_harundinacea|A
Photobacterium_gaetbulicola|A
Glaciecola_nitratireducens|AO
Pseudomonas_chlororaphis|A
Thermincola_potens|A
Desulfobacterium_autotrophicum|A
Desulfomonile_tiedjei|AD
Desulfobacula_toluolica|A
Desulfomonile_tiedjei|BA
Syntrophobacter_fumaroxidans|AO
Desulfobacula_toluolica|A
Syntrophobacter_fumaroxidans|A
Moorella_thermoacetica|AO

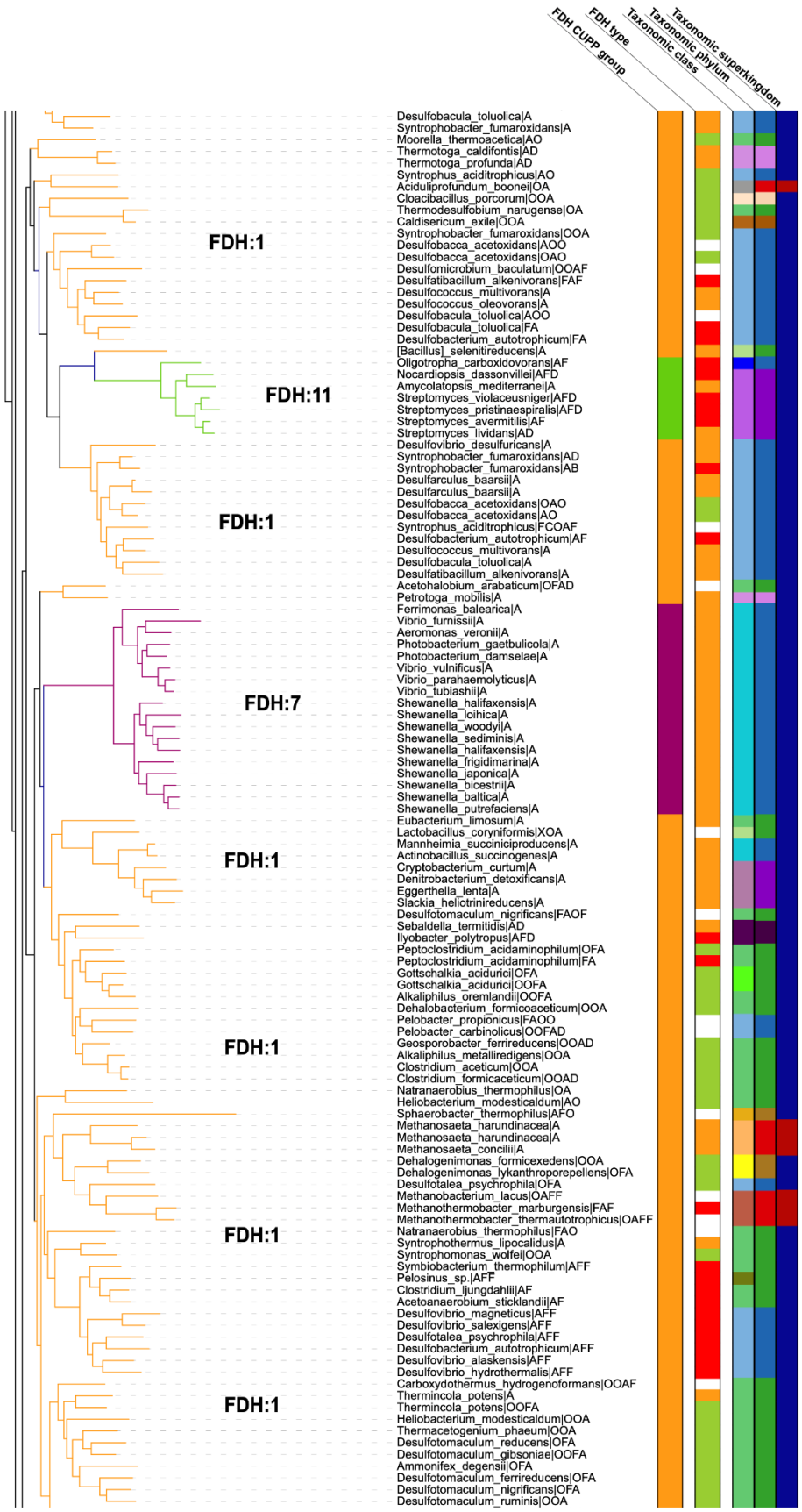
FDH CUPP group
FDH type
Taxonomic class
Taxonomic phylum
Taxonomic superkingdom
FDH:1
FDH:11
FDH:1
FDH:7
FDH:1
FDH:1
FDH:1
Desulfobacula_toluolica|A
Syntrophobacter_fumaroxidans|A
Moorella_thermoacetica|AO
Thermotoga_caldifontis|AD
Thermotoga_profunda|AD
Syntrophus_aciditrophicus|AO
Aciduliprofundum_boonei|OA
Cloacibacillus_porcorum|OOA
Thermodesulfobium_narugense|OA
Caldisericum_exile|OOA
Syntrophobacter_fumaroxidans|OOA
Desulfobacca_acetoxidans|AOO
Desulfobacca_acetoxidans|OAO
Desulfomicrobium_baculatum|OOAF
Desulfatibacillum_alkenivorans|FAF
Desulfococcus_multivorans|A
Desulfococcus_oleovorans|A
Desulfobacula_toluolica|AOO
Desulfobacula_toluolica|FA
Desulfobacterium_autotrophicum|FA
[Bacillus]_selenitireducens|A
Oligotropha_carboxidovorans|AF
Nocardiopsis_dassonvillei|AFD
Amycolatopsis_mediterranei|A
Streptomyces_violaceusniger|AFD
Streptomyces_pristinaespiralis|AFD
Streptomyces_avermitilis|AF
Streptomyces_lividans|AD
Desulfovibrio_desulfuricans|A
Syntrophobacter_fumaroxidans|AD
Syntrophobacter_fumaroxidans|AB
Desulfarculus_baarsii|A
Desulfarculus_baarsii|A
Desulfobacca_acetoxidans|OAO
Desulfobacca_acetoxidans|AO
Syntrophus_aciditrophicus|FCOAF
Desulfobacterium_autotrophicum|AF
Desulfococcus_multivorans|A
Desulfobacula_toluolica|A
Desulfatibacillum_alkenivorans|A
Acetohalobium_arabaticum|OFAD
Petrotoga_mobilis|A
Ferrimonas_balearica|A
Vibrio_furnissii|A
Aeromonas_veronii|A
Photobacterium_gaetbulicola|A
Photobacterium_damselae|A
Vibrio_vulnificus|A
Vibrio_parahaemolyticus|A
Vibrio_tubiashii|A
Shewanella_halifaxensis|A
Shewanella_loihica|A
Shewanella_woodyi|A
Shewanella_sediminis|A
Shewanella_halifaxensis|A
Shewanella_frigidimarina|A
Shewanella_japonica|A
Shewanella_bicestrii|A
Shewanella_baltica|A
Shewanella_putrefaciens|A
Eubacterium_limosum|A
Lactobacillus_coryniformis|XOA
Mannheimia_succiniciproducens|A
Actinobacillus_succinogenes|A
Cryptobacterium_curtum|A
Denitrobacterium_detoxificans|A
Eggerthella_lenta|A
Slackia_heliotrinireducens|A
Desulfotomaculum_nigrificans|FAOF
Sebaldella_termitidis|AD
Ilyobacter_polytropus|AFD
Peptoclostridium_acidaminophilum|OFA
Peptoclostridium_acidaminophilum|FA
Gottschalkia_acidurici|OFA
Gottschalkia_acidurici|OOFA
Alkaliphilus_oremlandii|OOFA
Dehalobacterium_formicoaceticum|OOA
Pelobacter_propionicus|FAOO
Pelobacter_carbinolicus|OOFAD
Geosporobacter_ferrireducens|OOAD
Alkaliphilus_metalliredigens|OOA
Clostridium_aceticum|OOA
Clostridium_formicaceticum|OOAD
Natranaerobius_thermophilus|OA
Heliobacterium_modesticaldum|AO
Sphaerobacter_thermophilus|AFO
Methanosaeta_harundinacea|A
Methanosaeta_harundinacea|A
Methanosaeta_concilii|A
Dehalogenimonas_formicexedens|OOA
Dehalogenimonas_lykanthroporepellens|OFA
Desulfotalea_psychrophila|OFA
Methanobacterium_lacus|OAFF
Methanothermobacter_marburgensis|FAF
Methanothermobacter_thermautotrophicus|OAFF
Natranaerobius_thermophilus|FAO
Syntrophothermus_lipocalidus|A
Syntrophomonas_wolfei|OOA
Symbiobacterium_thermophilum|AFF
Pelosinus_sp.|AFF
Clostridium_ljungdahlii|AF
Acetoanaerobium_sticklandii|AF
Desulfovibrio_magneticus|AFF
Desulfovibrio_salexigens|AFF
Desulfotalea_psychrophila|AFF
Desulfobacterium_autotrophicum|AFF
Desulfovibrio_alaskensis|AFF
Desulfovibrio_hydrothermalis|AFF
Carboxydothermus_hydrogenoformans|OOAF
Thermincola_potens|A
Thermincola_potens|OOFA
Heliobacterium_modesticaldum|OOA
Thermacetogenium_phaeum|OOA
Desulfotomaculum_reducens|OFA
Desulfotomaculum_gibsoniae|OOFA
Ammonifex_degensii|OFA
Desulfotomaculum_ferrireducens|OFA
Desulfotomaculum_nigrificans|OFA
Desulfotomaculum_ruminis|OOA

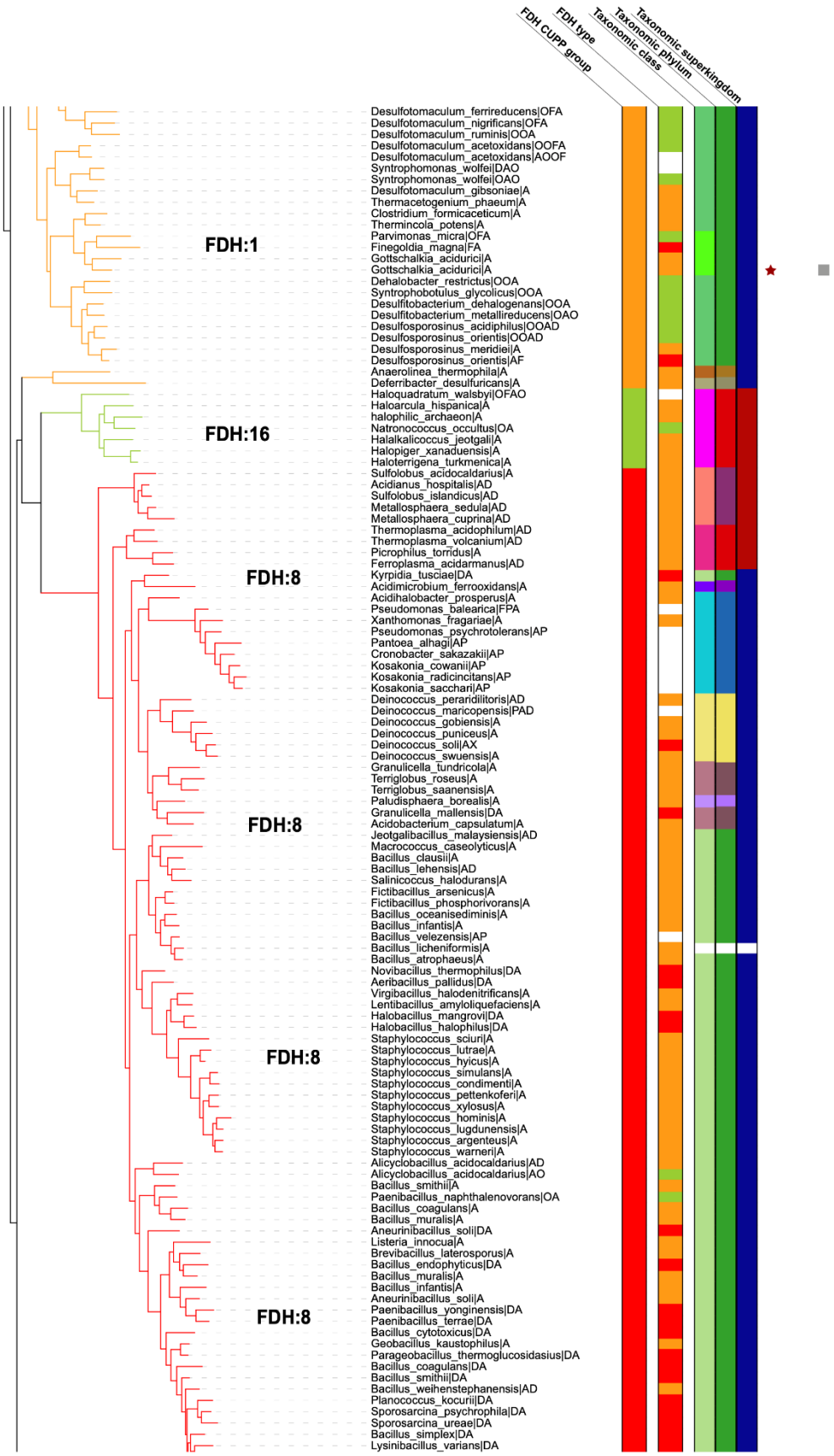
FDH CUPP group
FDH type
Taxonomic class
Taxonomic phylum
Taxonomic superkingdom
FDH:1
FDH:16
FDH:8
FDH:8
FDH:8
FDH:8
Desulfotomaculum_ferrireducens|OFA
Desulfotomaculum_nigrificans|OFA
Desulfotomaculum_ruminis|OOA
Desulfotomaculum_acetoxidans|OOFA
Desulfotomaculum_acetoxidans|AOOF
Syntrophomonas_wolfei|DAO
Syntrophomonas_wolfei|OAO
Desulfotomaculum_gibsoniae|A
Thermacetogenium_phaeum|A
Clostridium_formicaceticum|A
Thermincola_potens|A
Parvimonas_micra|OFA
Finegoldia_magna|FA
Gottschalkia_acidurici|A
Gottschalkia_acidurici|A
Dehalobacter_restrictus|OOA
Syntrophobotulus_glycolicus|OOA
Desulfitobacterium_dehalogenans|OOA
Desulfitobacterium_metallireducens|OAO
Desulfosporosinus_acidiphilus|OOAD
Desulfosporosinus_orientis|OOAD
Desulfosporosinus_meridiei|A
Desulfosporosinus_orientis|AF
Anaerolinea_thermophila|A
Deferribacter_desulfuricans|A
Haloquadratum_walsbyi|OFAO
Haloarcula_hispanica|A
halophilic_archaeon|A
Natronococcus_occultus|OA
Halalkalicoccus_jeotgali|A
Halopiger_xanaduensis|A
Haloterrigena_turkmenica|A
Sulfolobus_acidocaldarius|A
Acidianus_hospitalis|AD
Sulfolobus_islandicus|AD
Metallosphaera_sedula|AD
Metallosphaera_cuprina|AD
Thermoplasma_acidophilum|AD
Thermoplasma_volcanium|AD
Picrophilus_torridus|A
Ferroplasma_acidarmanus|AD
Kyrpidia_tusciae|DA
Acidimicrobium_ferrooxidans|A
Acidihalobacter_prosperus|A
Pseudomonas_balearica|FPA
Xanthomonas_fragariae|A
Pseudomonas_psychrotolerans|AP
Pantoea_alhagi|AP
Cronobacter_sakazakii|AP
Kosakonia_cowanii|AP
Kosakonia_radicincitans|AP
Kosakonia_sacchari|AP
Deinococcus_peraridilitoris|AD
Deinococcus_maricopensis|PAD
Deinococcus_gobiensis|A
Deinococcus_puniceus|A
Deinococcus_soli|AX
Deinococcus_swuensis|A
Granulicella_tundricola|A
Terriglobus_roseus|A
Terriglobus_saanensis|A
Paludisphaera_borealis|A
Granulicella_mallensis|DA
Acidobacterium_capsulatum|A
Jeotgalibacillus_malaysiensis|AD
Macrococcus_caseolyticus|A
Bacillus_clausii|A
Bacillus_lehensis|AD
Salinicoccus_halodurans|A
Fictibacillus_arsenicus|A
Fictibacillus_phosphorivorans|A
Bacillus_oceanisediminis|A
Bacillus_infantis|A
Bacillus_velezensis|AP
Bacillus_licheniformis|A
Bacillus_atrophaeus|A
Novibacillus_thermophilus|DA
Aeribacillus_pallidus|DA
Virgibacillus_halodenitrificans|A
Lentibacillus_amyloliquefaciens|A
Halobacillus_mangrovi|DA
Halobacillus_halophilus|DA
Staphylococcus_sciuri|A
Staphylococcus_lutrae|A
Staphylococcus_hyicus|A
Staphylococcus_simulans|A
Staphylococcus_condimenti|A
Staphylococcus_pettenkoferi|A
Staphylococcus_xylosus|A
Staphylococcus_hominis|A
Staphylococcus_lugdunensis|A
Staphylococcus_argenteus|A
Staphylococcus_warneri|A
Alicyclobacillus_acidocaldarius|AD
Alicyclobacillus_acidocaldarius|AO
Bacillus_smithii|A
Paenibacillus_naphthalenovorans|OA
Bacillus_coagulans|A
Bacillus_muralis|A
Aneurinibacillus_soli|DA
Listeria_innocua|A
Brevibacillus_laterosporus|A
Bacillus_endophyticus|DA
Bacillus_muralis|A
Bacillus_infantis|A
Aneurinibacillus_soli|A
Paenibacillus_yonginensis|DA
Paenibacillus_terrae|DA
Bacillus_cytotoxicus|DA
Geobacillus_kaustophilus|A
Parageobacillus_thermoglucosidasius|DA
Bacillus_coagulans|DA
Bacillus_smithii|DA
Bacillus_weihenstephanensis|AD
Planococcus_kocurii|DA
Sporosarcina_psychrophila|DA
Sporosarcina_ureae|DA
Bacillus_simplex|DA
Lysinibacillus_varians|DA

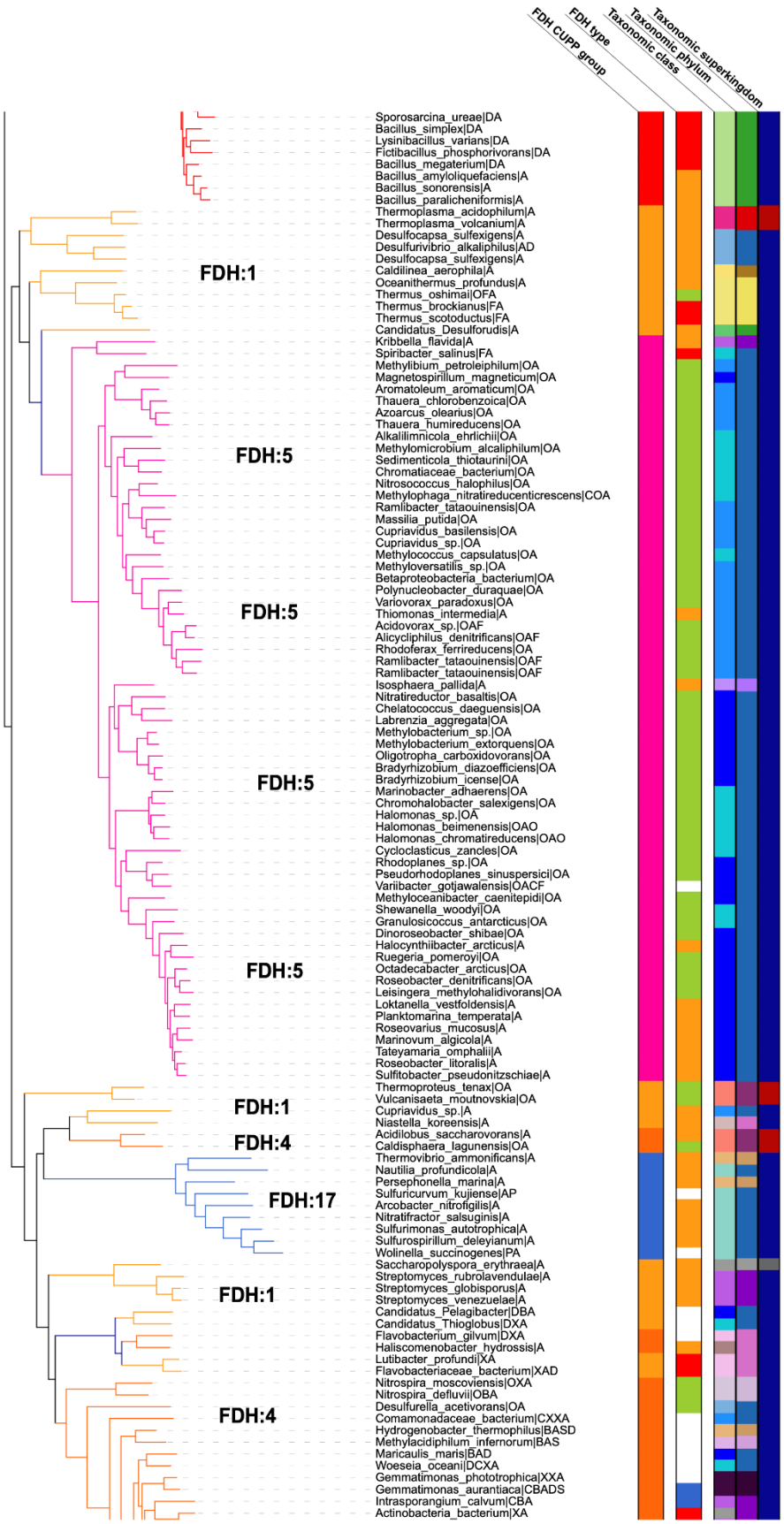
FDH CUPP group
FDH type
Taxonomic class
Taxonomic phylum
Taxonomic superkingdom
FDH:1
FDH:5
FDH:5
FDH:5
FDH:5
FDH:1
FDH:4
FDH:17
FDH:1
FDH:4
Sporosarcina_ureae|DA
Bacillus_simplex|DA
Lysinibacillus_varians|DA
Fictibacillus_phosphorivorans|DA
Bacillus_megaterium|DA
Bacillus_amyloliquefaciens|A
Bacillus_sonorensis|A
Bacillus_paralicheniformis|A
Thermoplasma_acidophilum|A
Thermoplasma_volcanium|A
Desulfocapsa_sulfexigens|A
Desulfurivibrio_alkaliphilus|AD
Desulfocapsa_sulfexigens|A
Caldilinea_aerophila|A
Oceanithermus_profundus|A
Thermus_oshimai|OFA
Thermus_brockianus|FA
Thermus_scotoductus|FA
Candidatus_Desulforudis|A
Kribbella_flavida|A
Spiribacter_salinus|FA
Methylibium_petroleiphilum|OA
Magnetospirillum_magneticum|OA
Aromatoleum_aromaticum|OA
Thauera_chlorobenzoica|OA
Azoarcus_olearius|OA
Thauera_humireducens|OA
Alkalilimnicola_ehrlichii|OA
Methylomicrobium_alcaliphilum|OA
Sedimenticola_thiotaurini|OA
Chromatiaceae_bacterium|OA
Nitrosococcus_halophilus|OA
Methylophaga_nitratireducenticrescens|COA
Ramlibacter_tataouinensis|OA
Massilia_putida|OA
Cupriavidus_basilensis|OA
Cupriavidus_sp.|OA
Methylococcus_capsulatus|OA
Methyloversatilis_sp.|OA
Betaproteobacteria_bacterium|OA
Polynucleobacter_duraquae|OA
Variovorax_paradoxus|OA
Thiomonas_intermedia|A
Acidovorax_sp.|OAF
Alicycliphilus_denitrificans|OAF
Rhodoferax_ferrireducens|OA
Ramlibacter_tataouinensis|OAF
Ramlibacter_tataouinensis|OAF
Isosphaera_pallida|A
Nitratireductor_basaltis|OA
Chelatococcus_daeguensis|OA
Labrenzia_aggregata|OA
Methylobacterium_sp.|OA
Methylobacterium_extorquens|OA
Oligotropha_carboxidovorans|OA
Bradyrhizobium_diazoefficiens|OA
Bradyrhizobium_icense|OA
Marinobacter_adhaerens|OA
Chromohalobacter_salexigens|OA
Halomonas_sp.|OA
Halomonas_beimenensis|OAO
Halomonas_chromatireducens|OAO
Cycloclasticus_zancles|OA
Rhodoplanes_sp.|OA
Pseudorhodoplanes_sinuspersici|OA
Variibacter_gotjawalensis|OACF
Methyloceanibacter_caenitepidi|OA
Shewanella_woodyi|OA
Granulosicoccus_antarcticus|OA
Dinoroseobacter_shibae|OA
Halocynthiibacter_arcticus|A
Ruegeria_pomeroyi|OA
Octadecabacter_arcticus|OA
Roseobacter_denitrificans|OA
Leisingera_methylohalidivorans|OA
Loktanella_vestfoldensis|A
Planktomarina_temperata|A
Roseovarius_mucosus|A
Marinovum_algicola|A
Tateyamaria_omphalii|A
Roseobacter_litoralis|A
Sulfitobacter_pseudonitzschiae|A
Thermoproteus_tenax|OA
Vulcanisaeta_moutnovskia|OA
Cupriavidus_sp.|A
Niastella_koreensis|A
Acidilobus_saccharovorans|A
Caldisphaera_lagunensis|OA
Thermovibrio_ammonificans|A
Nautilia_profundicola|A
Persephonella_marina|A
Sulfuricurvum_kujiense|AP
Arcobacter_nitrofigilis|A
Nitratifractor_salsuginis|A
Sulfurimonas_autotrophica|A
Sulfurospirillum_deleyianum|A
Wolinella_succinogenes|PA
Saccharopolyspora_erythraea|A
Streptomyces_rubrolavendulae|A
Streptomyces_globisporus|A
Streptomyces_venezuelae|A
Candidatus_Pelagibacter|DBA
Candidatus_Thioglobus|DXA
Flavobacterium_gilvum|DXA
Haliscomenobacter_hydrossis|A
Lutibacter_profundi|XA
Flavobacteriaceae_bacterium|XAD
Nitrospira_moscoviensis|OXA
Nitrospira_defluvii|OBA
Desulfurella_acetivorans|OA
Comamonadaceae_bacterium|CXXA
Hydrogenobacter_thermophilus|BASD
Methylacidiphilum_infernorum|BAS
Maricaulis_maris|BAD
Woeseia_oceani|DCXA
Gemmatimonas_phototrophica|XXA
Gemmatimonas_aurantiaca|CBADS
Intrasporangium_calvum|CBA
Actinobacteria_bacterium|XA

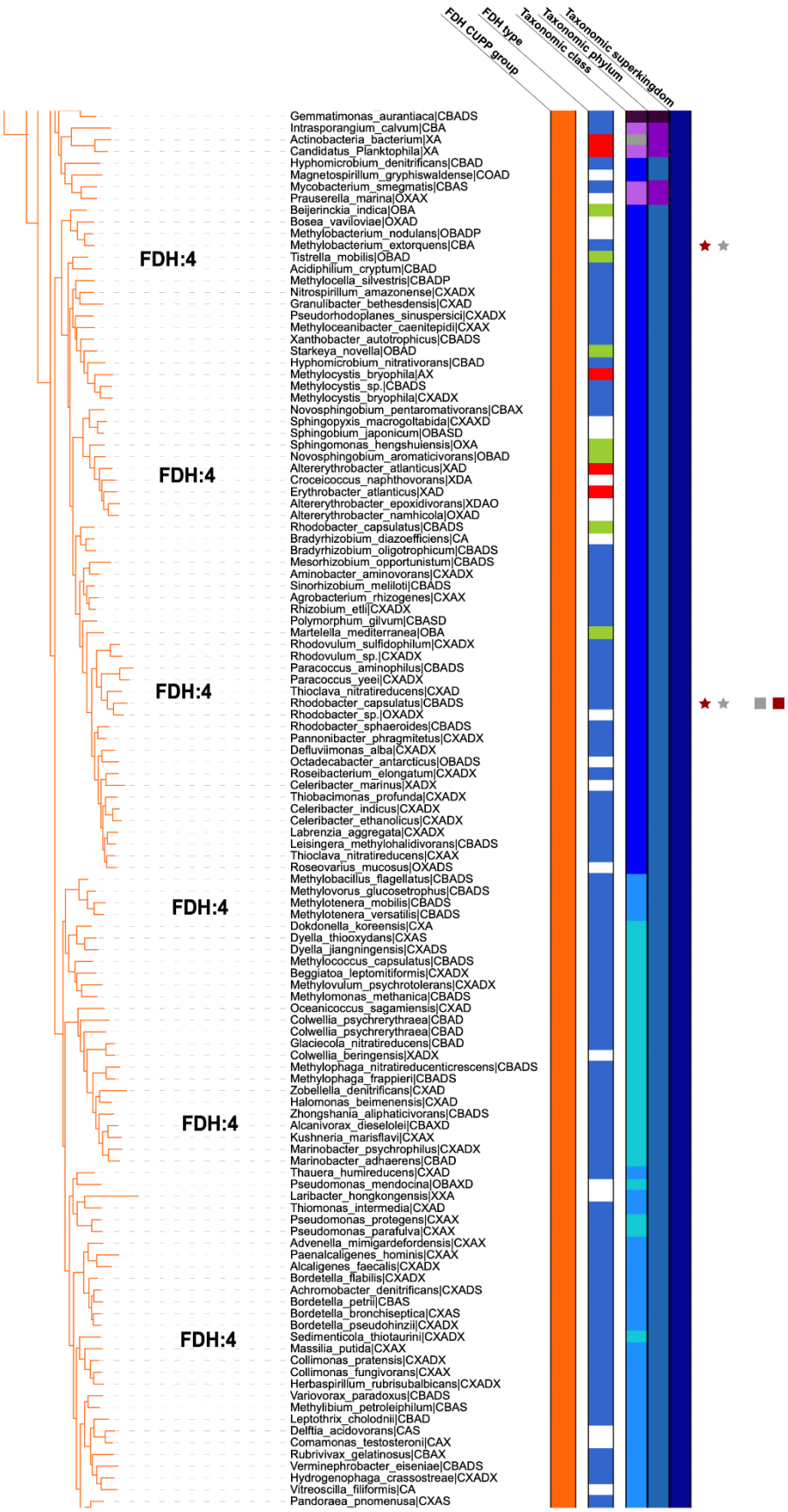
FDH CUPP group
FDH type
Taxonomic class
Taxonomic phylum
Taxonomic superkingdom
FDH:4
FDH:4
FDH:4
FDH:4
FDH:4
Gemmatimonas_aurantiaca|CBADS
Intrasporangium_calvum|CBA
Actinobacteria_bacterium|XA
Candidatus_Planktophila|XA
Hyphomicrobium_denitrificans|CBAD
Magnetospirillum_gryphiswaldense|COAD
Mycobacterium_smegmatis|CBAS
Prauserella_marina|OXAX
Beijerinckia_indica|OBA
Bosea_vaviloviae|OXAD
Methylobacterium_nodulans|OBADP
Methylobacterium_extorquens|CBA
Tistrella_mobilis|OBAD
Acidiphilium_cryptum|CBAD
Methylocella_silvestris|CBADP
Nitrospirillum_amazonense|CXADX
Granulibacter_bethesdensis|CXAD
Pseudorhodoplanes_sinuspersici|CXADX
Methyloceanibacter_caenitepidi|CXAX
Xanthobacter_autotrophicus|CBADS
Starkeya_novella|OBAD
Hyphomicrobium_nitrativorans|CBAD
Methylocystis_bryophila|AX
Methylocystis_sp.|CBADS
Methylocystis_bryophila|CXADX
Novosphingobium_pentaromativorans|CBAX
Sphingopyxis_macrogoltabida|CXAXD
Sphingobium_japonicum|OBASD
Sphingomonas_hengshuiensis|OXA
Novosphingobium_aromaticivorans|OBAD
Altererythrobacter_atlanticus|XAD
Croceicoccus_naphthovorans|XDA
Erythrobacter_atlanticus|XAD
Altererythrobacter_epoxidivorans|XDAO
Altererythrobacter_namhicola|OXAD
Rhodobacter_capsulatus|CBADS
Bradyrhizobium_diazoefficiens|CA
Bradyrhizobium_oligotrophicum|CBADS
Mesorhizobium_opportunistum|CBADS
Aminobacter_aminovorans|CXADX
Sinorhizobium_meliloti|CBADS
Agrobacterium_rhizogenes|CXAX
Rhizobium_etli|CXADX
Polymorphum_gilvum|CBASD
Martelella_mediterranea|OBA
Rhodovulum_sulfidophilum|CXADX
Rhodovulum_sp.|CXADX
Paracoccus_aminophilus|CBADS
Paracoccus_yeei|CXADX
Thioclava_nitratireducens|CXAD
Rhodobacter_capsulatus|CBADS
Rhodobacter_sp.|OXADX
Rhodobacter_sphaeroides|CBADS
Pannonibacter_phragmitetus|CXADX
Defluviimonas_alba|CXADX
Octadecabacter_antarcticus|OBADS
Roseibacterium_elongatum|CXADX
Celeribacter_marinus|XADX
Thiobacimonas_profunda|CXADX
Celeribacter_indicus|CXADX
Celeribacter_ethanolicus|CXADX
Labrenzia_aggregata|CXADX
Leisingera_methylohalidivorans|CBADS
Thioclava_nitratireducens|CXAX
Roseovarius_mucosus|OXADS
Methylobacillus_flagellatus|CBADS
Methylovorus_glucosetrophus|CBADS
Methylotenera_mobilis|CBADS
Methylotenera_versatilis|CBADS
Dokdonella_koreensis|CXA
Dyella_thiooxydans|CXAS
Dyella_jiangningensis|CXADS
Methylococcus_capsulatus|CBADS
Beggiatoa_leptomitiformis|CXADX
Methylovulum_psychrotolerans|CXADX
Methylomonas_methanica|CBADS
Oceanicoccus_sagamiensis|CXAD
Colwellia_psychrerythraea|CBAD
Colwellia_psychrerythraea|CBAD
Glaciecola_nitratireducens|CBAD
Colwellia_beringensis|XADX
Methylophaga_nitratireducenticrescens|CBADS
Methylophaga_frappieri|CBADS
Zobellella_denitrificans|CXAD
Halomonas_beimenensis|CXAD
Zhongshania_aliphaticivorans|CBADS
Alcanivorax_dieselolei|CBAXD
Kushneria_marisflavi|CXAX
Marinobacter_psychrophilus|CXADX
Marinobacter_adhaerens|CBAD
Thauera_humireducens|CXAD
Pseudomonas_mendocina|OBAXD
Laribacter_hongkongensis|XXA
Thiomonas_intermedia|CXAD
Pseudomonas_protegens|CXAX
Pseudomonas_parafulva|CXAX
Advenella_mimigardefordensis|CXAX
Paenalcaligenes_hominis|CXAX
Alcaligenes_faecalis|CXADX
Bordetella_flabilis|CXADX
Achromobacter_denitrificans|CXADS
Bordetella_petrii|CBAS
Bordetella_bronchiseptica|CXAS
Bordetella_pseudohinzii|CXADX
Sedimenticola_thiotaurini|CXADX
Massilia_putida|CXAX
Collimonas_pratensis|CXADX
Collimonas_fungivorans|CXAX
Herbaspirillum_rubrisubalbicans|CXADX
Variovorax_paradoxus|CBADS
Methylibium_petroleiphilum|CBAS
Leptothrix_cholodnii|CBAD
Delftia_acidovorans|CAS
Comamonas_testosteroni|CAX
Rubrivivax_gelatinosus|CBAX
Verminephrobacter_eiseniae|CBADS
Hydrogenophaga_crassostreae|CXADX
Vitreoscilla_filiformis|CA
Pandoraea_pnomenusa|CXAS

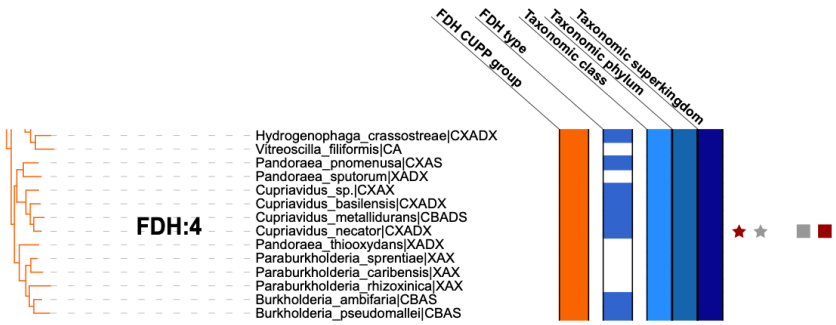

FDH Type

- Type 1: A, DA
- Type 2: (E)AB(E), AX(E), XA, AF, FA, XAD, AFD
- Type 3: Not able to annotate
- Type 4: ABC(E), ABP(E), AFC(E), ABCD, DABC(E), DABP(E), DAFCE
- Type 5: CBADS, CBADX, CXADS, CBAD, CXAD, CBAX, CBAS, CXAS, CXA
- Type 6: OA, OAF, OBAD, OAD, OXA, OXAD, AO, OBA, AOF, COA

Taxonomic superkingdom	Taxonomic phylum	Taxonomic class	Percentage of data (Phylum)
Archaea	Euryarchaeota	Thermococci Methanococci Methanobacteria Thermoplasmata Methanomicrobia Halobacteria	9.5 %
	Crenarchaeota	Thermoprotei	1.1 %
Bacteria	Proteobacteria	Alphaproteobacteria Betaproteobacteria Gammaproteobacteria Deltaproteobacteria Epsilonproteobacteria	64.3 %
	Firmicutes	Bacilli Clostridia Tissierellia Negativicutes Limnochordia	17.5 %
	Actinobacteria	Actinobacteria Acidimicrobiia Coriobacteriia Rubrobacteria	3.0 %
	Chloroflexi	Thermomicrobia Dehalococcoidia Anaerolineae Caldilineae	0.7 %
	Bacteroidetes	Saprospiria Chitinophagia Flavobacteriia	0.3 %
	Acidobacteria	Acidobacteriia	0.6 %
	Aquificae	Aquificae	0.5 %
	Caldiserica	Caldisericia	0.1 %
	Deferribacteres	Deferribacteres	0.1 %
	Deinococcus-Thermus	Deinococci	0.8 %
	Fusobacteria	Fusobacteriia	0.1 %
	Gemmatimonadetes	Gemmatimonadetes	0.1 %
	Nitrospirae	Nitrospira	0.2 %
	Planctomycetes	Planctomycetia	0.1 %
	Spirochaetes	Spirochaetia	0.1 %
	Synergistetes	Synergistia	0.1 %
	Thermotogae	Thermotogae	0.2 %
	Thermodesulfobacteria	Thermodesulfobacteria	0.2 %
	Verrucomicrobia	Methylacidiphilae	0.1 %
Unknown	Unknown	Unknown	0.2 %

CUPP group

- FDH:1
- FDH:2
- FDH:3
- FDH:4
- FDH:5
- FDH:6
- FDH:7
- FDH:8
- FDH:9
- FDH:10
- FDH:11
- FDH:12
- FDH:13
- FDH:14
- FDH:15
- FDH:16
- FDH:17

Known attributes

- Gene organization
- Subunit composition
- Crystal structure
- Formate oxidation
- CO_2 reduction

Appendix E. Solubility assay

The solubility assay was performed according to the below protocol.

- Spin down 1 mL sample, and wash with 200 µl Washing buffer and spin again for 5 min at 13,000 rpm
- Re-suspend pellets in 50 µl x OD_{600} cold solubilization buffers + 1 mM PMSF
- Sonicate at max intensity for 30 min in a cold water-bath (take out a 5 µl sample and reduce by adding 4x Laemmli loading buffer ⇨ Total Cell Lysate fraction (TCL))
- Spin 15 min at 13,000 rpm ⇨ keep both pellets (P) and supernatants (SN)
- Resuspend pellets in 50 µl x OD_{600} 1x Laemmli loading buffer and keep at RT (⇨ P)
- Add 1 ml ice-cold pure acetone to each supernatant and freeze for 20 min at -20°C
- Spin supernatants for 15 min at 13,000 rpm, remove acetone and let dry on the bench
- Resuspend faint white precipitates (bottom and inner surfaces of the eppendorf tubes) in 25 µl x OD_{600} 1x Laemmli loading buffer (⇨ SN)
- Boil pellets and supernatants samples for 3 min at 95°C
- Spin all samples for 15 min at 13,000 rpm, 4°C
- Load 5 µl of TCL, 15 µl of P and SN samples or 8 µl SN for Western Blot on 12% SDS gels and run for 15 min at 90 V and 1 hour at 150 V
- Continue with a Coomassie blue staining and a Western-Blotting anti-His tag
- Evaluate the proportion of proteins present in the SN = soluble proteins.

The buffers tested were with varying amounts of glycerol and salt (Table 14) and the proportion of proteins present in the SN fraction was evaluated (Figure 34 and Figure 35).

Table 14: Buffers used for solubility test.

Solubilization Buffer (10 ml)	**S1**	**S2**	**S3**	**S4**	**Washing buffer**
Tris-HCl pH 7.6 1M stock	50 mM (0.5 ml)	50 mM (0.5 ml)	50 mM (0.5 ml)	50 mM (0.5 ml)	50 mM (0.5 ml)
NaCl 5M stock	50 mM (0.1 ml)	150 mM (0.3 ml)	100 mM (0.2 ml)	500 mM (1.0 ml)	150 mM (0.3 ml)
Glycerol 100% stock	/	/	10% (1.0 ml)	/	/
MQ H_2O	9.3 ml	9.1 ml	8.2 ml	8.4 ml	9.2 ml

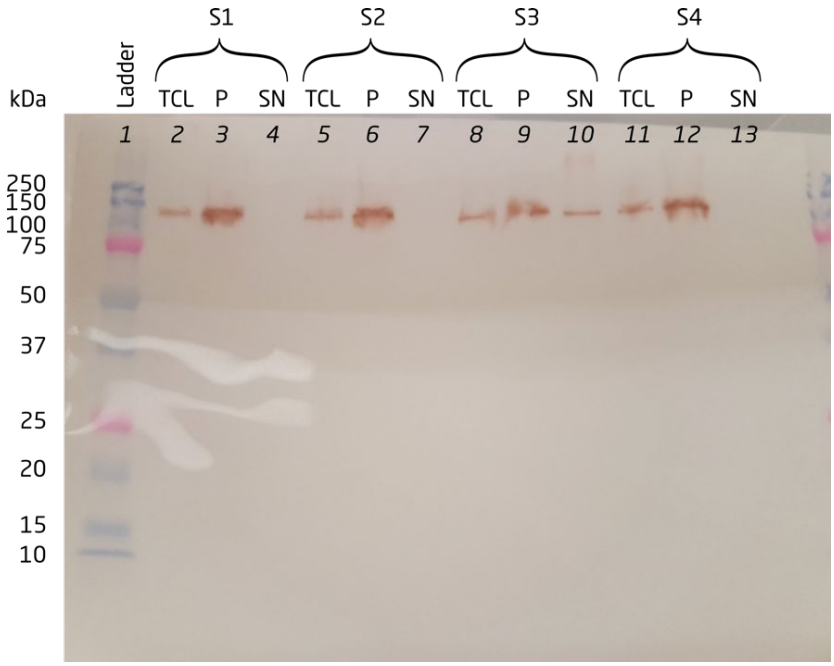

Figure 34: Western blot for alpha-tagged RcFDH. Buffers are described in Table 14. Ladder = DUAL color, TCL = total cell lysate, P = pellet, SN = supernatant.

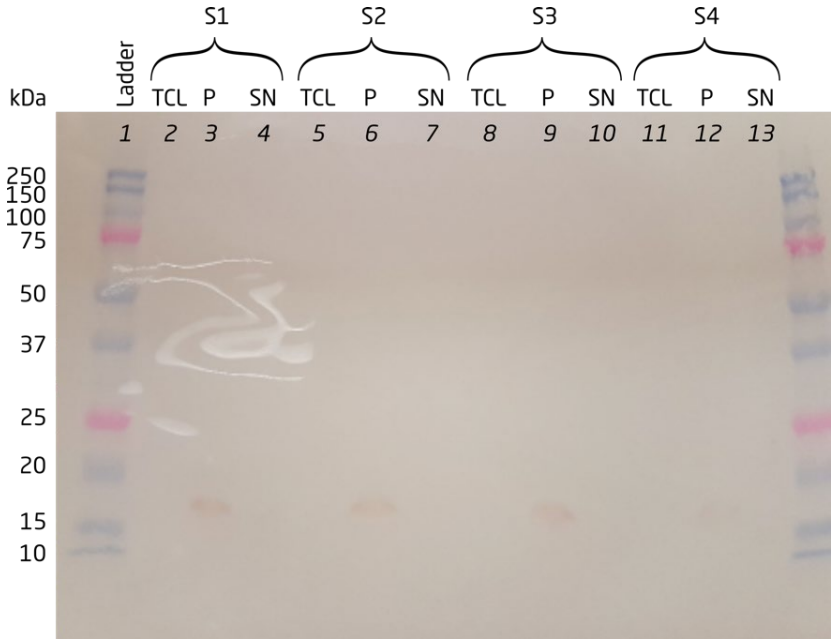

Figure 35: Western blot for gamma-tagged RcFDH. Buffers are described in Table 14. Ladder = DUAL color, TCL = total cell lysate, P = pellet, SN = supernatant.

While impossible to see in Figure 35, it actually contains the same pattern as can be seen in Figure 34. Here, RcFDH is only soluble when using the glycerol-containing buffer S3. Although a large amount of RcFDH is found in the insoluble fraction with this buffer, it can be argued that enough protein is in the soluble fraction to continue.

Appendix F. Co-factor saturation methodology

Co-factor saturation of enzyme samples were completed by laboratory technician Malgorzata Rizzi of DTU Environment as follows:

Elemental concentrations of Fe and Mo were measured on Agilent 7700x ICP-MS Inductive Coupled Plasma-Mass Spectrometer (ICP-MS). Sample with protein concentration between 0.5 and 1.5 mg/ml were used. Before the measurement, the samples were diluted 100x in 2% Suprapur HNO_3. The elements were analyzed in He mode. The sample uptake speed (nebulizer pump speed) was set to 0.1 rpm and the stabilization time to 40 sec. Integration time was set to 0.3 sec for He mode (He flow 5 mL/min). Processing of the data was carried out in the MassHunter 4.6 Workstation Software (v. C.01.06).

Appendix G. Materials and methods for cloning of expression vectors

Expression vectors were designed *in situ* and synthesized for this study. A total of six plasmids were ordered, two for each FDH variant. For each FDH variant, a construct with a His-tag on the N-terminal of the FdsG subunit as well as a construct with a His-tag on the N-terminal of the FdsA subunit was designed. All gene constructs were based on publicly available gene sequences sourced from the NCBI RefSeq database *(O'Leary et al., 2016)* (Table 15) and a common expression vector identical to the vector used by Hartmann et al. 2013 *(Hartmann and Leimkühler, 2013)*. Individual FDH operons were extracted as native sequences from full genomes and inserted into a modified pTrc expression vector. The gene constructs were synthesized and cloned into the expression vector by Genscript Biotech.

Table 15: Operon placement in the genomes of origin for RcFDH, RsFDH, and CnFDH (RefSeq).

Enzyme variant	Corresponding expression vectors	Genome ID	Genome name	Location of operon in genome
RcFDH	pTrc_RcFDH_gamma and pTrc_RcFDH_alpha	NC_014034.1	Rhodobacter capsulatus SB 1003, complete genome	3223340- 3229140 (complementary strand)
RsFDH	pTrc_RsFDH and pTrc_RsFDH_alpha	CP000661.1	Rhodobacter sphaeroides ATCC 17025, complete genome	2907382-2913283 (complementary strand)
CnFDH	pTrc_CnFDH and pTrc_CnFDH_alpha	NC_015726.1	Cupriavidus necator N-1 chromosome 1, complete sequence	657183-663287

The plasmids were transformed into competent *E. coli* DH5α cells and plated on LB agar plates with 100 µg/ml ampicillin. Individual transformant colonies were picked and cultured in LB medium with 100 µg/ml ampicillin overnight at 37 °C and 250 rpm. The outgrown culture was saved in 0.8 ml aliquots with 25% glycerol at -80 °C. Importantly, a decline in production yield was observed when using scrapes from a single glycerol stock repeatedly. Consistently high yields were achieved by only thawing and using an aliquot once.

Appendix H. Discussion on purification method

During execution of the research underlining this thesis, challenges regarding purification of the candidate FDHs arose. Both the solutions and challenges add to the story of recombinant type 5 FDH production as will discussed below. Additionally, the applied approach and future optimizations will be discussed.

Purification via IMAC is a commonly used method. A string of histidine residues, the so called 'His-tag', are coupled via a linker to an exposed part of the protein. The histidine residues of the His-tag have an affinity for metal-ions, with nickel ions being the most commonly applied. This is then exploited to separate tagged from native protein by first binding the tagged protein and washing unspecific protein, and then eluting the tagged protein by addition of imidazole. Imidazole, being chemically similar to the sidechain of histidine, also has affinity for metal ions and in high enough concentrations will displace and release the bound protein. As presented in the previous section, the constructs each contained a His-tag allowing use of IMAC to quickly reach a nearly pure solution of the given FDH variant.

However, although effective, IMAC purification does require considerations based on the protein of interest. For instance, given the propensity for nickel column to chelate metals, it does involve a risk when expressing metal-containing proteins. Additionally, nickel columns require the use of imidazole for elution, which can be another cause for concern. A solution could be an alternative form of affinity column, for instance a GST column (Tsai and Tainer, 2018). For this study it was not attempted to optimize via column material given the success with nickel columns in literature for type 5 FDH. It is, however, an interesting notion for potential future optimization.

Additional considerations involve used of pre-packed columns vs. gravity flow and use of salt for removing unspecific protein as discussed below.

Prepacked column vs. gravity flow system

In the work of this thesis, both methods were applied, starting with the pre-packed columns. Here, challenges with build-up of pressure on the pre-packed column was observed. To solve this issue, it was attempted to switch from HisTrap High Performance columns (containing a built-in filter) to HisTrap Fast Flow crude columns. The result of the switch in columns was only a delay in build-up of pressure. Filtering the supernatant through 0.45 µm filter paper prior to loading did not alleviate the build-up issues either. It was suspected that the FDH aggregated due to unknown complications with high protein concentration, which in turn built pressure and ruined the column. To alleviate these issues, gravity flow systems were applied instead. For the gravity flow method, however, one loses the informative protein absorbance chromatogram provided via the ÄKTA, but also circumvents the issue of pressure build-up. Additionally, the gravity flow method permits parallel purification, meaning all three type 5 FDH could be purified simultaneously.

High salt concentration for removal of unspecific protein

It is a well-known fact that salt concentration influence solubility of proteins. Additionally, salt concentration can be used to influence weak protein-protein interactions. As such, washing a protein-saturated nickel-column with buffer containing a different salt concentration, should influence unspecific protein bound to the His-tagged protein. An experiment was conducted with high salt concentration to enhance purity for RcFDH purified with pre-packed columns as described above.

Here the pre-packed column, with bound His-tagged RcFDH was washed with buffer containing 1 M NaCl for 1 CV, followed by washing the column without salt until conductivity returned to the previous baseline. The remaining protein on the column was eluted as described in Section 3.3.1 with imidazole. This resulted in two elution peaks: A “salt wash peak” and a “regular elution peak’. Interestingly, the latter regular peak showed significantly higher specific activity than the salt wash peak (data not shown). This result indicates that some unspecific binding to the His-tagged proteins is present, and that these proteins can be separated with a salt wash. A high salt wash was not included for type 5 FDH purified with gravity flow, and as such, the FDH studied for this thesis was not purified using this method.

Appendix I. Development of expression method

In accordance with existing knowledge on expression of complex metal-dependent FDHs, slow growth rates should enhance specific activity of purified FDHs by allowing increased co-factor saturation (Niks and Hille, 2018; Tsai and Tainer, 2018).

As described in Section 3.2, the expression method developed for this study used four different strains of *E. coli* expression strains transformed with pTrc_RcFDH_gamma. These were *E. coli* BL21 (DE3) pLysS, *E. coli* Rosetta2 (DE3), *E. coli* C43 (DE3), and *E. coli* BL21 (DE3). The strains were cultured in either LB medium or TB medium in combination with either high shaking speed (130 rpm) and low shaking speed (30 rpm) as described in detail below.

For expression, a single medium was used for both preculture and actual expression: Either LB or TB medium with 150 µg/ml ampicillin, 1 mM sodium molybdate. A 5 ml preculture were inoculated with 50 µl of the desired single-use glycerol stock, and then incubated at 37 °C and 130 rpm overnight. For expression, 2 l baffled Erlenmeyer shake flasks, each containing 500 ml expression medium, were inoculated with 1 ml preculture each and incubated at 37 °C and 130 rpm until OD600 reaching 0.4-0.8 (approximately 3 hours). The shake flasks with culture were then cooled by placing them on ice for 10 minutes before protein expression was induced with 50 µM IPTG. Shake flasks with cooled, induced culture were then incubated at 18 °C and either 130 rpm or 30 rpm for 24 hrs. Cells were harvested by centrifuging at 5,300 g for 15 min in a precooled (4 °C) centrifuge. From this point onwards, samples were kept at 4 °C or colder. Additionally, procedures were completed as quickly and efficiently as possible. For each gram of cell pellet, 10 ml of 40 mM potassium phosphate buffer, pH 7.5, with 10 mM KNO_3 and EDTA free protease inhibitor (cOmpleteTM Mini from Roche), were used to resuspend the pellet. The resuspended pellet was centrifuged at 8,000 g for 5 minutes. Discarding the supernatant, the pellet was stored at -20 °C.

The cell pellets were subsequently IMAC-purified as described in Section 3.3.1. The IMAC-pure RcFDH could then be assayed for formate oxidation activity as described in Section 4.2.1. Results are shown in Figure 36.

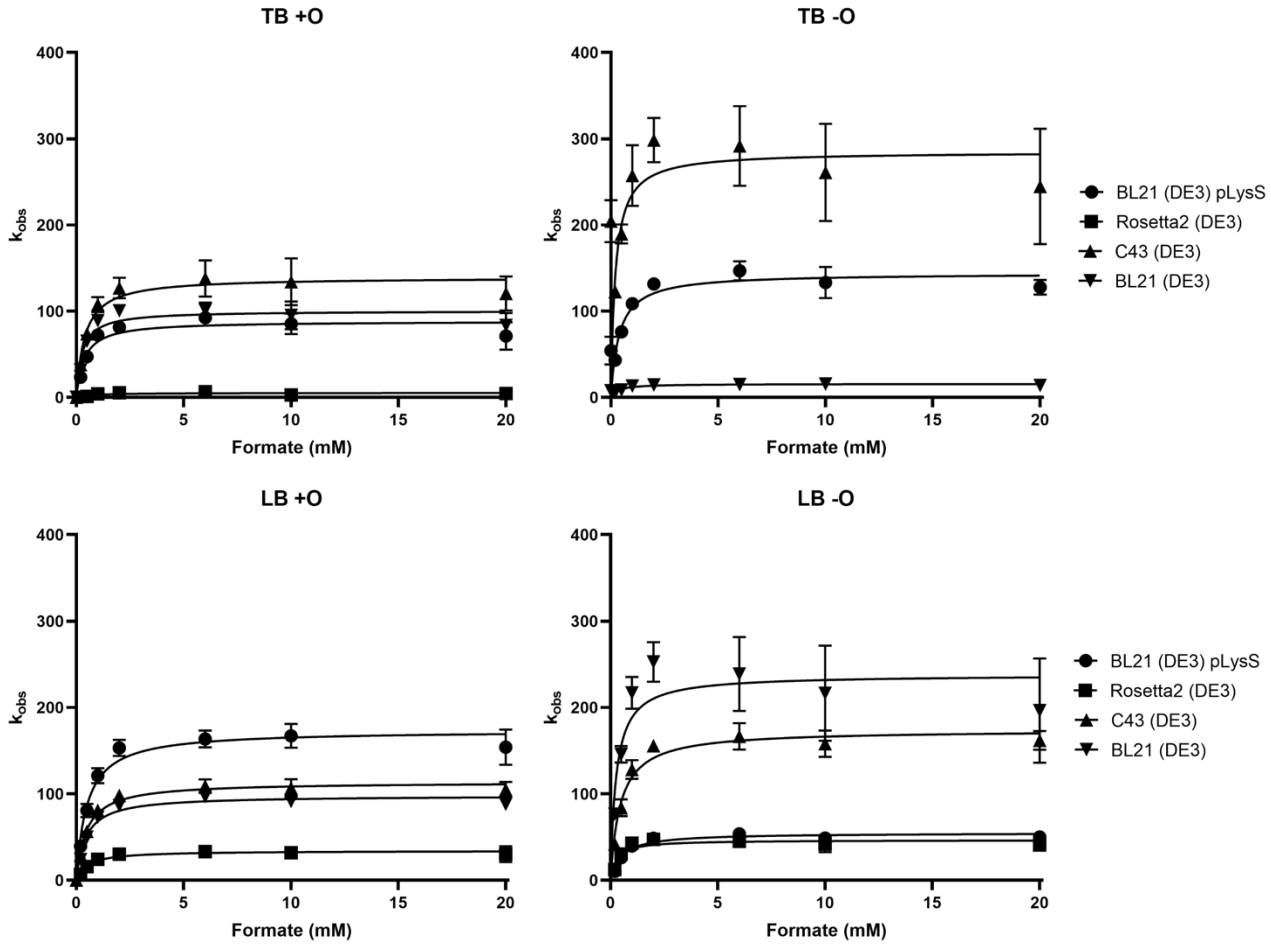

Figure 36: Formate oxidation activity for RcFDH expressed in four different E. coli *expression strains in either LB or TB media, and either with low stirring speed (-O) at 30 rpm or high stirring speed (+O) at 130 rpm.*

From Figure 36, RcFDH was observed to be expressed at lower oxygen concentrations due to low stirring, demonstrated higher formate oxidation activity. Additionally, it can be seen that RcFDH expressed in *E. coli* C43 (DE3) had the highest specific activity. However, a large degree of variation and no obvious pattern is observed.

Despite uncertainty, based on the observed results it was decided to proceed that TB medium and low stirring speed of 30 rpm since this condition allows the highest specific activity.

To verify that expression in *E. coli* C43 (DE3) indeed was the best expression strain, another batch of RcFDH was expressed as described above in this appendix. This time expression in *E. coli* C43 (DE3) was compared to expression in *E. coli* DH5α and *E. coli* MC1061 (Figure 37). Both of the new strains are not designed for expression but were employed in Hartmann and Leimkühler, 2013 and Yu et al, 2019.

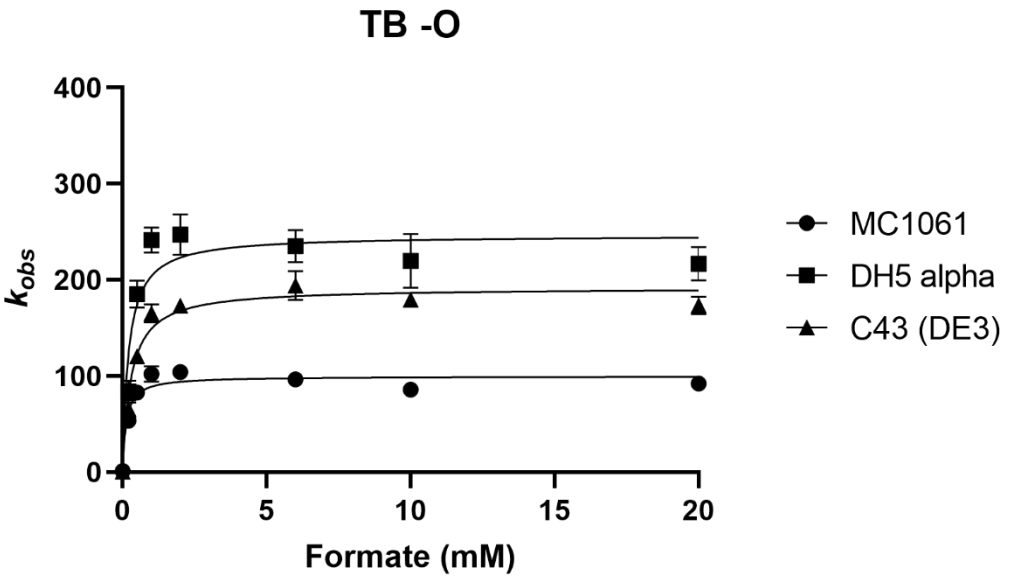

Figure 37: Formate oxidation activity for RcFDH expressed in three different E. coli expression strains in TB medium and low stirring speed (-O) at 30 rpm.

Interestingly, a lower formate oxidation activity for RcFDH expressed in *E. coli* C43 (DE3) was seen in this second expression relative to RcFDH expressed identically in the previous expression seen above (Figure 36). It is unknown, why the activity is different, but it underlines the large variation and lack of pattern observed previously.

Additionally, the RcFDH expressed in *E. coli* DH5α actually has higher specific activity compared to RcFDH expressed in *E. coli* C43 (DE3). In conclusion: Expression in optimized *E. coli* strains does not improve specific activity for type 5 FDHs compared to expression in non-optimized strains.

Appendix J. FDHs from a taxonomic and metabolic perspective

Taxonomy in relation to classification

The cataloged FDH genes of this study have origin in a diverse background. Both gram-positive bacterial phyla, as well as a broad selection of gram-negative phyla have been shown to contain FDH genes.

Interestingly, FDHs from proteobacteria comprise the vast majority of FDHs in the study. Proteobacteria is an enormous phylum comprising incredible diversity. Despite this, it is still noteworthy to observe such a dominance of proteobacterial FDH, especially when one takes into account that all sequences here are less than 90% identical with any other sequence included.

Unsurprisingly, there is a relation between taxonomy and formate dehydrogenase alpha subunit sequence. Meaning, clades of FDH alpha subunit sequences often fall within a single class and phylum. Archaeal FDHs are distinctly different from bacterial FDHs in terms of sequence, giving a clear separation between FDHs from the two taxonomic superkingdoms.

Metabolic profiles in relation to classification

Prokaryotic FDHs are considered to be very diverse in metabolic function (Maia et al., 2015). Interestingly, one organism may express multiple different FDHs (da Silva et al., 2011). For example, in *E. coli* the presence of three FDHs known as FDH-H, FDH-N, and FDH-O has been well documented, with the role of each individual FDH differing (Self, 2013).

It is possible that different versions of FDH will have different preferences for reaction direction (De Bok et al., 2003) or that FDH genes in the same organism may in fact be identical and allow the cell to react to varying formate concentrations (Lenger et al., 1997). As such, the role of FDHs can differ tremendously, even within the same organism. In essence, an organism with multiple FDH variants, will likely either have a more flexible metabolism, or simply be more dependent on formate as a key metabolite.

Interestingly, several metabolic pathways involve formate. By coupling the oxidation of formate to the reduction electron acceptors, prokaryotes can derive energy from formate to drive other reactions. For instance, *Wolinella succinogenes* uses FDH-based conversion of formate to drive nitrate reduction (Simon, 2002), and methanogens are able to use formate via FDHs to drive methanogenesis (Costa et al., 2010). Some organisms, such as methylotrophs, are able to use formate via FDH to regenerate reducing equivalents like NADH (Vorholt, 2002). Common for all of these is the fact that the FDH is most often applied for formate oxidation, the opposite of the application relevant for CCU. As is exemplified in Section 2.3, the FDH kinetic rate is often much higher with formate oxidation than for CO_2 reduction.

Interestingly, some FDHs are metabolically designed to perform CO_2 reduction. Particularly for acetogens via the WLP (Drake et al., 2008; Lemaire et al., 2020; Ljungdahl, 1986; Müller, 2019).

Appendix K. Pictures from purification

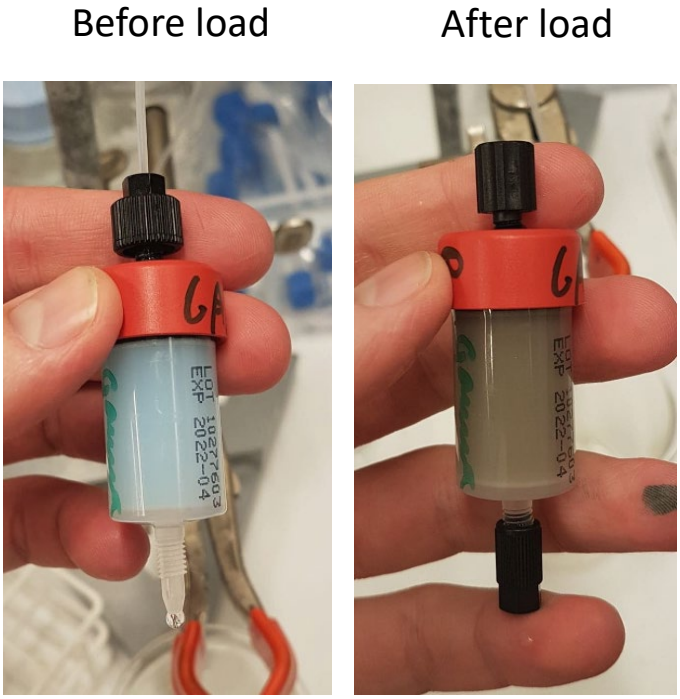

Figure 38. Pictures from purification before and after loading the 5 ml pre-packed HisTrap column.

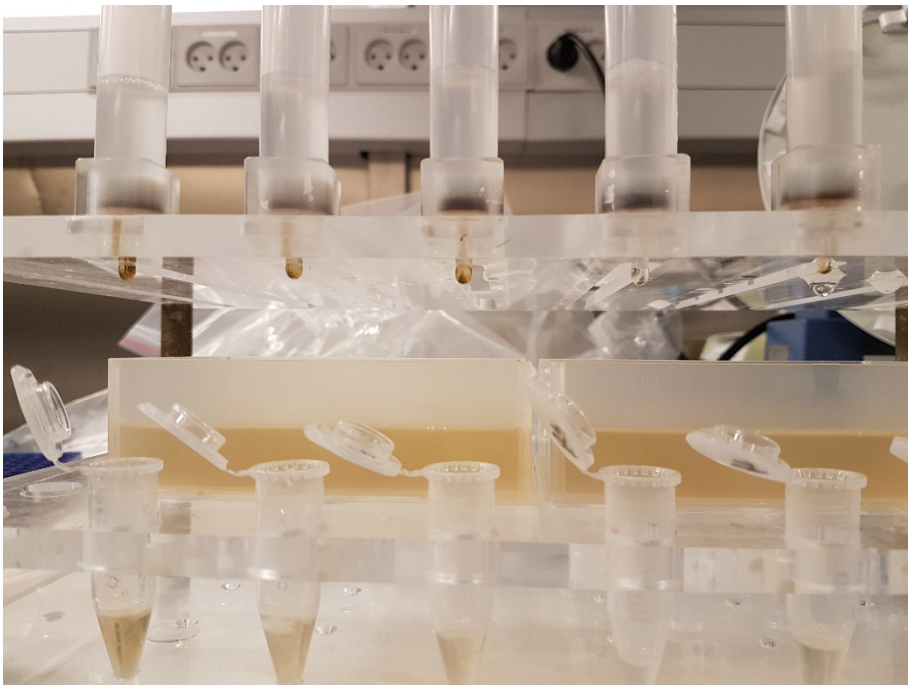

Figure 39: Picture of gravity flow IMAC purification run with parallel columns. Picture is taken during elution of FDH from column. Notice how the top of the column is turning white/blue as the protein is eluting. The bottom of the column is still dark from protein with brown drops starting to appear.

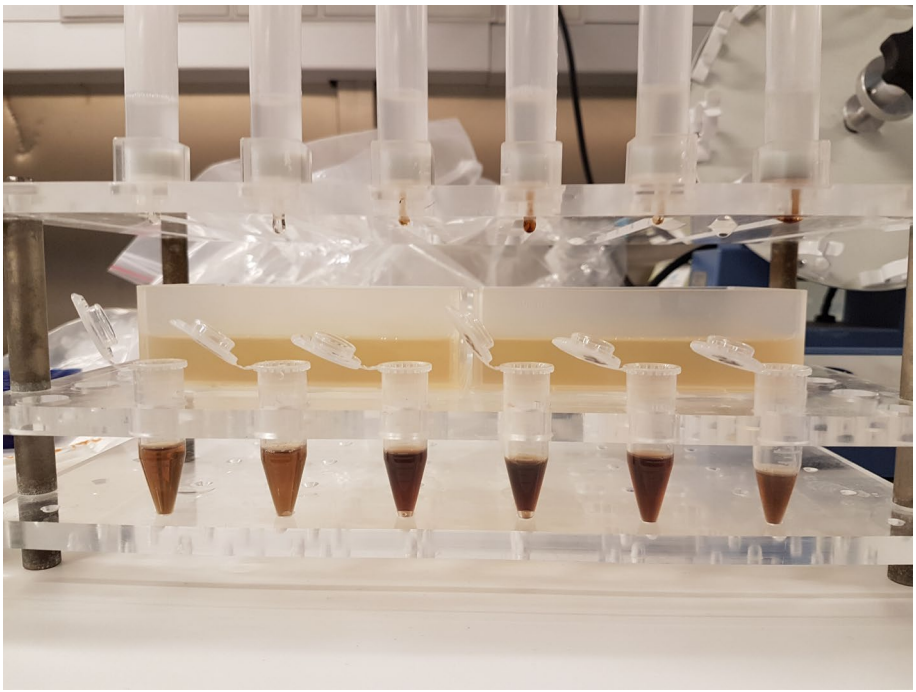

Figure 40: Picture of gravity flow IMAC purification run with parallel columns. Picture is taken at the end of elution of FDH from column. Notice the dark brown color of the eluted protein and the lack of color on the columns relative to Figure 39.

Appendix L. Supplementary figures

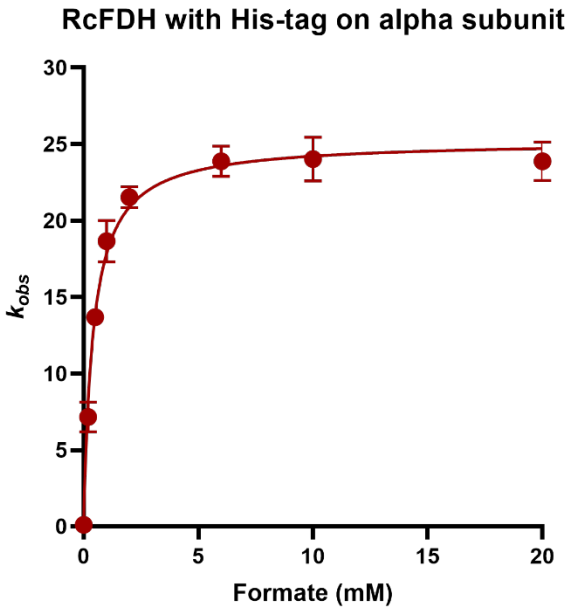

Figure 41: Observed catalytic rate of RcFDH expressed with His-tag placed on alpha subunit.

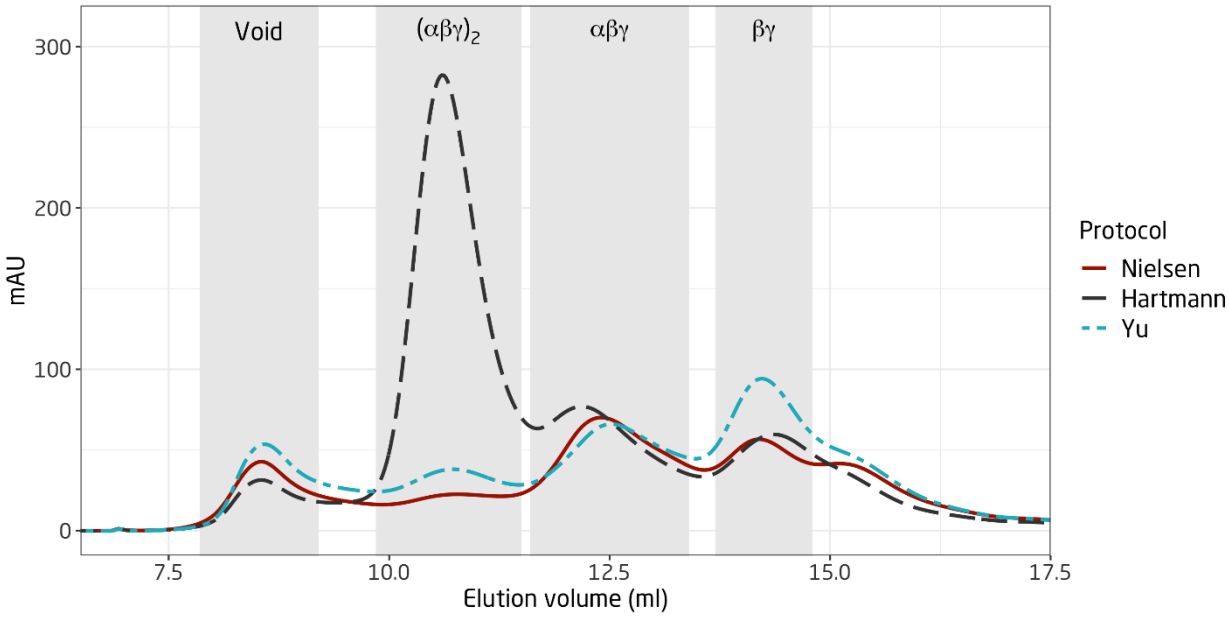

Figure 42: SEC chromatogram on RcFDH expressed with three different protocols. Each peak is marked with grey boxes and predicted subunit composition. SEC was performed on 24 ml Superdex^{TM} 200 10/300 column.

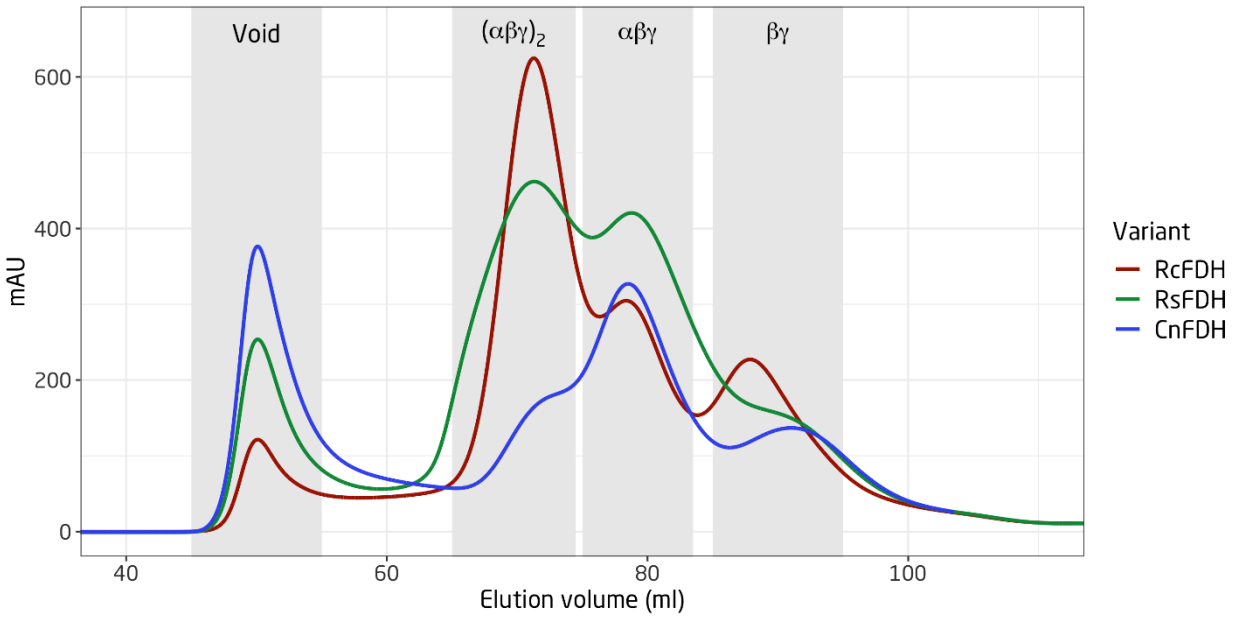

Figure 43: SEC Chromatogram on RcFDH, RsFDH and CnFDH expressed with the Hartmann protocol. Each peak is marked with grey boxes and predicted subunit composition. SEC was performed on 120 ml HiLoad™ Superdex™ 200 16/60 pg column.

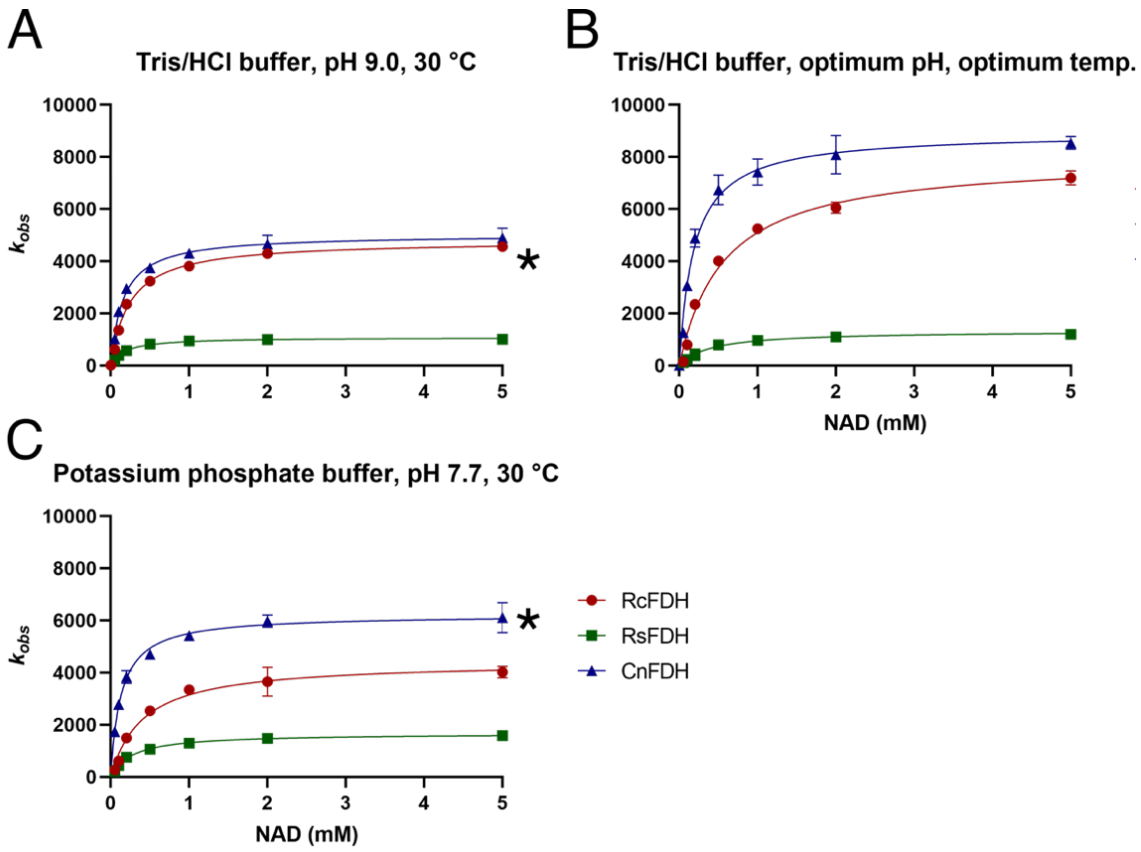

Figure 44: Steady state with formate saturation on the forward reaction (formate oxidation) for RcFDH, RsFDH, and CnFDH. '': reproduced result from literature* (Hartmann and Leimkühler, 2013; Niks et al., 2016). *Formate concentration was 6 mM and k_{obs} is calculated based on initial rate observed for first 10 seconds.*

Appendix M. Paper I: Classification and enzyme kinetics of formate dehydrogenases for biomanufacturing via CO_2 utilization

Paper I was published in Biotechnology Advances and is inserted on the following pages. The final published version hosted on Science Direct is available at:

https://doi.org/10.1016/j.biotechadv.2019.06.007

Biotechnology Advances 37 (2019) 107408

Contents lists available at ScienceDirect

Biotechnology Advances

journal homepage: www.elsevier.com/locate/biotechadv

Research review paper

Classification and enzyme kinetics of formate dehydrogenases for biomanufacturing via CO_2 utilization

Christian Førgaard Nielsen[a], Lene Lange[b], Anne S. Meyer[a,*]

[a] Protein Chemistry and Enzyme Technology Section, Department of Biotechnology and Biomedicine, Building 221, Technical University of Denmark, 2800 Kgs. Lyngby, Denmark
[b] LLa-Bioeconomy Research & Advisory, Karensgade 5, 2500 Valby, Denmark

ARTICLE INFO

Keywords:
CO_2 reduction
Carbon capture and utilization
Formate
Biocatalysis
FDH gene segment organization
FDH classification
Electrocatalysis

ABSTRACT

The reversible interconversion of formate ($HCOO^-$) and carbon dioxide (CO_2) is catalyzed by formate dehydrogenase (FDH, EC 1.17.1.9). This enzyme can be used as a first step in the utilization of CO_2 as carbon substrate for production of high-in-demand chemicals. However, comparison and categorization of the very diverse group of FDH enzymes has received only limited attention. With specific emphasis on FDH catalyzed CO_2 reduction to $HCOO^-$, we present a novel classification scheme for FDHs based on protein sequence alignment and gene organization analysis. We show that prokaryotic FDHs can be neatly divided into six meaningful subtypes. These sub-types are discussed in the context of overall structural composition, phylogeny of the gene segment organization, metabolic role, and catalytic properties of the enzymes. Based on the available literature, the influence of electron donor choice on the efficacy of FDH catalyzed CO_2 reduction is quantified and compared. This analysis shows that methyl viologen and hydrogen are several times more potent than NADH as electron donors. Hence, the new FDH classification scheme and the electron donor analysis provide an improved base for developing FDH-facilitated CO_2 reduction as a viable step in the utilization of CO_2 as carbon source for green production of chemicals.

1. Introduction

Increased atmospheric CO_2 levels are a direct cause of global warming and climate change (IPCC, 2018). To reduce continued CO_2 emissions and warming, alternatives to current fossil fuel derived production routes need to be developed and implemented. Over the last decade there has been a substantial increase in research towards developing technologies, partnerships, and catalysts to facilitate the conversion of CO_2 into industrially relevant chemical building blocks and high-in-demand chemical products. In recent years, enzymes have gained a footing within the global chemical industry due to their low reaction temperature and energy requirements, and their high selectivity. The field of CO_2 capture and conversion, where enzymatic approaches have received a great deal of attention recently, reflects this trend (Cotton et al., 2018; Goeppert et al., 2014; Marpani et al., 2017a; Sultana et al., 2016). On top of the general advantages of using enzymatic approaches, biocatalysts are indeed able to effectively interact with CO_2 as a substrate and promote electron transfer reactions beyond the first coordination sphere. This is uncommon for non-biological approaches (Appel et al., 2013).

CO_2 is a substrate or a product in a vast number of different enzymatically catalyzed reactions in biology. The various pathways for incorporation of carbon into biomass, including those not limited to photosynthesis, are indeed well-studied (Bar-Even et al., 2012). Shi et al. have recently provided a thorough overview of the most important biological, enzymatically catalyzed reactions involving CO_2 (Shi et al., 2015). Of the many diverse reactions, the conversion of CO_2 to formate ($HCOO^-$) is attractive because it gives a product that is a kinetically stable liquid chemical at ambient temperature. Unlike the alternative attractive potential of incorporating CO_2 through carboxylation (Glueck et al., 2010), formate can be produced without any other (co-factor) reagents than energy in the form of electrons as well as free protons.

Formate dehydrogenases (FDHs, EC 1.17.1.9, formerly EC 1.2.1.2) predominantly catalyze the oxidation of formate to CO_2 (Eq. (1)), but have also been shown to catalyze the reverse reaction, namely reduction of CO_2 (Eq. (2)).

$$HCOO^- \rightleftharpoons CO_2 + H^+ + 2e^- \quad (1)$$

$$CO_2 + H^+ + 2e^- \rightleftharpoons HCOO^- \quad (2)$$

* Corresponding author.
E-mail address: asme@dtu.dk (A.S. Meyer).

https://doi.org/10.1016/j.biotechadv.2019.06.007
Received 25 February 2019; Received in revised form 26 May 2019; Accepted 10 June 2019
Available online 12 June 2019

Formate, often in the form of formic acid, is used extensively in food and feed preservation and as a pH regulator in other applications. The use of formate has been strongly advocated as an energy storage compound for the hydrogen economy (Mellmann et al., 2016; Singh et al., 2015) or as fuel for fuels cells (An and Chen, 2017). It was argued in a recent review that formate was the most suitable feedstock to support chemoautotrophic growth which could be an efficient alternative to photosynthesis driven biotechnology (Claassens et al., 2018). Alternatively, design of novel pathways in microorganisms like *E. coli* could allow growth of the bacterium on formate (Bar-Even et al., 2013).

The objective of this review is to present an overview of FDH as a catalyst for CO_2 reduction to formate, paving the way for further conversion to value-added products. By such conversion, CO_2 is exploited as an (available and accessible) carbon resource instead of being a nuisance and a threat for global livelihood. The urgency of developing negative emission technologies, of which development of FDHs to accomplish efficient CO_2 conversion may be an essential part, is accentuated by the recent daunting projections that CO_2 emissions are still increasing. Hence, the global atmospheric CO_2 concentration has recently reached 405 ppm (Le Quéré et al., 2018) and the recent data indicate a renewed increase of 2.7% in global CO_2 emissions for 2018, which is a steep growth compared to the 1.6% increase in 2017 (Figueres et al., 2018, Le Quéré et al., 2018).

This review summarizes the current state of knowledge regarding FDHs in relation to the exploitation of these enzymes in Carbon Capture and Use. We present a new sequence-based classification of FDHs and discuss how the individual FDH enzyme groups are suited for CO_2 reduction. We also examine reaction rates, efficiencies of different common electron donor principles, and stability/robustness of the enzymes. Our goal with this survey is to provide an advanced understanding of FDH enzymes and improve the decision base for selecting the right enzymes and corresponding electron donors for biocatalytic CO_2 reduction.

2. Formate dehydrogenase classification

Formate dehydrogenases are fascinating enzymes, with an astounding range of diversity in terms of structure, subunit composition and metabolic function. While many FDHs are soluble enzymes catalyzing a single reaction, others are part of large, sometimes membrane-bound complexes, which comprise other functions interwoven with formate oxidation or CO_2 reduction.

The mechanisms that allow biocatalytic interconversion between formate and CO_2 are fundamental and prevalent across all kingdoms of living organisms. These biocatalytic functions are essential for most living organisms, therefore an extremely high number of different FDHs exist.

Two distinct classes of FDH enzymes, with distinctly different structure and catalytic mechanism, have been observed – metal-dependent FDHs, and metal-independent FDHs – based on metal content and related mechanism of the reaction in the active sites (Maia et al., 2017). Others divide FDHs into NAD-dependent or NAD-independent (Choe et al., 2014), which essentially is an analogous division to metal-dependent and metal-independent, albeit less distinct since 'NADH-independent' variants may still utilize NADH.

While sharing EC number and facilitating the same reaction, the metal-dependent and metal-independent FDHs are distinctly different, and are consequently discussed separately.

2.1. Metal-independent formate dehydrogenases

Metal-independent variants of FDHs appear to have been studied more than the metal-dependent FDHs. FDH from the yeast *Candida boidinii* is by far the best studied of the metal-independent enzymes – probably because this enzyme is commercially available – followed by FDH from the Gram-negative bacterium *Pseudomonas* sp.101 (Sultana et al., 2016; Tishkov and Popov, 2006). Interestingly, metal-independent FDHs are sometimes hailed as the superior solution (Takacs et al., 2017) while at other times they are simply dismissed as slow and therefore not a relevant option for CO_2 reduction applications (Cotton et al., 2018).

The metal independent FDHs are a remarkably uniform group of enzymes. These enzymes have been proposed to be of the D-specific 2-hydroxy acid dehydrogenase family because they share characteristics of other dehydrogenases in this family (Vinals et al., 1993). Further subgrouping makes little sense for the metal-independent class.

2.2. Metal-dependent formate dehydrogenases

Metal-dependent FDHs are commonly viewed as molybdo-enzymes (with occasional tungsten substitution) and are grouped as a subfamily of the 'DMSO reductase family' (Hille et al., 2014). This very diverse family is one of four families within the molybdo-enzymes, a collection of exclusively prokaryote enzymes that share overall structure and spectroscopic properties (Zhang and Gladyshev, 2008). The family is named after its first structurally characterized member (Schneider et al., 1996).

In 2007 Rothery et al. defined a family called 'complex iron-sulfur molybdo-enzyme', which encompasses several distinct types of enzymes based on co-factors and subunit composition (Rothery et al., 2008). Later, in 2013, Grimaldi et al. coined the term Mo/W-bisPGD enzymes (Grimaldi et al., 2013). This term covers enzymes with a molybdopterin cofactor, specifically a Mo/*W*-bis(pyranopterin guanosine dinucleotide) co-factor in one of its active sites, and replaces the denomination 'DMSO reductase family'.

2.2.1. Proposed formate dehydrogenase classification scheme

The metal-dependent FDHs exhibit considerable diversity in both metabolic function, cellular localization, co-factors, and structure. However, no sub-classification or categorization scheme exists for these enzymes. In a recent review, the diversity and biological function of the 29 best described metal-dependent FDHs from 24 different prokaryotes are discussed (Hartmann et al., 2015). Three issues are raised that are imperative in relation to introducing further grouping of metal-dependent FDH.

First, like many other prokaryote protein complexes, multi-subunit FDHs appear to be encoded mainly in operons. The diversity in subunit composition is reflected in the gene organization.

Second, while the molybdopterin co-factor (Mo/W-bisPGD) is ubiquitous in the active site across all metal-dependent FDH, the additional co-factor content shows significant variation. Commonly, between one and five of the electron transporting iron sulfur cofactors are present. These often vary in conformation and structural location. Additionally, often either a heme group, a flavin adenine dinucleotide (FAD), or a flavin mononucleotide (FMN) is present. Interestingly, gene segment organization and co-factor use appear to be correlated (Table 1).

Third, the chaperone genes, which have been suggested as necessary for proper maturation and assembly of proto-FDH with the Mo/*W*-bis-PGD cofactor are not always present in the operon encoding the FDH enzyme (Hartmann et al., 2015). These chaperone genes are commonly referred to as *fdhD* and *fdhE*, although inconsistencies in nomenclature are frequent. For example, the genes *fdsC* of *Cupriavidus necator* are homologs to *fdhD* in most other FDH containing prokaryotes.

Based on these three points of consideration, i.e. subunit composition, cofactors, and presence of chaperone genes in the operon, a new categorization comprised of six types of metal-dependent FDHs is proposed (Table 1).

As discussed later, this categorization does not distinguish between FDHs that incorporate tungsten and FDHs that incorporate molybdenum. Neither does this type of categorization involve differentiation between FDHs that have SeCys or Cys as their coordinating

Table 1
The six proposed types of metal-dependent FDHs shown with gene organization, subunit composition and characterizing co-factor. The gene organization is shown with generic abbreviations to accommodate discrepancies. 'A': alpha (α) subunit gene, 'B': beta (β) subunit gene, 'C': gamma (γ) subunit gene, 'D': fdhD, 'E': fdhE, 'S': Delta subunit chaperone gene.

Type	Gene organization	Subunit composition (per monomer)	Characterizing Co-factor
1	fdhA	α	None
	FdhA and fdhB	αβ	None
2	fdhAB	αβ	None
	fdhDABE	αβ	None
3	fdhAB	α + FAD F420	FAD
	fdhCABD	α + FAD F420	FAD
4	fdhABC (fdnGHI[a])	αβγ	Heme
	fdhABCE	αβγ	Heme
	fdhABEC	αβγ	Heme
	fdhEABCD	–	Heme
5	fdhCBAD	αβγ	FMN
	fdhCBADS	αβγ	FMN
6	With NADH oxidoreductase	–	–

[a] *E. coli* gene nomenclature for FDH-N (nitrate-inducible FDH), corresponding to the fdhABC gene structure.

cysteine residue. Though the catalytic rates of the enzyme are known to be affected by the type of metal (tungsten or molybdenum) and the type of coordinating cysteine residue, these are often interchangeable and cannot form the basis of a classification.

A sequence based homology analysis of the conserved FDH α-subunit sequences from the 23 currently described FDHs was conducted and each sequence was annotated with the corresponding categorization type (Fig. 1). Genetic code is now known to be flexible across organisms (Ling et al., 2016), so to minimize organism specific translation bias, amino acid sequences translated from annotated genomes were used.

2.2.2. Phylogenetic analysis of metal-dependent formate dehydrogenases

A total of 1597 FDH α-subunit sequences were extracted, based on RefSeq genome annotation, from full genomes. Neighboring genes were logged and the resulting gene structure used to annotate individual FDH α-subunit sequences with a type.

FDH alpha subunit sequence data were reduced to 965 sequences of less than 90% identity using CD-hit (Li and Godzik, 2006). The sequences were aligned using MAFFT multiple sequence aligner software v. 7, (Katoh and Standley, 2013) on the MAFFT online service (Katoh et al., 2017). The alignment was analyzed with RAxML maximum likelihood software (Stamatakis, 2014) using a LG amino acid replacement matrix (Le and Gascuel, 2008) through the CIPRES server system (Miller et al., 2010).

To annotate the sequences with gene segment organization, the neighboring genes to the alpha subunit were inspected. The four genes upstream and four genes downstream were inspected. This exercise required a heavy reliance on the Refseq annotation of genes. Coding strand and location for each gene was logged to allow order and direction of gene structure.

The phylogenetic tree in Fig. 2 corroborates the validity of the six metal-dependent FDH categorization types proposed in this study

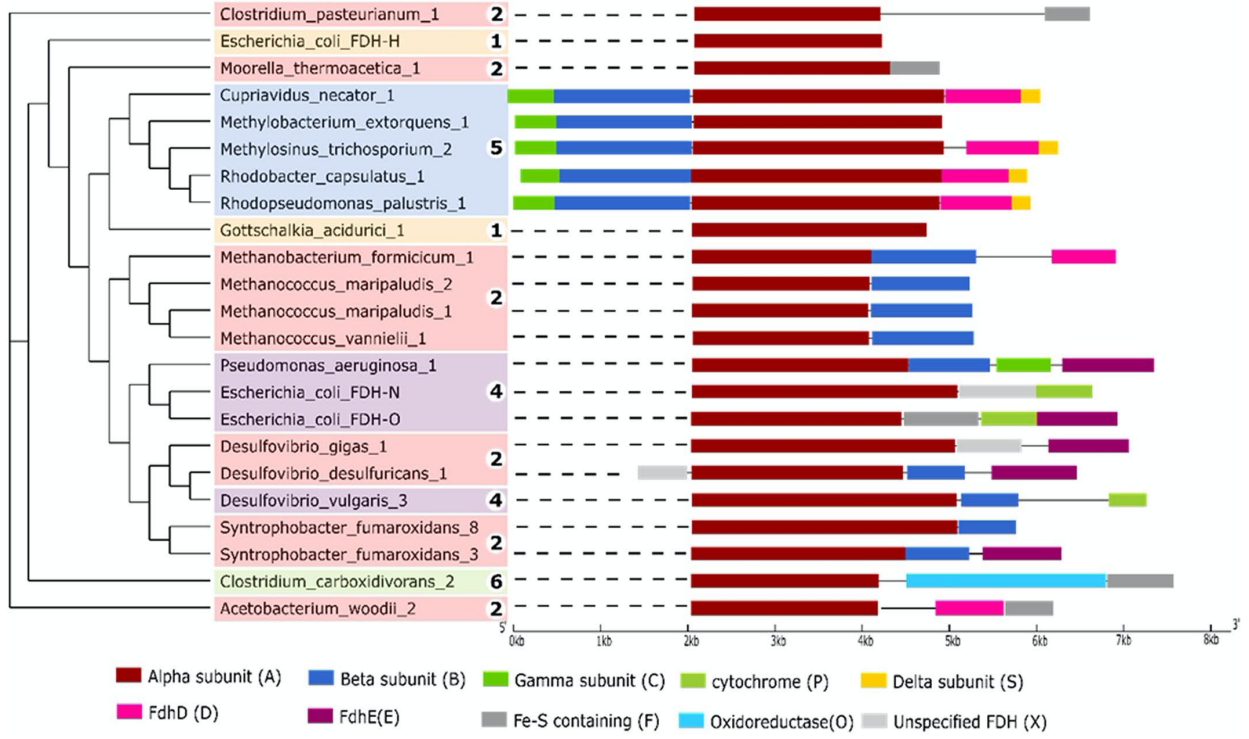

Fig. 1. Distribution of the 23 currently known metal-dependent FDHs in the six suggested new FDH categorization types mapped in relation to alpha subunit amino acid sequence homology analysis. The genes corresponding to each of the 23 enzymes were included only when it was possible to correlate the described enzyme to the encoding genes in an RefSeq annotated genome of the origin organism. Ten different annotations were logged, including FDH subunits, cytochrome (all types), sulfurtransferase FdhD, FDH accessory protein FdhE, and NAD(P)H related oxidoreductases. Genes annotated as Fe-S containing or as an unspecified formate dehydrogenase subunit were also included. Encircled numbers 1–6 signify categorization type. Each individual enzyme is named according to microbial origin. Numbers added to the microbial names indicate the relevant operon number of the FDH-operons in the genome, e.g. Syntrophobacter_fumaroxidans_3 and _8 denominates the 3rd and 8th FDH operon in the *Syntrophobacter fumaroxidans* genome.

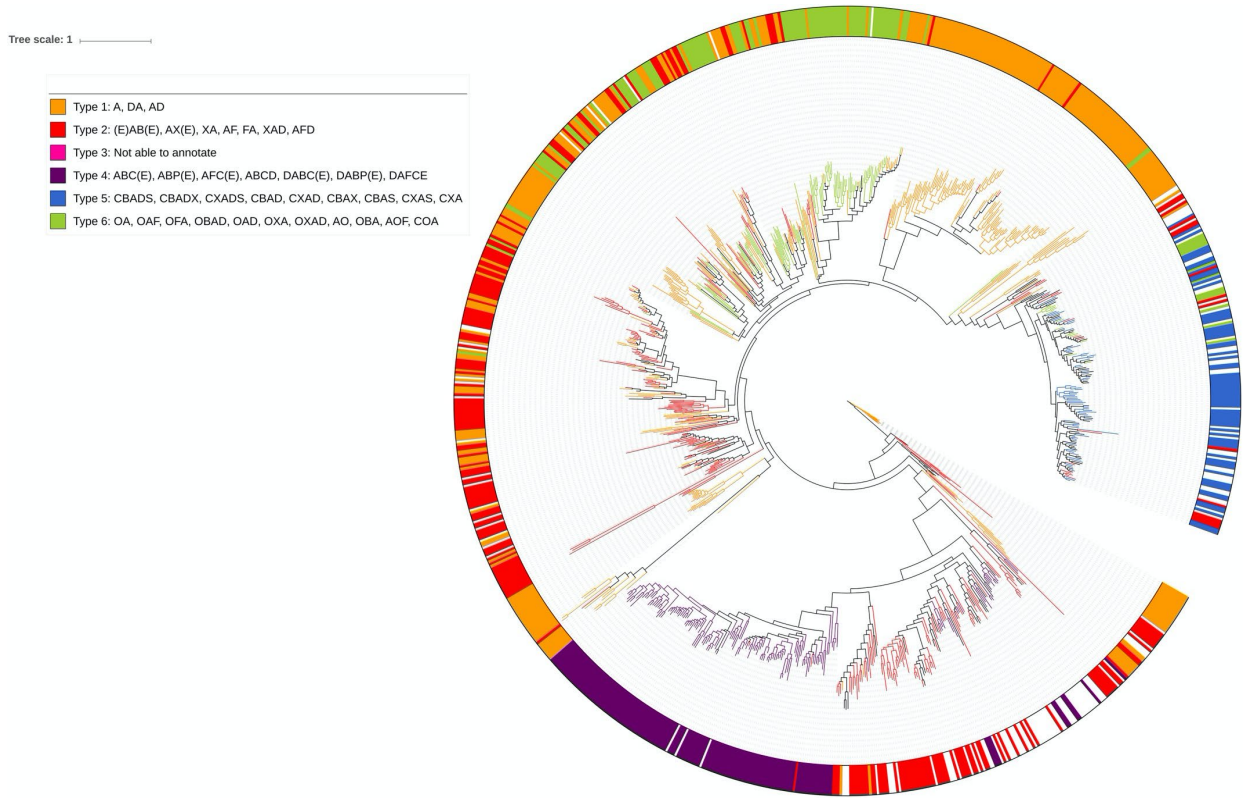

Fig. 2. Phylogenetic tree generated based on alignment of 965 metal-dependent FDH alpha subunit sequences. Inter-sequence identity was reduced to a maximum of 90% between any two sequences. Each branch tip represent a single sequence. Each sequence is annotated with an FDH type based on gene segment organization. Gene segment organization is defined as the genetic makeup of the surrounding genes of a given FDH alpha subunit sequence. Here 'A': alpha (α) subunit, 'B': beta (β) subunit, 'C': gamma (γ) subunit, 'D': accessory sulfurtranferase fdhD, 'E': accessory protein fdhE, 'S': delta subunit, 'X': unspecified formate dehydrogenase subunit, 'O': NADH-quinone oxidoreductase related subunit, 'F': 4Fe-4S containing protein, and 'P': cytochrome formate dehydrogenase subunit.

(Table 1). Despite uncertainties related to non-systematic errors in RefSeq annotation quality, nomenclature inconsistencies, varying sequence lengths, and high biological complexity, the metal-dependent FDH alpha subunit grouping produced meaningful phylogenetic correlations corresponding to the proposed FDH classification types. The phylogenetic tree in Fig. 2, shows that particularly the groupings of type 1 and all of type 4 form distinct clades. Type 1 is also observed mixed with type 2 and type 6. Type 5, which has the most distinct genes organization profile, forms a group of less defined clades. It was not possible to annotate sequences with type 3 because it was not possible to discriminate between beta-subunit of type 2 versus the FAD containing beta-subunit of type 3.

3. Formate dehydrogenase diversity

3.1. Subunit composition and gene segment organization

Metal-independent FDHs are monomeric globular proteins that present either one or two identical active sites. The variant from *Candida boidinii* (CbFDH) is the best studied and a prime example of the feature that no co-factor is part of the FDH enzyme structure. Metal-independent FDHs are highly structurally conserved across the kingdoms of life (Fig. 3).

Metal-dependent FDHs share structurally similar alpha-subunits that as mentioned form the basis for the above phylogenetic tree (Fig. 2). The alpha-subunits are typically between 80 and 95 kDa in size and include the hallmark active site containing Mo/W-bisPGD. The structure and co-factor composition are highly similar to other enzymes with similar function, i.e. the NADH dehydrogenases (Hille et al., 2014).

FdhD and FdhE are chaperone proteins, and FdhD, also referred to as FdsC, has been shown to bind the molybdopterin cofactor (Böhmer et al., 2014). Along with the third type of chaperone, FdsD, the FdhD and FdhE are not part of the active FDH enzyme but instead have been proposed to be essential for FDH assembly and maturation (Hartmann et al., 2015). Type 5 metal-dependent FDHs are typically co-encoded with *fdsC* and *fdsD* in their gene organization, whereas the other FDH types are co-encoded, if at all, with *fdhD* and *fdhE*.

Metal-dependent FDHs are highly diverse and are observed to have monomer, heterodimer, or heterotrimer conformations. The additional subunits to the main 'alpha subunit(s)' are denominated the 'beta subunit' (20–35 kDa) and 'gamma-subunit' (12–18 kDa), respectively. Currently, only the crystal structures of the metal-dependent FDH-H and FDH-N from *E. coli* along with an FDH from *Desulfovibrio gigas* (DgFDH, which is equivalent to '*Desulfovibrio_gigas_1*', Fig. 1), have been solved (Fig. 3).

In *Gottschalkia acidiurici 9a* (*Clostridium acidiurici*) a pair of FDH genes have been observed to differ slightly. This pair of FDHs, combined with an electron-bifurcating module and an hydrogenase-like module, form a complex able to catalyze a coupled reaction with both ferredoxin and NADH (Kearny and Sagers, 1972; Wang et al., 2013a). Interestingly, many different variants of this configuration with FDH, electron-bifurcating modules and a hydrogenase are observed for FDHs across several anaerobic bacteria or archaea, most notably in the hydrogenase/FDH complexes of *Acetobacterium woodii* (Schuchmann and Müller, 2013), *Moorella thermoacetica* (Wang et al., 2013b), or

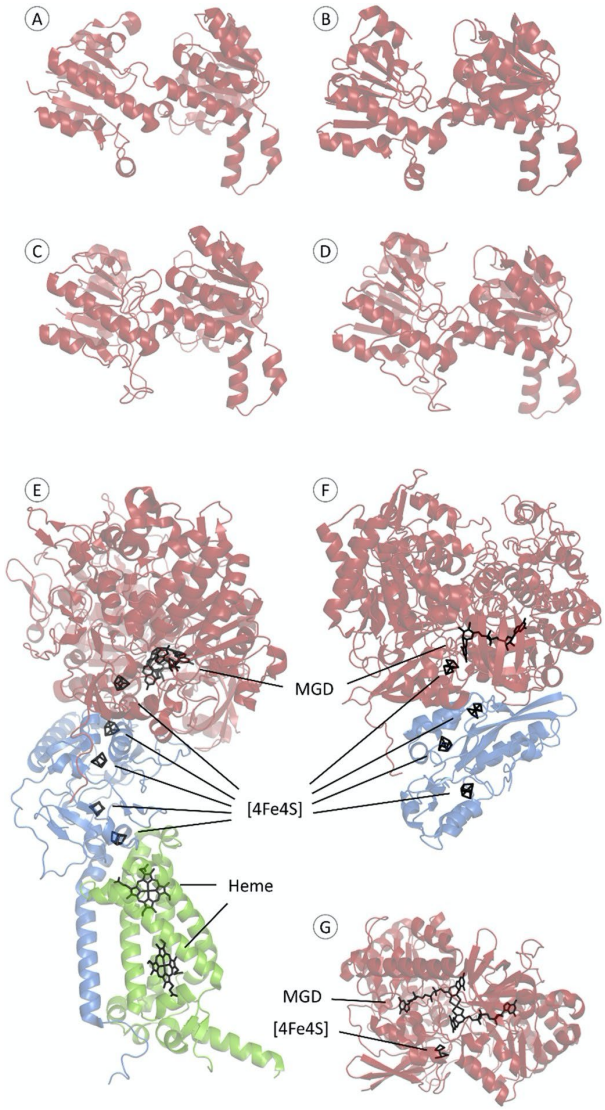

Fig. 3. Overview of the currently available unique crystal structures of FDH enzymes. Main subunits with the formate/CO_2 catalyzing active site are shown in red, with additional subunits shown in blue and green. A) metal-independent FDH of Arabidopsis thaliana (3JTM) (Shabalin et al., 2010), (B) metal-independent FDH of Candida boidinii (5DNA) (Guo et al., 2016), (C) metal-independent FDH of Pseudomonas sp. 101 (2GO1) (Filippova et al., 2005), (D) metal-independent FDH of Granucella mallencis MP5ACTX8 (4XYG) (Fogal et al., 2015), (E) metal-dependent FDH-N of Escherichia coli (1KQG) (Jormakka et al., 2003), (F) metal-dependent FDH of Desulfovibrio gigas (1H0H) (Raaijmakers et al., 2002), (G) metal-dependent FDH-H of Escherichia coli (2IV2) (Raaijmakers and Romão, 2006). (For interpretation of the references to color in this figure legend, the reader is referred to the web version of this article.)

Thermoanaerobacter kuvui (Schwarz et al., 2018).

Another example of FDH as a part of a larger electron-transporting complex is found in the methanogenic organism *Methanothermobacter wolfeii*. In this species, FDH activity is observed in a massive 800 kDa complex that facilitates a twostep reduction of CO_2 to formate and then to formyl-methanofuran. These examples elucidate the diversity contained among the FDHs classified here under 'type 1' because this type is solely characterized by having an FDH alpha subunit in the gene structure and none of the other more defining subunits or chaperones. As such, type 1 FDHs, and also to some extent type 2 FDHs, show the highest diversity of the six suggested FDH types in terms of tertiary structure.

3.2. Structure and mechanism

Metal-independent FDHs function simply by facilitating the close proximity of NAD^+ and formate or NADH and CO_2 to allow hydride and electron transfer between the two molecules (Castillo et al., 2008). In general, the reaction catalyzed by metal-independent FDHs is relatively more in favor of formate oxidation than CO_2 reduction as compared to the metal-dependent FDH reaction catalysis. We interpret the enzyme structure, governing the energy reorganization at catalysis, and the reaction mechanism involving NADH/NAD+ (or NADPH/NADP+) as being responsible for this favoring of formate oxidation over CO_2 reduction.

The well-known metal-independent FDH from *Candida boidinii* has been engineered to accept NADP(H) instead of the native NAD(H) (Andreadeli et al., 2008; Wu et al., 2009), but examples of FDHs naturally using NADP(H) are seen as well (Alpdağtaş et al., 2018; Hatrongjit and Packdibamrung, 2010). Nonetheless, the metal-independent FDHs are in general limited to using only NADH or in rare cases NADP(H) as electron carrier co-substrate.

For metal-dependent FDHs the catalytic mechanism is also quite well understood. In short, the molybdenum or tungsten of the Mo/W-bisPGD in the active site, presents a terminal sulfur residue. Then, the metal-dependent FDHs direct electrons through a 'wire' of FeS groups in order to reduce this heavy metal sulfo group in the active site, and this reduced heavy metal sulfo group then acts as hydride donor for the reduction of CO_2 to formate. The mechanism is reversed for formate oxidation to CO_2 (Maia et al., 2017). The wire of FeS groups can transport electrons over surprisingly long distances, for example, a distance of more than 90 Å has been demonstrated in FDH-N from *E. coli* (Jormakka et al., 2003). Interestingly, compared to the metal-independent FDHs, the mechanism for metal-dependent FDHs inherently allows a broader variety of electron donors. Besides NADH, metal-dependent FDHs have thus been described to interact with a wide variety of physiological redox partners, including cytochromes, ferredoxins, coenzyme F_{420}, and membrane quinols (Hille et al., 2014).

The Mo/W-bisPGD active site topology appears to be similar across different metal-dependent FDH variants, with the main variations being the heavy metal (either Mo or W) in the active site co-factor as well as the conformation-directing residue (either Cys or SeCys). The effect of these discrepancies on the enzyme activity is not fully understood, although enzymes with W-containing co-factors and SeCys as coordinating residue have been shown to be more prone to CO_2 reduction than enzymes with Mo-containing with Cys as coordinating residue (De Bok et al., 2003).

More significant variations are observed in the opposite end of the electron transfer chain. As mentioned above, during catalysis, metal-dependent FDHs direct electrons through an FeS mediated electron transfer chain (Jormakka et al., 2003). The electron source and the mechanism by which the electrons are guided into this electron chain differ significantly among the metal-dependent FDHs. When the FDH is soluble and not part of a multi-function complex, flavin mononucleotide (FMN), flavin adenine dinucleotide (FAD), or heme groups are common co-factors that facilitate electron uptake and electron release from the enzyme. NADH is a predominant electron donor for metal-dependent FDHs for catalyzing CO_2 conversion to formate, but other electron donors are also observed (and discussed below). In the context of the six proposed FDH types (Table 1), the type 4 defining heme group co-factor is known to reduce cytochrome during formate oxidation to CO_2 (Elantak et al., 2005), whilst FAD and FMN are unique to type 3 and type 5, respectively.

Table 2
Overview of FDHs described in the literature to reduce CO_2. The species name of the organism producing the FDH variant is given as unique identifier for the FDH variant. If available, the type and amount of electron donor used to reduce CO_2 is given along with pH for the given experiment. The class is defined as either metal-dependent (Metal) or metal-independent (Non-metal). Type refers to types proposed in the categorization scheme of this study. Enzyme catalytic reaction rate and specificity constant are for CO_2 reduction. Properties of formate oxidation are not given.

ID	Organism	Electron donor	Donor conc	Exp. pH	Class	Type	k_{cat} (red)	K_m CO_2	k_{cat}/K_m	Reference
			(mM)				(s^{-1})	(mM)		
SfFDH	*Syntrophobacter fumaroxidans*	MV^{2+}	1		Metal	2	282	–	–	(De Bok et al., 2003)
DdFDH	*Desulfovibrio desulfuricans*	MV^{2+}	0.2	7	Metal	2	47	0.02	2968	(Maia et al., 2016)
EcFDH (FDH-H)	*Escherichia coli*	MV^{2+}	0.1	7	Metal	1	1	8.3	0.1	(Bassegoda et al., 2014)
DvFDH	*Desulfovibrio vulgaris*	MV^{2+}	1		Metal	4	3	–	–	(da Silva et al., 2011)
AwFDH (FDH2)	*Acetobacterium woodii*	MV^{2+}	5	7	Metal	2	372	3.8	97.9	(Schuchmann and Müller, 2013)
SfFDH	*Syntrophobacter fumaroxidans*	Electrode	–		Metal	2	112	–	–	(Reda et al., 2008)
EcFDH (FDH-H)	*Escherichia coli*	Electrode	–		Metal	1	112	8.3	13.5	(Bassegoda et al., 2014)
EcFDH (FDH-H)	*Echerichia coli*	Electrode	–		Metal	1	–	2.5		(Yuan et al., 2018)
DdFDH	*Desulfovibrio desulfofuricans*	Electrode	–		Metal	2	–	–	–	(Cordas et al., 2019)
DvFDH	*Desulfovibrio vulgaris*	Electrode	–		Metal	3	11	–	–	(Miller et al., 2019)
AwFDH	*Acetobacter woodii*	Hydrogen	–		Metal	2	28	3.8	7.4	(Schuchmann and Müller, 2013)
TkFDH	*Thermoanaerobacter kuvui*	Hydrogen	–		Metal	2	2654	–	–	(Schwarz et al., 2018)
CbFDH	*Candida boidinii*	NADH	1	7.5	Non-metal	–	0.1	–	–	(Altas et al., 2017)
CbFDH	*Candida boidinii*	NADH	0.15	7.1	Non-metal	–	0.02	2.6	0.01	(Choe et al., 2014)
TsFDH	*Thiobacillus sp. KNK65MA*	NADH	0.15	7	Non-metal	–	0.3	0.95	0.34	(Choe et al., 2014)
CcFDH	*Clostridium carboxidivorans*	NADH	0.2		Metal	6	0.08	–	–	(Alissandratos et al., 2013)
RcFDH	*Rhodobacter capsulatus*	NADH	0.2		Metal	5	1.48	–	–	(Hartmann and Leimkühler, 2013)
PoFDH	*Pseudomonas oxalaticus*	NADH	100		Non-metal	–	3	40	0.08	(Ruschig et al., 1976)
CnFDH	*Cupriavidus necator*	NADH	0.2	7	Metal	5	11	2.7	4.07	(Yu et al., 2017)
MtFDH	*Myceliophthora thermophila*	NADH	1	6	Non-metal	–	0.1	0.44	0.23	(Altas et al., 2017)
CtFDH	*Chaetomium thermophilum*	NADH	1	5	Non-metal	–	0.02	3.29	0.01	(Altas et al., 2017)
CmFDH	*Candida methylica*	NADH	1	8	Non-metal	–	0.01	0.01	1.00	(Altas et al., 2017)

3.3. Role of formate dehydrogenase in nature

Formate, and by extension FDHs, play a critical role in several biological contexts. FDHs exist as soluble proteins and may be found both in the periplasm and in the cytoplasm of microorganisms or, alternatively, bound as membrane-bound proteins or as part of a membrane bound multifunction complex. Taxonomically, metal-dependent FDHs are predominantly found in prokaryotes, while metal-independent FDHs are found across all kingdoms of living organisms (Hille et al., 2014).

3.3.1. Formate dehydrogenase in eukaryotes

In larger mammals, understanding the role of formate has been hampered by difficulties in studying its influence experimentally. However, there are indications that formate serves as an important one-carbon metabolite and may have a critical role in fetal development (Brosnan and Brosnan, 2016).

The physiological role of FDH in plants is complex and is yet to be completely elucidated. It is, however, clear that FDHs have a significant role in stress response (Alekseeva et al., 2011).

3.3.2. Formate dehydrogenase in prokaryotes

Microorganisms, specifically bacteria and archaea, which depend on the Wood-Ljungdahl pathway for utilization of carbon dioxide as a building block for biosynthesis, use FDH in the first step towards formation of acetate that in turn directly enters the central metabolism. The Wood-Ljungdahl pathway consists of an Eastern and a Western branch, where 1 mol of acetate is generated or consumed for every 2 mol of CO_2, depending on the direction of the pathway (Ragsdale, 1997). In the Eastern branch, CO_2 is incorporated through formate and in the Western branch through carbon monoxide. Interestingly, the Western branch is unique to acetogens, methanogens and sulfate reducers (Ragsdale, 2008). The Wood-Ljungdahl pathway can be considered as a CO_2-reducing electron sink that in combination with other modules allows acetogens to conserve energy (Schuchmann and Müller, 2014).

Methanogens are strictly anaerobic archaea under the phylum *Euryarchaeaota*, which are found in a wide range of environments (Holmes and Smith, 2016). Methanogens utilize a very limited range of substrates, usually mainly CO_2 and H_2. For hydrogenotrophic methanogens, such as *Methanococcus spp.,* formate may act as an energy source (Nishio and Nakashimada, 2013; Wood et al., 2003).

Due the diverse metabolic roles of formate, a single organism may encode multiple, structurally different FDHs in its genome, with the individual FDH variants able to serve different purposes (da Silva et al., 2011). For example, in *Syntrophobacter fumaroxidans* two FDH variants are encoded in the genome, with one favoring formate oxidation and the other slightly favoring CO_2 reduction (De Bok et al., 2003). *Wolinella succinogenes,* a close relative to *Helicobacter pylori*, has two identical FDH encoding genes in its genome (*fdhI* and *fdhII*). The organism uses the resulting FDH enzymes to oxidize formate and transfer the resulting electrons to one of two reductases involved in growth. The two FDH encoding gene copies in the genome allow *W. succinogenes* to respond to presence of formate by expressing both *fdhI* and *fdhII* rather than just *fdhI*. During growth with formate, both genes are expressed which results in a six-fold increase in FDH levels relative to growth without formate (Lenger et al., 1997).

FDHs can be considered versatile metabolic tools, applicable in any context involving formate, regardless of whether the context involves formate as a recyclable metabolite, as a precursor for higher metabolites, or use of formate as a source of electrons to drive other reactions. One organism may have several genes encoding FDH in its genome. These genes either allow simple up or downregulation of FDH expression in the cell, like for *W. succinogenes*, or alternatively allow the cell to apply FDH with different preferences for direction of the reaction.

4. Comparison of metal vs. non-metal formate dehydrogenase kinetics

As regards the practical application of FDH for CO_2 reduction, currently different 17 metal-dependent and metal-independent FDHs have been characterized based on their catalytic properties, including turnover number (Table 2). Currently, there are no published studies involving pilot or industrial scale use of any kind of FDH for CO_2

reduction, and the results discussed here will consequently revolve around reactions and processes characterized at lab scale.

Except for FDHs belonging to our suggested new categorization type 3, all of the proposed FDH types can be annotated to known and described FDHs. Clearly, one of the key considerations for FDH catalyzed CO_2 reduction is the electron donor. A recent review has highlighted that a majority of studies involving FDH apply an excess of the natural electron donor NADH to shift equilibrium towards CO_2 reduction (Sultana et al., 2016). Other reducing agents, most popularly methyl viologen (MV^{2+}), have also been applied. As is evident (Table 2), the catalytic properties and turnover (k_{cat}) span a wide range and appear to be influenced by the type of electron donor employed.

4.1. NADH as electron donor

Initially demonstrated by Obert and Dave in 1999 (Obert and Dave, 1999), FDH combined with variants of formaldehyde dehydrogenase ($F_{ald}DH$) and alcohol dehydrogenase (ADH) has been studied extensively as a cascade reaction using NADH as electron donor. This system allows a six e^- reduction of CO_2 over three sequential steps and yields low levels of methanol (Luo et al., 2015; Marpani et al., 2017a). Research involving this cascade reaction constitutes the majority of research conducted on reducing CO_2 with FDH and NADH as electron donor for each step of the reaction. For this reason, the regeneration of the NADH is essential, and various technologies, including electrochemical and/or bio-electrochemical systems have been suggested (Alissandratos and Easton, 2015; Srikanth et al., 2017). The most commonly used strategy at lab scale is synchronous in situ conversion of NAD+ directly to NADH by addition of a suitable second enzyme and a second substrate (Hummel and Gröger, 2014; Marpani et al., 2017a, 2017b; Obert and Dave, 1999). Additionally, NADH is by far the most common electron donor used in the studies available in the literature describing both metal-dependent and metal-independent FDHs. CO_2 reduction with NADH as electron donor has been demonstrated to function optimally under acidic conditions (Baskaya et al., 2010). However, this is unique for the proximity mechanism of the metal-independent FDHs. Metal-dependent FDHs function better under neutral (Yu et al., 2017) or slightly basic conditions (Hartmann and Leimkühler, 2013). Despite being the most frequently applied electron donor, NADH is unstable and challenging to work with (Zhang et al., 2018).

4.2. Other chemical electron donors

Methylviologen (MV^{2+}), also known as 1,1′-dimethyl-4,4′-bipyridinium dichloride, is a popular artificial electron donor to use as a replacement for NADH. FDH from *Syntrophobacter fumaroxidans* (De Bok et al., 2003; Reda et al., 2008), *Desulfovibrio desulfuricans* (Maia et al., 2016), *Desulfovibrio vulgaris* (Finn et al., 2017), and *Escherichia coli* (Bassegoda et al., 2014) have been characterized with MV^{2+} as electron donor. Recent research even demonstrated how use of a new viologen derivative, 1,1′-diaminoethyl-4,4′-bipyridinium salt, allowed a 28-fold increase of k_{cat}/K_M relative to MV^{2+} (Ikeyama and Amao, 2017).

Finally, the recently discovered so-called hydrogen dependent carbon dioxide reductase (HDCR) from *Acidobacterium woodii* has been demonstrated to reduce CO_2 with molecular hydrogen (H_2) as the electron donor. When the kinetics of the FDH subunit with MV^{2+} as electron donor are compared, the specificity rate constant with MV^{2+} as electron donor is $372\,s^{-1}$, which is much higher than with H_2 at $28\,s^{-1}$ (Table 2).

4.3. Electrochemical approaches

There appears to be two distinct “schools” for enzymatic electrochemical reduction of CO_2; electrons are either supplied directly, with the enzyme immobilized on an electrode or, alternatively, indirectly through a mediator molecule.

4.3.1. Direct electrocatalysis

For direct electro catalysis, the method of immobilization is an essential parameter influencing the efficacy of electron conduction from electrode to active site (Sakai et al., 2018). Direct electro catalysis through the application of various oxidoreductases is receiving increasing attention (Milton and Minteer, 2017) due to the exciting potential of substituting co-reagents with cheap electricity. In relation to FDH, electrochemical approaches appear particularly promising due to the ability of metal-dependent FDH to channel electrons between structurally distant locations on the enzyme. In nature, NADH or other molecules serve as electron donors that allow electrons to be transferred along FeS-groups to ultimately reduce the molybdenum/tungsten in the active site.

As was demonstrated by Reda et al., the metal-dependent FDH from *S. fumaroxidans* (SfFDH) was able to efficiently reduce CO_2 with an electrode as electron donor (Reda et al., 2008). Later, Bassegoda et al. demonstrated that FDH-H from *E. coli* was able to reduce CO_2 at similar rates, but at pH 7.0 rather than at pH 5.9 as used for SfFDH (Bassegoda et al., 2014; Reda et al., 2008). Recently, a study from the Spormann group at Stanford demonstrated the ability of the massive multi-subunit multi-function heterodisulfide reductase supercomplex of *Methanococcus maripaludis* to adhere to a graphite electrode and directly reduce CO_2 to formate. Importantly, an unprecedented stable activity was demonstrated over a 5-day time period, which is by far the longest recorded (Lienemann et al., 2018).

Of the FDHs that have been investigated in a bioelectrochemical setting without using any electron mediators, only the FDH-H from *E. coli* has been characterized in relation to CO_2 affinity (Axley and Grahame, 1991; Yuan et al., 2018). With MV^{2+} as electron donor, SfFDH has a higher k_{cat} than EcFDH but according to De Bok et al., the CO_2 affinity could not be measured for SfFDH (De Bok et al., 2003). In fact, currently, only EcFDH (FDH-H) have been characterized for both efficiency and CO_2 affinity in a direct bioelectrochemical context.

4.3.2. Indirect electrocatalysis

The indirect method involves continuous reduction of the desired electron donor in solution, which thus allows soluble non-immobilized FDH to catalyze reduction of CO_2. This method has been applied using either the metal-independent CbFDH (Kim et al., 2014; Schlager et al., 2016) or metal-dependent FDH (Sakai et al., 2015, 2016, 2017). In this regard, Sakai et al. have done extensive work with a tungsten-containing FDH from *Methylobacterium extorquens* AM1 using NADH, MV^{2+}, and the little used 1,1′-trimethylene-2,2′- bipyridinium dibromide (TQ) as indirect electron mediator (Sakai et al., 2015, 2016, 2017).

4.4. Comparison of formate dehydrogenase kinetics for CO_2 reduction

In a recent review on metal-dependent FDHs, Maia et al. conclude that no clear trend is evident between FDH structure and reduction activity (Maia et al., 2017). Whilst the current kinetic data on metal-dependent FDH are limited, especially in terms of CO_2 affinity, a holistic comparison of all characterized FDHs reveals interesting tendencies (Fig. 4). In order to quantitatively compare the kinetic properties of FDHs, we compared the kinetics data for enzymes characterized at mesophilic conditions with identical electron donors (Table 2). The data were gathered via a manually curated literature search.

Not only is NADH clearly the inferior electron donor but the NADH dependent metal-independent FDHs also have both lower specificity constant and lower catalytic rate by orders of magnitude when compared to systems including metal-dependent FDHs (Fig. 4). From the data (Fig. 4) it is evident that the FDH from *Acetobacterium woodii,* AwFDH (Table 2) in general has high k_{cat} values compared to the other

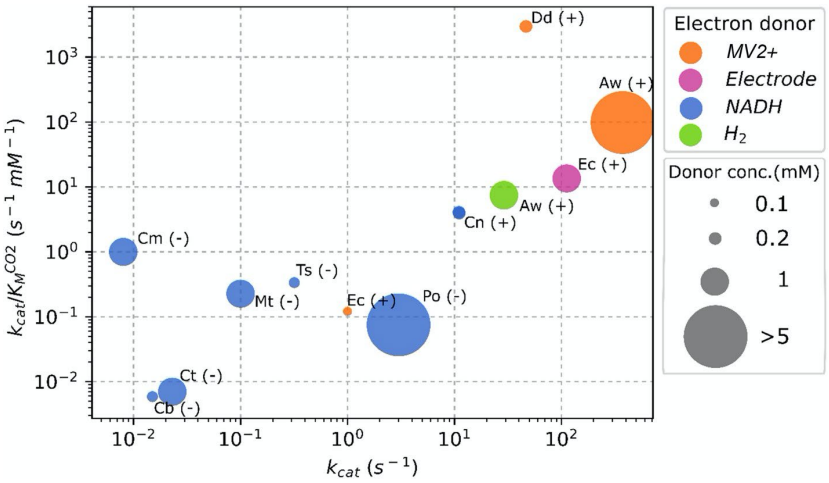

Fig. 4. The properties of kinetically characterized FDHs available in the current literature. These 11 FDH are the only ones to be described both in terms of specific rate constant and CO_2 affinity of all known and described FDHs. The properties are visualized by plotting the specificity constant data k_{cat}/K_M as a function of the specific rate constant, k_{cat}, with the type and concentration of electron donor visualized by color and size of markers. (−): metal-independent FDH, (+): metal-dependent FDH. Cm: *Candida methylica*, Cb: *Candida boidinii*, Ct: *Chaetomium thermophilum*, Mt.: *Myceliophthora thermophile*, Ts: *Thiobacillus sp.* KNK65MA, Ec: *Escherichia coli* (Electrode at 150 mV overpotential), Po: *Pseudomonas oxilatus* (100 mM NADH), Cn: *Cupriavidus necator*, Dd: *Desulfovibrio desulfuricans*, Aw: *Acetobacterium woodii*.

FDHs, but also that the k_{cat} of the AwFDH with MV^{2+} as electron donor substrate has higher k_{cat} than with H_2 (Fig. 4). Interestingly, the newly characterized HDCR from *Thermoanaerobacter kuvui* has been demonstrated to catalyze the by far highest rate for hydrogenation of CO_2 to formate (Schwarz et al., 2018). The CO_2 affinity for this enzyme is unknown, but with the enzymes inherent thermal stability it is a supremely interesting candidate for further study.

Among the FDHs, the enzyme that exhibits the highest k_{cat}/K_m of all enzymes assessed is the FDH of *Desulfovibrio desulfuricans,* DdFDH with MV^{2+} as electron donor (Fig. 4). This is largely due to is very high affinity for CO_2. Very recently, this specific enzyme was characterized with protein film voltammetry and shown to be a promising candidate for a bioelectrochemical system (Cordas et al., 2019).

When comparing FDH on electrodes, the catalytic rate is measured as a current density. The current density of SfFDH immobilized on graphite was 80 μA at 0.8 V (presumably vs SHE), compared to 62 μA at 0.66 V vs SHE for FDH-H from *E. coli* (EcFDH) immobilized on cobaltocene (Yuan et al., 2018). In other words, the current density observed for SfFDH was higher but also observed at higher potential. It is likely that the current density observed with EcFDH will be even higher than 80 μA when at 0.8 V vs SHE. Due to differences in immobilization method it is difficult to conclude whether the success for EcFDH is due to applied method or actual enzymatic properties. It is however interesting, that rates up to 112 s^{-1} were reported for SfFDH in a system where CO_2 is the only substrate beyond energy delivered as electrons.

The substrate concentration is dependent on pH simply because the equilibrium between aqueous CO_2 (acidic conditions), HCO_3^- (neutral conditions), and CO_3^{2-} (alkaline conditions) differs with pH. In the calculation of FDH dissociation constants towards bicarbonate, the dissociation constant was converted to the corresponding dissociation constant towards CO_2 (K_M^{CO2}), as described previously (Cotton et al., 2018).

5. Application perspectives

In order to apply an FDH as a biocatalyst for efficient CO_2 conversion to manufacture chemicals and chemical building blocks, a number of practical issues with regard to enzyme and reaction set-up must be considered. The robustness of enzymes can be improved by protein engineering (Bommarius et al., 2010; Chen and Zeng, 2016), including tolerance towards reaction extremes beyond common biological reaction conditions. Recently, carbonic anhydrase from *Desulfovibrio vulgaris* was engineered to be stable at conditions relevant for CO_2 capture and utilization at high temperatures and alkaline pH (Alvizo et al., 2014). Additionally, a different and more direct way of avoiding loss of activity is through immobilization of the enzyme which often significantly stabilizes the protein (Marpani et al., 2017a). With CO_2 reduced in an electrode set-up, immobilization is an inherent prerequisite.

For FDHs in general, reversible interconversion between CO_2 and formate, depending on the individual FDH enzyme, results in complex relationships between CO_2 and formate concentration in a given solution. Due to the often much higher FDH affinity for formate than for CO_2, these relationships will potentially create limits to the extent of CO_2 conversion (Maia et al., 2016). To circumvent these limits, formate must be continuously removed.

Variants of metal-dependent FDHs – the obvious candidate for FDH-mediated CO_2 reduction – have been discredited due to their oxygen sensitivity (Bassegoda et al., 2014). The mechanism behind the oxygen sensitivity is not fully understood. In general, FDHs with W-bisMGD and SeCys as coordinating residue are more prone to oxygen sensitivity. However, an exception is the tungsten-containing MeFDH of *Methylobacterium extorquens* AM1 (Laukel et al., 2003). While fewer FDHs with Mo-bisMGD and Cys coordinating residues are oxygen sensitive, many still are. Two oxygen-tolerant candidates are the metal-dependent variants RcFDH and CnFDH from *Rhodobacter capsulatus* and *Cupriavidus necator*, respectively, which have been shown to be able to reduce CO_2 in the presence of oxygen (Hartmann and Leimkühler, 2013; Yu et al., 2017, 2019). Both RcFDH and CnFDH are of type 5 in the new categorization proposed here, with MeFDH being closely related to these in terms of alpha sequence homology and gene segment organization. Focusing on FDHs of type 5 may allow circumvention of the otherwise severe oxygen sensitivity observed for some variants of metal-dependent FDHs. Moreover, FDHs of type 5 may hold the key to understanding why some FDHs are oxygen sensitive and others are not.

The complex structure and delicate assembly requirements for metal-dependent FDHs create challenges in terms of recombinant expression (Ihara et al., 2015), especially in terms of potential secretion of the protein. Most FDH enzymes studied for CO_2 reduction have been wild-type enzymes isolated from the cytoplasm or periplasm of the organism from which the enzyme is derived. Despite the challenges, it has long been shown possible to produce recombinant selenocysteine containing proteins in *E. coli* (Arnér et al., 1999). Therefore it is not unreasonable to envisage heterogeneous production of recombinant FDH containing both selenocysteine and tungsten. Furthermore, maturation of the molybdenum co-factor has been well studied (Iobbi-Nivol and Leimkühler, 2013) as has the assembly of the co-factor and proto-enzyme (Hartmann et al., 2015).

In 2013, successful heterologous expression of a metal-dependent cytoplasmic, and soluble, FDH from *Rhodobacter capsulatus* (RcFDH)

was achieved in *E. coli* (Hartmann and Leimkühler, 2013). In 2013 also, expression of a monomer metal-dependent FDH from *Clostridium carboxidivorans* was reported (Alissandratos et al., 2013). Efforts to enhance the commonly applied metal-independent CbFDH by protein engineering have been made (Carter et al., 2014), but little to no research efforts have gone into engineering metal-dependent variants.

Finally, until now, use of FDH for biomanufacturing of formate from CO_2 has been tested only in small lab scale set-ups providing limited insight into how such a process would function at a larger scale. In the context of applying FDH for reduction of CO_2 to formate, a device able to efficiently supply electrons through FDH to CO_2 would have to be developed and tested to evaluate the potential. However, increased independence of economy of scale is a significant advantage in biomanufacturing because this independence permits smaller and more adaptable production facilities (Clomburg et al., 2017).

Of significant note, relative to application of FDH for CO_2 reduction, are systems employing whole-cell microbial biocatalysts with CO_2 as substrate. Here focus has been on molecular hydrogen or direct electrocatalysis to drive catalysis. Studies with engineered *E. coli* or variants of *Desulfovibrio* spp. have demonstrated high production levels of formate from CO_2 and H_2 (Alissandratos et al., 2014; Mourato et al., 2017; Roger et al., 2018). In addition, microbial electrosynthesis (MES) technology, applying a range of different organisms, have been studied and applied for using CO_2 to produce organic acids and alcohols (Kracke et al., 2018; Le et al., 2018; Mateos et al., 2018; Roy et al., 2016; Zhang et al., 2019). Interestingly, the use of CO_2 for MES have been estimated to be economically feasible (Christodoulou et al., 2017), underlining the possibilities within this field of CO_2 utilization.

Extending the discussion of which technology is best suited for CO_2 conversion, would naturally also result in inclusion of non-biological approaches. Here, homogenous and electrochemical catalysts have made significant advances in recent years (Qiao et al., 2014; Sordakis et al., 2017), not to mention the thermochemically driven technologies based on heterogeneous catalysts (Ma et al., 2009; Otto et al., 2015). However, to the best of our knowledge – while several excellent reviews present large parts of the diverse Carbon Capture and Use, CUU, technologies under development – there is no quantitative comparison yet. In this context, with prospects of abundant and cheap renewable electricity, FDH mediated CO_2 conversion may prove to be an attractive option for the development of a Carbon Capture and Use market. We believe that an FDH based electro catalyst will prove a strong contender for the exact purpose of producing formate from crude low-concentration CO_2 sources and cheap electricity at small-scale settings. Hopefully, the classification scheme proposed in this study will help future studies and commercially oriented attempts to select potent FDH candidates to fully exploit the potential of FDH-mediated conversion of CO_2 as a first step towards utilizing CO_2 as the carbon resource it really is.

Acknowledgment

This study was funded by the Technical University of Denmark and partially funded by the BioValue SPIR, Strategic Platform for Innovation and Research on value added products from biomass, which is co-funded by The Innovation Fund Denmark, Case No: 0603-00522B.

References

Alekseeva, A.A., Savin, S.S., Tishkov, V.I., 2011. NAD (+)-dependent formate dehydrogenase from plants. Acta Nat. 3, 38–54.

Alissandratos, A., Easton, C.J., 2015. Biocatalysis for the application of CO_2 as a chemical feedstock. Beilstein J. Org. Chem. 11, 2370–2387. https://doi.org/10.3762/bjoc.11.259.

Alissandratos, A., Kim, H.-K., Matthews, H., Hennessy, J.E., Philbrook, A., Easton, C.J., 2013. *Clostridium carboxidivorans* strain P7T recombinant formate dehydrogenase catalyzes reduction of CO_2 to formate. Appl. Environ. Microbiol. 79, 741–744. https://doi.org/10.1128/AEM.02886-12.

Alissandratos, A., Kim, H.K., Easton, C.J., 2014. Formate production through carbon dioxide hydrogenation with recombinant whole cell biocatalysts. Bioresour. Technol. 164, 7–11. https://doi.org/10.1016/j.biortech.2014.04.064.

Alpdağtaş, S., Yücel, S., Kapkaç, H.A., Liu, S., Binay, B., 2018. Discovery of an acidic, thermostable and highly NADP+ dependent formate dehydrogenase from *Lactobacillus buchneri* NRRL B-30929. Biotechnol. Lett. 40, 1135–1147. https://doi.org/10.1007/s10529-018-2568-6.

Altas, N., Aslan, A.S., Karatas, E., Chronopoulou, E., Labrous, N.E., Binay, B., 2017. Heterologous production of extreme alkaline thermostable NAD+-dependent formate dehydrogenase with wide-range pH activity from *Myceliophthora thermophila*. Process Biochem. 61, 110–118. https://doi.org/10.1016/j.procbio.2017.06.017.

Alvizo, O., Nguyen, L.J., Savile, C.K., Bresson, J. a, Lakhapatri, S.L., Solis, E.O.P., Fox, R.J., Broering, J.M., Benoit, M.R., Zimmerman, S. a, Novick, S.J., Liang, J., Lalonde, J.J., 2014. Directed evolution of an ultrastable carbonic anhydrase for highly efficient carbon capture from flue gas. Proc. Natl. Acad. Sci. U. S. A. 111, 16436–16441. https://doi.org/10.1073/pnas.1411461111.

An, L., Chen, R., 2017. Mathematical modeling of direct formate fuel cells. Appl. Therm. Eng. 124, 232–240. https://doi.org/10.1016/j.applthermaleng.2017.06.020An, L., Chen, R., 2016. Direct formate fuel cells: A review. J. Power Sources 320, 127–139. doi:10.1016/j.jpowsour.2016.04.082.

Andreadeli, A., Platis, D., Tishkov, V., Popov, V., Labrou, N.E., 2008. Structure-guided alteration of coenzyme specificity of formate dehydrogenase by saturation mutagenesis to enable efficient utilization of NADP+. FEBS J. 275, 3859–3869. https://doi.org/10.1111/j.1742-4658.2008.06533.x.

Appel, A.M., Bercaw, J.E., Bocarsly, A.B., Dobbek, H., DuBois, D.L., Dupuis, M., Ferry, J.G., Fujita, E., Hille, R., Kenis, P.J.A., Kerfeld, C.A., Morris, R.H., Peden, C.H.F., Portis, A.R., Ragsdale, S.W., Rauchfuss, T.B., Reek, J.N.H., Seefeldt, L.C., Thauer, R.K., Waldrop, G.L., 2013. Frontiers, opportunities, and challenges in biochemical and chemical catalysis of CO_2 fixation. Chem. Rev. 113, 6621–6658. https://doi.org/10.1021/cr300463y.

Arnér, E.S.J., Sarioglu, H., Lottspeich, F., Holmgren, A., Böck, A., 1999. High-level expression in *Escherichia coli* of selenocysteine-containing rat thioredoxin reductase utilizing gene fusions with engineered bacterial-type SECIS elements and co-expression with the selA, selB and selC genes. J. Mol. Biol. 292, 1003–1016. https://doi.org/10.1006/jmbi.1999.3085.

Axley, M.J., Grahame, D.A., 1991. Kinetics for formate dehydrogenase of *Escherichia coli* formate-hydrogenlyase. J. Biol. Chem. 266, 13731–13736.

Bar-Even, A., Noor, E., Milo, R., 2012. A survey of carbon fixation pathways through a quantitative lens. J. Exp. Bot. 63, 2325–2342. https://doi.org/10.1093/jxb/err417.

Bar-Even, A., Noor, E., Flamholz, A., Milo, R., 2013. Design and analysis of metabolic pathways supporting formatotrophic growth for electricity-dependent cultivation of microbes. Biochim. Biophys. Acta Bioenerg. 1827, 1039–1047. https://doi.org/10.1016/j.bbabio.2012.10.013.

Baskaya, F.S., Zhao, X., Flickinger, M.C., Wang, P., 2010. Thermodynamic feasibility of enzymatic reduction of carbon dioxide to methanol. Appl. Biochem. Biotechnol. 162, 391–398. https://doi.org/10.1007/s12010-009-8758-x.

Bassegoda, A., Madden, C., Wakerley, D.W., Reisner, E., Hirst, J., 2014. Reversible interconversion of CO_2 and formate by a molybdenum-containing formate dehydrogenase. J. Am. Chem. Soc. 136, 15473–15476. https://doi.org/10.1021/ja508647u.

Böhmer, N., Hartmann, T., Leimkühler, S., 2014. The chaperone FdsC for *Rhodobacter capsulatus* formate dehydrogenase binds the bis-molybdopterin guanine dinucleotide cofactor. FEBS Lett. 588, 531–537. https://doi.org/10.1016/j.febslet.2013.12.033.

Bommarius, A.S., Blum, J.K., Abrahamson, M.J., 2010. Status of protein engineering for biocatalysts: how to design an industrially useful biocatalyst. Curr. Opin. Chem. Biol. 15, 194–200. https://doi.org/10.1016/j.cbpa.2010.11.011.

Brosnan, M.E., Brosnan, J.T., 2016. Formate: the neglected member of one-carbon metabolism. Annu. Rev. Nutr. 36, 369–388. https://doi.org/10.1146/annurev-nutr-071715-050738.

Carter, J.L.L., Bekhouche, M., Noiriel, A., Blum, L.J., Doumèche, B., 2014. Directed evolution of a formate dehydrogenase for increased tolerance to ionic liquids reveals a new site for increasing the stability. ChemBioChem 15, 2710–2718. https://doi.org/10.1002/cbic.201402501.

Castillo, R., Oliva, M., Martí, S., Moliner, V., 2008. A theoretical study of the catalytic mechanism of formate dehydrogenase. J. Phys. Chem. B 112, 10012–10022. https://doi.org/10.1021/jp8025896.

Chen, Z., Zeng, A.P., 2016. Protein engineering approaches to chemical biotechnology. Curr. Opin. Biotechnol. https://doi.org/10.1016/j.copbio.2016.07.007.

Choe, H., Joo, J.C., Cho, D.H., Kim, M.H., Lee, S.H., Jung, K.D., Kim, Y.H., 2014. Efficient CO_2-reducing activity of NAD-dependent formate dehydrogenase from *Thiobacillus sp.* KNK65MA for formate production from CO_2 gas. PLoS One 9 (7), e103111. https://doi.org/10.1371/journal.pone.0103111.

Christodoulou, X., Okoroafor, T., Parry, S., Velasquez-Orta, S.B., 2017. The use of carbon dioxide in microbial electrosynthesis: advancements, sustainability and economic feasibility. Biochem. Pharmacol. 18, 390–399. https://doi.org/10.1016/j.jcou.2017.01.027.

Claassens, N.J., Sánchez-Andrea, I., Sousa, D.Z., Bar-Even, A., 2018. Towards sustainable feedstocks: a guide to electron donors for microbial carbon fixation. Curr. Opin. Biotechnol. 50, 195–205. https://doi.org/10.1016/j.copbio.2018.01.019.

Clomburg, J.M., Crumbley, A.M., Gonzalez, R., 2017. Industrial biomanufacturing: the future of chemical production. Science 355 (38), eaag0804. https://doi.org/10.1126/science.aag0804.

Cordas, C.M., Campaniço, M., Baptista, R., Maia, L.B., Moura, I., Moura, J.J.G., 2019. Direct electrochemical reduction of carbon dioxide by a molybdenum-containing formate dehydrogenase. J. Inorg. Biochem. 196, 110694. https://doi.org/10.1016/j.jinorgbio.2019.110694.

Cotton, C.A., Edlich-Muth, C., Bar-Even, A., 2018. Reinforcing carbon fixation: CO_2 reduction replacing and supporting carboxylation. Curr. Opin. Biotechnol. 49, 49–56.

https://doi.org/10.1016/j.copbio.2017.07.014.
da Silva, S.M., Pimentel, C., Valente, F.M.A., Rodrigues-Pousada, C., Pereira, I.A.C., 2011. Tungsten and molybdenum regulation of formate dehydrogenase expression in *Desulfovibrio vulgaris* Hildenborough. J. Bacteriol. 193, 2909–2916. https://doi.org/10.1128/JB.00042-11.
De Bok, F.A.M., Hagedoorn, P.L., Silva, P.J., Hagen, W.R., Schiltz, E., Fritsche, K., Stams, A.J.M., 2003. Two W-containing formate dehydrogenases (CO_2-reductases) involved in syntrophic propionate oxidation by *Syntrophobacter fumaroxidans*. Eur. J. Biochem. 270, 2476–2485. https://doi.org/10.1046/j.1432-1033.2003.03619.x.
Elantak, L., Dolla, A., Durand, M.C., Bianco, P., Guerlesquin, F., 2005. Role of the tetrahemic subunit in *Desulfovibrio vulgaris* Hildenborough formate dehydrogenase. Biochemistry 44, 14828–14834. https://doi.org/10.1021/bi0515366.
Figueres, C., Le Quéré, C., Mahindra, A., Bäte, O., Whiteman, G., Peters, G., Guan, D., 2018. Emissions are still rising: ramp up the cuts. Nature 564, 27–30. https://doi.org/10.1038/d41586-018-07585-6.
Filippova, E.V., Polyakov, K.M., Tikhonova, T.V., Stekhanova, T.N., Boiko, K.M., Popov, V.O., 2005. Structure of a new crystal modification of the bacterial NAD-dependent formate dehydrogenase with a resolution of 2.1 Å Crystallogr. Rep. 50, 796–800. https://doi.org/10.2210/PDB2GO1/PDB.
Finn, R.D., Attwood, T.K., Babbitt, P.C., Bateman, A., Bork, P., Bridge, A.J., Chang, H.Y., Dosztanyi, Z., El-Gebali, S., Fraser, M., Gough, J., Haft, D., Holliday, G.L., Huang, H., Huang, X., Letunic, I., Lopez, R., Lu, S., Marchler-Bauer, A., Mi, H., Mistry, J., Natale, D.A., Necci, M., Nuka, G., Orengo, C.A., Park, Y., Pesseat, S., Piovesan, D., Potter, S.C., Rawlings, N.D., Redaschi, N., Richardson, L., Rivoire, C., Sangrador-Vegas, A., Sigrist, C., Sillitoe, I., Smithers, B., Squizzato, S., Sutton, G., Thanki, N., Thomas, P.D., Tosatto, S.C.E., Wu, C.H., Xenarios, I., Yeh, L.S., Young, S.Y., Mitchell, A.L., 2017. InterPro in 2017-beyond protein family and domain annotations. Nucleic Acids Res. 45, D190–D199. https://doi.org/10.1093/nar/gkw1107.
Fogal, S., Beneventi, E., Cendron, L., Bergantino, E., 2015. Structural basis for double cofactor specificity in a new formate dehydrogenase from the acidobacterium *Granulicella mallensis* MP5ACTX8. Appl. Microbiol. Biotechnol. 99, 9541–9554. https://doi.org/10.1007/s00253-015-6695-x.
Glueck, S.M., Gümüs, S., Fabian, W.M.F., Faber, K., 2010. Biocatalytic carboxylation. Chem. Soc. Rev. 39, 313–328. https://doi.org/10.1039/B807875K.
Goeppert, A., Czaun, M., Jones, J.-P., Surya Prakash, G.K., Olah, G.A., 2014. Recycling of carbon dioxide to methanol and derived products – closing the loop. Chem. Soc. Rev. 43, 7995–8048. https://doi.org/10.1039/C4CS00122B.
Grimaldi, S., Schoepp-Cothenet, B., Ceccaldi, P., Guigliarelli, B., Magalon, A., 2013. The prokaryotic Mo/W-bisPGD enzymes family: a catalytic workhorse in bioenergetic. Biochim. Biophys. Acta Bioenerg. 1827, 1048–1085. https://doi.org/10.1016/j.bbabio.2013.01.011.
Guo, Q., Gakhar, L., Wickersham, K., Francis, K., Vardi-Kilshtain, A., Major, D.T., Cheatum, C.M., Kohen, A., 2016. Structural and kinetic studies of formate dehydrogenase from *Candida boidinii*. Biochemistry 55, 2760–2771. https://doi.org/10.1021/acs.biochem.6b00181.
Hartmann, T., Leimkühler, S., 2013. The oxygen-tolerant and NAD + -dependent formate dehydrogenase from *Rhodobacter capsulatus* is able to catalyze the reduction of CO_2 to formate. FEBS J. 280, 6083–6096. https://doi.org/10.1111/febs.12528.
Hartmann, T., Schwanhold, N., Leimkühler, S., 2015. Assembly and catalysis of molybdenum or tungsten-containing formate dehydrogenases from bacteria. Biochim. Biophys. Acta Proteins Proteom. 1854, 1090–1100. https://doi.org/10.1016/j.bbapap.2014.12.006.
Hatrongjit, R., Packdibamrung, K., 2010. A novel NADP + -dependent formate dehydrogenase from *Burkholderia stabilis* 15516: screening, purification and characterization. Enzym. Microb. Technol. 46, 557–561. https://doi.org/10.1016/j.enzmictec.2010.03.002.
Hille, R., Hall, J., Basu, P., 2014. The mononuclear molybdenum enzymes. Chem. Rev. 114, 3963–4038. https://doi.org/10.1021/cr400443z.
Holmes, D.E., Smith, J.A., 2016. Biologically produced methane as a renewable energy source. Adv. Appl. Microbiol. 97, 1–61. https://doi.org/10.1016/bs.aambs.2016.09.001.
Hummel, W., Gröger, H., 2014. Strategies for regeneration of nicotinamide coenzymes emphasizing self-sufficient closed-loop recycling systems. J. Biotechnol. 191, 22–31. https://doi.org/10.1016/j.jbiotec.2014.07.449.
Ihara, M., Kawano, Y., Fujiwara, Y., Kodo, T., Mizuguchi, M., Mochiduki, Y., Kodoh, K., Okabe, A., Matsuno, I., 2015. Expression systems for soluble metal-dependent formate dehydrogenase. J. Photochem. Photobiol. A Chem. 313, 154–162. https://doi.org/10.1016/j.jphotochem.2015.06.028.
Ikeyama, S., Amao, Y., 2017. An artificial co-enzyme based on the viologen skeleton for highly efficient CO_2 reduction to formic acid with formate dehydrogenase. ChemCatChem 9, 833–838. https://doi.org/10.1002/cctc.201601188.
Iobbi-Nivol, C., Leimkühler, S., 2013. Molybdenum enzymes, their maturation and molybdenum cofactor biosynthesis in *Escherichia coli*. Biochim. Biophys. Acta Bioenerg. 1827, 1086–1101. https://doi.org/10.1016/j.bbabio.2012.11.007.
IPCC, 2018. Summary for policymakers. In: Masson-Delmotte, V., Zhai, P., Pörtner, H.O., Roberts, D., Skea, J., Shukla, P.R. ... World Meteorological Organization (Eds.), Global Warming of 1.5°C. An IPCC Special Report on the Impacts of Global Warming of 1.5°C above Pre-industrial Levels and Related Global Greenhouse Gas Emission Pathways, in the Context of Strengthening the Global Response to the Threat of Climate Change, Sustainable Development, and Efforts to Eradicate Poverty. Geneva, Switzerland.
Jormakka, M., Byrne, B., Iwata, S., 2003. Formate dehydrogenase - A versatile enzyme in changing environments. Curr. Opin. Struct. Biol. 13, 418–423. https://doi.org/10.1016/S0959-440X(03)00098-8.
Katoh, K., Standley, D.M., 2013. MAFFT multiple sequence alignment software version 7: improvements in performance and usability. Mol. Biol. Evol. 30, 772–780. https://doi.org/10.1093/molbev/mst010.
Katoh, K., Rozewicki, J., Yamada, K.D., 2017. MAFFT online service: multiple sequence alignment, interactive sequence choice and visualization. Brief. Bioinform. 1–7. https://doi.org/10.1093/bib/bbx108.
Kearny, J.J., Sagers, R.D., 1972. Formate dehydrogenase from *Clostridium acidiurici*. J. Bacteriol. 109, 152–161.
Kim, S., Kim, M.K., Lee, S.H., Yoon, S., Jung, K.D., 2014. Conversion of CO_2 to formate in an electroenzymatic cell using *Candida boidinii* formate dehydrogenase. J. Mol. Catal. B Enzym. 102, 9–15. https://doi.org/10.1016/j.molcatb.2014.01.007.
Kracke, F., Lai, B., Yu, S., Krömer, J.O., 2018. Balancing cellular redox metabolism in microbial electrosynthesis and electro fermentation – a chance for metabolic engineering. Metab. Eng. 45, 109–120. https://doi.org/10.1016/j.ymben.2017.12.003.
Laukel, M., Chistoserdova, L., Lidstrom, M.E., Vorholt, J.A., 2003. The tungsten-containing formate dehydrogenase from *Methylobacterium extorquens* AM1: purification and properties. Eur. J. Biochem. 270, 325–333. https://doi.org/10.1046/j.1432-1033.2003.03391.x.
Le, S.Q., Gascuel, O., 2008. An improved general amino acid replacement matrix. Mol. Biol. Evol. 25, 1307–1320. https://doi.org/10.1093/molbev/msn067.
Le Quéré, C., Andrew, R.M., Friedlingstein, P., Sitch, S., Hauck, J., Pongratz, J., Pickers, P.A., Korsbakken, J.I., Peters, G.P., Canadell, J.G., Arneth, A., Arora, V.K., Barberos, L., Bastos, A., Bopp, L., Chevallier, F., Chini, L.P., Ciais, P., Doney, S.C., Gkritzalis, T., Goll, D., Harris, I., Haverd, V., Hoffmann, F.M., Hoppema, M., Houghton, R.A., Hurtt, G., Ilyina, T., Jain, A.K., Johannessen, T., Jones, C.D., Kato, E., Keeling, R.F., Goldewijk, K.K., Landschützer, P., Lefèvre, N., Lienert, S., Liu, Z., Lombardozzi, D., Metzl, N., Munro, D.R., Nabel, J., Nakaoka, S., Neill, C., Olsen, A., Ono, T., Patra, P., Peregon, A., Peters, W., Peylin, P., Pfeil, B., Pierrot, D., Poulter, B., Rehder, G., Resplandy, L., Robertson, E., Rocher, M., Rödenbeck, C., Schuster, U., Schwinger, J., Séférian, R., Skjelvan, I., Steinhoff, T., Sutton, A., Tans, P.P., Tian, H., Tilbrook, B., Tubiello, F.N., van der Laan-Luijkx, I.T., vander der Werf, G.R., Viovy, Walker, A.P., Wiltshire, A.J., Wright, R., Zaehle, S., Zheng, B., 2018. Global carbon budget 2018. Earth Syst. Sci. Data 10, 2141–2194. https://doi.org/10.5194/essd-10-2141-2018.
Le, Q.A.T., Kim, H.G., Kim, Y.H., 2018. Electrochemical synthesis of formic acid from CO_2 catalyzed by *Shewanella oneidensis* MR-1 whole-cell biocatalyst. Enzym. Microb. Technol. 116, 1–5. https://doi.org/10.1016/j.enzmictec.2018.05.005.
Lenger, R., Herrmann, U., Gross, R., Simon, J., Kroger, A., 1997. Structure and function of a second gene cluster encoding the formate dehydrogenase of *Wolinella succinogenes*. Eur. J. Biochem. 246, 646–651.
Li, W., Godzik, A., 2006. Cd-hit: a fast program for clustering and comparing large sets of protein or nucleotide sequences. Bioinformatics 22, 1658–1659. https://doi.org/10.1093/bioinformatics/btl158.
Lienemann, M., Deutzmann, J.S., Milton, R.D., Sahin, M., Spormann, A.M., 2018. Mediator-free enzymatic electrosynthesis of formate by the *Methanococcus maripaludis* heterodisulfide reductase supercomplex. Bioresour. Technol. 254, 278–283. https://doi.org/10.1016/j.biortech.2018.01.036.
Ling, J., O'Donoghue, P., Söll, D., 2016. Genetic code flexibility in microorganisms: novel mechanisms and impact on physiology. Microbiol. Nat. Rev. 13, 707–721. https://doi.org/10.1038/nrmicro3568.Genetic.
Luo, J., Meyer, A.S., Mateiu, R.V., Pinelo, M., 2015. Cascade catalysis in membranes with enzyme immobilization for multi-enzymatic conversion of CO_2 to methanol. New Biotechnol. 32, 319–327. https://doi.org/10.1016/j.nbt.2015.02.006.
Ma, J., Sun, N., Zhang, X., Zhao, N., Xiao, F., Wei, W., Sun, Y., 2009. A short review of catalysis for CO_2 conversion. Catal. Today 148, 221–231. https://doi.org/10.1016/j.cattod.2009.08.015.
Maia, L.B., Fonseca, L., Moura, I., Moura, J.J.G., 2016. Reduction of carbon dioxide by a molybdenum-containing formate dehydrogenase: a kinetic and mechanistic study. J. Am. Chem. Soc. 138, 8834–8846. https://doi.org/10.1021/jacs.6b03941.
Maia, L.B., Moura, I., Moura, J.J.G., 2017. Molybdenum and tungsten-containing formate dehydrogenases: aiming to inspire a catalyst for carbon dioxide utilization. Inorgan. Chim. Acta 455, 350–363. https://doi.org/10.1016/j.ica.2016.07.010.
Marpani, F., Pinelo, M., Meyer, A.S., 2017a. Enzymatic conversion of CO_2 to CH_3OH via reverse dehydrogenase cascade biocatalysis: quantitative comparison of efficiencies of immobilized enzyme systems. Biochem. Eng. J. https://doi.org/10.1016/j.bej.2017.08.011.
Marpani, F., Sárossy, Z., Pinelo, M., Meyer, A.S., 2017b. Kinetics based reaction optimization of enzyme catalysed reduction of formaldehyde to methanol with synchronous cofactor regeneration. Biotechnol. Bioeng. 114, 2762–2770. https://doi.org/10.1002/bit.26405.
Mateos, R., Escapa, A., Vanbroekhoven, K., Patil, S.A., Moran, A., Pant, D., 2018. Microbial electrochemical technologies for CO_2 and its derived products valorization. In: Microbial Electrochemical Technology. Elsevier, pp. 777–796. https://doi.org/10.1016/b978-0-444-64052-9.00032-7.
Mellmann, D., Sponholz, P., Junge, H., Beller, M., 2016. Formic acid as a hydrogen storage material – development of homogeneous catalysts for selective hydrogen release. Chem. Soc. Rev. 45, 3954–3988. https://doi.org/10.1039/C5CS00618J.
Miller, M.A., Pfeiffer, W., Schwartz, T., 2010. Creating the CIPRES Science Gateway for inference of large phylogenetic trees. In: 2010 Gateway Computing Environments Workshop (GCE). IEEE, pp. 1–8. https://doi.org/10.1109/GCE.2010.5676129.
Miller, M., Robinson, W.E., Oliveira, A.R., Heidary, N., Kornienko, N., Warnan, J., Pereira, I.A.C., Reisner, E., 2019. Interfacing formate dehydrogenase with metal oxides for the reversible electrocatalysis and solar-driven reduction of carbon dioxide. Angew. Chem. Int. Ed. 4601–4605. https://doi.org/10.1002/anie.201814419.
Milton, R.D., Minteer, S.D., 2017. Direct enzymatic bioelectrocatalysis: differentiating between myth and reality. J. R. Soc. Interface 14, 20170253. https://doi.org/10.1098/rsif.2017.0253.
Mourato, C., Martins, M., Da Silva, S.M., Pereira, I.A.C., 2017. A continuous system for biocatalytic hydrogenation of CO_2 to formate. Bioresour. Technol. 235, 149–156.

https://doi.org/10.1016/j.biortech.2017.03.091.
Nishio, N., Nakashimada, Y., 2013. Manufacture of biogas and fertilizer from solid food wastes by means of anaerobic digestion. In: Food Industry Wastes. Elsevier, pp. 121–133. https://doi.org/10.1016/B978-0-12-391921-2.00007-X.
Obert, R., Dave, B.C., 1999. Enzymatic conversion of carbon dioxide to methanol: enhanced methanol production in silica sol−gel matrices. J. Am. Chem. Soc. 121, 12192–12193. https://doi.org/10.1021/ja991899r.
Otto, A., Grube, T., Schiebahn, S., Stolten, D., 2015. Closing the loop: captured CO_2 as a feedstock in the chemical industry. Energy Environ. Sci. 8, 3283–3297. https://doi.org/10.1039/C5EE02591E.
Qiao, J., Liu, Y., Hong, F., Zhang, J., 2014. A review of catalysts for the electroreduction of carbon dioxide to produce low-carbon fuels. Chem. Soc. Rev. 43, 631–675. https://doi.org/10.1039/C3CS60323G.
Raaijmakers, H.C.A., Romão, M.J., 2006. Formate-reduced *E. coli* formate dehydrogenase H: the reinterpretation of the crystal structure suggests a new reaction mechanism. J. Biol. Inorg. Chem. 11, 849–854. https://doi.org/10.1007/s00775-006-0129-2.
Raaijmakers, H., Macieira, S., Dias, J.M., Teixeira, S., Bursakov, S., Huber, R., Moura, J.J.G., Moura, I., Romão, M.J., Dias, M., Teixeira, S., Bursakov, S., Huber, R., Moura, J.J.G., Moura, I., Roma, M.J., De Qui, D., 2002. Gene sequence and the 1.8 Å crystal structure gene sequence and the 1.8 Å of the tungsten-containing formate dehydrogenase from *Desulfovibrio gigas*. Structure 10, 1261–1272. https://doi.org/10.1016/S0969-2126(02)00826-2.
Ragsdale, S.W., 1997. The eastern and Western branches of the Wood/Ljundahl pathway: how the east and west were won. Biofactors 6, 3–11.
Ragsdale, S.W., 2008. Enzymology of the woods-Ljundahl pathway of acetogenesis. Ann. N. Y. Acad. Sci. 1125, 129–136. https://doi.org/10.1196/annals.1419.015. Enzymology.
Reda, T., Plugge, C.M., Abram, N.J., Hirst, J., 2008. Reversible interconversion of carbon dioxide and formate by an electroactive enzyme. Proc. Natl. Acad. Sci. 105, 10654–10658. https://doi.org/10.1073/pnas.0801290105.
Roger, M., Brown, F., Gabrielli, W., Sargent, F., 2018. Efficient hydrogen-dependent carbon dioxide reduction by *Escherichia coli*. Curr. Biol. 28, 140–145. https://doi.org/10.1016/j.cub.2017.11.050.
Rothery, R.A., Workun, G.J., Weiner, J.H., 2008. The prokaryotic complex iron–sulfur molybdoenzyme family. Biochim. Biophys. Acta Biomembr. 1778, 1897–1929. https://doi.org/10.1016/j.bbamem.2007.09.002.
Roy, S., Schievano, A., Pant, D., 2016. Bioresource technology electro-stimulated microbial factory for value added product synthesis. Bioresour. Technol. 213, 129–139. https://doi.org/10.1016/j.biortech.2016.03.052.
Ruschig, U., Müller, U., Willnow, P., Höpner, T., 1976. CO_2 reduction to formate by NADH catalysed by formate dehydrogenase from *Pseudomonas oxalaticus*. Eur. J. Biochem. 79, 325–330. https://doi.org/10.1111/j.1432-1033.1976.tb11021.x.
Sakai, K., Hsieh, B.-C., Maruyama, A., Kitazumi, Y., Shirai, O., Kano, K., 2015. Interconversion between formate and hydrogen carbonate by tungsten-containing formate dehydrogenase-catalyzed mediated bioelectrocatalysis. Sens. Bio-Sens. Res. 5, 90–96. https://doi.org/10.1016/j.sbsr.2015.07.008.
Sakai, K., Kitazumi, Y., Shirai, O., Takagi, K., Kano, K., 2016. Efficient bioelectrocatalytic CO_2 reduction on gas-diffusion-type biocathode with tungsten-containing formate dehydrogenase. Electrochem. Commun. 73, 85–88. https://doi.org/10.1016/j.elecom.2016.11.008.
Sakai, K., Sugimoto, Y., Kitazumi, Y., Shirai, O., Takagi, K., Kano, K., 2017. Direct electron transfer-type bioelectrocatalytic interconversion of carbon dioxide/formate and NAD+/NADH redox couples with tungsten-containing formate dehydrogenase. Electrochim. Acta 228, 537–544. https://doi.org/10.1016/j.electacta.2017.01.112.
Sakai, K., Xia, H. qi, Kitazumi, Y., Shirai, O., Kano, K., 2018. Assembly of direct-electron-transfer-type bioelectrodes with high performance. Electrochim. Acta 271, 305–311. https://doi.org/10.1016/j.electacta.2018.03.163.
Schlager, S., Dumitru, L.M., Haberbauer, M., Fuchsbauer, A., Neugebauer, H., Hiemetsberger, D., Wagner, A., Portenkirchner, E., Sariciftci, N.S., 2016. Electrochemical reduction of carbon dioxide to methanol by direct injection of electrons into immobilized enzymes on a modified electrode. ChemSusChem 9, 631–635. https://doi.org/10.1002/cssc.201501496.
Schneider, F., Löwe, J., Huber, R., Schindelin, H., Kisker, C., Knäblein, J., 1996. Crystal structure of dimethyl sulfoxide reductase from *Rhodobacter capsulatus* at 1.88 Å resolution. J. Mol. Biol. 263, 53–69.
Schuchmann, K., Müller, V., 2013. Direct and reversible hydrogenation of CO_2 to formate by a bacterial carbon dioxide reductase. Science 342, 1382–1385. https://doi.org/10.1126/science.1244758.
Schuchmann, K., Müller, V., 2014. Autotrophy at the thermodynamic limit of life: a model for energy conservation in acetogenic bacteria. Nat. Rev. Microbiol. 12, 809–821. https://doi.org/10.1038/nrmicro3365.
Schwarz, F.M., Schuchmann, K., Müller, V., 2018. Hydrogenation of CO_2 at ambient pressure catalyzed by a highly active thermostable biocatalyst. Biotechnol. Biofuels 11, 237. https://doi.org/10.1186/s13068-018-1236-3.
Shabalin, I.G., Serov, A.E., Skirgello, O.E., Timofeev, V.I., Samygina, V.R., Popov, V.O., Tishkov, V.I., Kuranova, I.P., 2010. Recombinant formate dehydrogenase from *Arabidopsis thaliana*: preparation, crystal growth in microgravity, and preliminary X-ray diffraction study. Crystallogr. Rep. 55, 806–810. https://doi.org/10.1134/S1063774510050159.
Shi, J., Jiang, Y., Jiang, Z., Wang, X., Wang, X., Zhang, S., Han, P., Yang, C., 2015. Enzymatic conversion of carbon dioxide. Chem. Soc. Rev. 44, 5981–6000. https://doi.org/10.1039/c5cs00182j.
Singh, A.K., Singh, S., Kumar, A., 2015. Hydrogen energy future with formic acid: a renewable chemical hydrogen storage system. Catal. Sci. Technol. 6, 12–40. https://doi.org/10.1039/C5CY01276G.
Sordakis, K., Tang, C., Vogt, L.K., Junge, H., Dyson, P.J., Beller, M., Laurenczy, G.G., 2017. Homogeneous Catalysis for Sustainable Hydrogen Storage in Formic Acid and Alcohols. vol. 118. pp. 372–433. https://doi.org/10.1021/acs.chemrev.7b00182.
Srikanth, S., Alvarez-Gallego, Y., Vanbroekhoven, K., Pant, D., 2017. Enzymatic electrosynthesis of formic acid through carbon dioxide reduction in a bioelectrochemical system: effect of immobilization and carbonic anhydrase addition. Chemphyschem 18 (22), 3174–3181. https://doi.org/10.1002/cphc.201700017.
Stamatakis, A., 2014. RAxML version 8: a tool for phylogenetic analysis and post-analysis of large phylogenies. Bioinformatics 30, 1312–1313. https://doi.org/10.1093/bioinformatics/btu033.
Sultana, S., Sahoo, P.C., Martha, S., Parida, K., 2016. A review of harvesting clean fuels from enzymatic CO_2 reduction. RSC Adv. 6, 44170–44194. https://doi.org/10.1039/C6RA05472B.
Takacs, M., Makhlynets, O.V., Tolbert, P.L., Korendovych, I.V., 2017. Secretion of functional formate dehydrogenase in *Pichia pastoris*. Protein Eng. Des. Sel. 30, 381–386. https://doi.org/10.1093/protein/gzx010.
Tishkov, V.I., Popov, V.O., 2006. Protein engineering of formate dehydrogenase. Biomol. Eng. 23, 89–110. https://doi.org/10.1016/j.bioeng.2006.02.003.
Vinals, C., Depiereux, E., Feytmans, E., 1993. Prediction of structurally conserved regions of D-specific hydroxy acid dehydrogenases by multiple alignment with formate dehydrogenase. Biochem. Biophys. Res. Commun. 192, 182–188. https://doi.org/10.1006/bbrc.1993.1398.
Wang, S., Huang, H., Kahnt, J., Thauer, R.K., 2013a. *Clostridium acidurici* electron-bifurcating formate dehydrogenase. Appl. Environ. Microbiol. 79, 6176–6179. https://doi.org/10.1128/AEM.02015-13.
Wang, S., Huang, H., Kahnt, J., Thauer, R.K., 2013b. A reversible electron-bifurcating ferredoxin- and NAD-dependent [FeFe]-hydrogenase (HydABC) in *Moorella thermoacetica*. J. Bacteriol. 195, 1267–1275. https://doi.org/10.1128/JB.02158-12.
Wood, G.E., Haydock, A.K., Leigh, J.A., 2003. Function and regulation of the formate dehydrogenase genes of the methanogenic archaeon *Methanococcus maripaludis*. J. Bacteriol. 185, 2548–2554. https://doi.org/10.1128/JB.185.8.2548–2554.2003.
Wu, W., Zhu, D., Hua, L., 2009. Site-saturation mutagenesis of formate dehydrogenase from *Candida bodinii* creating effective NADP+-dependent FDH enzymes. J. Mol. Catal. B Enzym. 61, 157–161. https://doi.org/10.1016/j.molcatb.2009.06.005.
Yu, X., Niks, D., Mulchandani, A., Hille, R., 2017. Efficient reduction of CO_2 by the molybdenum-containing formate dehydrogenase from *Cupriavidus necator* (*Ralstonia eutropha*). J. Biol. Chem. 292, 16872–16879. https://doi.org/10.1074/jbc.M117.785576.
Yu, X., Niks, D., Ge, X., Liu, H., Hille, R., Mulchandani, A., 2019. Synthesis of formate from CO_2 gas catalyzed by an O_2-tolerant NAD-dependent formate dehydrogenase and glucose dehydrogenase. Biochemistry. 58, 1861–1868. https://doi.org/10.1021/acs.biochem.8b01301.
Yuan, M., Sahin, S., Cai, R., Abdellaoui, S., Hickey, D.P., Minteer, S.D., Milton, R.D., 2018. Creating a low-potential redox polymer for efficient electroenzymatic CO_2 reduction. Angew. Chem. Int. Ed. 57, 6582–6586. https://doi.org/10.1002/anie.201803397.
Zhang, Y., Gladyshev, V.N., 2008. Molybdoproteomes and evolution of molybdenum utilization. J. Mol. Biol. 379, 881–899. https://doi.org/10.1016/j.jmb.2008.03.051.
Zhang, Z., Xu, B., Luo, J., Solms, N., He, H., Zhang, Y., Pinelo, M., Zhang, S., 2018. Ionic liquids as bifunctional cosolvents enhanced CO_2 conversion catalysed by NADH-dependent formate dehydrogenase. Catalysts 8, 304. https://doi.org/10.3390/catal8080304.
Zhang, Z., Song, Y., Zheng, S., Zhen, G., Lu, X., Takuro, K., Xu, K., Bakonyi, P., 2019. Electro-conversion of carbon dioxide (CO_2) to low-carbon methane by bioelectromethanogenesis process in microbial electrolysis cells: the current status and future perspective. Bioresour. Technol. 279, 339–349. https://doi.org/10.1016/j.biortech.2019.01.145.

Appendix N. Paper II: Enzyme reaction kinetics and O_2 tolerance of bacterial formate dehydrogenases for CO_2 utilization

Paper II is in preparation for submission to Journal of CO_2 Utilization. It is inserted on the following pages.

Enzyme reaction kinetics and O_2 tolerance of bacterial formate dehydrogenases for CO_2 utilization

Nielsen, Christian F.[1], Morth, J. Preben[1], and Meyer, Anne S.[1*]

[1] Department of Biotechnology and Biomedicine, Technical University of Denmark, Kgs. Lyngby, Denmark

E-mail: asme@dtu.dk

Received xxxxxx
Accepted for publication xxxxxx
Published xxxxxx

Abstract

Enzymatic conversion of CO_2 is an interesting approach for carbon capture and utilization. This study presents a characterization of three metal-dependent, recombinantly expressed formate dehydrogenases, originating from *Rhodobacter capsulatus* (RcFDH), *Rhodobacter sphearoides* (RsFDH), and *Cupriavidus necator* (CnFDH). The enzymes are characterized in terms of their reaction kinetics as well as their oxygen tolerance and pH and temperature optima for both the reduction of CO_2 and the oxidation of formate.

It was observed that the reduction of CO_2 had a higher optimum temperature and lower optimum pH than the oxidation of formate for all three enzymes. When comparing the three enzymes at their respective optima for CO_2 conversion, CnFDH had the highest turnover of CO_2. All three enzymes were oxygen sensitive in the dimeric heterotrimer $(\alpha\beta\gamma)_2$ conformation, even in the presence of KNO_3 whereas the monomeric heterotrimer $\alpha\beta\gamma$ of RsFDH was stable in the presence of high concentrations (10 mM) of KNO_3.

In conclusion, the three enzyme variants of this study hold potential as candidates for enzymatic CCU with CnFDH being the current best candidate. However, issues with oxygen sensitivity will have to be overcome for efficient large-scale implementation.

Keywords: Carbon capture and utilization; Formate dehydrogenase; Enzyme kinetics; Oxygen tolerance

1. Introduction

Through carbon capture and utilization (CCU), CO_2 can be used as carbon resource and hereby substitute petrochemical production pathways that are based on fossil fuels [1]. As such, CCU has the potential to substitute net CO_2 emitting processes with net-neutral or even net-negative CO_2 emitting processes. An effective consortium of CCU technologies would reduce dependence on fossil fuels and help mitigate the drastic climate changes we are just beginning to experience [2].

Enzymatic solutions are of interest because they are effective, selective and mild. Within CCU, enzymes have been studied as catalysts for converting CO_2 to existing in-demand chemical products. Particularly the enzyme class formate dehydrogenases (FDHs) is of interest. FDHs selectively catalyze the interconversion between CO_2 and formate (Eq. 1). For this study, formate oxidation is referred to as the 'forward reaction', given that it is the more common reaction direction in nature and also the reaction inferred by the very name of the enzyme. Correspondingly, CO_2 reduction will be referred to as the 'reverse reaction'.

$$HCO_2^- \rightleftharpoons CO_2 + H^+ + 2e^- \quad (Eq. 1)$$

FDHs are of particular interest because they are the only enzymes capable of utilizing CO_2 and electrons as the only two substrates for conversion to a liquid chemical product. All other enzymatic reactions with CO_2 involve either complex co-substrates or result in gaseous products.

In terms of diversity, FDHs can be divided into metal-dependent FDHs and metal-independent FDHs. The variants of the metal-dependent FDHs have demonstrated much higher conversion rates than the metal-independent FDHs and are poised to be applied for direct electrochemistry [3]. Essentially, some metal-dependent FDHs are able to directly use electrons from an electrode to reduce CO_2 to formate at high rates and with perfect selectivity, while metal-independent FDHs are not.

Recently, two variants of metal-dependent FDHs have been postulated to be oxygen tolerant in the presence of KNO_3 [4-7]. These are the intracellular soluble heterotrimer FDHs from *Rhodobacter capsulatus* (RcFDH), and from *Cupriavidus necator* (CnFDH). Specifically, RcFDH has been characterized by Hartmann and Leimkühler in 2013 while CnFDH has been characterized by Yu et al. in both 2017 and 2019. Oxygen tolerance is an obvious parameter of interest, in relation to application, since anaerobic operations are costly. As such, the postulated oxygen tolerance for RcFDH and CnFDH become critical. However, to the best of our knowledge, every other metal-dependent FDH is distinctly oxygen sensitive. We speculate that RcFDH and CnFDH indeed also exhibit oxygen sensitivity, albeit to a lesser extent than other metal-dependent FDHs.

Additionally, we argue that the larger diversity among metal-dependent FDHs allow further sub-classification. For this purpose we recently published a novel classification scheme for metal-dependent FDHs based on subunit composition, co-factor content, and gene organization [8]. In this scheme metal-dependent FDHs are divided into six 'types'. Interestingly, the two postulated oxygen tolerant metal-dependent FDHs – RcFDH and CnFDH – both fall solidly within the subdivision 'type 5'. Type 5 FDHs are characterized by CBADS gene organisation and the use of a flavin mononucleotide (FMN) co-factor.

We expressed RcFDH and CnFDH heterologously along with a third type 5 FDH originating from *Rhodobacter sphearoides* (RsFDH). RsFDH has not previously been characterized and was included for comparison. Additionally, *R. sphaeroides* is closely related to *R. capsulatus* and is known to perform both anaerobic and aerobic metabolism. As such, it is likely that proteins from *R. sphaeroides* are somewhat oxygen tolerant.

RcFDH, CnFDH, and RsFDH are heterotrimers composed of an alpha (α), beta (β) and gamma (γ) subunit. (Figure 1). Additionally, two chaperones FdsD and FdsS are co-expressed along with the three subunits of the enzyme [9,10]. The enzymes are all known for containing ancient and versatile molybdenum co-factors [11]. In these cases, a bis-molypdopterin guanine dinucleotide (bis-MGD) co-factor that can be expressed in *E. coli* [12]. All three organisms of origin, although different, are known to thrive in microaerophilic ecological niches [13–15].

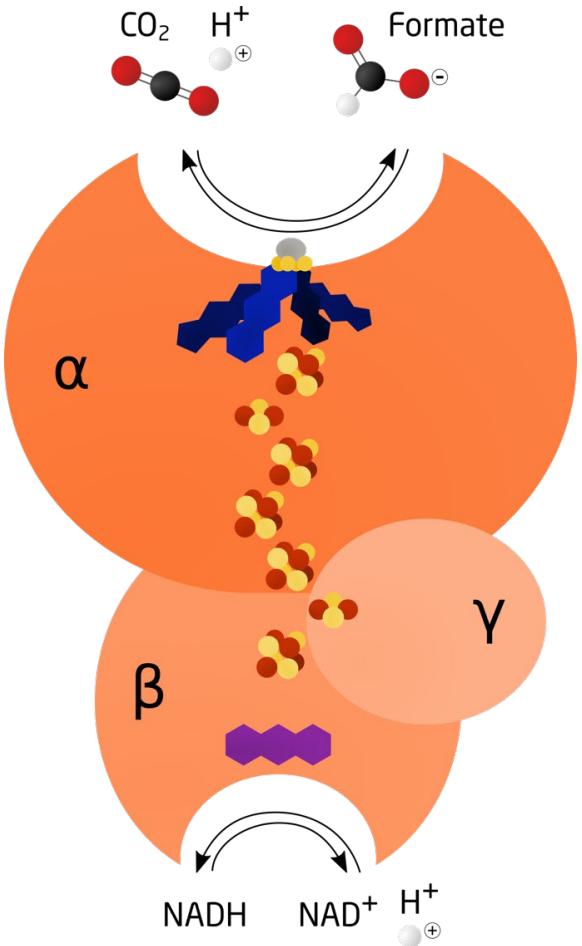

Figure 1: Model of generalised proposed structure of the cytosolic FDHs of Rhodobacter capsulatus *and* Cupriavidus necator. *Based on sequence homology, it is assumed that the cytosolic FDH of* Rhodobacter sphaeroides *can also be represented by the model. The active enzymes are composed of an FdsA ('α', ~105 kDa), FdsB ('β', 52-55 kDa), and FdsG ('γ', 15-19 kDa) subunits, composed interchangeably in either αβγ or $(αβγ)_2$ comformations. Each αβγ harbours nine distinct co-factors. The α-subunit contains four [Fe4-S4] clusters and one [Fe2-S2] cluster along with the distinctive Mo-bis-MGD co-factor present in the main CO_2 reducing/formate oxidizing active site. The β-subunit contains a single [Fe4-S4] cluster as well as the FMN of the secondary NADH oxidizing/NAD^+ reducing active site. Finally, the γ-subunit contains a single [Fe2-S2] cluster. While the Mo-bis-MGD and FMN co-factors facilitate the reactions at either active site, the FeS clusters transfer electrons between the two active sites [16].*

Despite a similar gene organization, we speculated that type 5 FDHs of different origin might differ in their kinetic properties with respect to the rate-rations of the forward and reverse reaction, their pH-temperature optima, and perhaps even their oxygen tolerance – all aspects of significance in relation to any future application for CCU. Examining and comparing these enzymes may divulge insights into defining characteristics related to application. Additionally, by benchmarking against the studies by Hartmann and Leimkühler and Yu et al., we tie together previous results as well as test their validity and reproducibility.

2. Results and discussion

2.1 Expression and purification

RcFDH, RsFDH, and CnFDH native gene operons were synthesized and cloned into an pTrc expression vector. A 6-mer His-tag was placed N-terminally of the gamma-subunit. Given the end-location of the gamma subunit in the operon, positioning the His-tag on the gamma subunit allowed previous studies to amplify the operon with PCR and clone into the expression vector, instead of full de novo synthesis. The three enzymes were expressed in *E. coli* DH5α strains as described previously [6]. Four interesting observations were made during expression and purification.

Firstly, in an attempt to optimize yield, we also synthesized a version of the gene operon with the His-tag positioned on the N-terminal of the alpha subunit instead of on N-terminal of the gamma subunit. The hypothesis was that a His-tag on the largest subunit would increase retention on the nickel column used for purification. Although the solubility of the proteins with His-tag on the alpha subunit, assessed qualitatively with western blot and SDS-PAGE, was comparable to protein expressed with His-tag on the gamma subunit, the specific activity was a factor 1000 lower (data not shown).

Secondly, in a book chapter of Methods in Enzymology from 2018, Niks and Hille state that slowing the rate of growth for the expression strain, improves incorporation of the molybdenum center [17]. It is known from previous studies that heterologously expressed metal-dependent FDHs do not have full co-factor saturation [5,6]. As a result, in an attempt to optimize co-factor saturation, we expressed RcFDH at different temperatures (18 or 30 °C) and with minimum or low shaking (30 or 130 rpm). At 30 °C and 130 rpm we experienced not only the highest yield but also the highest specific activity (data not shown). As such, no clear benefit was observed from producing type 5 metal-dependent FDHs at lower temperature than 30 °C or lower shaking speed than 130 rpm.

Thirdly, we clearly observed a near complete precipitation of the protein when frozen in the presence of imidazole.

Finally, it has previously been observed that RcFDH appears as both a monomeric heterotrimer (αβγ) as well as a dimeric heterotrimer ($(\alpha\beta\gamma)_2$) [6]. For this study, during SEC purification, RcFDH, RsFDH, and CnFDH eluted as masses corresponding to the dimeric heterotrimer, monomeric heterotrimer as well as the βγ incomplete composition. Additionally, the specific activity of the αβγ and $(\alpha\beta\gamma)_2$ conformations were near identical, leading us to believe that enzyme may exist in an equilibrium between the monomeric and dimeric state.

2.2 Optimum conditions

To compare the enzymes in a meaningful manner, we designed an experiment using response surface methodology to gauge the global pH and temperature activity optimum. The purified enzymes were studied using a standard kinetic assay following either absorbance or fluorescence of NADH.

Based on previous studies with RcFDH and CnFDH we set the ranges for pH between pH 5 to pH 9 and temperature from 20 °C to 50 °C. A central composite design was used. At least 13 datapoints were measured for each experiment. We were then able to fit a quadratic polynomial surface model to the obtained sets of measurements without significant lack of fit and a R-squared value of minimum 0.9. Plotting the predicted fit (Figure 2, next page), we were able to obtain the predicted global pH vs. temperature optimum (Table 1).

Table 1: Global optimum combination of pH and temperature for maximum activity of RcFDH, RsFDH and CnFDH. Optimum given for both forward and reverse reaction.

	RcFDH		**RsFDH**		**CnFDH**	
	Forward	**Reverse**	**Forward**	**Reverse**	**Forward**	**Reverse**
pH (95% CI)	**8.7** (7.8-9.6)	**8.4** (7.8-9.0)	**8.2** (7.2-9.0)	**7.4** (7.0-7.8)	**7.5** (7.1-7.9)	**7.3** (6.6-8.0)
Temperature (°C) (95% CI)	**37** (33-41)	**41** (38-44)	**34** (30-38)	**50** (47-52)	**40** (38-42)	**46** (42-50)

Interestingly, the global optimum is consistently at a higher temperature and lower pH for the reverse reaction relative to the forward reaction.

Although the reverse reaction is at optimum at a lower pH then for the forward reaction, the difference is not nearly as significant as expected. In contrast to our original hypothesis, the three enzymes turned out to have relatively similar reaction optima, potentially related to the similar ecological niches that the three organisms of origin inhabit.

It has previously been shown by Yu et al. that CnFDH solely uses aqueous CO_2 ($CO_{2(aq)}$) as its substrate [4]. For this study, we also observed a significant reduction in activity when attempting to use bicarbonate as substrate under anaerobic conditions (data not shown). It is likely, that other studies using bicarbonate as CO_2-substrate for other metal-dependent FDHs, are measuring either a diaphorase unspecific activity at aerobic conditions or activity with $CO_{2(aq)}$ derived from dissociation of bicarbonate. In this regard, it is difficult to reliably report substrate concentrations.

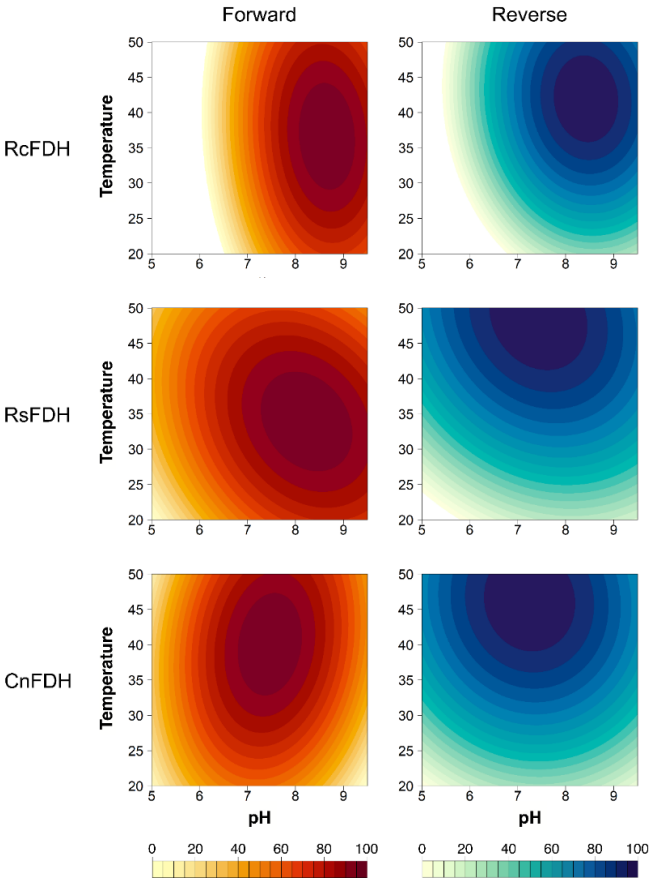

Figure 2: Relative predicted rate with pH 5 to pH 9.5 and 20 °C to 50 °C. Rate given as relative to highest rate with 100 being the highest predicted rate.

Soluble CO_2 exists in a pH-dependent equilibrium between carbonic acid, bicarbonate, and carbonate. Acidic conditions favor carbonic acid, physiological pH favors bicarbonate, and basic conditions favor carbonate [18]. Knowing that CnFDH is only active on $CO_{2(aq)}$, which again is in equilibrium with carbonic acid, it can be hypothesized that low pH should favor increased CO_2 reduction activity. For all three type 5 FDHs studied here, the optimum pH is indeed lower for the reverse reaction relative to the forward reaction. However, the observed differences are nearly negligible and surprisingly, the optimum pH values are even slightly basic for all three variants. This is in contrast to our expectation of a significantly lower optimum and acidic pH for the reverse reaction.

The explanation is likely to be found in the manner with which we provided $CO_{2(aq)}$. Instead of bicarbonate, reaction buffer was saturated with CO_2 in a gaseous form ($CO_{2(g)}$). According to Henry's law, $CO_{2(aq)}$ at ambient conditions reach a concentration of approximately 29.5 mM [19]. Dissolved $CO_{2(aq)}$ does not readily react with water to create carbonic acid. Instead the majority of $CO_{2(aq)}$ remains as $CO_{2(aq)}$ which could help explain why we did not observe acidic pH optimum for reverse reaction.

Based on the results of this analysis, we conclude that the CnFDH variant has lower pH optima than the other tested enzymes, but in general, there is no significant difference in the pH between the forward and reverse reactions. Additionally, we can conclude that there is no significant difference between the optimum for the forward and reverse reaction.

2.3 Co-factor saturation

RcFDH and CnFDH have both previously been predicted to contain a total of five [Fe4-S4] and two [Fe2-S2] complexes [4,6]. Assuming a similar co-factor composition for RsFDH, each mole of enzyme should contain 24 moles of iron and 1 mole of molybdenum. Molybdenum and iron concentrations were quantified with inductive coupled plasma-mass spectrometry (ICP-MS). Based on the protein concentration a co-factor saturation could be estimated (Table 2).

Table 2: Estimated metal content in percentage of maximum possible metal concentration for the respective enzymes. Uncertainty given as a single standard deviation.

	RcFDH		RsFDH		CnFDH	
	$(\alpha\beta\gamma)_2$	$\alpha\beta\gamma$	$(\alpha\beta\gamma)_2$	$\alpha\beta\gamma$	$(\alpha\beta\gamma)_2$	$\alpha\beta\gamma$
Mo % saturation	**60** ± 1.2	**70** ± 0.5	**43** ± 4.3	**44** ± 1.2	**63** ± 2.4	**87** ± 1.1
Fe % saturation	**65** ± 0.5	**44** ± 0.7	**58** ± 0.9	**50** ± 0.5	**46** ± 1.8	**50** ± 0.5

It has previously been shown that heterologously expressed type 5 FDHs do not have full co-factor saturation: Hartmann and Leimkühler [6] reported 39% molybdenum and 48% iron saturation for RcFDH in $(\alpha\beta\gamma)_2$ conformation. Compared to those numbers, our FDH populations have slightly higher saturation. Additionally, it can be observed that the iron saturations in the three enzymes' $\alpha\beta\gamma$ fractions are very similar and this fraction was used for the kinetic studies enabling a reasonable direct comparison of the three enzymes.

2.4 Kinetic characterization

Following estimation of optimum pH and temperature for activity, a comparison of maximum activity was possible. Furthermore, as mentioned in the introduction, to compare with previous work two additional conditions were included. For the forward reaction Hartmann et. al performed standard assays at 30 °C at pH 9.0 in a Tris/HCl buffer. Similarly, Yu et al. also performed a standard assay at 30 °C but at pH 7.7 and in a potassium phosphate buffer. Turnover number, $K_{M,formate}$ and $K_{M,\ NAD}$ presented in Table 3 were calculated based on initial rate (Figure 3).

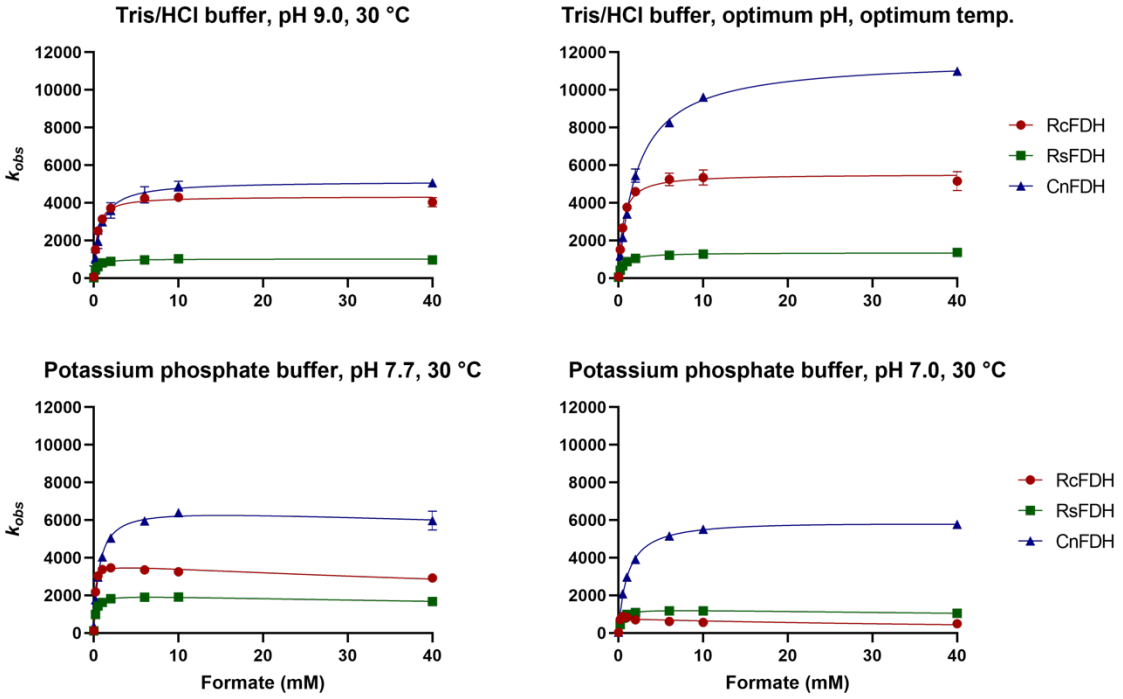

Figure 3: Comparison of steady state kinetics of formate oxidation between the heterologously expressed type 5 FDHs. All reactions were performed at 30 °C, at aerobic conditions, and 2 mM NAD^+.

Table 3: Observed forward reaction kinetic parameters. For each value a confidence interval (CI) at 95% confidence is given. ND: Not determined. '-': Not applicable.

		Forward reaction (Formate oxidation)			
		k_{cat} (min^{-1}) (95% CI)	**$K_{M,formate}$ (mM)** (95% CI)	**K_{M,NAD^+} (mM)** (95% CI)	**$K_{i,formate}$ (mM)** (95% CI)
RcFDH	Tris/HCl buffer, Optimum conditions (36.5 °C, pH 8.7)	5520 (5300 – 5740)	0.49 (0.41 – 0.59)	0.57 (0.47 – 0.68)	-
	Tris/HCl buffer, 30 °C, pH 9.0	4330 (4200 – 4470)	0.36 (0.31 – 0.42)	0.24 (0.29-0.29)	-
	KPO_4 buffer, 30 °C, pH 7.7	3660 (3480 – 3840)	0.12 (0.09 – 0.19)	0.41 (0.31 – 0.54)	147 (96 – 267)
	KPO_4 buffer, 30 °C, pH 7.0	760 (710-860)	0.02 (0.00-0.04)	ND	56 (29-107)
RsFDH	Tris/HCl buffer, Optimum conditions (33.8 °C, pH 8.2)	1350 (1300 -1390)	0.52 (0.44 – 0.62)	0.40 (0.28 – 0.57)	-
	Tris/HCl buffer, 30 °C, pH 9.0	1010 (940 – 1090)	0.29 (0.19 – 0.42)	0.18 (0.14 – 0.21)	-
	KPO_4 buffer, 30 °C, pH 7.7	2030 (1950 – 2110)	0.21 (0.18 – 0.25)	0.27 (0.22 – 0.35)	201 (137 – 345)
	KPO_4 buffer, 30 °C, pH 7.0	1290 (1240-1340)	0.33 (0.29-0.39)	ND	180 (129-278)
CnFDH	Tris/HCl buffer, Optimum conditions (40.1 °C, pH 7.5)	11640 (11380– 11890)	2.30 (2.12 – 2.47)	0.19 (0.15 – 0.23)	-
	Tris/HCl buffer, 30 °C, pH 9.0	5140 (4880 – 5420)	0.80 (0.63 – 1.02)	0.16 (0.13 – 0.19)	-
	KPO_4 buffer, 30 °C, pH 7.7	6770 (6340 – 7250)	0.63 (0.51 – 0.78)	0.13 (0.11 – 0.15)	-
	KPO_4 buffer, 30 °C, pH 7.0	6110 (5890-6370)	1.07 (0.95-1.20)	ND	-

Benchmarking the activity measured for the forward reaction in this study, the observed turnover number for RcFDH of 4330 min^{-1} at 30 °C and pH 9.0 is directly comparable to the observed turnover of 2189 min^{-1} measured by Hartmann and Leimkühler, 2013. In this study, they reported a saturation of 39% Mo and 48% Fe. Additionall,y this work quantified the flavin saturation to approximately 68% [6]. For the present study, we observe a higher Mo saturation and comparable Fe saturation, leading us to hypothesize that the higher level of Mo may be the reason for the near doubling in the turnover number compared to the previous experiment. Additionally, we hypothesize that our fast enzyme population is more loosly associated with the substrate due to an observed Michaelis-Menten constants of the reaction substrates ($K_{M,formate}$ of 0.36 and $K_{M,NAD}$+ of 0.24), compared to the previous work ($K_{M,formate}$ of 0.28 and $K_{M,NAD}$+ of 0.17).

Similarly, we can benchmark the results for CnFDH. Yu et al., 2019 expressed and characterized CnFDH. Here they reported an observed turnover number of 5940 min^{-1} with a co-factor saturation of approximately 50%. The co-factor saturation was estimated by comparing observed turnover number with turnover number

observed for natively expressed CnFDH and assuming 100% co-factor saturation in the natively expressed enzyme population [5]. In the present study, the measured turnover number under identical conditions was 6770 min^{-1}. With a 50% saturation of Fe observed for CnFDH in this study, the observed activity nicely corresponds to the activity observed in the previous study by Yu. et al., 2019.

For CO_2 reduction (the reverse reaction) the steady-state kinetics measurements were performed under anaerobic conditions and using gas-saturated buffers. From the initial rates presented in Figure 4, it is evident that CnFDH, like for the forward reaction, has a significantly higher turnover than the two other tested FDHs. The calculations of $K_{M,CO2}$ (Table 4), however reveal that the saturation was incomplete.

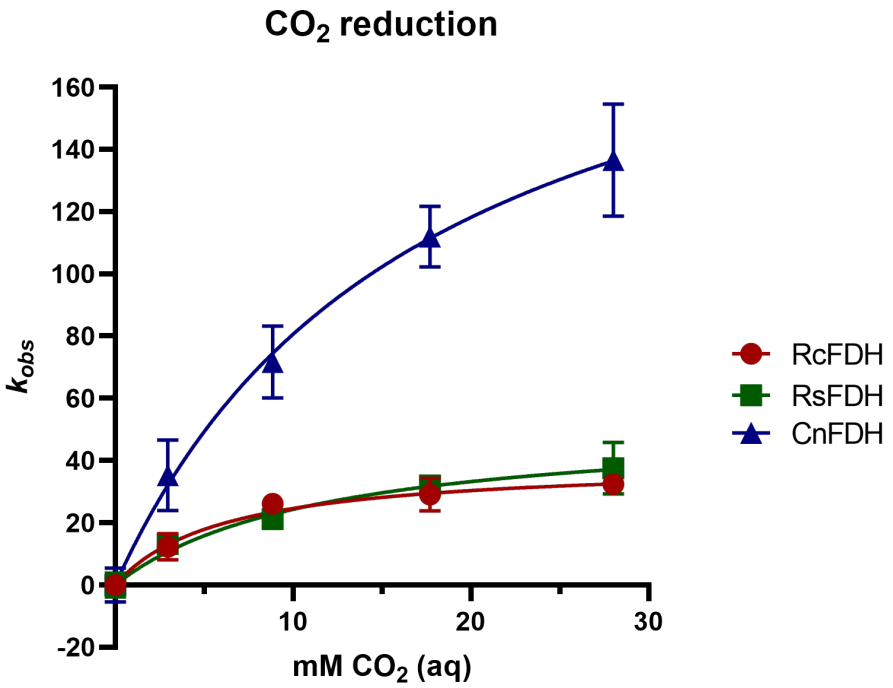

Figure 4: Comparison of steady state kinetics of CO_2 reduction for heterologously expressed type 5 FDHs. Reactions were completed at optimum pH and optimum temperature determined in this study. All reactions were completed in 100 mM potassium phosphate, 100 mM Tris/HCl buffer with 0.2 mM NADH, at ambient pressure and in anaerobic conditions. The range of CO_2 substrate concentrations were achieved by mixing buffer saturated with either nitrogen or CO_2.

Table 4: Observed reverse reaction kinetic parameters. For each value a confidence interval (CI) at 95% confidence is given when possible.

		Reverse reaction (CO_2 reduction)	
		k_{cat} (min^{-1}) (95% CI)	**$K_{M,CO2}$ (mM)** (95% CI)
RcFDH	Optimum temp., optimum pH	39.5 (33.0-50.0)	6.1 (3.1-12.4)
	30 °C, pH 7.0	36.1	-
RsFDH	Optimum temp., optimum pH	52.5 (39.4-80.4)	11.6 (5.3-27.4)
	30 °C, pH 7.0	43.6	-
CnFDH	Optimum temp., optimum pH	221 (172-320)	17.5 (9.9-34.2)
	30 °C, pH 7.0	127	-

Compared to the previous work by Hartmann and Leimkühler, 2013 in RcFDH, where a turnover number of 89 min^{-1} was measured [6], this study achieves a much lower activity. Similarly, comparing the results for CnFDH to those of Yu et al., 2017 [4] where a turnover number of 660 min^{-1} was obtained, it is evident that the experiments performed here are not optimal. This is corroborated by comparing the $K_{M,CO2}$ of 17.5 mM measured in this study to the $K_{M,CO2}$ of 2.7 mM from Yu et al., 2017 [4].

Based on these experiments it can be concluded that CnFDH is by far the most efficient of the three tested enzymes both in terms of formate oxidation and CO_2 reduction. However, we also conclude that our applied methodology did not allow for proper saturation with substrate during the reverse reaction and consequently is likely not representative of the catalytic rates achievable with this enzyme.

2.5 Stability and oxygen tolerance

Some metal-dependent FDHs have been shown to be oxygen sensitive [20-22], and due to the complexity and price of running anaerobic experiments, it is much more realistic that enzymatic CO_2 conversion on a large scale required for proper CCU would be run under aerobic conditions. As a result, it was deemed highly important to test the oxygen tolerance of the three type 5 FDHs in this study. Previous studies have claimed both RcFDH and CnFDH to be oxygen tolerant in the presence of KNO_3 [6,7,23]. Due to the high degree of similarity between RsFDH and the other previously characterized enzymes, it is natural to hypothesize that oxygen tolerance should extend to this variant as well.

We tested the oxygen tolerance of the three variants in both αβγ and $(αβγ)_2$ conformations using either 0.5 or 10 mM KNO_3, with measurements performed for the activity of the forward reaction over a 10-minute period (Figure 5). Here, it is observed that the activity gradually declines over the first 6-8 minutes for all tested variants except the RsFDH $(αβγ)_2$ conformation with 10 mM KNO_3. However, fitting a one phase decay model revealed that using 10 mM KNO_3 results in greater stabilization with only 10-14% activity reduction compared to 20-31% reduction at 0.5 mM KNO_3. Interestingly, the absolute initial activity was the same for all tested conditions, which is contradictory to previously published data claiming that nitrate ions act as a competitive inhibitor of FDHs [23].

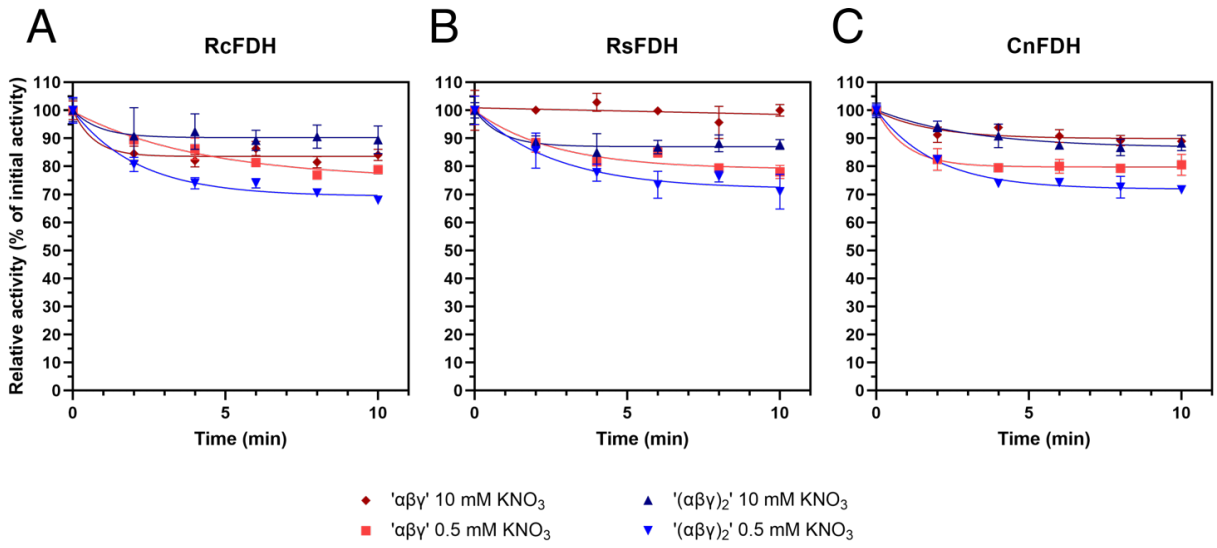

Figure 5: Oxygen tolerance of enzymes, A) RcFDH, B) RsFDH, and C) CnFDH. Formate oxidation activity were measured on enzyme incubated in 25 °C Tris/HCl buffer, pH 8 with either 0.5 mM or 10 mM KNO_3. Importantly the buffer was prepared and stored at aerobic conditions prior to introduction of enzyme. FDH in either αβγ (circle and square) or $(αβγ)_2$ (triangles) were studied. Experiments were performed in duplicates.

Interestingly, we also observe that the three enzyme variants more or less show the same pattern of activity reduction, all with very limited differences between the αβγ and $(αβγ)_2$ conformations. If anything, the αβγ conformation is slightly more stable, potentially indicating some sort of destabilization or exposure of the enzymes' oxygen sensitive domain by dimerization. It could also be due to a larger percentage of correctly assembled protein. Furthermore, temperature also had an effect, which was observed as no loss of activity when the enzymes where stored on ice.

Overall, the oxygen sensitivity experiments show that only RsFDH αβγ was oxygen tolerant. However, while the rest of the tested forms show a significant reduction in activity, the activity also plateaus after the initial phase of exposure to oxygen, which was supported by measurements after 20 and 40 minutes (data not shown). The underlying mechanism could be either a heterogenous enzyme population, in which only a fraction of enzymes is oxygen sensitive, or the formation of an equilibrium between the FDH-oxygen affinity and FDH-nitrate affinity. Interestingly, when stored on ice, no loss of activity was observed over time (8 hours).

For RcFDH and CnFDH, we see a larger difference between activity at high and low KNO_3 for αβγ than we do for $(\alpha\beta\gamma)_2$. This could be due to a higher percentage of incomplete or vulnerable protein. It could also be because the oxygen labile sites are somehow protected when the enzyme is in a dimer confirmation.

3. Conclusions

Conversion of CO_2 directly to a liquid chemical, formic acid, is possible through the utilization of the FDH enzyme class. This study heterologously expressed three variants, RcFDH, RsFDH, and CnFDH, in *E. coli* DH5α strains and characterized them in terms of their reaction kinetics and oxygen tolerance.

The expression of these enzymes led to four main recommendations: First, the His-tag to be used in purification should be placed on the gamma subunit rather than the alpha subunit of the protein to retain activity. Secondly, the expression yields similar co-factor saturation when carried out at 30 °C and shaking at 130 rpm relative to 18 °C and 30 rpm. This allows for faster growth. Thirdly, presence of imidazole results in protein precipitation upon freezing and should consequently be avoided. Finally, the three variants all showed both monomeric heterotrimer (αβγ) and dimeric heterotrimer ($(\alpha\beta\gamma)_2$) conformations with near identical specific activities.

Regarding pH and temperature optima, the three enzyme variants all have higher optimum temperatures for the oxidation of formate (forward reaction) than the reduction of CO_2 (reverse reaction). Surprisingly, no significant difference was found for pH optima between the forward and reverse reactions, but CnFDH displayed a preference for lower pH values.

When characterizing the co-factor content of these heterologously expressed FDHs, we observed slightly higher saturation for the molybdenum and iron complexes than reported previously, but we were not close to full saturation. The $(\alpha\beta\gamma)_2$ conformation generally had higher saturation, but the iron levels for the three variants in the αβγ were highly comparable.

Overall, the kinetics experiments revealed that CnFDH had the largest turnover of the three variants, both for the forward and reverse reactions. However, comparisons of the results of this study to those in the literature revealed that the experimental conditions for the reverse reactions may not have been optimal.

Finally, the oxygen sensitivity in the presence of KNO_3 was similar between the tested variants, with almost all displaying a reduction upon oxygen exposure. Surprisingly, our tested variant RsFDH αβγ was fully oxygen tolerant at the highest tested KNO_3 concentration (10 mM) marking this as a potential candidate for future optimizations.

If able to combine the oxygen stability of RsFDH and the high conversion activity of CnFDH with an optimized setup that allows for full CO_2 saturation, one would have a strong candidate for large-scale enzymatic of CO_2. Hopefully, future work will derive such a variant.

4. Materials and methods

4.1 Gene constructs and cloning

Expression vectors were designed *in situ* and synthesized for this study. A total of six plasmids were ordered, two for each FDH variant. For each FDH variant, a construct with a His-tag on the N-terminal of the FdsG subunit as well as a construct with a His-tag on the N-terminal of the FdsA subunit were designed. All gene constructs were based on publicly available gene sequences sourced from the NCBI refseq database [24] (Table 5 below), and a common expression vector identical to the vector used by Hartmann and Leimkühler, 2013 [6]. Individual FDH operons were extracted as native sequences from full genomes and inserted into a modified pTrc expression vector. The gene constructs were synthesized and cloned into the expression vector by Genscript Biotech.

Table 5: Operon information for the enzyme variants RcFDH, RsFDH, and CnFDH retrieved from the RefSeq database.

Enzyme variant	Corresponding expression vectors	Genome ID	Genome name	Location of operon in genome
RcFDH	pTrc_RcFDH_gamma and pTrc_RcFDH_alpha	NC_014034.1	*Rhodobacter capsulatus SB 1003,* complete genome	3223340- 3229140 (complementary strand)
RsFDH	pTrc_RsFDH and pTrc_RsFDH_alpha	CP000661.1	*Rhodobacter sphaeroides ATCC 17025,* complete genome	2907382-2913283 (complementary strand)
CnFDH	pTrc_CnFDH and pTrc_CnFDH_alpha	NC_015726.1	*Cupriavidus necator N-1 chromosome 1,* complete sequence	657183-663287

The plasmids were transformed into competent *E. coli* DH5α and plated on LB agar plates with 100 µg/ml ampicillin. Individual transformant colonies were picked and cultured in LB media with 100 µg/ml ampicillin overnight at 37 °C and 250 rpm. The outgrown culture was saved in 0.8 ml aliquots with 25% glycerol at -80 °C. Importantly, we observed a decline in production yield when using scrapes from a singly glycerol repeatedly. High consistent yields were achieved by only thawing and using an aliquot once.

4.2 Expression and purification

For expression a single media was used for both preculture and actual expression: LB media with 150 µg/ml ampicillin, 1 mM sodium molybdate and 20 µM isopropyl β-D-1-thiogalactopyranoside (IPTG). A 5 ml preculture were inoculated with 50 µl of the desired single-use glycerol stock, and then incubated at 37 °C and 130 rpm overnight. For expression, 2 l baffled Erlenmeyer shake flasks, each containing 500 ml expression media, were inoculated with 1 ml preculture each and incubated for 24 hours at 30 °C and 130 rpm. Cells were harvested by centrifuging at 5300 g for 15 min in a precooled (4 °C) centrifuge. From this point onwards, samples were kept at maximum 4 degrees or colder. Additionally, procedures were completed as quickly and efficiently as possible. For each gram of cell pellet, 10 ml of 40 mM potassium phosphate buffer, pH 7.5, with 10 mM KNO_3 and EDTA free protease inhibitor (cOmplete™ Mini from Roche), were used to resuspend the pellet. The resuspended pellet was centrifuged at 8000 g for 5 minutes. Discarding the supernatant, the pellet was stored at -20 °C.

For purification, the cell pellets were first gently thawed and resuspended. For every gram of cell pellet 10 ml of precooled 40 mM potassium phosphate buffer, pH 7.5, with 10 mM KNO_3 were used to resuspend. The cell suspension was lysed once in a STANSTED Pressure Cell Homogenizer SPCH-10 at 1.35 kbar and subsequently centrifuged at 21.000 g for 1 hr in a precooled centrifuge. The supernatant was mixed with 0.2 ml Ni Sepharose™ HP resin per 1 g of lysed cell pellet and allowed to gently mix for 45 minutes. The resin/lysate mixture were then added to an empty gravity 25 ml flow column from BIO-RAD and allowed to settle. The formed nickel resin column should appear dark grey/brown due to high saturation of the [Fe_4-S_4]-containing

protein. Typically, a 1 ml column volume (CV) were used, corresponding to protein from 5 g of lysed cell pellet per column. The column was washed with 25 CV of first 75 mM potassium phosphate buffer, pH 7.5, with 10 mM KNO_3 and 10 mM imidazole followed by 25 CV 75 mM potassium phosphate buffer, pH 7.5, with 10 mM KNO_3 and 20 mM imidazole. The enzymes were then eluted with 5 CV 75 mM potassium phosphate buffer, pH 7.5, with 10 mM KNO_3 and 250 mM imidazole. The eluted enzyme solution should have a dark brown color, similar to a thin cup of coffee. Immediately following elution, the protein solution was buffer exchanged to 75 mM potassium phosphate buffer, pH 7.5, with 10 mM KNO_3 using PD10 buffer exchange columns (Sephadex™ G-25 M), flash frozen in aliquots in liquid nitrogen with argon gas in the headspace, and stored at -80 °C.

The enzyme solutions of all three variants are known or presumed to be comprised a heterogeneous mix of the active heterotrimer-dimer, the heterotrimer-monomer and the incomplete βγ constellation. For each variant a 15-20 mg/ml 2 ml solution were prepared and loaded onto a HiLoad™ 16/60 Superdex™ 200 pg column equilibrated with 75 mM potassium phosphate buffer, pH 7.5, with 10 mM KNO_3. Fractions were collected conservatively to represent each of the resulting peaks (Peak 1: corresponding to FDH in $(\alpha\beta\gamma)_2$ confirmation, peak 2: corresponding to FDH in αβγ confirmation), flash frozen with argon gas headspace and stored at -80 °C. Sample purity were confirmed with SDS-PAGE. Routine activity assays were performed as by measuring change in absorbance over time at 340 nm (Extinction coefficient for NADH is 6220 M^{-1} cm^{-1} at 340 nm). Standard conditions were pH 9 Tris/Hcl buffer with 2 mM NAD^+ and 6 mM formate. Protein concentration were determined at 280 nm using an extinction coefficient based on predictions with the Quest Calculate™ Protein Concentration Calculator (see Table 6 below).

Table 6: Predicted weights and extinction coefficients of the three FDHs based on protein sequence and co-factor content. The predicted weight is assuming 100% co-factor saturation and includes the His-tag and gamma-tail of the plasmid construct.

FDH variant	Predicted weight (kDa)	Extinction coefficient at 280 nm (M^{-1} cm^{-1})
RcFDH	179,310	167,960
RsFDH	182,380	148,210
CnFDH	185,010	146,260

4.3 Enzymatic reaction assay

For kinetic characterization of the forward reaction (formate oxidation), assays were performed under aerobic conditions. Conversely, kinetic characterization of the reverse reaction (CO_2 reduction) were performed under anaerobic conditions.

For estimating a global pH and temperature combinatory optimum, a response surface modelling (RSM) approach was applied. In JMP statistical software, a central composite design was created with pH 5 to pH 9 as the first range of parameters and 20 °C to 50 °C as the second range of parameters. Default settings were accepted, and measurement were performed in randomized order. For each condition, pH was adjusted at the relevant temperature. An overlapping assay buffer of 100 mM acetate, 100 mM potassium phosphate, 100 mM Tris base were used to cover the full range.

For determining the forward reaction optimum, the activity rate at individual conditions was followed by measuring the absorbance of NADH at 340 nm. The reaction was started by addition of enzyme to a pre-tempered solution of assay buffer with 2 mM NAD and 6 mM sodium formate with measurements once per second for 100 seconds. Typically, the first 10 seconds were used to calculate the initial rate.
For determining the reverse reaction optimum, fluorescence of NADH, exited at 340 nm and with emission at 445 nm, was used to measure activity rate. Fluorescence of NADH is temperature dependent [25] causing lower sensitivity at higher temperatures. Additionally, NADH fluorescence correlates logarithmically with concentration of NADH [26]. To address these issues, standards were made at the relevant temperatures. Finally, NADH is known to oxidize to NAD^+ over time, requiring a need to use fresh stock solutions of NADH

and verify concentration with absorbance before use. CnFDH and RcFDH are known to catalyze a diaphorase side reaction with NADH in the presence of oxygen [4,6], requiring complete removal of oxygen at reaction conditions to avoid false positive activity. Assay buffers at relevant pHs with 0.2 mM NADH were degassed and saturated with either nitrogen or CO_2 and stored in sealed vials. Saturation with CO_2 causes a drop in pH, requiring adjustment of pH after saturation. Again, adjustment of pH was also done at relevant temperature. A 1.4 ml quartz cuvette with four windows and a screwcap with replaceable septum seal, was used to control reaction conditions. The sealed quartz cuvette was purged with inert nitrogen gas before assay buffer was added with gastight Hamilton syringes through septum. Nitrogen saturated buffer was used as a negative control for unspecific activity and CO_2 saturated buffer to assess activity. Reaction was started with addition of enzyme through septum with gastight Hamilton syringe to pre-tempered reaction solution. Fluorescence was followed for 100 seconds. Typically, the first 10 seconds were used to calculate initial rate. Measurements were done in duplicates.

Turnover number and substrate affinity were determined at three conditions for the forward reaction: potassium phosphate buffer, pH 7.7 at 30 °C, Tris/HCl buffer, pH 9.0 at 30 °C, and Tris/HCl buffer, optimum pH at optimum temperature. For each condition, steady state kinetics were determined at sodium formate concentrations of 0-40 mM paired with 2 mM NAD, and at NAD^+ concentrations of 0-5 mM paired with 6 mM sodium formate. The assay was performed in triplicates following the methodology described above for the RSM study.

For the reverse reaction, turnover number and substrate affinity were only determined only at optimum conditions, supplemented with a single measurement at maximum possible substrate concentration at the 'standard' condition: potassium phosphate buffer, pH 7.0 at 30 °C. By mixing nitrogen and CO_2 saturated buffers, a substrate range of 0% to 95% CO_2 saturation was achieved.. The assay was performed in triplicates following the methodology described above for the RSM study. A 100 mM potassium phosphate, 100 mM Tris/HCl buffer were used for assays at optimum conditions.

4.4 Co-factor quantification

Elemental concentrations of Fe and Mo were measured on Agilent 7700x ICP-MS Inductive Coupled Plasma-Mass Spectrometer (ICP-MS). Sample with protein concentration between 0.5 and 1.5 mg/ml were used. Before the measurement, the samples were diluted 100x in 2% Suprapur HNO_3. The elements were analyzed in He mode. The sample uptake speed (nebulizer pump speed) was set to 0.1 rpm and the stabilization time to 40 sec. Integration time was set to 0.3 sec for He mode (He flow 5 mL/min). Processing of the data was carried out in the MassHunter 4.6 Workstation Software (v. C.01.06).

4.5 Oxygen tolerance study

FDH in either $(\alpha\beta\gamma)_2$ or $\alpha\beta\gamma$ confirmation in 75 mM potassium phosphate buffer, pH 7.5, with 10 mM KNO_3 at 0.5-1.5 mg/ml concentrations, were diluted 20-fold in 100 mM Tris/HCl buffer, pH 8.0, with or without KNO_3. Importantly, the buffer was exposed to ambient air conditions prior to addition of enzyme. Formate oxidation activity was measured the resulting FDH solutions (now at either 0.5 mM or 10 mM KNO_3), as described previously, immediately and then every 2 minutes for 10 minutes.

Acknowledgements

-

References

"Quest Calculate™ Protein Concentration Calculator." AAT Bioquest, Inc, 20 Aug. 2020, https://www.aatbio.com/tools/calculate-protein-concentration.

[1] F.D. Meylan, V. Moreau, S. Erkman, CO2 utilization in the perspective of industrial ecology, an overview, J. CO2 Util. 12 (2015) 101–108. https://doi.org/10.1016/j.jcou.2015.05.003.

[2] C. Hepburn, E. Adlen, J. Beddington, E.A. Carter, S. Fuss, N. Mac Dowell, J.C. Minx, P. Smith, C.K. Williams, The technological and economic prospects for CO2 utilization and removal, Nature. 575 (2019) 87–97. https://doi.org/10.1038/s41586-019-1681-6.

[3] T. Reda, C.M. Plugge, N.J. Abram, J. Hirst, Reversible interconversion of carbon dioxide and formate by an electroactive enzyme, Proc. Natl. Acad. Sci. 105 (2008) 10654–10658. https://doi.org/10.1073/pnas.0801290105.

[4] X. Yu, D. Niks, A. Mulchandani, R. Hille, Efficient reduction of CO2by the molybdenum-containing formate dehydrogenase from Cupriavidus necator (Ralstonia eutropha), J. Biol. Chem. 292 (2017) 16872–16879. https://doi.org/10.1074/jbc.M117.785576.

[5] X. Yu, D. Niks, X. Ge, H. Liu, R. Hille, A. Mulchandani, Synthesis of Formate from CO2 Gas Catalyzed by an O2-Tolerant NAD-Dependent Formate Dehydrogenase and Glucose Dehydrogenase, Biochemistry. 58 (2019) 1861–1868. https://doi.org/10.1021/acs.biochem.8b01301.

[6] T. Hartmann, S. Leimkühler, The oxygen-tolerant and NAD+-dependent formate dehydrogenase from Rhodobacter capsulatus is able to catalyze the reduction of CO2 to formate, FEBS J. 280 (2013) 6083–6096. https://doi.org/10.1111/febs.12528.

[7] D. Niks, J. Duvvuru, M. Escalona, R. Hille, Spectroscopic and kinetic properties of the molybdenum-containing, NAD+-dependent formate dehydrogenase from Ralstonia eutropha, J. Biol. Chem. 291 (2016) 1162–1174. https://doi.org/10.1074/jbc.M115.688457.

[8] C.F. Nielsen, L. Lange, A.S. Meyer, Classification and enzyme kinetics of formate dehydrogenases for biomanufacturing via CO2 utilization, Biotechnol. Adv. 37 (2019) 107408. https://doi.org/10.1016/j.biotechadv.2019.06.007.

[9] T. Hartmann, N. Schwanhold, S. Leimkühler, Assembly and catalysis of molybdenum or tungsten-containing formate dehydrogenases from bacteria, Biochim. Biophys. Acta - Proteins Proteomics. 1854 (2015) 1090–1100. https://doi.org/10.1016/j.bbapap.2014.12.006.

[10] N. Böhmer, T. Hartmann, S. Leimkühler, The chaperone FdsC for Rhodobacter capsulatus formate dehydrogenase binds the bis-molybdopterin guanine dinucleotide cofactor, FEBS Lett. 588 (2014) 531–537. https://doi.org/10.1016/j.febslet.2013.12.033.

[11] D. Niks, R. Hille, Molybdenum- and tungsten-containing formate dehydrogenases and formylmethanofuran dehydrogenases: Structure, mechanism, and cofactor insertion, Protein Sci. 28 (2019) 111–122. https://doi.org/10.1002/pro.3498.

[12] S. Leimkühler, The biosynthesis of the molybdenum cofactors in Escherichia coli, Environ. Microbiol. 22 (2020) 2007–2026. https://doi.org/10.1111/1462-2920.15003.

[13] P.F. Weaver, J.D. Wall, H. Gest, Characterization of Rhodopseudomonas capsulata, Arch. Microbiol. 105 (1975) 207–216. https://doi.org/10.1007/BF00447139.

[14] A. Pohlmann, W.F. Fricke, F. Reinecke, B. Kusian, H. Liesegang, R. Cramm, T. Eitinger, C. Ewering, M. Pötter, E. Schwartz, A. Strittmatter, I. Voß, G. Gottschalk, A. Steinbüchel, B. Friedrich, B. Bowien, Genome sequence of the bioplastic-producing “Knallgas” bacterium Ralstonia eutropha H16, Nat. Biotechnol. 24 (2006) 1257–1262. https://doi.org/10.1038/nbt1244.

[15] C. Mackenzie, J.M. Eraso, M. Choudhary, H.R. Jung, X. Zeng, P. Bruscella, Á. Puskás, S. Kaplan, Postgenomic adventures with Rhodobacter sphaeroides, Annu. Rev. Microbiol. 61 (2007) 283–307. https://doi.org/10.1146/annurev.micro.61.080706.093402.

[16] M. Jormakka, S. Törnroth, B. Byrne, S. Iwata, Molecular Basis of Proton Motive Force Generation: Structure of Formate Dehydrogenase, Science (80-.). 295 (2002) 1863–1868. http://science.sciencemag.org/content/sci/295/5561/1863.full.pdf (accessed June 26, 2018).

[17] D. Niks, R. Hille, Reductive activation of CO2 by formate dehydrogenases, 1st ed., Elsevier Inc., 2018. https://doi.org/10.1016/bs.mie.2018.10.013.

[18] C.B. Andersen, Understanding carbonate equilibria by measuring alkalinity in experimental and natural systems, J. Geosci. Educ. 50 (2002) 389–403. https://doi.org/10.5408/1089-9995-50.4.389.

[19] P.L. Hayden, Carbonate Chemistry Applied to the Beverage Production of Still Water, (2003) 1–12. https://irp-cdn.multiscreensite.com/01ad9a08/files/uploaded/Carbonate Chemistry.pdf.

[20] K. Schuchmann, V. Muller, Direct and Reversible Hydrogenation of CO2 to Formate by a Bacterial Carbon Dioxide Reductase, Science (80-.). 342 (2013) 1382–1385. https://doi.org/10.1126/science.1244758.

[21] T. Reda, C.M. Plugge, N.J. Abram, J. Hirst, Reversible interconversion of carbon dioxide and formate by an electroactive enzyme, Proc. Natl. Acad. Sci. 105 (2008) 10654–10658. https://doi.org/10.1073/pnas.0801290105.

[22] A. Bassegoda, C. Madden, D.W. Wakerley, E. Reisner, J. Hirst, Reversible Interconversion of CO 2 and Formate by a Molybdenum- Containing Formate Dehydrogenase, J. Am. Chem. Soc. 136 (2014) 15473–15476.

[23] J. Friedebold, B. Bowien, Physiological and biochemical characterization of the soluble formate dehydrogenase, a molybdoenzyme from Alcaligenes eutrophus, J. Bacteriol. 175 (1993) 4719–4728. https://doi.org/10.1128/jb.175.15.4719-4728.1993.

[24] N.A. O'Leary, M.W. Wright, J.R. Brister, S. Ciufo, D. Haddad, R. McVeigh, B. Rajput, B. Robbertse, B. Smith-White, D. Ako-Adjei, A. Astashyn, A. Badretdin, Y. Bao, O. Blinkova, V. Brover, V. Chetvernin, J. Choi, E. Cox, O. Ermolaeva, C.M. Farrell, T. Goldfarb, T. Gupta, D. Haft, E. Hatcher, W. Hlavina, V.S. Joardar, V.K. Kodali, W. Li, D. Maglott, P. Masterson, K.M. McGarvey, M.R. Murphy, K. O'Neill, S. Pujar, S.H. Rangwala, D. Rausch, L.D. Riddick, C. Schoch, A. Shkeda, S.S. Storz, H. Sun, F. Thibaud-Nissen, I. Tolstoy, R.E. Tully, A.R. Vatsan, C. Wallin, D. Webb, W. Wu, M.J. Landrum, A. Kimchi, T. Tatusova, M. DiCuccio, P. Kitts, T.D. Murphy, K.D. Pruitt, Reference sequence (RefSeq) database at NCBI: current status, taxonomic expansion, and functional annotation, Nucleic Acids Res. 44 (2016) D733–D745. https://doi.org/10.1093/nar/gkv1189.

[25] B. Zelent, T. Troxler, J.M. Vanderkooi, Temperature Dependence for Fluorescence of β-NADH in Glycerol/Water Solution and in Trehalose/Sucrose Glass, J. Fluoresc. 17 (2006) 37–42. https://doi.org/10.1007/s10895-006-0146-0.

[26] P. Held, Determination of NADH Concentrations with the Synergy TM 2 Multi-Detection Microplate Reader using Fluorescence or Absorbance, BioTek. (2007) 6. http://www.biotek.com/resources/docs/NADH_App_Note.pdf.